THE GEOCHEMISTRY OF SEDIMENTS OF THE PANAMA BASIN, EASTERN EQUATORIAL PACIFIC OCEAN

by

Thomas Frederick Pedersen,

B.Sc(Hons), British Columbia.

Thesis presented for the degree of

DOCTOR OF PHILOSOPHY

of the University of Edinburgh,
in the Faculty of Science

May, 1979

Declaration

This thesis has been composed by me, and except where specified in the text, all the work presented here is my own.

ABSTRACT

A study of some of the many factors which collectively govern the composition of hemipelagic sediments in the Panama Basin is reported. Emphasis is placed on diagenetic processes. The mineralogy, elemental composition (C, Na, Mg, Al, Si, P, S, Cl, K, Ca, Ti, Cr, Mn, Fe, Co, Ni, Cu, Zn, Br, Rb, Sr, Zr, Mo, I and Ba) and interstitial water chemistry ($Si(OH)_4$, NH_4^+, PO_4^{3-}, SO_4^{2-}, alkalinity, Mn^{2+}, Fe^{2+}, and total I) of a suite of shallow (< 2 m) sediment cores have been investigated.

The Panama Basin is characterized by complex circulation, exceptional euphotic zone productivity and sediment compositions ranging from foraminiferal ooze in the Galapagos Islands area to hemipelagic clays in the northeast.

Throughout the Basin, sediments which are reducing at depth are mantled by a manganese oxide-rich surface layer. Upon burial MnO_2 dissolves increasing the interstitial manganese concentration to levels limited by precipitation of manganese-bearing carbonate. The occurrence in one core of an authigenic mineral of composition $(Mn_{51}Ca_{45}Mg_4)CO_3$ is linked to chemical and physical controls on nucleation in sediments. Fe, Mg, K, Si and smectite are enriched in one horizon of a Galapagos Spreading Centre core, evincing historical hydrothermal activity.

The molybdenum distribution parallels that of manganese in the sediments. Diagenetic recycling and scavenging of sea water Mo by oxides produce an enriched surface layer. Coprecipitation of Mo with iron monosulphides probably limits the pore water concentration. Ni, Co, Cu and Zn are enriched in the oxide layer of the biogenic sediments alone. Rapid accumulation and complexation by organic ligands in the carbon-rich terrigenous clays may inhibit adsorption of the metals by surficial oxides. Organic matter appears to be a major host for Ni, Co

and Zn at depth in Galapagos-area sediments. This relationship is contingent upon the initial concentration of the metals by the oxides. Iodine and bromine are strongly associated with organic matter in the sediments. I/C_{org} and Br/C_{org} ratios suggest that iodine is much more labile than bromine during diagenesis. Interstitial iodine profiles indicate that there is a small benthic flux of iodine to bottom water.

Diagenetic modelling shows that there is excess dissolved phosphate in pore waters, apparently produced by dissolution of skeletal hydroxyapatite.

Radiocarbon dating and accumulation rate calculations demonstrate that climate has had a major effect on sediment deposition in the Galapagos Islands area during the past 50,000 years.

TABLE OF CONTENTS

CHAPTER ONE

INTRODUCTION

In the past decade, chemical oceanographic research has seen the development of an increasing tendency to study only one specific aspect of a geochemical system. This is often the case in the investigation of the complex biogeochemistry of marine sediments where integrated studies of the many processes influencing sediment composition are uncommon. To some extent, this scarcity reflects limits imposed upon sediment work by areal constraints since within a particular portion of the oceans sedimentation may be characterized by detrital, biogenic, organic or hydrothermal inputs, but rarely reflects all four.

The hemipelagic sediments of the topographically-enclosed Panama Basin in the eastern equatorial Pacific constitute an exception to this generality for they are subject, over a distance of less than 1000 km, to known hydrothermal activity as well as distinct deposition of terrigenous, biogenous and organic components. The Basin therefore functions as a microcosm of oceanic sedimentary processes and for this reason has increasingly warranted the attention of marine geochemists over the past several years.

Considerable work has been carried out on mineralogy, biogenic sediment distribution and texture, radiolarian paleoecology, tectonic evolution and hydrothermal activity. Despite such intense investigation, the chemistry of sediments in the Panama Basin has received little attention. It is this subject which will be primarily studied in this thesis.

The Panama Basin was chosen as an appropriate area for the study of factors affecting sediment composition not only because it is influenced by a diversity of depositional processes but also, equally importantly, because it encompasses some of the most productive surface waters in the oceans. As a consequence the sediments are relatively enriched in organic matter; bacterially-mediated decomposition

of this material initiates diagenetic reactions which play a major role in determining the eventual composition of the sediments.

In this thesis several aspects of sediment composition will be considered. Mineralogy and major and minor element analyses, including organic carbon, will be used to develop a broad overview of areal and vertical variations in the sediments.

Recent research has outlined significant hydrothermal effusion into bottom water in the south-central Panama Basin (Lonsdale, 1977a; Lupton et al, 1977; Weiss et al, 1977; Corliss et al, 1978, 1979) and indications that this activity influences element distributions will be discussed within the context of both mineralogy and major element chemistry.

Since publication of the widely-cited paper by Lynn and Bonatti (1965) on manganese diagenesis, a greater awareness of the importance of post-depositional chemical effects on sediment composition has been fostered amongst marine geochemists. It is increasingly being recognized that precipitation, dissolution and exchange reactions in sediments play a dynamic role in governing the distribution of a number of elements. Such processes are given special consideration in this work, particularly in the cases of manganese and trace element chemistry.

The post-depositional behaviour of manganese will be explained on the basis of its distribution in interstitial water, solid hydrogenous and authigenic phases and its association with textural variations in the sediments. The partitioning and distribution of trace elements will be considered with cognisance of the possible importance of diagenesis in influencing element behaviour. Particular emphasis will be placed on the transition metals since surprisingly little is known of their geochemistry, especially in hemipelagic sediments.

The association of the halogens, iodine and bromine, with organic

matter will be investigated in this thesis with the intention of elucidating possible contrasts in the post-depositional behaviour of the two elements. The effects of diagenesis on controlling the exchange of iodine between sediments and sea water in the Panama Basin will also be considered.

Since the composition of interstitial solution is sensitive to certain subtle changes in the solid phase, pore water analyses will be used to define the nature and extent of early diagenetic reactions in the sediments, paramount among which is organic matter decomposition. An attempt will be made to account for the distribution of metabolites in solution.

Finally, the recognition that Pleistocene climatic fluctuations have influenced the sedimentary record has important implications concerning compositional variations within sediments. Most of the research in this field has dealt only with the distribution in the sediment column of biogenic material and its oxygen isotopic composition. In this study, consideration of the effects of climatic change on depositional processes will be extended by critically examining the distribution with time of elements in organic, biogenic and terrigenous phases.

Analytical work for this research was performed on a suite of cores collected on a traverse across the Panama Basin during cruise 2/1976 of R.R.S. Shackleton. Coring stations were chosen in order to sample a range of sediments influenced by varying degrees of biogenic, terrigenous and possibly hydrothermal deposition. The locations of those studied are listed in Table 1.1 and shown in Fig. 1.1. Core collection and handling methodology are outlined in Appendix A (p. 140) along with a brief description of the sediments.

The cores collected by the author were supplemented by samples from a box core raised by a team from the Scripps Institution of

Oceanography during the Pleiades Leg II cruise in May-June, 1976.

Table 1.1 Locations and water depths of cores collected for this thesis.

Core	Depth (m, uncorrected)	Latitude	Longitude
P1	3422	1°17.7'S	94°37.4'W
P2	3510	1°24.65'S	92°58.83'W
P5	1540	0°54.57'S	87°51.08'W
Pleiades Box Core	2716[1]	0°36.13'N	86°08.24'W
P6	2712	0°52.34'N	86°07.73'W
P7	3085	2°36.26'N	83°59.18'W
P8	4093	4°37.24'N	82°59.17'W
P9	3075	5°15.67'N	79°44.51'W
P10	4007	6°27.5'N	78°25.8'W
P11	3847	6°48.28'N	78°35.35'W
P12	3491	7°08.66'N	78°43.92'W
P13	1803	7°31.3'N	78°54.5'W

[1] corrected depth.

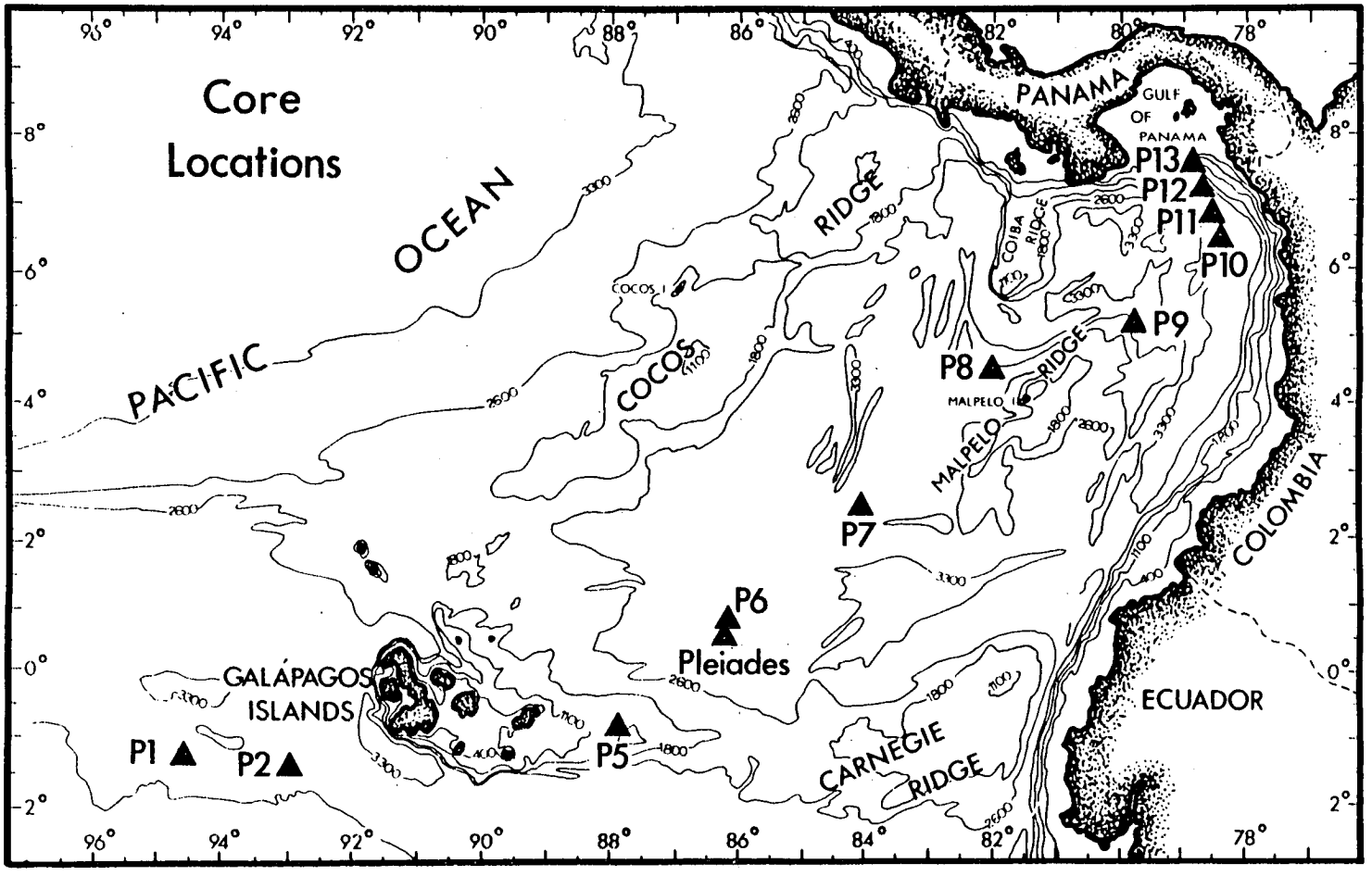

Fig. 1.1 Locations of cores studied in this thesis.

CHAPTER TWO

PHYSICAL CHARACTERISTICS OF THE PANAMA BASIN

2.1 Physiography

To the north and east the Panama Basin is bordered by the continental margins of Central and northwestern South America while the Cocos and Carnegie submarine ridges bound its western and southern limits respectively (Fig. 2.1). The Cocos Ridge extends approximately 1100 km southwestwards from the continental margin at the Costa Rica - Panama border, where it forms the southern terminus of the Middle America Trench, towards the Galapagos Archipelago. Depths on the ridge range from sea level at Cocos Island to about 2000 m (Chase et al, 1970). Four saddles have been located (Fig. 2.1): the Cocos Gap at 6° 15' N, with a crestal depth of 1800 m (Dowding, 1977) and three passages toward the southern end with depths of 2010 m (3° 40' N), 2110 m (2° 20' N), and 2140 m (1° 15' N) (Lonsdale, 1977b,p. 1066). The 1000 km long Carnegie Ridge extends eastward at about 1° S latitude from the Galapagos Islands to the continental margin of central Ecuador where it terminates the northern end of the Peru-Chile Trench. A broad saddle with a sill depth of 2330 m (Lonsdale, 1977b)divides the ridge into two equal-length segments.

Two internal ridges, the Coiba Ridge, which extends about 250 km from the continental margin off central Panama, and the central Malpelo Ridge divide the Panama Basin into eastern and western sub-basins. The Coiba Gap, a 3600 m deep (van Andel, 1973) narrow trough separates the two ridges and provides the primary link between the sub-basins.

Major tectonic features of the Panama Basin are shown in Fig. 2.2. The active Galapagos Spreading Centre forms part of the boundary between the Cocos and Nazca lithospheric plates and is offset by a series of north-south striking transform faults, principal of which is the Coiba Fracture Zone at 83° W which forms the eastern terminus of the Cocos Plate. Hey et al (1977) report a half-spreading rate of

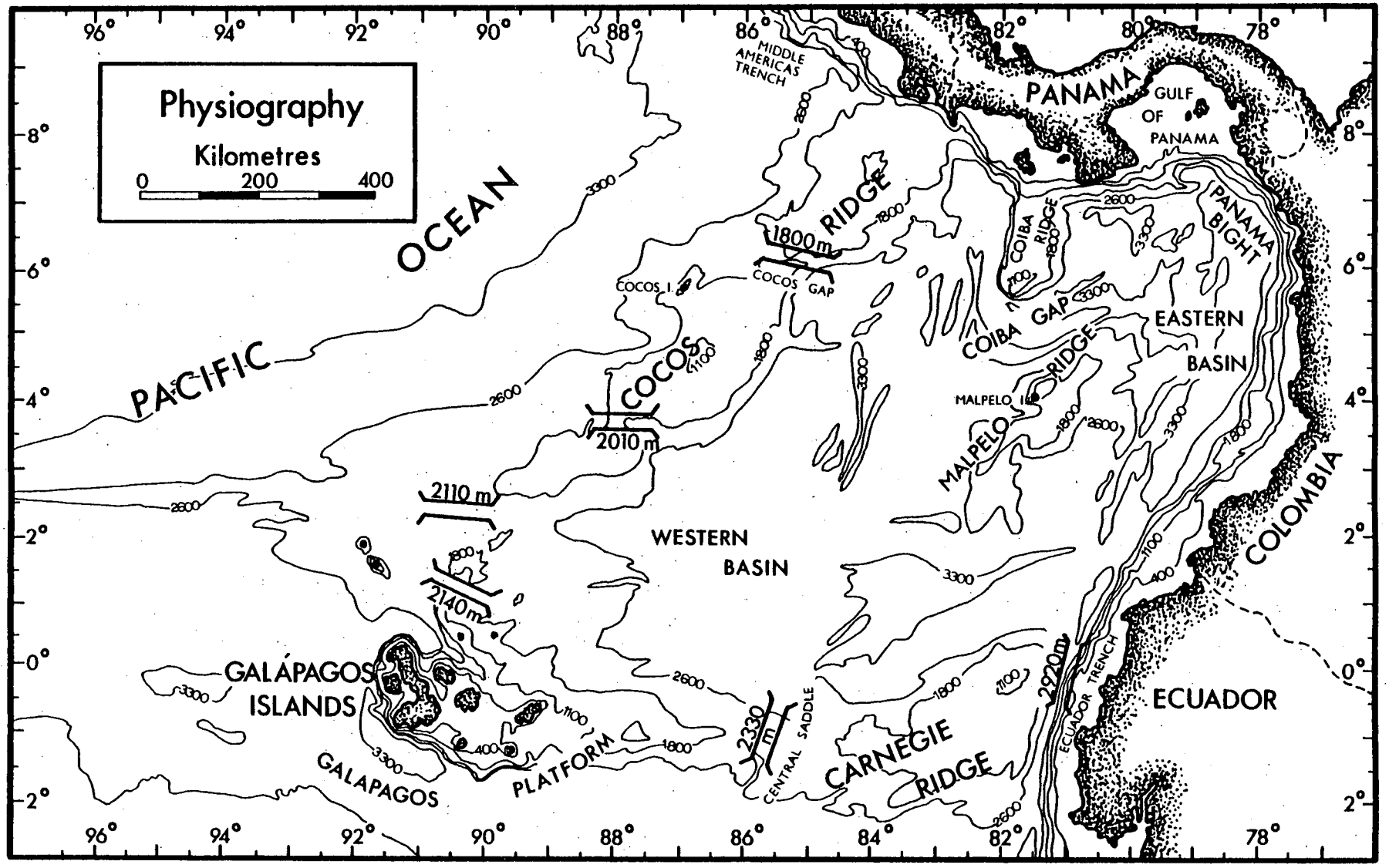

Fig. 2.1 Physiographic features of the Panama Basin.
Bathymetry is after Chase et al (1970). Isobaths are in metres.

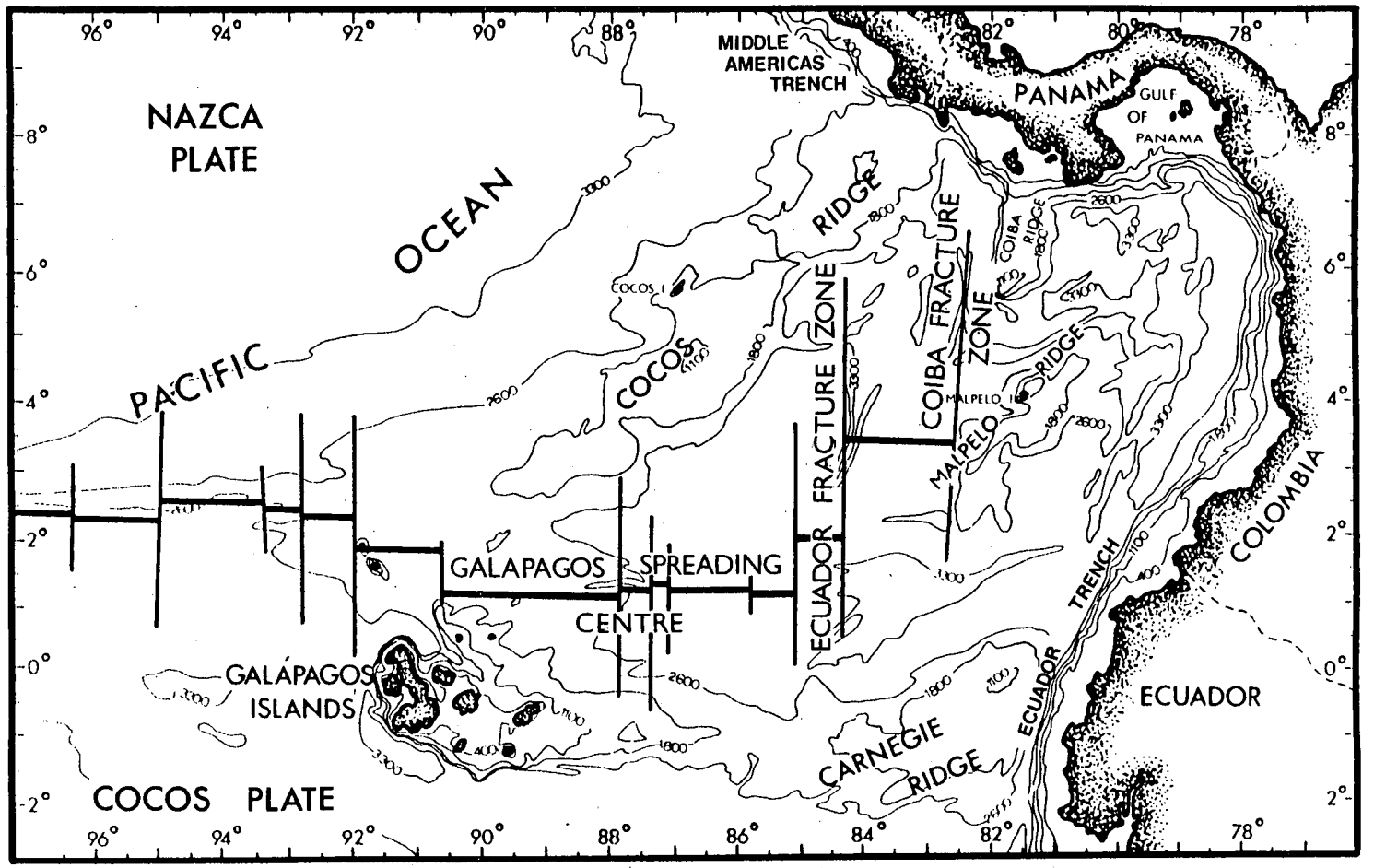

Fig. 2.2 Major tectonic features of the Panama Basin (after Hey, 1977).

21-36 mm yr^{-1} for the spreading centre, considerably less than the 71 mm yr^{-1} half-rate they report for the East Pacific Rise.

Aseismicity characterizes the Cocos and Carnegie Ridges (van Andel et al, 1971); judging by the distribution of recent earthquake epicentres (Fig. 3, Heath and van Andel, 1973), the Coiba and Malpelo Ridges are similarly aseismic. Prevailing tectonic theory supports motion of the Cocos and Nazca Plates away from a Galapagos hotspot (marked at present by the volcanically active Galapagos Islands), causing formation of the Cocos and Carnegie Ridges (Holden and Dietz, 1972; Hey, 1977; Hey et al, 1977). Generally, seismic activity within the Basin is confined to transform faults, with only very low magnitude earthquakes being recorded from the spreading centre crest (Macdonald and Mudie, 1974). Although much of Central America and western South America is subject to severe contemporary seismicity, Panama has been free of volcanic activity throughout the Quaternary (Terry, 1956). This quiescence resulted when the subduction zone seaward of Panama and northernmost South America was plugged by underthrusting of the Cocos and Carnegie Ridges, probably during the Pliocene as indicated by Fig. 7 of Hey (1977).

Sediment thickness in the Panama Basin varies locally as a function of circulation and topography but can be allied generally to the age of the underlying crust, at least for the Western Basin. Sediment accumulation is negligible (<3 m) within 10 km of the spreading centre (Klitgord and Mudie, 1974) but exceeds 500 m on Mid-Miocene basalt in the north of the Basin (Heath and van Andel, 1973, Fig. 11).

2.2 Hydrography

The complex surface circulation of the Panama Basin is now quite well understood and has been summarized by Wyrtki (1965, 1966, 1967),

Forsbergh (1969), Stevenson (1970) and Dinkelman (1974). Although considerable work is yet required to describe much of the midwater circulation, bottom water inflow and circulation have been described by Laird (1971) and more recently by Lonsdale (1977b).

Major features of the surface circulation are outlined in Fig. 2.3. Large-scale changes in the circulation pattern relate directly to variation in intensity and direction of the trade-wind systems. Since the Panama Basin lies within the seasonal migration zone of the trade-wind and doldrums belt, surface waters are successively influenced by the northeast trades, the equatorial calm belt, and the southeast trades (Dinkelman, 1974). The Inter-tropical Convergence (I.T.C.), where the trade-winds converge within the buffering zone of the doldrums, is at its southern maximum (just north of the equator) during southern summer and migrates to about 10-12° N during southern winter (July-September). The I.T.C. is the principal influence on the development of the eastward-moving N. Equatorial Countercurrent in the Basin (Wyrtki, 1965). The Countercurrent is well developed during southern winter, mostly flowing counterclockwise around the upwelling zone of the Costa Rica Dome and entering the N. Equatorial Current, but its penetration into the Basin is progressively reduced as the I.T.C. shifts southward, and it disappears from the area during the southern summer. Fig. 2.3 illustrates this marked seasonal variation.

Cool, nutrient-rich water of the Peru Current strongly affects the southern Panama Basin surface water. During southern winter and spring the current is well defined and deflects increasingly westward as it flows north toward the equator and contributes to the South Equatorial Current. A portion of the Peru Current continues to flow northward entraining some N. Equatorial Countercurrent water and continental runoff and forms the Colombia Current (Fig. 2.3). This, in

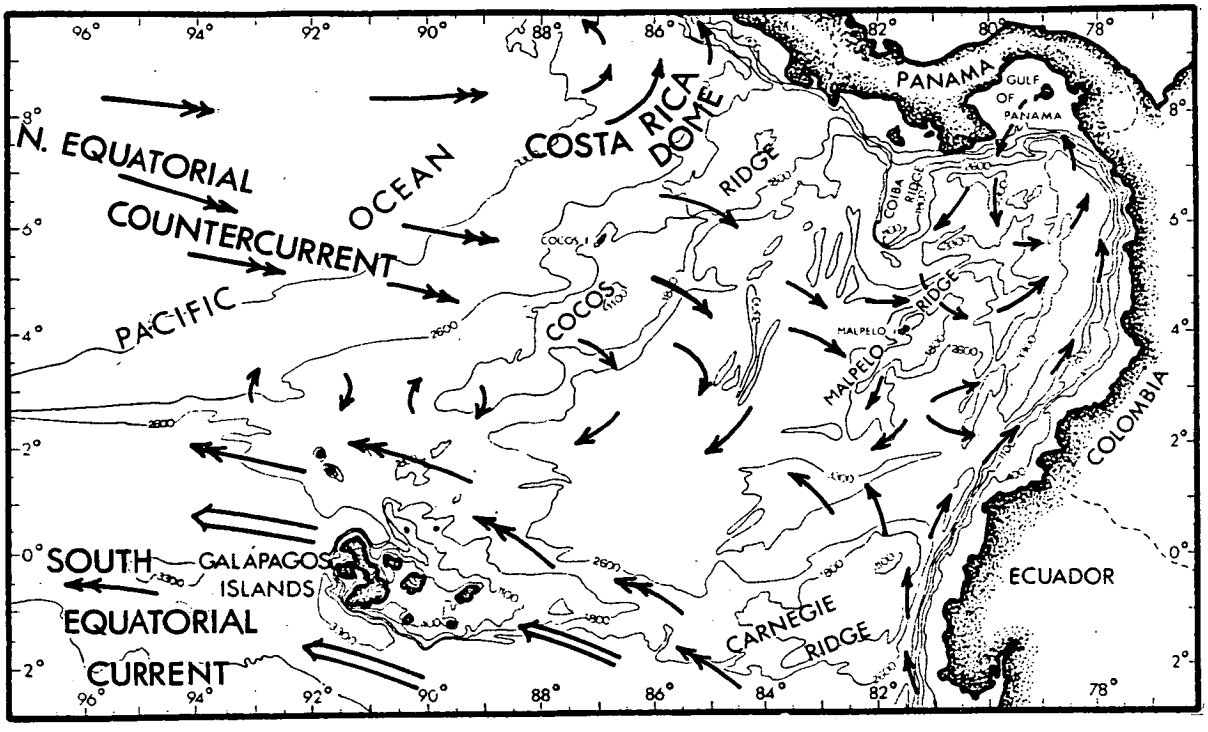

(a) Southern winter

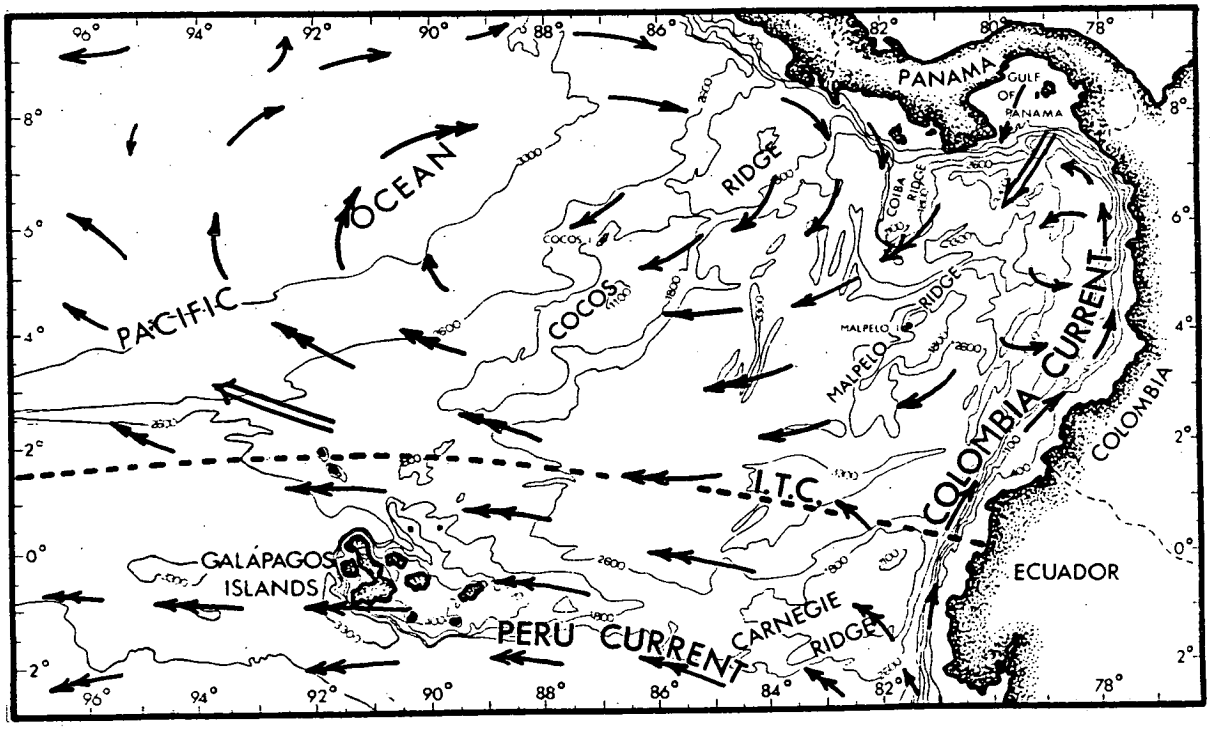

(b) Southern summer

Fig. 2.3 Surface circulation in the eastern equatorial Pacific (after Wyrtki, 1965).

turn, forms the eastern branch of a counter-clockwise circulation cell in the Panama Bight. In southern summer, the Peru Current weakens as the southeast trade-winds shift southward. During this period, a large, sluggish anticyclonic eddy dominates the outer Basin circulation (Fig. 2.3b) and the Panama Bight cell and Colombia Current are strengthened upon being confined to the coastal area.

Subsurface circulation in the Panama Basin is little understood at present. Stevenson and Taft (1971) and Pak and Zaneveld (1973) present the most recent reports on the behaviour of the Equatorial Undercurrent, known equally well as the Cromwell Current, east of the Galapagos Islands. The Undercurrent flows around the Islands, mostly on the northern side, and extends eastward at a depth of 100-250 m to at least 86° 30' W before eventually dying out as a result of strong vertical mixing. Interruption of the flow by the Islands generates eddies of various sizes (Pak and Zaneveld, 1973) which probably complicate subsurface circulation in the Western Basin. There is some evidence that a portion of the Undercurrent water curls around and adds to the South Equatorial Current (Wyrtki, 1967). In the Eastern Basin, Stevenson (1970) reports the existence of a southbound current at depth 0-250 m just west of the Colombia Current. Dinkelman (1974) suggests this might merge into the southward-flowing Peru-Chile Undercurrent but supporting evidence is not yet available. Based on a study of mineral distribution in the surface sediments of the Panama Basin, Heath et al (1974) advocate that dispersal of some clay minerals over much of the southern half of the Basin is facilitated by southerly or southwesterly-moving intermediate-depth (300-2000 m) currents; however, no hydrographic data to support this theory is yet available.

Bottom water enters the Panama Basin through the Ecuador Trench (sill depth 2920 m) at the eastern end of the Carnegie Ridge (Laird,

1971; Lonsdale, 1977b). This inflow is a well defined 230-300 m thick layer of bottom water originating from the Peru Basin; its circulation is shown in Fig. 2.4. Initially, the water diverges into two branches: one flows westward through the Carnegie-Malpelo Pass and then spreads across the Western Basin; the other flows northeast parallel to the base of the South American continental slope before curling westward and spilling through the Coiba Gap into the northern part of the Western Basin.

Considerable exchange probably occurs across the central saddle on the Carnegie Ridge. Using limited hydrographic data, Lonsdale (1977b) suggests that there is a slow, broad inflow across the saddle which, not being dense enough to spill down to the Basin floor, generally defines the upper limit of distinctive Basin water. However, the barchan-like dunes which occur on the north flank of the sill (Lonsdale and Malfait, 1974) indicate episodic cascading inflow of dense water across the sill. Laird (1971) and Kowsmann (1973) postulate that water also leaves the Basin across the Carnegie saddle. Therefore, it seems possible that a very broad southerly drift of warmer, less dense Basin water occurs just above the slow inflow discussed by Lonsdale (1977b), possibly balancing the inflowing bottom water.

Constant renewal of Panama Basin Bottom Water is indicated by the increase in dissolved oxygen content with depth. The principal force driving the renewal appears to be the addition of geothermal heat within the Basin, especially along the Galapagos Spreading Centre where discharging plumes of warm water have been observed (Weiss et al, 1977). Lonsdale (1977b) calculates the inflow rate to be 0.35×10^6 m^3 s^{-1} (0.35 sv), a volume sufficient to fill the Panama Basin up to the Carnegie Ridge central sill depth (2300 m) in less

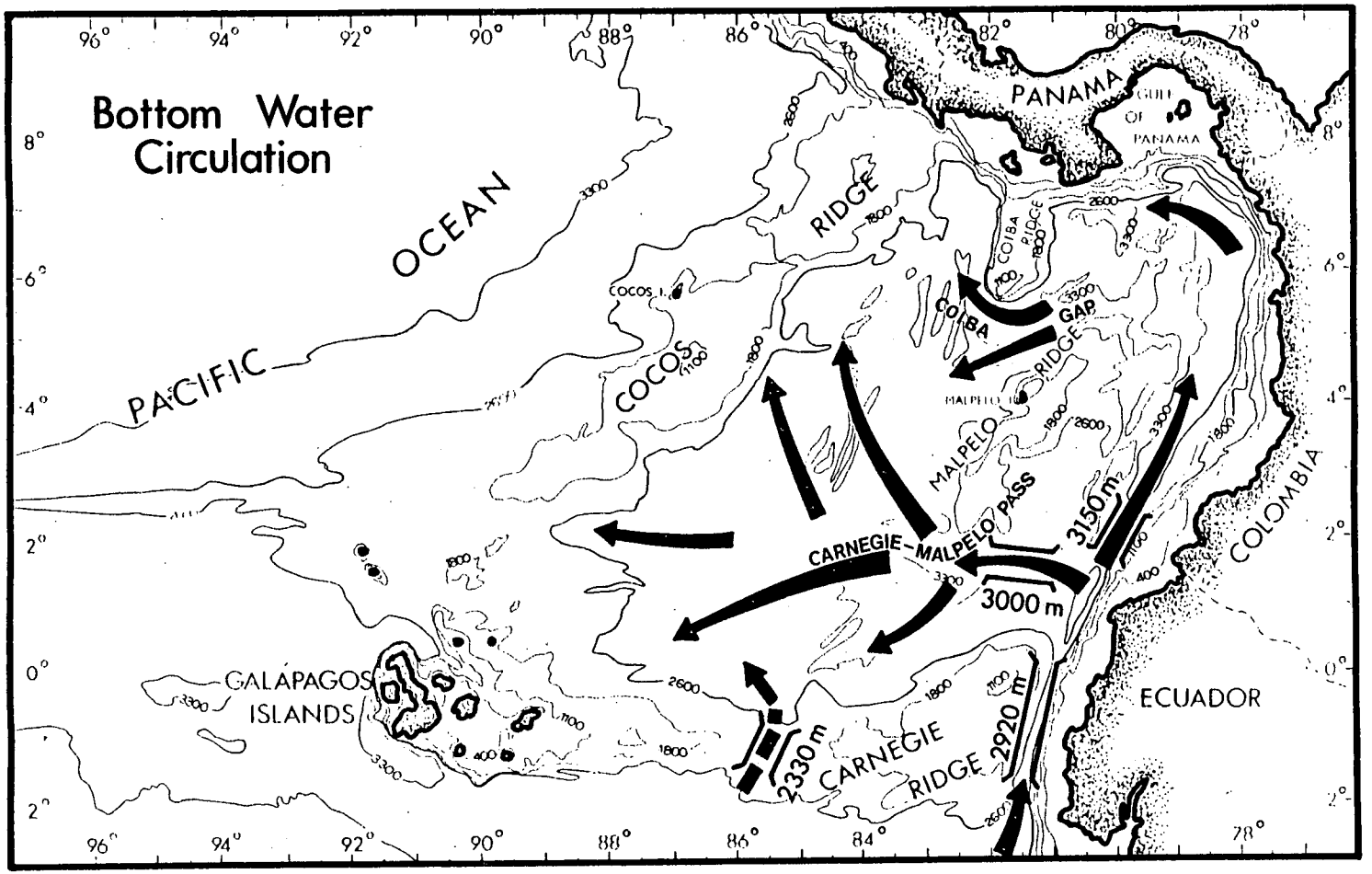

Fig. 2.4 Bottom water circulation in the Panama Basin (after Lonsdale, 1977b).

than 50 yr.

2.3 Biological productivity

The level of biological productivity in the Panama Basin is among the highest found in the world's oceans and relates directly to two features: rapid upwelling over parts of the Basin, and the widespread shallow thermocline. Average euphotic zone productivity for Panama Basin waters is shown in Fig. 2.5.

Upwelling of NO_3^- and PO_4^{3-} - rich subsurface water is pronounced along the equatorial divergence zone, being exemplified by Equatorial Undercurrent water cropping out near the Galapagos Archipelago. Along the western margin of South America upwelling enriches the coastal waters adjacent to the Peru and Colombia Currents; domal upwelling in the Panama Bight, associated with the counter-clockwise gyre developed there (Stevenson, 1970), supports high productivity in much of the remainder of the Eastern Basin. In addition, the shallow (25-50 m deep) thermocline occurring over large areas of the Panama Basin lies within the euphotic zone; phytoplankton are thus able to withdraw nutrients directly from the enriched thermocline waters (Ryther, 1963).

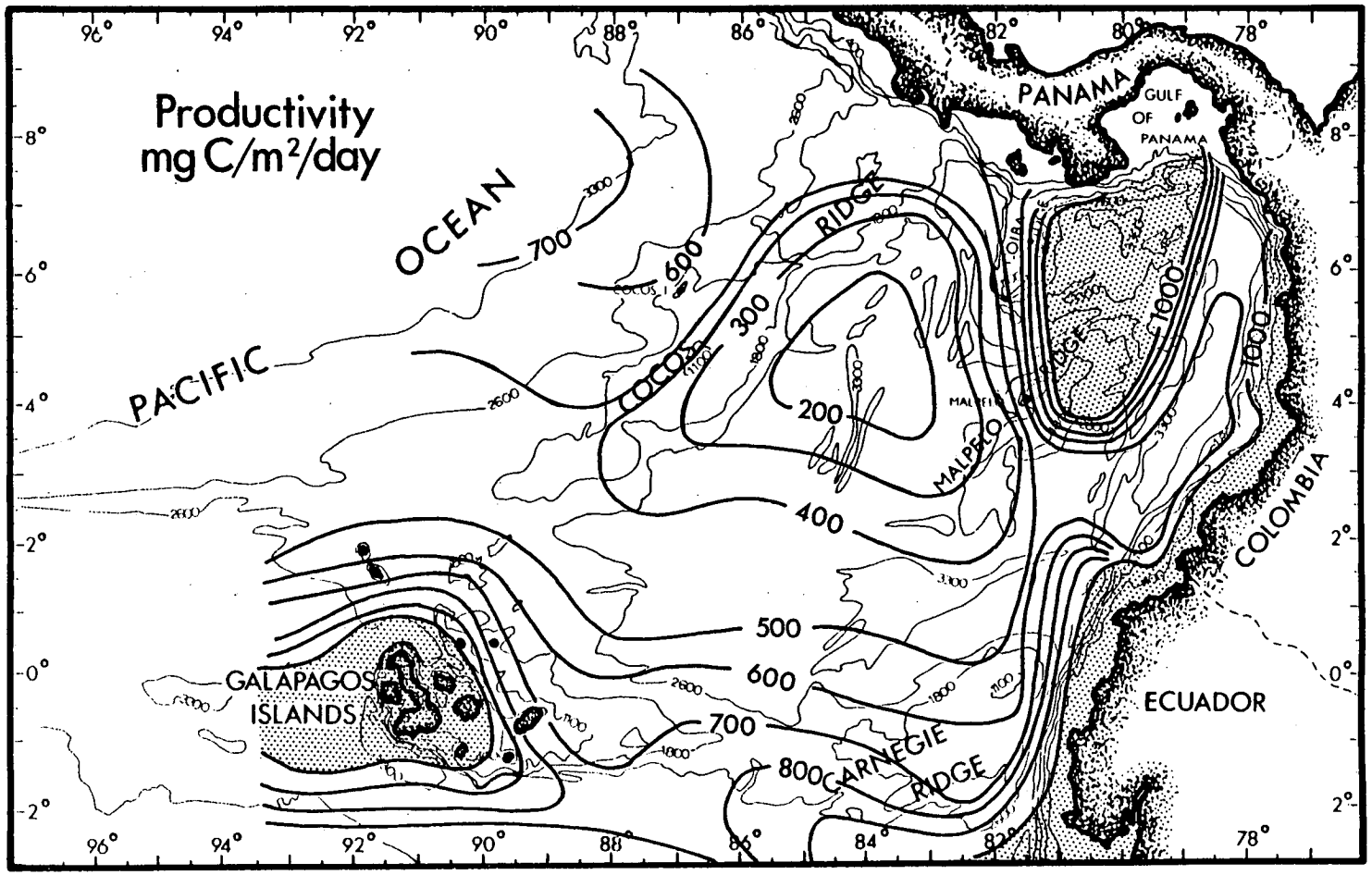

Fig. 2.5 Average productivity in the Panama Basin integrated over the euphotic zone (after Moore et al, 1973).

CHAPTER THREE

MINERALOGY

3.1 Introduction

Knowledge of mineral distributions in Panama Basin sediments provides a primary framework within which areal and vertical chemical variations may be evaluated. Accordingly, ten surface and thirty subsurface samples (from P2, P6 and P8) were examined by X-ray diffraction of oriented mounts following removal of calcium carbonate, amorphous iron and manganese oxides and, to some extent, opal. In addition, unoriented pressed powders representing eleven chemically untreated samples were X-rayed. Preparation techniques and instrument conditions are detailed in Appendix B.

A previous description of the mineralogy of Panama Basin surface sediments has been provided by Heath et al (1974) and that presented here complements their work.

3.2 Mineral identification

Quartz: The pronounced sharp 101 peak at 3.34 Å (26.66° 2θ) and a less intense 100 peak at 4.26 Å (20.85° 2θ) were used to identify quartz in unoriented powder mounts. The occurrence of the mineral in oriented mounts could not be confirmed because of background interference from the ceramic tile used in the preparation procedure; this interference is discussed in Appendix B.

Feldspar: A strong peak at 3.18 Å (28.04° 2θ) and a less intense 4.04 Å (21.98° 2θ) reflection indicated the presence of feldspar in unoriented powder mounts. The often complex 3.18 Å peak was considered to represent total feldspars (Heath, 1969) and the 4.04 Å peak plagioclase (Peterson and Goldberg, 1962; Heath, 1969).

Amphibole: A typically sharp reflection at 8.5 Å (10.4° 2θ) indicated the presence of amphibole.

Clay minerals

Smectite was distinguished by a peak with a spacing of ~14 Å at 50% humidity which shifted to ~17.4-17.6 Å following solvation by ethylene glycol. Heating to 400°C fully collapsed the d-spacing to ~10 Å, as shown in Fig. 3.1.

Chlorite was identified by a sequence of peaks at 14 Å (001), 7 Å (002), and 3.5 Å (003) which were not affected by glycolation. The interference-free 3.5 Å reflection was the most diagnostic since the large smectite (001) peak commonly masked the 14 Å chlorite spacing, even in glycolated samples, and the (001) kaolinite reflection directly overlapped chlorite (002). Boiling for 30 min in 10% HCl eliminated the (003) peak (Fig. 3.2a). Heating to 550°C destroyed the 7 Å chlorite + kaolinite reflection and intensified chlorite (001) (Fig. 3.1). The (001) reflection persisted to >850°C which indicated that at least some of the chlorite is well crystallized (Heath, 1969).

Kaolinite was recognized by a sequence of reflections at 7.14 Å (001), 3.59 Å (002) and 2.38 Å (003) which were unaffected by glycolation and disappeared upon heating to 550°C (Fig. 3.1). Biscaye (1965) reported that slow scanning ($\frac{1}{8}^{\circ}$ 2θ min^{-1}) of the 24-26° range resolves the 3.5 Å chlorite reflection from kaolinite (002) provided both peaks yield similar intensities. In Panama Basin samples where both minerals occurred, the slow-scan intensity of the chlorite (003) reflection was generally about twice that of kaolinite (002), thus allowing only partial resolution as shown in Fig. 3.2b.

Illite. Reflections at 10 Å (001) and 5 Å (002) unaffected by glycolation were attributed to illite.

The zeolite clinoptilolite-heulandite was recognized principally by a strong 8.9-9 Å (020) reflection. A less intense peak at 7.9 Å

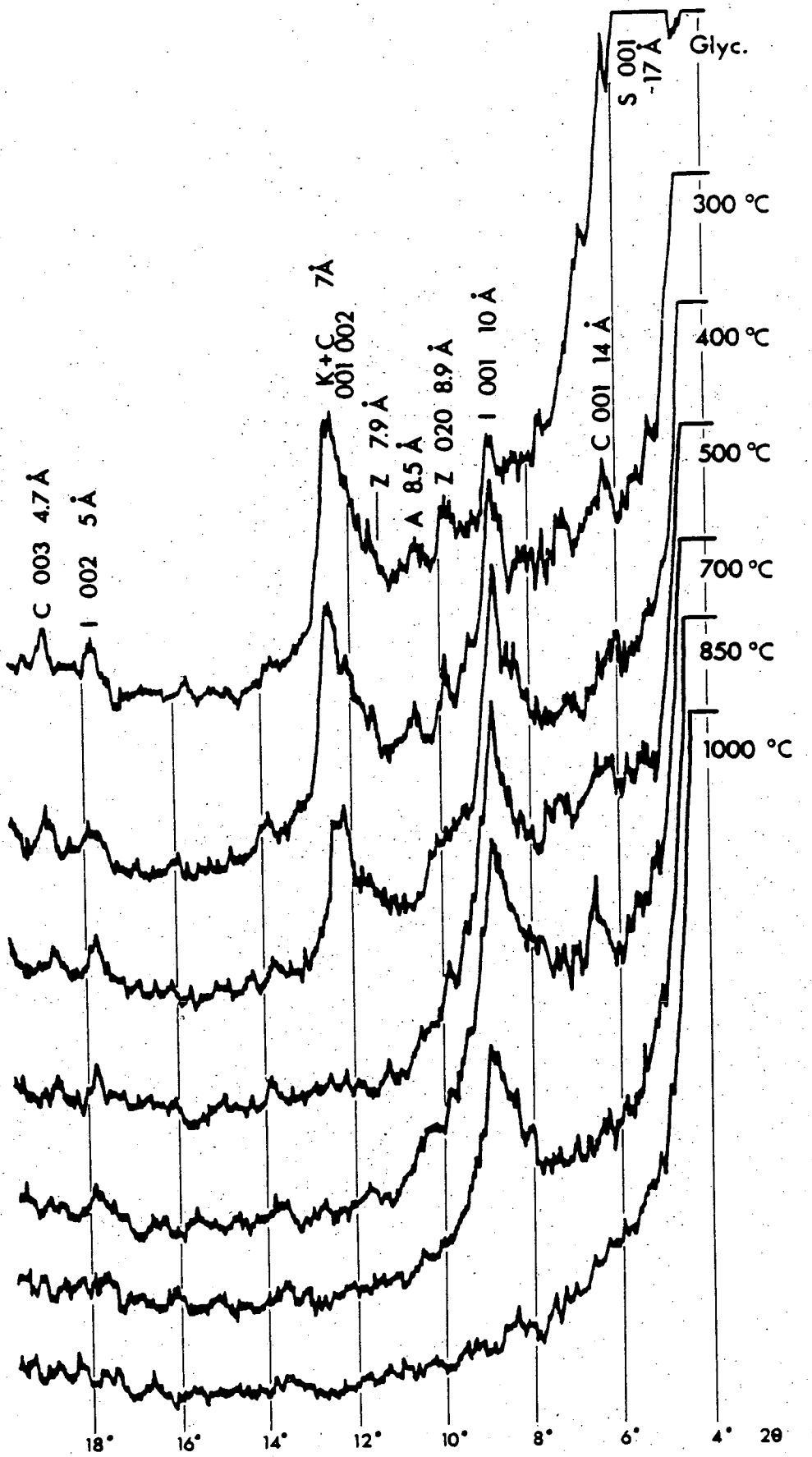

Fig. 3.1 Step-heating effects on sample P8:0-4:
All temperatures were held for one hour.
S = smectite, C = chlorite, I = illite,
Z = clinoptilolite-heulandite, A = amphibole,
and K + C = kaolinite + chlorite.

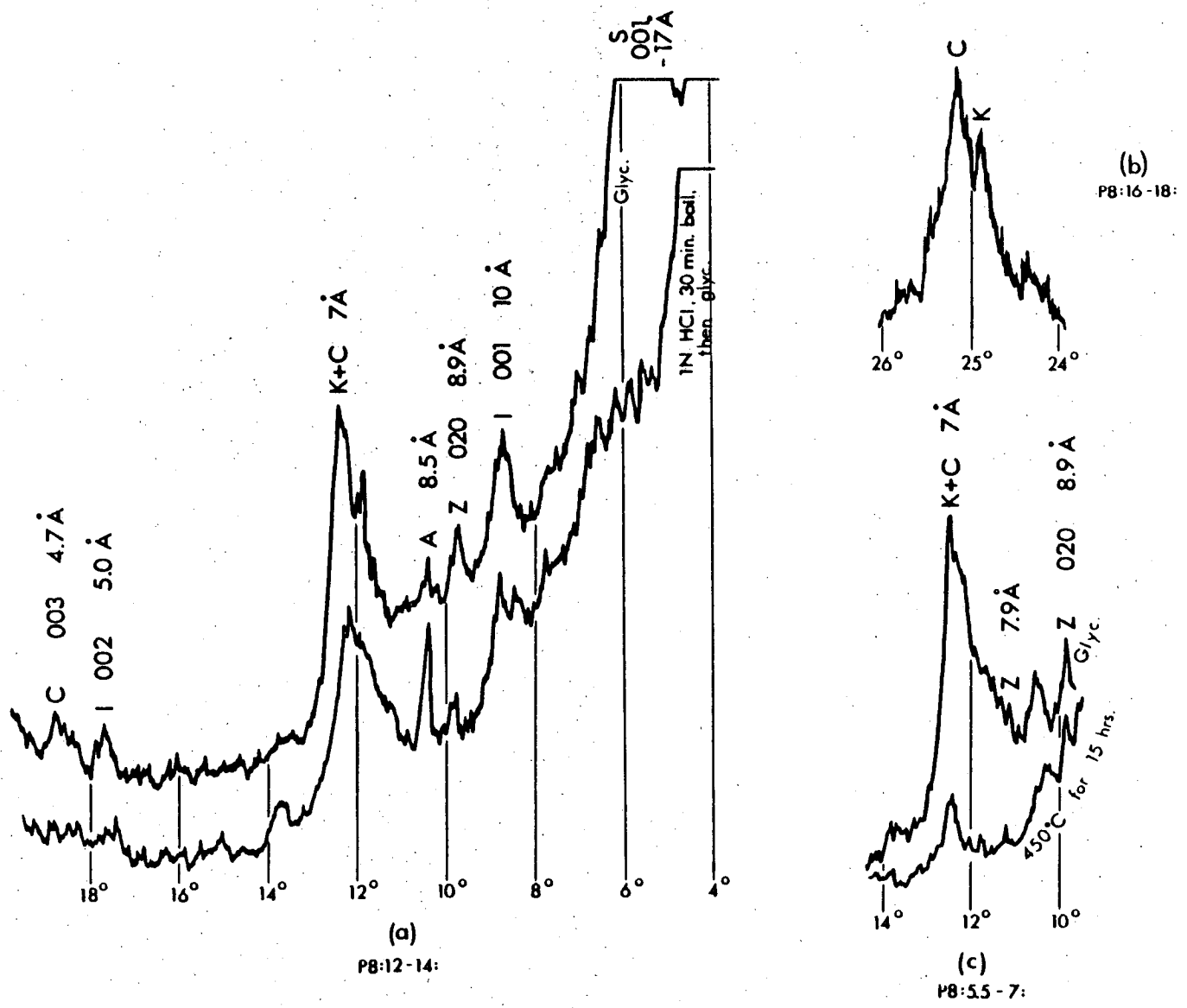

Fig. 3.2 (a) diffractograms of sample P8:12-14: before and after boiling for 30 min in 1N HCl;
(b) slow-scan ($\frac{1}{8}^{o}$ 2θ min^{-1}) resolution of chlorite (003) from kaolinite (002);
(c) response of the zeolite peaks to prolonged heating at 450°C.

occurred sporadically, being frequently masked by the shoulder of the 7 Å chlorite + kaolinite reflection. Heating at 450°C for 15 hours did not affect the diffraction pattern (Fig. 3.2c). Mumpton (1960) reported that heulandite becomes amorphous after overnight heating at ~350°C, while clinoptilolite is unaffected. Hence, it is concluded that the zeolite phase present is principally clinoptilolite.

3.3 Mineral distribution

This section will outline the mineral distribution within a suite of chemically analyzed cores and surface sediments. The discussion will deal principally with clay minerals since these form the bulk of the non-biogenic fraction. No attempt has been made to quantify concentrations of minerals present as it is well known that semi-quantitative clay mineral analysis by X-ray diffractometry is subject to serious difficulty. Factors as diverse as crystallinity differences, compositional variations due to isomorphous substitution of cations, oriented mount preparation techniques, and grain size ranges specific to certain clay minerals inhibit the utility of standard mixtures in semi-quantitative work and cast doubt on correlations of mineral suites having different provenance (Archer, 1969). However, a general assessment of important areal and vertical mineralogic variation in the sediments is necessary. Therefore, peak height ratios on glycolated samples have been determined directly, without application of weighting factors. Peak heights were chosen in preference to peak areas since the high concentration of smectite present in all samples prevented consistent peak area determinations for other minerals in the range 10.5-6.5 Å.

Biogenic opal and calcite dominate much of the large western portion of the Basin and the Galapagos Platform area and become

subordinate to terrigenous material only in nearshore regions and in the Eastern Basin. The general distribution of both minerals, as mapped by Moore et al (1973), is shown in Fig. 3.3. Unoriented mount diffractometry of core top samples clearly defines the biogenic-terrigenous sediment division; cores P1-P7 are composed largely of calcite with opal (identified by a broad background centred on 22° 2θ) and P8-P13 largely of terrigenous minerals.

The non-biogenic fraction of all samples is composed of smectite with subordinate amounts of chlorite, kaolinite, illite, quartz, feldspars, amphibole and occasional clinoptilolite and volcanic glass shards. Coarse terrigenous minerals, primarily quartz, feldspars, hornblende, and pyroxene, are most abundant on the continental margin, as would be expected. The quartz 4.26 Å/ total clay 4.5 Å peak height ratio decreases steadily from ~1.8 on the upper continental slope off the Gulf of Panama (core P13) to ~1.0 in the centre of the Western Basin biogenic sediments (Table 3.1), demonstrating the expected seaward increase in clays relative to detrital particles of larger grain size. The inordinately high Q 4.26 Å/clay 4.5 Å ratio in P13 relative to P10, P11 and P12 suggests either a greater input of clays to the northeasternmost basin than to the slope or possible removal of the fine fraction by winnowing, producing a lag deposit of coarser material. The latter suggestion implies slower accumulation and is supported by microscopic identification of ovoid to spherical, pale to bright green glauconite (?) pellets in P13, possibly formed by alteration of faecal pellets. The mineral was not observed in any other cores but Kowsmann (1973) reported its irregular occurrence in some Panama Basin shelf and ridge sediments.

The general seaward decrease in the smectite 001/illite 002 and smectite 001/K + C 7 Å ratios (Table 3.1) opposes the relative increase

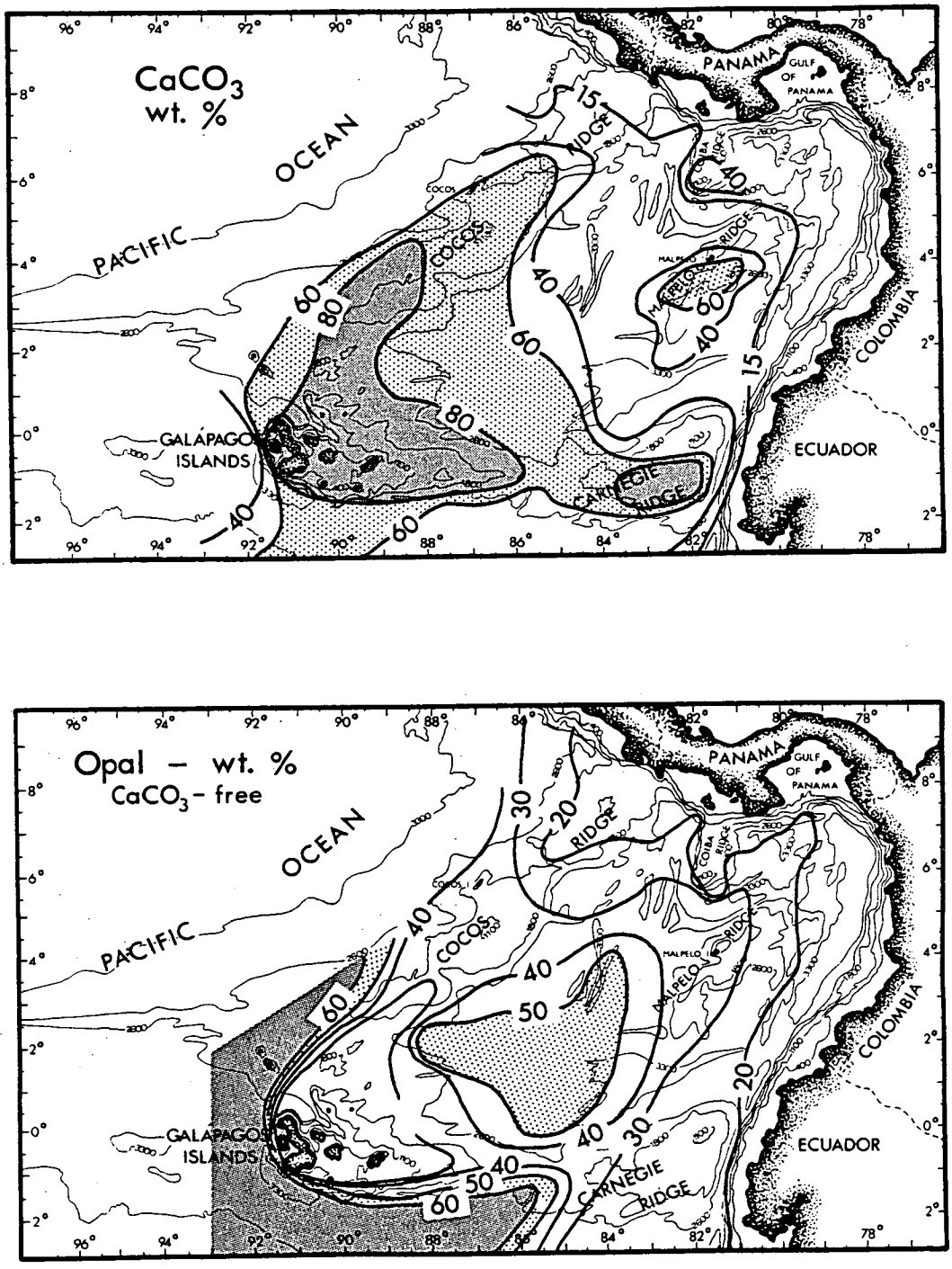

Fig. 3.3 $CaCO_3$ and opal distributions in Panama Basin surface sediments (after Moore et al, 1973). Moore et al calculated the $CaCO_3$ content from total carbon analyses, but since they failed to take into account the 1-2% organic carbon content of the sediments, the isocons are in error by up to 15 wt. %. The 15% isocon should, in fact, be 0 wt. %, as will become evident in Chapter Four.

Table 3.1 Selected X-ray diffractogram peak height ratios in Panama Basin sediments. S = smectite, I = illite, K + C = kaolinite + chlorite, Q = quartz, n.m. = not measurable.

Sample	Glycolated oriented mounts		Unoriented mounts
	S 001 / I 002	S 001 / K+C 7A	Q 4.26 Å / Total clay 4.5 Å
P13:0-2:	5.0	5.25	1.83
P12:0-1.5:	3.5	3.41	1.26
P11:0-3:	3.6	3.07	1.21
P10:0-2:	3.2	2.65	1.18
P9:0-2:	2.9	3.24	1.09
P8:0-4:	2.6	2.49	1.07
P7:0-2:	2.7	3.38	1.06
P6:0-1:	I n.m.	2.96	1.0
P5:0-1.5:	2.0	2.79	Clay n.m.
P2:0-1:	I n.m.	2.3	Clay n.m.

of finer-grained smectite with distance from source observed in other areas (e.g. Gibbs, 1977). This suggests that there is no common source for the clay minerals. Smectite concentration is proportionately highest in core P13, near the shelf, but is considerably reduced in the northeastern basin sediments (P10-P12), probably due to dilution by chlorite, kaolinite, and illite contributed from the continent to the east. These observations concur with the study of Heath et al (1974) who outlined sources for chlorite, kaolinite and illite in western Colombia and northern Ecuador and suggested that terrigenous smectite was derived mainly from western Panama and Costa Rica. Despite the significant input of the other clay minerals, smectite is quite clearly the dominant clay in the Eastern Basin. This observation is equally true throughout the rest of the Panama Basin and west of the Galapagos Islands where the smectite content greatly exceeds that of other non-biogenic minerals.

It is unclear what proportion of the smectite in the sediments investigated here can be attributed to authigenesis. As pyroclastic debris occurs only irregularly in the samples examined, with the exception of core P8 which contains the highest proportion of glass shards, most of the smectite is probably terrigenous. No cores were collected from the areas of known glass shard concentration (Kowsmann, 1973) which were shown by Heath et al (1974) to contain authigenic smectite.

Clinoptilolite was clearly identified only in core P8; a possible peak at 9.8° 2θ in oriented mount diffractograms from other Eastern Basin cores (P11, P12, P13) could only be ascribed very tentatively to the zeolite. It is generally agreed that clinoptilolite forms authigenically in sediments from alteration of high-SiO_2 volcanic glass (Hathaway and Sachs, 1965; Hay, 1966; Petzing and Chester, 1979). Its occurrence throughout core P8 may be related genetically to the significant content of glass shards in the core.

Clinoptilolite has been previously observed in the Pacific in Tertiary northeastern equatorial sediments (Heath, 1969), in association with altered volcanic debris in equatorial DSDP cores (Cook and Zemmels, 1971, 1972), and in Miocene to Recent sediments in the northern Panama Basin (Petzing and Chester, 1979). In addition Cronan (1974) stated that clinoptilolite has been found in sediments near the coast of Central America where rhyolitic glass is abundant. The mineral is usually found in pre-Pleistocene sediments; younger occurrences are often ascribed to reworking (Cronan, 1974). Therefore, its presence throughout the rapidly accumulating (Chapter Four) sediments of core P8 suggests that it may have been contributed from reworked proximal shelf or ridge sediments.

Kaolinite and chlorite occur in significant quantities in all

samples within the confines of the Panama Basin. Although high opal concentrations in the Galapagos Rise area west of the Galapagos Islands dilute the non-biogenic fraction, kaolinite 001 and 002 peaks are present in P2 sample diffractograms but only a trace of chlorite is evident. The reason for this segregation of chlorite and kaolinite is unclear but it may be related to aeolian transport of continental dust in the eastern equatorial Pacific area. In the vicinity of the Galapagos Archipelago, dust contains several times more kaolinite than chlorite (Prospero and Bonatti, 1969).

Illite is a significant component in all cores within the Basin but only trace quantities are observed west of the Galapagos Islands. Heath et al (1974) proposed that the mineral is widely distributed from a principal source near the Colombia-Ecuador border by bottom and intermediate-depth currents.

The vertical distribution of minerals in the non-biogenic fraction of the sediments was examined in cores P2, P6 and P8. Mineralogical contrast with the surface sediments was noted in only two horizons, one near the base of core P8 and the other near 40 cm depth in P6. Although scattered glass shards were observed throughout core P8, abundant volcanic debris was encountered only at the bottom of the core (165-183 cm). Microscopic examination of a sample taken from the 175-183 cm interval revealed a high proportion (20-30%) of clear, colourless glass shards in association with clear, mostly anhedral, highly angular quartz grains and abundant coarse opaque minerals including subhedral amphibole, biotite flakes and feldspars. Rarer brown anhedral crystals of high refractive index were thought to be zircon. Oriented mount diffractometry of the same sample showed the kaolinite, chlorite, illite, amphibole, zeolite and dominant smectite reflections typical of the entire core but, compared to sediments higher in the column,

all peaks were reduced in intensity, probably as a result of dilution by the shards. Relative to the kaolinite-chlorite 7 Å peak, the clinoptilolite reflection in the bottom sample was about 15-20% more intense than in the rest of the core (Table 3.2). It is tempting to ascribe this increase to alteration of the shards. Unfortunately, this suggestion cannot be confirmed since it may be equally due to a decrease in the kaolinite-chlorite input.

Table 3.2 Selected X-ray diffractogram peak height ratios in glycolated oriented mount samples from cores P6 and P8. S = smectite, Z = zeolite (clinoptilolite), K + C = kaolinite + chlorite.

Sample	$\frac{S\ 001}{K+C\ 7Å}$	$\frac{Z}{K+C\ 7Å}$	Sample	$\frac{S\ 001}{K+C\ 7Å}$
P8:0-4:	2.49	0.79	P6:0-1:	2.96
P8:5.5-7:	2.59	0.78		
P8:8.5-10:	3.34	0.80		
P8:12-14:	3.80	0.77	P6:18-20:	4.26
P8:16-18:	2.61	0.71		
P8:21-24:	3.50	0.65	P6:35-40:	7.80
P8:28-32:	3.18	0.66		
P8:40-45:	2.67	0.64		
P8:55-60:	3.21	0.58	P6:50-55:	6.38
P8:70-75:	2.91	0.66		
P8:85-90:	2.77	0.64	P6:65-70:	5.00
P8:100-105:	3.32	0.63		
P8:115-120:	3.79	0.65		
P8:120-125:	2.86	0.63	P6:85-90:	4.57
P8:135-140:	3.21	0.70		
P8:150-155:	3.61	0.71	P6:125-130:	3.38
P8:160-165:	3.38	0.71		
P8:170-175:	3.70	0.72		
P8:175-183:	3.71	0.91	P6:145-150:	3.35

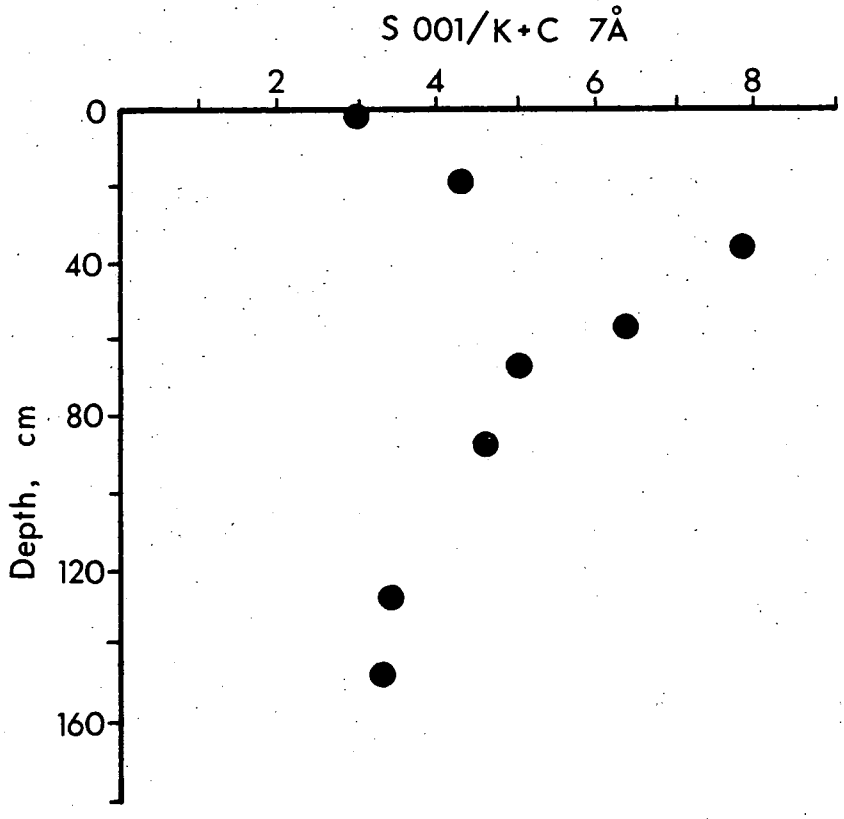

Fig. 3.4 Variation of the smectite peak intensity relative to the kaolinite + chlorite 7Å reflection in core P6.

In order to determine the refractive index of the glass, approximately thirty shards were hand-picked from the ash and mounted on a slide coated with softened gelatin (Nayudu, 1962). Using standard immersion oils, the refractive index was determined to be 1.516-1.520, indicating a silica content in the glass of 65-66% (Williams et al, 1954, p. 28). This high (rhyodacitic) SiO_2 content is consistent with the rhyolitic nature of volcanic debris found in sediments near the Central American coast (Cronan, 1974).

The overall occurrence of minerals in the non-biogenic fraction of core P6 differs from that in P8 only in the apparent absence of clinoptilolite and a dearth of glass shards. Vertical mineral distribution in the core is not uniform, however. A pronounced relative increase in

smectite intensity occurs between 20 and 70 cm depth (Table 3.2; Fig. 3.4). Microscopic examination of the sediment showed a complete lack of pyroclastic material which, coupled with the absence of zeolite reflections on diffractograms, indicates a source for the smectite increase other than *in situ* alteration. Chemical evidence presented in the following chapter assists in resolving the smectite distribution.

CHAPTER FOUR

MAJOR ELEMENT CHEMISTRY

4.1 Introduction

The distribution of major elements in marine sediments is controlled by the relative proportions of terrigenous minerals, biologic detritus, and authigenic and hydrogenous phases. In this chapter variations of and within these four components in Panama Basin sediments will be investigated with the objective of outlining some of the processes governing the incorporation of major elements into hemipelagic sediments.

It is intended initially to describe the areal and vertical distribution of elements associated mainly with biogenous materials. The vertical distribution will be used to establish a stratigraphic framework that will facilitate correlation of sediment horizons over a wide area. This framework will place certain constraints on the description and interpretation of the distribution of some of the remaining elements.

The confusion inherent in describing variations of an element in a multi-component sediment will be reduced in this study by the frequent application of inter-element ratios. Since aluminium in marine sediments is associated practically exclusively with terrigenous minerals, it can be used as an index of the content of detrital aluminosilicates present. The proportions of an element known to occur in terrigenous and biogenous phases, for example, can thus be resolved by choosing an element/Al ratio typical of aluminosilicates; any excess of the element may then be assigned to the non-lithogenous fractions. Additionally, variations in element/Al ratios can illustrate relative mineralogical changes within a suite of sediments, free of sympathetic correlations produced by biogenic dilution of detrital or hydrogenous components.

In order to properly clarify element distributions, allowance must be made for the diluting effects of residual sea salt. In this thesis, therefore, all element analyses are considered on a salt-free basis and

in some instances, both a salt- and carbonate-free basis. Equations used for dilution corrections are presented in Appendix B.

Major element concentrations were determined on fused glass discs by X-ray fluorescence spectrometry using a Philips PW 1450 automatic spectrometer. Organic carbon was analyzed by dry combustion of $CaCO_3$-free samples in a Leco carbon analyzer. Analytical methods are fully described in Appendix B and all element concentrations and inter-element ratio data are listed in Appendix C.

4.2 Distribution of Si and Ca

Silicon is partitioned between terrigenous and certain biogenous phases in Panama Basin sediments; the surface distribution pattern of both can be readily outlined by use of Si/Al ratios. The biogenic and terrigenous silica contents of each surface sample have been calculated by this method and are listed in Table 4.1.

Four factors controlling opaline silica distribution in the Panama Basin have been outlined previously (Moore et al, 1973). These are: (a) winnowing, which removes opaline material from shallow areas and deposits it in pelagic zones; (b) dilution by terrigenous detritus; (c) primary productivity; and (d) dissolution, which, like winnowing, tends to preferentially remove finer, more delicate grains. In this study the distribution shows moderate correlation with the pattern of primary productivity (Fig. 2.5) in the overlying water column. High opal concentrations ($\sim$55%, salt- and carbonate-free) typify the Galapagos Platform sediments where there is reduced dilution from terrigenous minerals, as shown by the low terrigenous SiO_2 content in that area. Sample P5:0-1.5: differs from sediments west of the Galapagos Archipelago in having a high $SiO_{2\ terrig.}$ content in company with the highest $SiO_{2\ biog.}$ concentration. This may reflect increased input to

Table 4.1 Partitioning of silica between biogenic and terrigenous phases in Panama Basin area surface sediments.

Sample	Si/Al	Wt.% SiO_2, salt- and $CaCO_3$-free	
		Biogenic[1]	Terrigenous
P1:0-2:	14.36	55.2	12.3
P2:0-1:	12.07	55.0	15.3
P5:0-1.5:	7.45	55.8	30.2
Pleiades(PL-2)	5.25	24.8	24.8
P6:0-1:	4.92	23.3	26.8
P7:0-2:	3.98	20.0	39.2
P8:0-2:	3.08	7.5	43.6
P9:0-2:	3.07	7.9	46.9
P10:0-2:	2.63[2]	~0	49.8
P11:0-3:	2.64	~0	48.9
P12:0-1.5:	2.63	~0	50.0
P13:0-2:	3.04	7.7	49.2

[1] The biogenic fraction may include hydrogenous silica. It is well known that hydrothermal basalt leachates are enriched in dissolved silica and, in hydrothermally active areas such as the Galapagos Spreading Centre, some amorphous silica may be precipitated. Unfortunately, it is not possible here to differentiate amorphous silica of biogenic and hydrothermal origins.

[2] Value chosen as the Si/Al ratio of the terrigenous fraction (2.63). Microscopic examination of the sediment in this sample revealed an almost total lack of opaline silica; only a few diatoms were observed. This ratio compares well with that for average argillaceous pelagic sediment (2.7; Chester, 1965) and, as expected, is less than the value of 3.07 for the average pelagic sediment compiled by El Wakeel and Riley (1961) which includes siliceous deposits.

the immediate area of minerals physically weathered from the Galapagos Islands.

Opal is increasingly dominated by terrigenous silica as the continent is approached. The diatom and radiolarian concentrations are very small in the Eastern Basin despite relatively high productivity, especially of diatoms (Moore et al, 1973), in upwelled nearshore waters. The reason for this distribution is simply one of dilution; the sedimentation rate of non-biogenic detritus in the Eastern Basin is very high (Moore et al, 1973; Heath et al, 1974) and obscures the input of biogenic particles.

Calcium is also partitioned between terrigenous and biogenous phases, but unlike Si, the former fraction contributes only a very minor amount to the total Ca concentration. Hence, calcium values, expressed as $CaCO_3$ (Table 4.2), essentially illustrate the distribution of biogenic carbonate in the surface sediments. It is evident that the distribution bears no direct relationship to primary productivity; instead, it may be controlled by the dual processes of dissolution and/or dilution.

Table 4.2 $CaCO_3$ concentrations in Panama Basin surface sediments.

Sample	% $CaCO_3$ (salt-free)[1]	Water depth (m, uncorrected)
P1:0-2:	63.1	3422
P2:0-1:	50.0	3510
P5:0-1.5:	90.5	1540
Pleiades(PL-2)	62.5	2716[2]
P6:0-1:	67.4	2712
P7:0-2:	50.6	3085
P8:0-2:	0.5	4093
P9:0-2:	1.5	3075
P10:0-2:	1.6	4007
P11:0-3:	0.8	3847
P12:0-1.5:	1.6	3491
P13:0-2:	2.1	1803

[1] Values for P1-P7 were calculated from Ca concentrations (see p. 172); P8-P13 concentrations were calculated from the difference between total C and organic C.

[2] Corrected depth.

The calcite compensation depth (CCD) in the central Panama Basin is about 3.4 km (Moore et al, 1973) but it is known that this horizon shoals in nearshore areas (Kennett, 1966). Berger (1970) suggested that the common lack of carbonates in hemipelagic sediments may be partly due to shoaling of the lysocline in the overlying waters. Moore et al (1973) consequently concluded that an increased rate of dissolution in the nearshore area of the Eastern Basin was responsible for the low carbonate concentrations observed along the continental margin. However, since opal, which dissolves at a rate largely independent of depth, is diluted by the large terrigenous input to Eastern Basin sediments, it is probable that $CaCO_3$ is similarly affected. It is therefore likely that both dissolution and, to a lesser extent, dilution are important in reducing the calcite content from high levels on the Galapagos Platform to < 2% in the Eastern Basin (Table 4.2).

The distribution of the silicon content with depth, relative to aluminium, is shown in Fig. 4.1. The Si/Al ratio was plotted in preference to carbonate-free silicon since, in the biogenic sediments, it most clearly defines the relative variation between the lithogenous and non-lithogenous silica-bearing phases. The dominant feature in the western Galapagos Platform area sediments (P1 and P2) is the gradual relative silica increase at depth. In P1 a maximum is reached at about 120 cm; below this depth the ratio decreases rapidly in response to what probably were conditions unfavourable for enhanced deposition of silica at the time of sedimentation. Cores P2 and P6 show similar Si/Al increases with depth. Other data discussed below indicate that the basal Si/Al decrease observed in P1 would have been seen in these two cores had they been longer. Two other features are notable in the profiles of Fig. 4.1. In core P6 there is a sharp Si/Al peak at 40 cm depth, and in P8 the concentration of glass shards in the ash at the

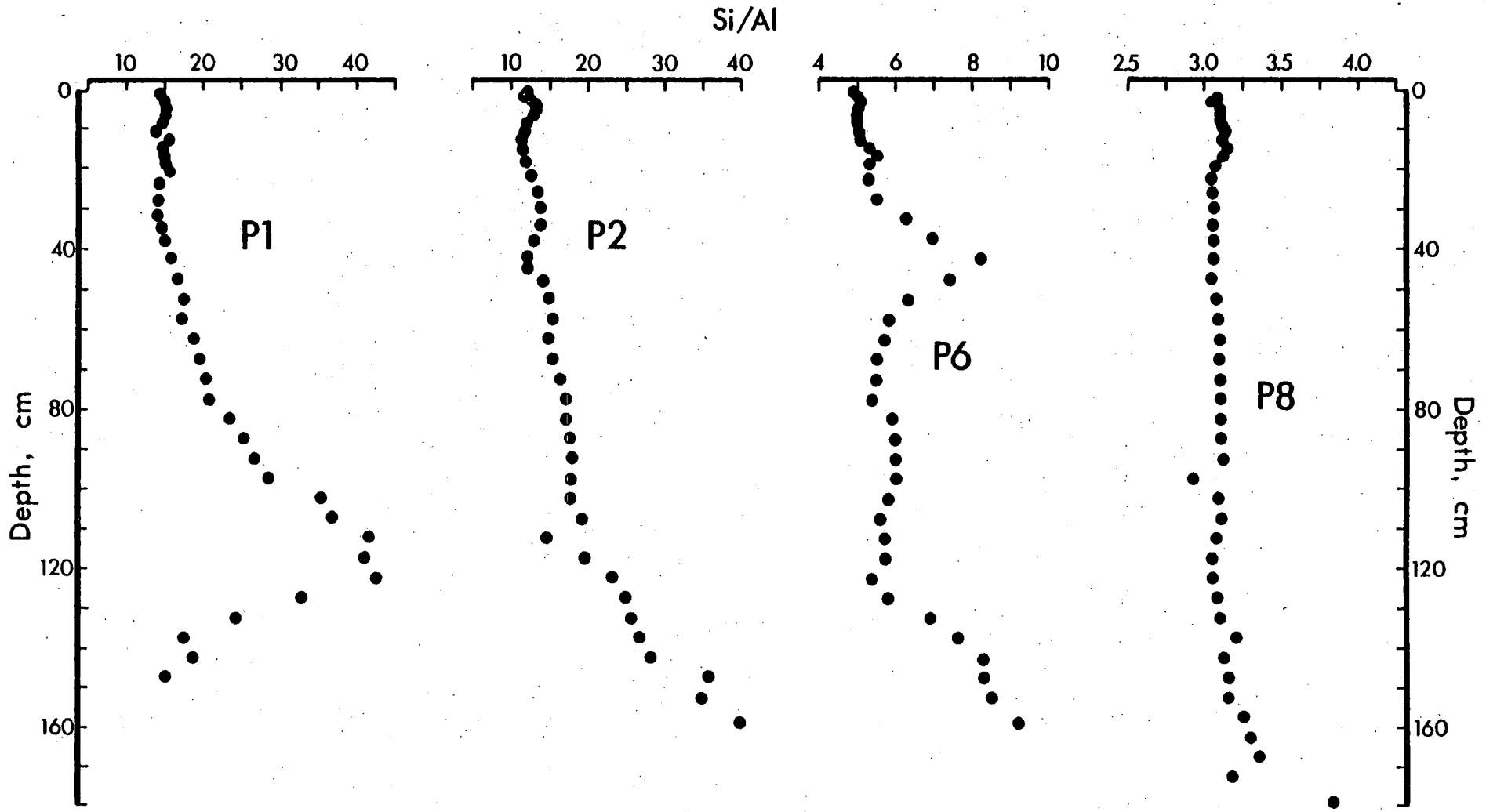

Fig. 4.1 Profiles of the Si/Al ratio in Panama Basin area sediments. Note the different scales for cores P6 and P8.

base of the core, described previously, is clearly reflected in the 20% increase in the Si/Al ratio.

Considerable variation exists in calcium content with depth in the biogenic sediments of cores P1, P2 and P6 (Table C.1, pp. 171 - 190). Since these fluctuations record changes with time in the relative input of the terrigenous and dominant biogenic fractions, they establish a convenient stratigraphy in each core. The utility of this time-based framework in correlating sediments in the equatorial Panama Basin area is discussed in some detail in section 4.4.

4.3 Distribution of organic carbon and phosphorus

The concentrations of organic carbon (C_{org}) and phosphorus in surface sediments are listed in Table 4.3. Salt-free C_{org} levels range from 0.48 to 2.58%, with the highest values occurring in the sediments of the Eastern Basin and the lowest in the Galapagos Platform area.

Although it has been noted that there is a considerable input of riverborne sediment to the Eastern Basin (Heath et al, 1974), it is unlikely that this contributes measurably to the organic carbon content observed there. Several studies have shown that the stable carbon isotopic composition of organic matter in recent marine sediments is identical to that of marine plankton (Degens and Mopper, 1976); the only exceptions are estuarine and some very nearshore shelf sediments. The organic matter in Panama Basin sediments is therefore interpreted as being predominantly of organic origin. This conclusion is supported by $\delta^{13}C$ analyses for organic carbon in core P8 (Table 4.4); the values lie within the range typical for organic carbon in open marine sediments (-19 to -22 per mil, Degens, 1969).

The occurrence of high C_{org} concentrations in the Eastern Basin sediments is not simply a reflection of higher productivity but rather

Table 4.3 Salt-free organic carbon and phosphorus concentrations in Panama Basin surface sediments.

Sample	% C_{org}	% P_{total} [1]	% P_{org} [2]	% $P_{detrital}$ [3]	% $P_{skeletal}$ [4]
P1:0-2:	0.59	0.047	0.007	0.005	0.035
P2:0-1:	0.71	0.062	0.009	0.008	0.045
P5:0-1.5:	0.56	0.035	0.007	0.003	0.025
Pleiades(PL-2)	0.50	0.061	0.006	0.010	0.045
P6:0-1:	0.78	0.060	0.010	0.009	0.041
P7:0-2:	0.74	0.067	0.007	0.021	0.039
P8:0-2:	2.58	0.074	0.031	0.047	-0.004 [5]
P9:0-2:	1.87	0.063	0.023	0.050	-0.010
P10:0-2:	1.87	0.095	0.023	0.053	0.020
P11:0-3:	2.06	0.082	0.025	0.052	0.005
P12:0-1.5:	2.14	0.080	0.026	0.053	0.001
P13:0-2:	2.11	0.099	0.026	0.052	0.021

[1] From Table C.1 (Appendix C).

[2] Based on organic carbon concentrations assuming a C:P molar ratio of 212 (wt. ratio = 82). Justification for such a value is found in Chapter Seven.

[3] Based on aluminium concentrations (Table 6.1) assuming a P:Al ratio in the terrigenous fraction of 0.006. This value is typical of deeper sediments in core P8 (Table C.1) where organic P may have been largely oxidized, and matches that of average argillaceous pelagic sediment (Chester, 1965).

[4] $\% P_{skeletal} = \% P_{total} - (\% P_{org} + \% P_{detrital})$

[5] Negative values indicate the considerable uncertainty in these calculations. Choice of the P:Al ratio and C:P molar ratio is defined by ranges only; they are therefore somewhat arbitrary.

of the high degree of preservation of organic detritus in rapidly accumulating sediments where organic compounds are only briefly exposed to free oxygen. Fig. 2.5 suggests that sediments underlying the productive Galapagos Platform area should be subject to an organic carbon input flux roughly equivalent to that for the Eastern Basin. The observed disparity in C_{org} concentrations between the two areas is probably a function of differing total sedimentation rates; a higher loss of organic carbon by oxidation near the sediment-water interface would occur in the more slowly-accumulating Galapagos area sediments. In consequence these sediments have a thicker oxidized layer as noted in the core descriptions (Appendix A) and as observed by Lynn and Bonatti (1965).

Vertical distribution patterns for organic carbon are displayed in Fig. 4.2. The three carbonate-rich cores P1, P2 and P6 have strikingly similar C_{org} profiles characterized by an initial decrease in the upper 20 cm followed by a peak between 30 and 70 cm depth which reaches a maximum of 2.5% C_{org} in P6. In contrast, core P8 has a surface concentration of 2.58% which decreases fairly regularly to less than half that value at 180 cm depth.

The general decrease in C_{org} concentrations observed in the upper horizons of the carbonate cores and throughout P8 are probably due to bacterial metabolization - this claim is supported by pore water chemistry, discussed in Chapter Seven. The carbon peaks present at depth in the Galapagos Platform (P1 and P2) and Spreading Centre (P6) cores may represent periods of greatly enhanced productivity in the eastern equatorial Pacific (see Arrhenius, 1952). Productivity increases will be reflected in the sediment record by higher organic carbon concentrations providing the increase is sufficiently large to survive subsequent organic diagenesis.

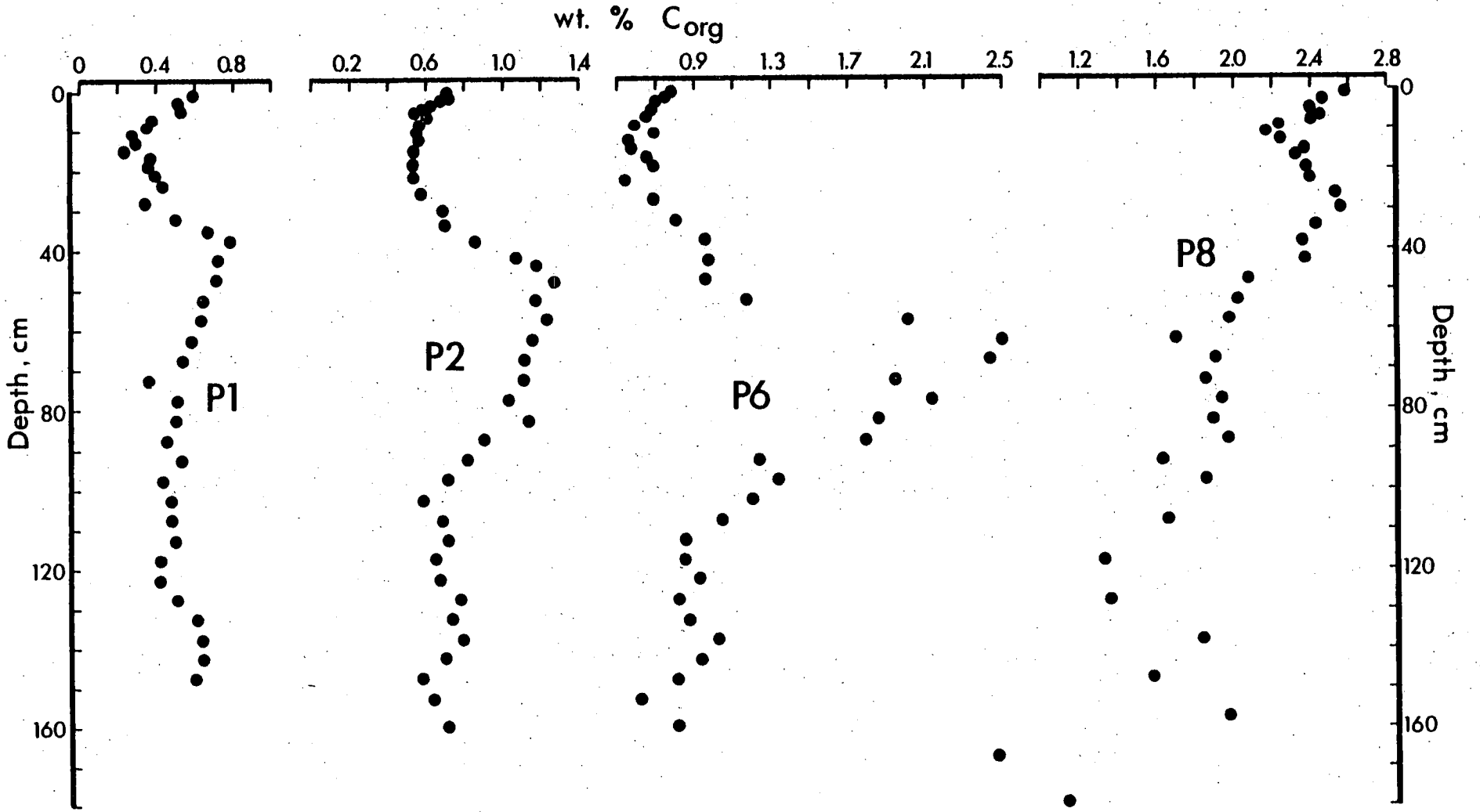

Fig. 4.2 Organic carbon profiles in Panama Basin area sediments. The data are on a salt-free basis.

Since a number of workers have noted a positive association between the distribution of biogenic carbonate and phosphorus in marine sediments (e.g. El Wakeel and Riley, 1961), it is incorrect to consider phosphorus distribution on a carbonate-free basis; it is discussed here on a salt-free level only.

Phosphorus occurs in marine sediments principally in four phases: inorganic skeletal debris, detrital apatite, organic matter, and a disordered ferriphosphate. The latter phase, which often occurs in dispersed iron oxides and in oxide coatings on mineral grains, is present in significant quantities in many metalliferous sediments (Berner, 1973; Froelich et al, 1977) but it is thought to be quantitatively unimportant in Panama Basin sediments. Limited support for this contention is given by the plot of "excess" Fe versus "non-lithogenous" P (Fig. 4.3) which demonstrates an absence of any significant iron-phosphorus association in surface sediments.

The distribution of phosphorus in surface sediments can be clarified by estimating the relative contributions of the element from each of detrital, skeletal and organic phases, as in Table 4.3. These calculations show that detrital apatite is the main P-bearing component in the largely terrigenous sediments of the Eastern Basin and indicate that skeletal phosphorus predominates in the Western Basin and Galapagos area sediments. The pattern of primary productivity in the Panama Basin suggests that the flux of skeletal apatite to the sediments (a function of fish distribution, which is related to primary productivity) should be very roughly similar in the Eastern Basin and in the Galapagos area. The reason for the lower $P_{skeletal}$ concentrations in the former must, like opal, be extensive dilution by terrigenous detritus. In contrast, Eastern Basin sediments have a higher organic phosphorus content since rapid sedimentation there encourages preservation of organic matter

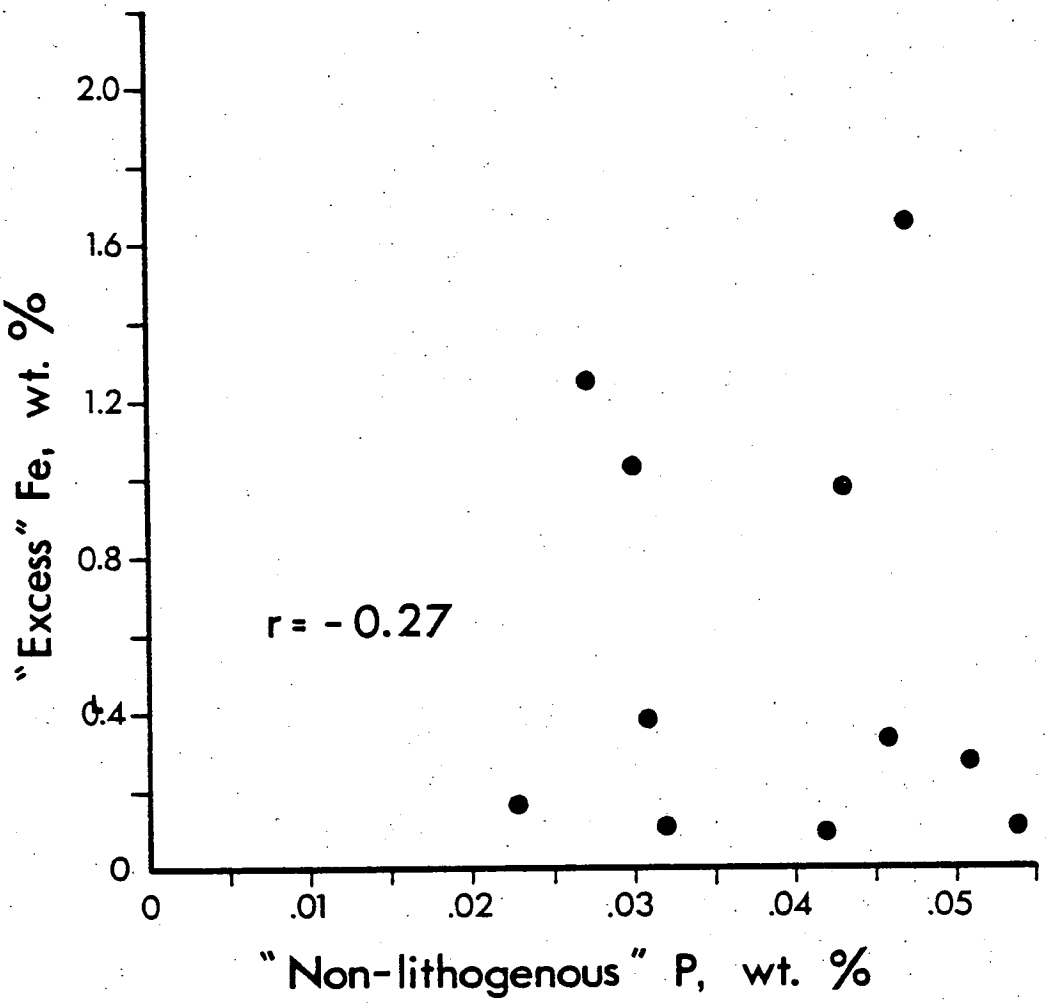

Fig. 4.3 "Excess" Fe versus "Non-lithogenous" P in Panama Basin surface sediments, calculated by assuming Fe/Al (lithogenous) = 0.66 and P/Al (lithogenous) = 0.006.

(p. 33). The vertical distribution of salt-free phosphorus is shown in Fig. 4.4. In each core, total phosphorus concentrations decrease with depth. In the carbonate-rich sediments, where skeletal apatite is the predominant P-bearing phase, the phosphorus decrease is 150-250 ppm over the length of each core. Below 120 cm in P1, a slight reversal in the trend of lower P concentration with depth is evident. The progressive increase in salt-free aluminium in this zone (Table C.1, p. 175) reflects a greater relative lithogenous input which, assuming a P/Al ratio of 0.006 (Table 4.3), contributes sufficient apatite to entirely account for the phosphorus increase. In core P8, where skeletal apatite is quantitatively unimportant relative to organically-bound P, the phosphorus concentration decreases in the top metre by roughly 250 ppm. An increase in concentration of the element near the base of the core is likely due to lithogenous apatite associated with the pyroclastic debris occurring there.

Thermodynamic considerations and nutrient regeneration calculations (Chapter Seven) suggest that skeletal apatite may be dissolving in the sediments and it seems likely that this dissolution, coupled with the diffusive loss of phosphate to overlying sea water, might well account for the observed phosphate decreases in cores P1, P2 and P6. However, a different mechanism is required to explain the phosphorus decrease in the terrigenous sediments of core P8.

It is well known that organic phosphorus is a very labile element in organic material undergoing bacterial oxidation (see section 7.3). In core P8, the surface sediments contain an estimated 0.031 % P_{org} and about 0.047 % of detrital P (Table 4.3). The total phosphorus concentration decreases exponentially with depth to about 80 cm where it reaches a constant level of 0.045-0.048 %, which is in good agreement with the detrital P content in the core (Fig. 4.4). The constancy

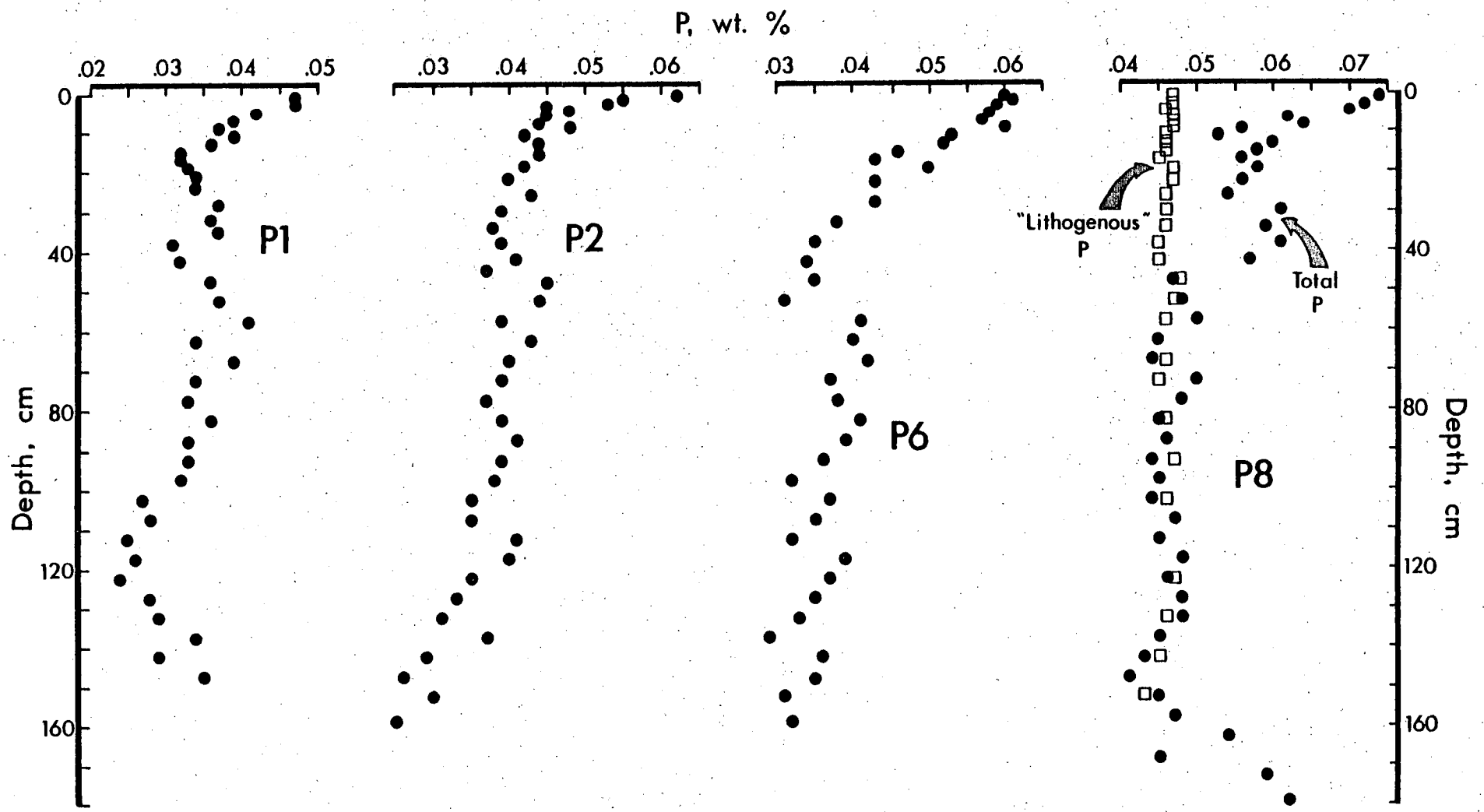

Fig. 4.4 Phosphorus distributions in Panama Basin area cores, on a salt-free basis. The "lithogenous" P content in P8 is calculated assuming P/Al (lithogenous) = 0.006.

between 80 and 140 cm depth suggests that most of the organic phosphorus has been metabolized to dissolved phosphate in the period represented by the upper 80 cm of sediment accumulation. Therefore, it would appear that diagenesis of organic matter can account for the observed decrease in the total phosphorus content of the core.

4.4 Carbonate and organic carbon stratigraphy

The distribution of a cyclical series of high calcium carbonate concentrations with depth in many equatorial Pacific sediments has been documented by a number of workers (e.g. Arrhenius, 1952; Hays et al, 1969; Broecker, 1971; Shackleton and Opdyke, 1973; Thompson and Saito, 1974). It has been shown that the stratigraphy defined by the carbonate peaks offers a means of correlating sediment horizons over a wide area in the Pacific, and it can be applied successfully to this work.

The distribution of calcium carbonate in cores P1, P2 and P6 is shown in Fig. 4.5 along with the top 2 m of a core collected from a site about 300 km southwest of the Galapagos Islands, described by Arrhenius (1952). The profiles of the four cores are sufficiently similar to permit reasonable correlation.

A greater degree of confidence in the correlations is provided by the organic carbon distribution. Prior to this research, the only investigation of the vertical distribution of organic carbon in eastern equatorial Pacific sediments was that of Arrhenius (1952) who found prominent bands of high C_{org} content at depth in several cores. Similar increases in organic carbon concentrations occur in all three carbonate-rich cores examined here. The carbon peaks correspond directly with the high concentration in the top metre of Galapagos-area core SW 39 (Arrhenius, 1963), as shown in Fig. 4.6. The correlations provided by the carbon peaks are stratigraphically consistent with those

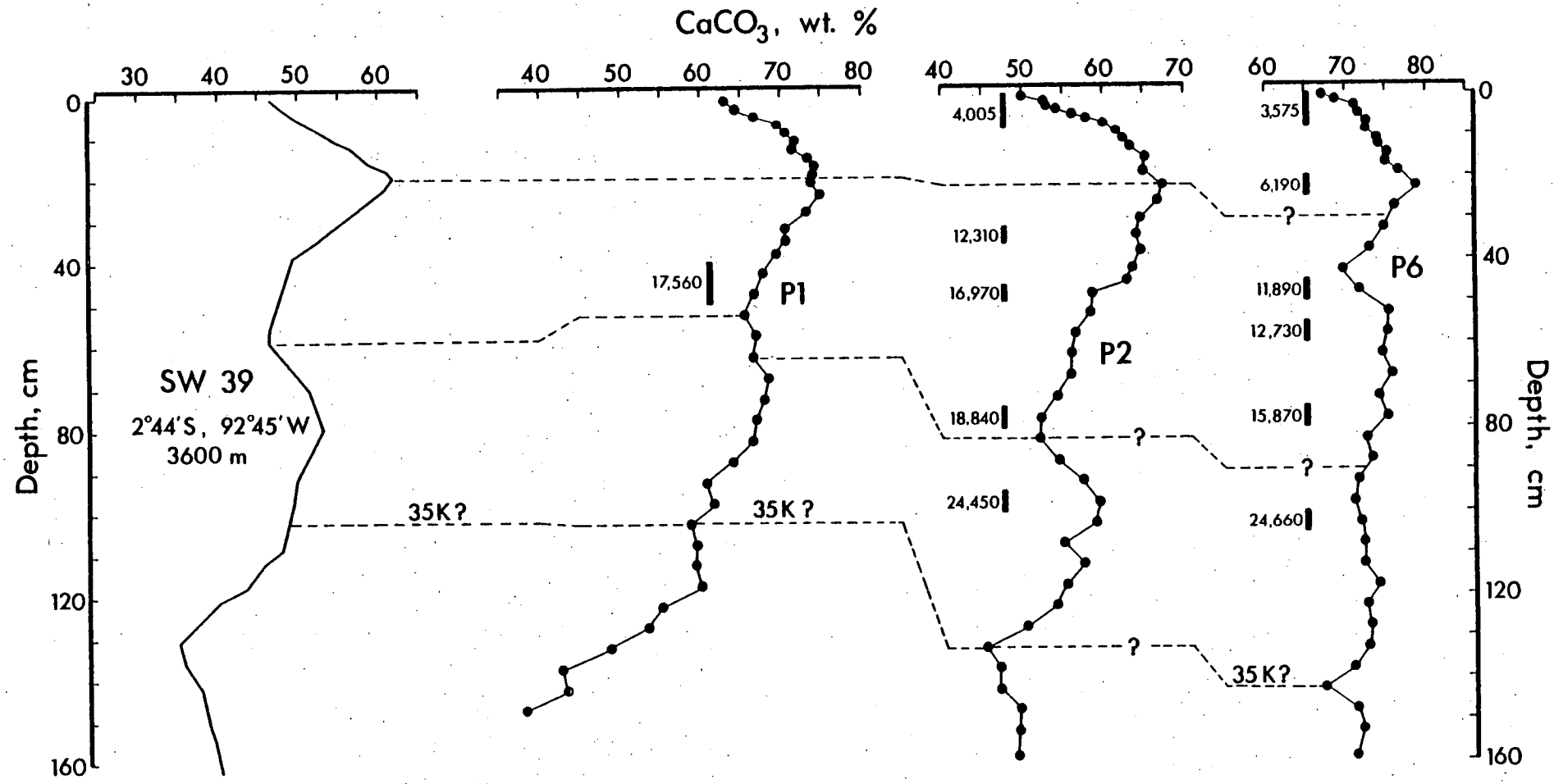

Fig.4.5 Calcium carbonate distributions in Panama Basin area cores, with radiocarbon dates from Table 4.4. The profile for core SW 39 is after Arrhenius (1952) and the 35,000 year (35K) horizon at 102 cm depth in that core is abstracted from Luz and Shackleton (1975). Correlations are aided by the organic carbon distributions of Fig. 4.6 and by the radiocarbon dates.

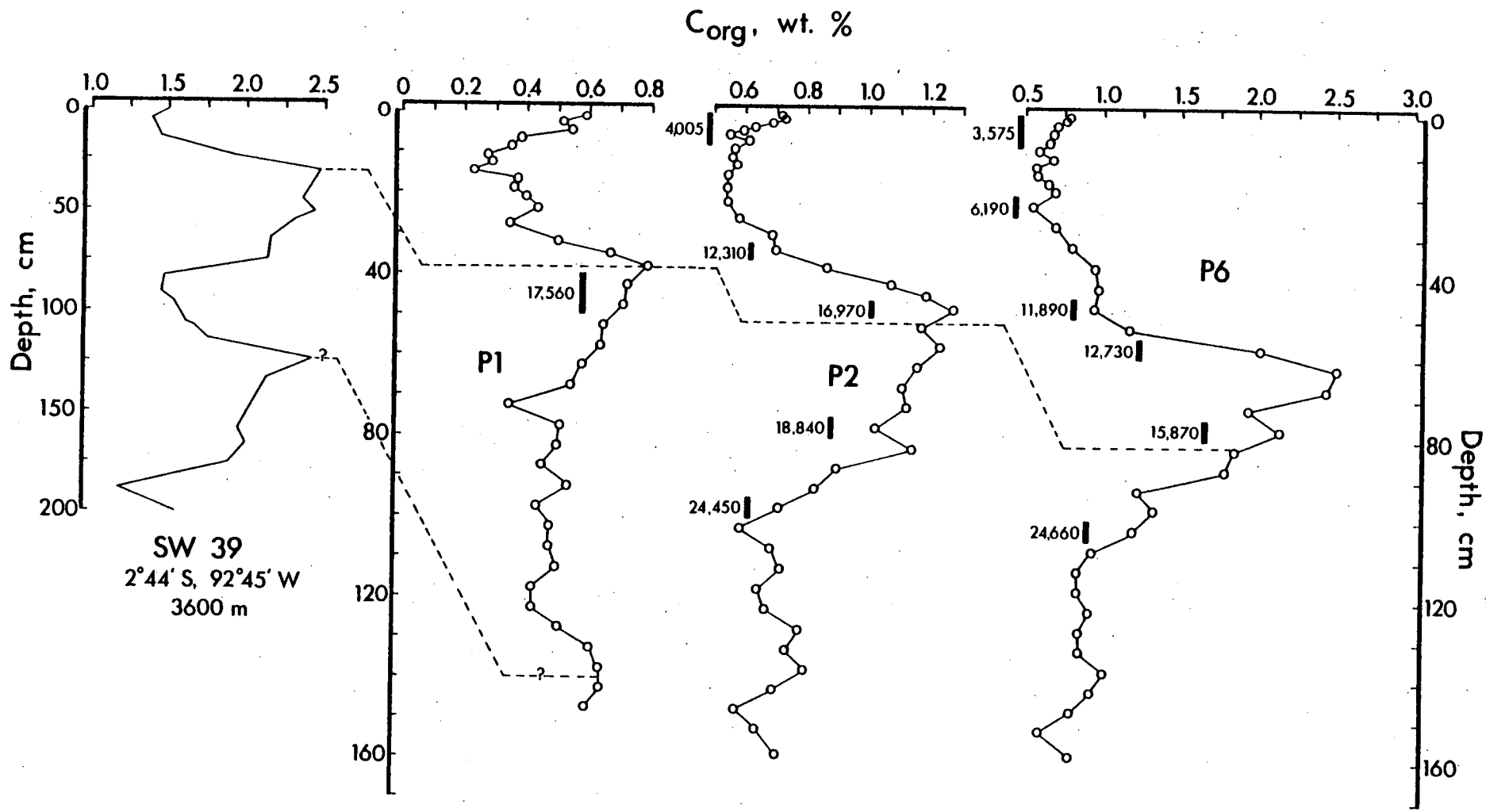

Fig. 4.6 Correlations between organic carbon peaks in Panama Basin area cores. The carbon profile for core SW 39 is after Arrhenius (1963). The radiocarbon dates are listed in Table 4.4

indicated by the $CaCO_3$ profiles. Processes controlling the distributions of both components are discussed in Chapter Eight.

Age dating of cores and sedimentation rates

In order to determine sedimentation rates in the cores studied here, twelve carbonate-rich samples were radiometrically dated using ^{14}C. The results are listed in Table 4.4 and have been plotted in Figs. 4.5 and 4.6. The large number of dates obtained establishes reasonably precise time-control on the observed carbon-carbonate stratigraphy. An additional, tentative date (35,000 yr) has been abstracted from the literature by correlating core SW 39 with core V21-33 described by Luz and Shackleton (1975). The latter core has good time-control, afforded by detailed oxygen isotopic stratigraphy matched to the oxygen isotope time scale of Broecker and van Donk (1970).

Using the radiometric dates, average net sedimentation rates can be estimated. For cores P1, P2 and P6 the average Holocene (roughly the last 11,000 yr) rates are 2.6, 2.8 and 4.0 cm $10^{-3}yr^{-1}$, respectively.

A large number of Holocene sedimentation rates have been calculated for Panama Basin area cores, mainly by Swift (1977). These are listed in Table 4.5 and plotted in Fig. 4.7 along with the values determined here. The rates are typically one to two orders of magnitude higher than those for pelagic sediments and are characteristically variable over short distances.

A relatively high sedimentation rate for core P8 has been implied previously by the postulated dilution of biogenic constituents in the core. The radiocarbon results, however, indicate the presence of "old" carbon, both organic and inorganic, in the sediments, suggesting a low sedimentation rate. In order to resolve the apparent paradox presented by these contrasting lines of evidence, several points require consideration: (a) severe analytical difficulties were encountered in

Table 4.4 Radiocarbon ages of Panama Basin sediment samples, calculated using a ^{14}C half-life of 5730 years.

Core	Sample Depth (cm)		^{14}C age $\pm$ 1 σ (years)	$\delta^{13}C$ (per mil, PDB)
P1	40-50		17560 $\pm$ 225	0.4
P2	0-8		4005 $\pm$ 115	0
	32-36		12310 $\pm$ 180	-1.0
	46-50		16970 $\pm$ 280	-0.5
	75-80		18840 $\pm$ 460	-0.4
	95-100		24450 $\pm$ 580	-0.2
P6	0-8		3575 $\pm$ 95	1.2
	20-25*		6190 $\pm$ 210	-
	45-50		11890 $\pm$ 155	0.8
	55-60*		12730 $\pm$ 210	-
	75-80		15870 $\pm$ 190	1.1
	100-105		24660 $\pm$ 530	1.7
P8	40-60	Carbonate	21170 $^{+2310}_{-1790}$	0
		Organic	18540 $\pm$ 230	-21.1
	65-80*		40,000 ?	-
	95-115	Carbonate	20760?	0
		Organic	35,900 ?	-21.7

* Asterisked samples were dated at the Physical Research Laboratory, Ahmedabad, courtesy of Dr. B. L. K. Somayajulu.
All other samples were dated by the Radiocarbon Laboratory, Scottish Universities Research and Reactor Centre, East Kilbride.

Table 4.5 Published and calculated Holocene sedimentation rates in the eastern equatorial Pacific.

Core	Location Lat.	Long.(°W)	Sedimentation Rate (cm $10^{-3}yr^{-1}$)	Source
V15-32	3°15'S	82°30'	8.6	Swift (1977)
V17-43	1°52'N	82°37'	3.4	"
V17-44	3°34'S	85°07'	5.5	"
V19-25	2°28'N	81°42'	7.0	"
V19-27	0°28'S	82°04'	6.7	"
V19-28	2°22'S	84°39'	6.2	"
V19-29	3°35'S	83°56'	7.3	"
V19-30	3°23'S	83°31'	10.0	"
V21-26	4°36'N	82°44'	12.2	"
V21-212	2°50'N	85°08'	3.4	"
V21-214	3°50'N	80°38'	8.0	"
RC8-102	1°25'S	86°51'	7.2	"
RC8-103	1°16'N	85°10'	13	"
RC10-52	3°52'N	83°56'	30	"
RC13-142	4°28'N	82°26'	28.3	"
RIS 29	2°18'N	89°27'	7.7	"
RIS 30	1°13'N	88°31'	11.5	"
RIS 32	0°09'S	85°59'	29	"
Y69-71	0°06'N	86°29'	9.1	Dinkelman (1974)
Y69-72	1°01'N	87°27'	9.6	Swift (1977)
Y69-73	1°27'N	87°56'	8.9	Dinkelman (1974)
Y69-74	2°02'N	88°19'	8.8	Swift (1977)
Y69-105	0°09'N	84°03'	8.8	Pisias (1976)
Y69-106	2°59'N	86°33'	2.5	"
Y71-3-10	1°13'S	82°17'	17	Swift (1977)
Y71-3-11	0°17'S	83°16'	8.7	"
Y71-3-24	1°06'S	85°01'	39	"
Y71-3-30	0°21'S	85°29'	27.5	"
P1	1°18'S	94°37'	2.6	This study
P2	1°25'S	92°59'	2.8	"
P6	0°52'N	86°08'	4.0	"

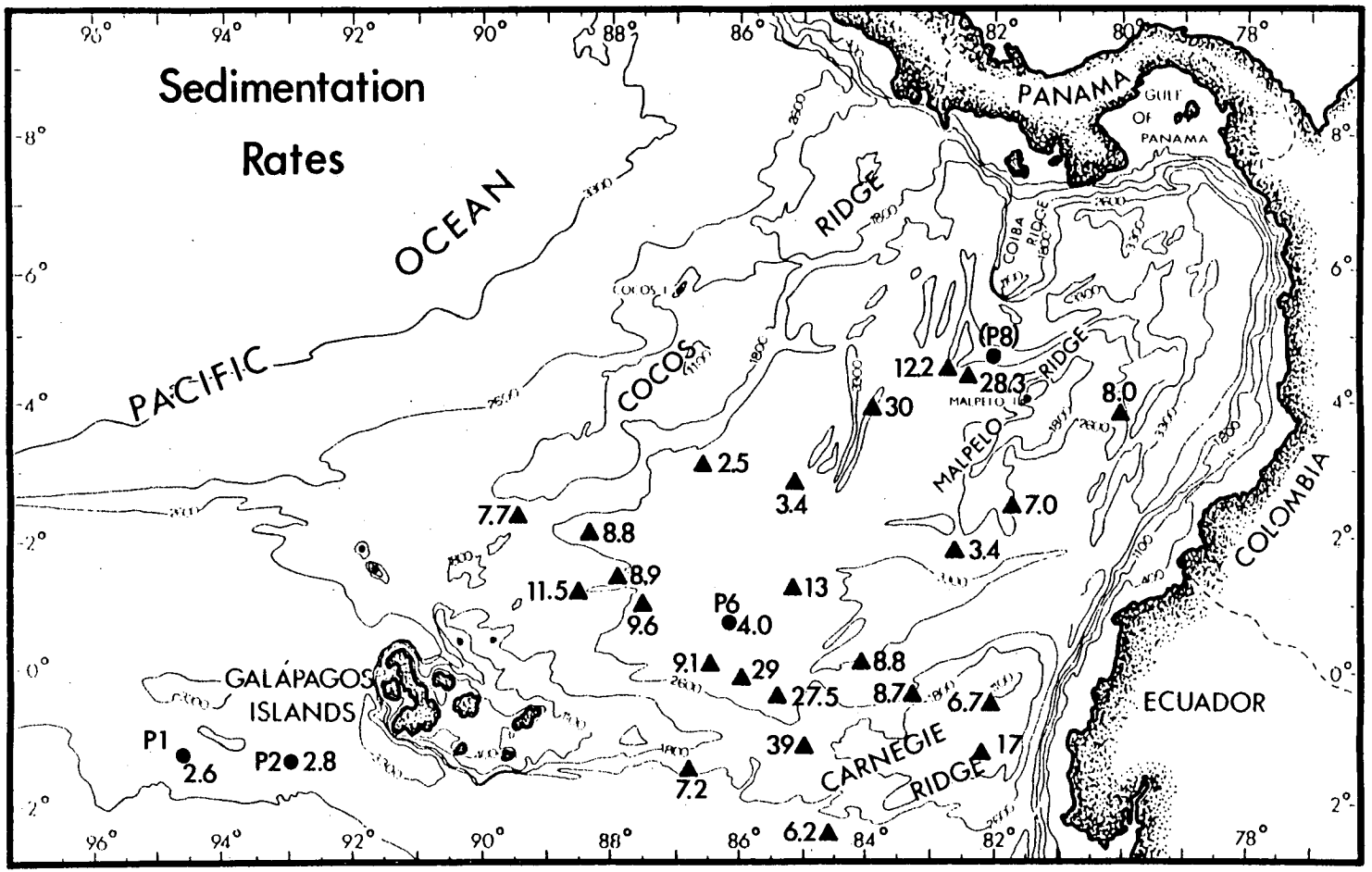

Fig. 4.7 Published and calculated net sedimentation rates for Holocene Panama Basin sediments, in cm $10^{-3}yr^{-1}$.

attempting to date the $CaCO_3$-poor P8 sediments (D.D. Harkness, pers. comm.) and the results should be viewed with caution; (b) core P8 lies in the Coiba Gap below the Coiba and Malpelo Ridges and this area has a very high measured bulk accumulation rate (Swift, 1977), attributable to both rapid sedimentation of terrigenous clays and an influx of sediment eroded from proximal ridge and slope deposits; (c) both the low opal and the relatively high organic carbon contents in P8 imply a high sedimentation rate in the core, which one would expect from its location; and (d) the presence of clinoptilolite throughout the core (Chapter Three) indicates some input of reworked Pleistocene sediment which must contain "old", relatively refractory carbon. The net conclusion is that the inconsistent radiocarbon dates probably result from inclusion of reworked "old" organic and inorganic carbon in the sediments. All evidence other than the ^{14}C dates suggests a relatively high sedimentation rate for the core.

4.5 Distribution of lithogenous elements

Within the lithogenous fraction, variations in the concentrations of elements are best illustrated by element/Al ratios since these are independent of dilution by biogenic components. Titanium, potassium, magnesium, and iron distributions will be described in this section although, as will become evident, the term "lithogenous" does not strictly apply to all.[1]

---

[1] Sodium is omitted from this discussion since corrections for salt sodium based on Cl analyses can introduce substantial error in biogenic sediments where the combined error in analyses of high Na and Cl concentration is transmitted to a small terrigenous sodium content. As a result, corrected sodium concentrations in such sediments lack sufficient precision to be of use in explaining areal and vertical variation.

Titanium

Titanium in sediments occurs principally in the oxides ilmenite, rutile, and anatase (Rankama and Sahama, 1950) and is found to a lesser degree replacing Al in clay mineral lattices (Correns, 1954). Rutile and ilmenite are highly resistant to weathering and are therefore the most common detrital minerals, especially in the heavy mineral fraction in sediments (Goldschmidt, 1954); anatase may be authigenic (Arrhenius, 1963; Deer et al, 1966) or of detrital origin, following formation in the Ti-enriched residues of chemically-weathered basalts (Blatt et al, 1972). The principal occurrence of the element in the coarse-grained heavy mineral fraction renders the Ti/Al ratio useful as a sensitive indicator of the relative concentration of heavy terrigenous minerals.

In the Panama Basin, surface sediments exhibit a range of Ti/Al ratios (Table 4.6) which clearly outline two titanium sources. Ratios increase landward from the centre of the Basin, from 0.043 at core P7 to 0.071 at P13, indicating an increasing concentration of heavy minerals as their continental source is approached. The high ratio in P13:0-2: is consistent with the microscopically-observed concentration in that sample (noted in Chapter Three) of coarse opaque heavy minerals.

Table 4.6 Ti/Al and K/Al ratios in Panama Basin surface sediments.

Sample	Ti/Al	K/Al
P1:0-2:	0.058	0.235
P2:0-1:	0.066	0.195
P5:0-1.5:	0.072	0.157
Pleiades (PL-2)	0.044	0.206
P6:0-1:	0.048	0.200
P7:0-2:	0.043	0.172
P8:0-2:	0.059	0.137
P9:0-2:	0.057	0.140
P10:0-2:	0.060	0.127
P11:0-3:	0.062	0.121
P12:0-1.5:	0.064	0.123
P13:0-2:	0.071	0.126

Similar high Ti/Al ratios occur near the Galapagos Archipelago, 0.066 for P2:0-1: and 0.072 for P5:0-1.5:. McBirney and Williams (1969) report that the tholeiitic and alkali basalts which form the islands frequently contain substantial titaniferous augite, ilmenite and titaniferous magnetite; Ti concentrations in those rocks range up to 2.52% Ti. Since the Galapagos climate is extremely arid, one would expect retardation of chemical weathering of the basalts with a consequent lack of laterite development. Hence, the titanium enrichment (relative to Al) in proximal sediments must be due to input of primary detrital Ti-bearing minerals from erosion of the Galapagos Islands, rather than secondary minerals such as anatase. Dispersion of the detrital minerals is rather limited; to the northeast samples PL-2 and P6:0-1: have low Ti/Al ratios (0.044 and 0.048 respectively) and to the west there is an obvious Ti/Al decrease with increasing distance from the islands. The pattern suggests that, at the present time, transport of most of the locally-derived heavy detritus is limited to a radius of less than a few hundred kilometres from the archipelago.

Profiles of the vertical distribution of the Ti/Al ratio are displayed in Fig. 4.8. Variation with depth is essentially absent in core P8 but is significant in the biogenic cores where several features are noteworthy. The upper 15-20 cm of P1, P2 and P6, representing deposition over the last 10,000 years or so, have generally low Ti/Al ratios; average ratios are higher in the 10,000-40,000 year interval in the sediments, especially at about the 40-50 cm ($\sim$15,000 yr) level in P2. Below 120 cm ($\sim$ 40,000 yr) in P1, a progressive decrease in the ratio occurs. Since neither titanium nor aluminium in these sediments are subject to diagenetic remobilization processes, the fluctuations in the ratios must represent changes with time in the depositional regime in the eastern equatorial Pacific. A possible mechanism to

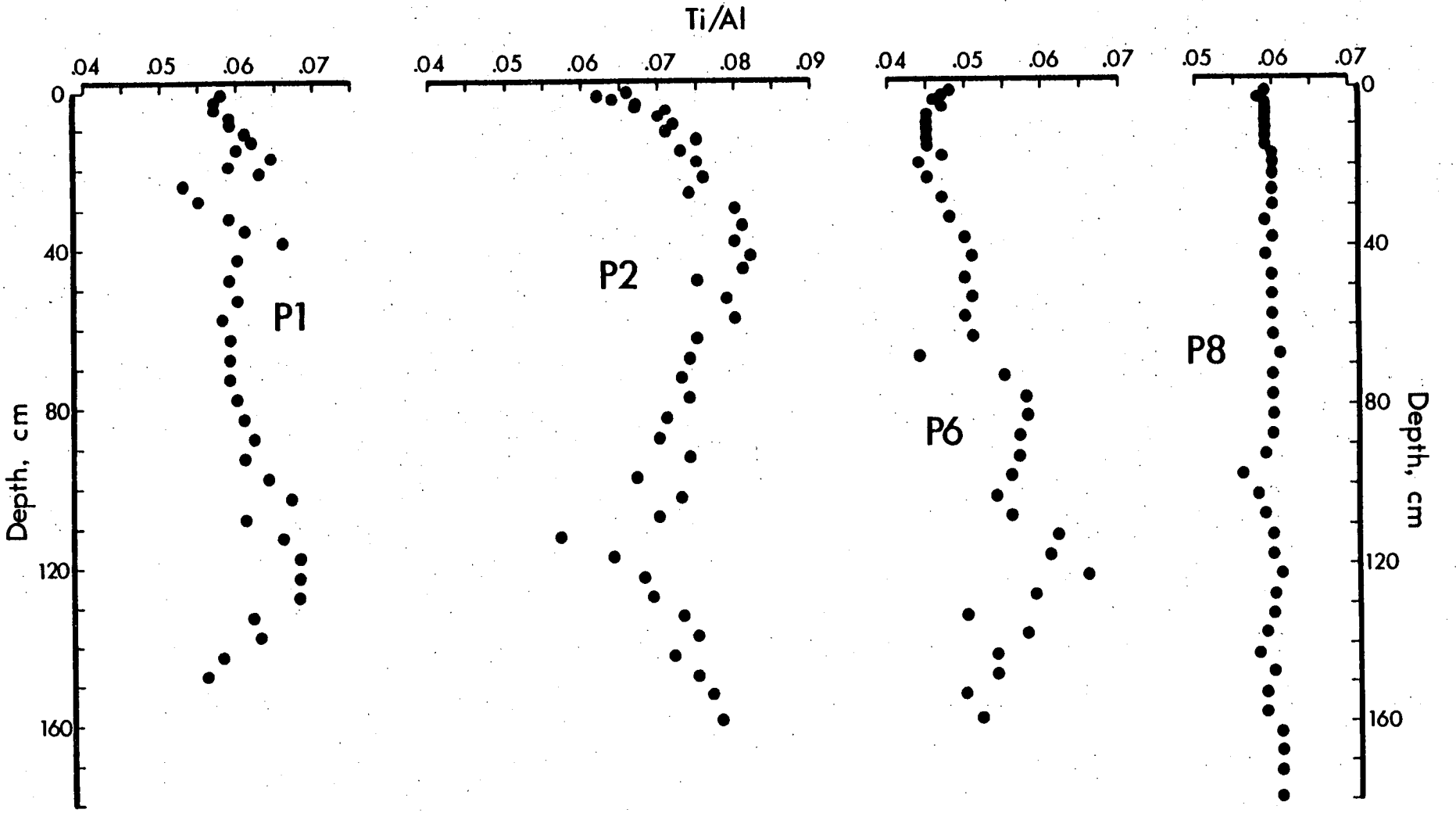

Fig. 4.8 Distribution of the Ti/Al ratio with depth in Panama Basin sediments.

account for such changes over the 50,000 year interval spanned by the cores is discussed in Chapter Eight.

Potassium

The K/Al ratio in surface sediments (Table 4.6) increases seaward from ~0.13 near Panama (P13:0-2:) to more than 0.20 west of the Galapagos Islands (P1:0-2:). Since illite is the principal host for potassium in these sediments and smectite is by far the dominant Al-bearing mineral (Chapter Three), the trend of the K/Al ratio suggests that the illite content increases in a seaward direction relative to smectite. Lower K/Al values near the Galapagos Archipelago (~0.17 for P2:0-1: and 0.16 for P5:0-1.5:) probably reflect local input of Al-bearing, K-depleted detrital minerals (such as plagioclase and undefined ferromagnesian minerals) from the adjacent islands. There may also be authigenic potassium-free smectite forming from basaltic debris in these sediments (Heath et al, 1974).

Variations in K/Al at depth (Fig. 4.9) generally indicate the relative proportions of smectite and illite in the lithogenous fraction of the sediments. In this regard, the decrease in K/Al ratios in the upper horizons of the cores imply that the Basin area as a whole has been receiving less illite relative to smectite in the recent past. However, two features digress from this generalization. Firstly, the relative potassium increase at the base of core P8 is more probably due to the K-feldspar content in the pyroclastic material than to an illite increase. Secondly, the sharp K/Al increase centred at 40 cm depth in core P6 cannot simply reflect illite/smectite ratios since smectite (Chapter Three), magnesium, and especially iron are also enriched in this zone.

Potassium enrichments in iron-rich oceanic sediments have not been previously discussed, probably due to a common lack of K analyses in

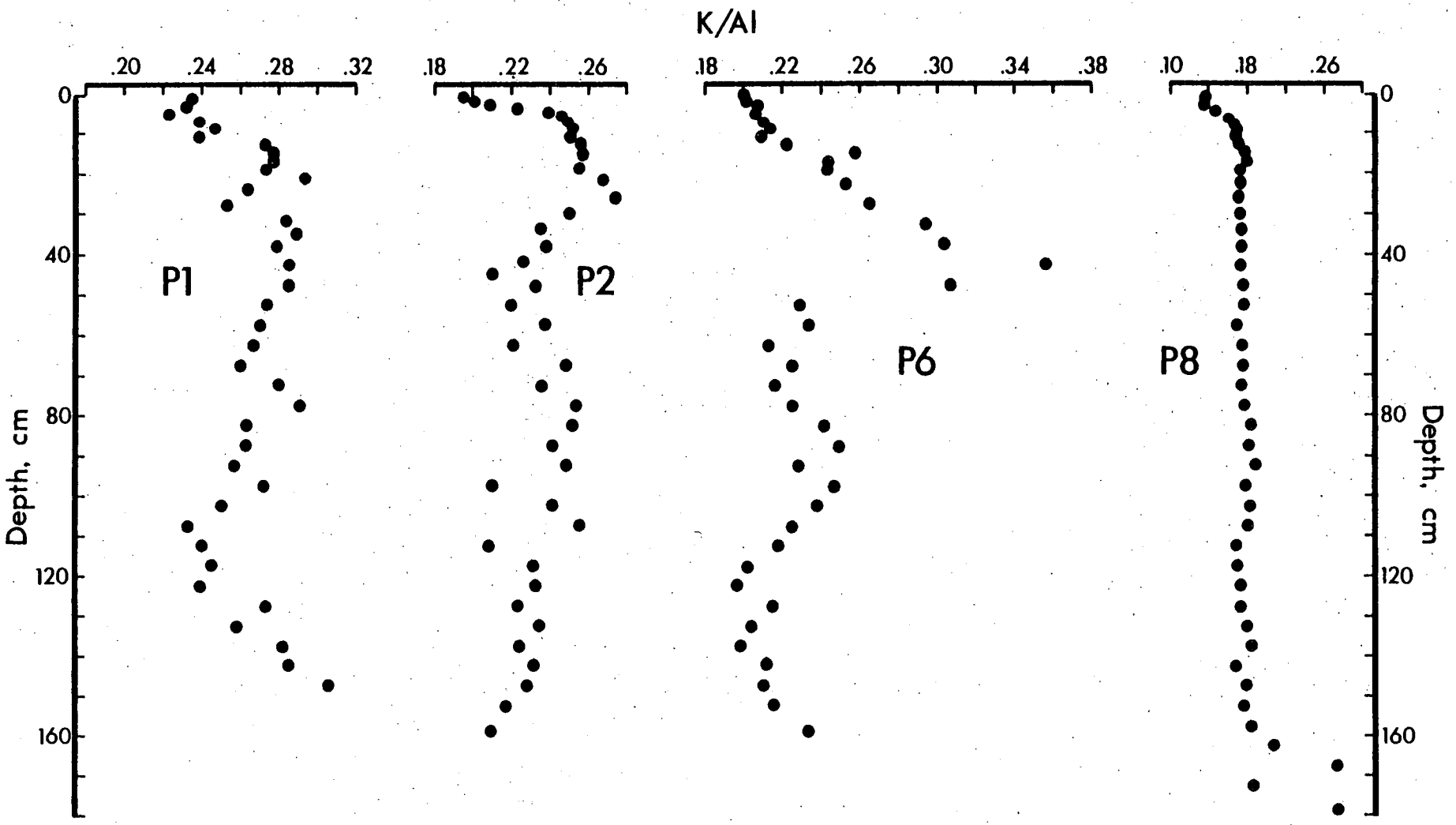

Fig. 4.9 Profiles of the salt-free K/Al ratio in Panama Basin area cores.

such material. However, data available in the reports of some workers suggest that enrichment does occur. The analyses of Bischoff and Rosenbauer (1977) of a mixed terrigenous-metalliferous sediment from the DOMES area near the Clarion Fracture zone yield a K/Al ratio of 0.42, uncorrected for salt, whereas nearby non-metalliferous sediments show considerably smaller ratios ($\sim$0.33). Sayles and Bischoff (1973) show in data for Bauer Deep sediments (core 14) salt-free K/Al ratios of 0.44-0.75 while sediments 500 km to the east (core 11) have K/Al values ranging from 0.22-0.30. Potassium, therefore, seems to be clearly enriched in metalliferous sediments although the site(s) in which it resides is open to question. The large radius of the potassium ion (1.33 Å) precludes its substitution for Fe or Mg in mineral lattices but it may be adsorbed from sea water onto interlayer sites in the Fe-smectite (nontronite ?) phase or onto hydrogenous oxides.

Iron and magnesium

Relative to aluminium, iron and magnesium show no systematic variation in Basin surface sediments (Table 4.7). Fe/Al ratios range from 0.68 to 0.88 and Mg/Al from 0.22 to 0.28 (cf. average pelagic clay, Fe/Al = 0.77, Mg/Al = 0.25, Turekian and Wedepohl, 1961).

Table 4.7 Fe/Al and Mg/Al ratios in Panama Basin surface sediments, on a salt-free basis.

Sample	Fe/Al	Mg/Al
P1:0-2:	0.778	0.284
P2:0-1:	0.743	0.265
P5:0-1.5:	0.882	0.255
Pleiades (PL-2)	0.830	0.279
P6:0-1:	0.839	0.277
P7:0-2:	0.756	0.233
P8:0-2:	0.710	0.252
P9:0-2:	0.682	0.216
P10:0-2:	0.769	0.238
P11:0-3:	0.782	0.238
P12:0-1.5:	0.785	0.227
P13:0-2:	0.848	0.252

Plots of Mg versus Al and Fe versus Al (Fig. 4.10) show that in the Galapagos area and central basin sediments, aluminosilicate minerals host all of the magnesium and very nearly all of the iron. The lack of an intercept on the ordinate of the Mg-Al graph indicates significantly that biogenic calcite in these sediments contains essentially no magnesium. In the case of iron, the small intercept ($< 0.1\%$ Fe) suggests that the element occurs to a hardly-significant extent in a non-aluminosilicate component, possibly oxide.

The distributions of both elements covary with depth as illustrated in Figs. 4.11 and 4.12. Cores P1 and P2 have very similar profiles although average ratios are marginally lower in the latter.

Between 20 and 60 cm depth in core P6, well-defined Mg/Al and Fe/Al increases occur, apparently in association with the K/Al and Si/Al increases described earlier. In addition, X-ray diffractometry results (p. 22) show a clear increase in the relative smectite content in this zone. The existence of a very strong association between smectite and iron and magnesium in the core is revealed by the plots of Fe/Al and Mg/Al versus smectite/kaolinite + chlorite 7Å in Fig. 4.13. The correlative enrichments of several elements plus smectite in this horizon may be due to a specific depositional event as discussed in the following section.

Hydrothermal nature of the sediment

Many iron- and manganese-enriched sediments of the Eastern Pacific are considered to be of hydrothermal-volcanic origin (Böstrom and Peterson, 1966; Böstrom and Peterson, 1969; Böstrom et al, 1969; Bender et al, 1971; Sayles and Bischoff, 1973; Dymond et al, 1973; Dymond and Veeh, 1975; and Sayles et al, 1975). The enrichments are generally believed to be produced by selective precipitation from solution of Fe, Si and other elements leached from recently-emplaced basalt by hot,

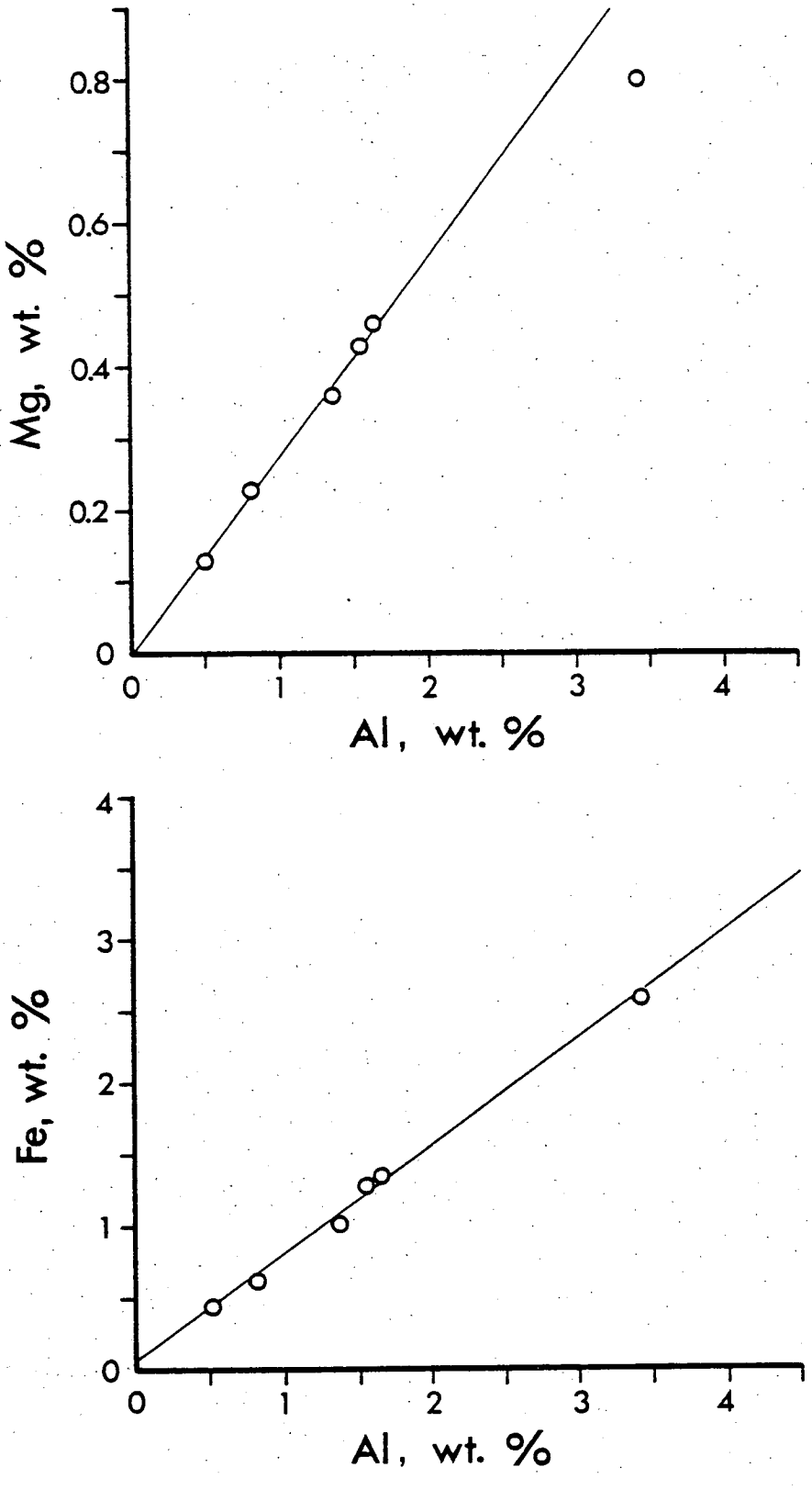

Fig. 4.10 Correlations between magnesium and aluminium and iron and aluminium in carbonate-rich Panama Basin surface sediments, all on a salt-free basis.

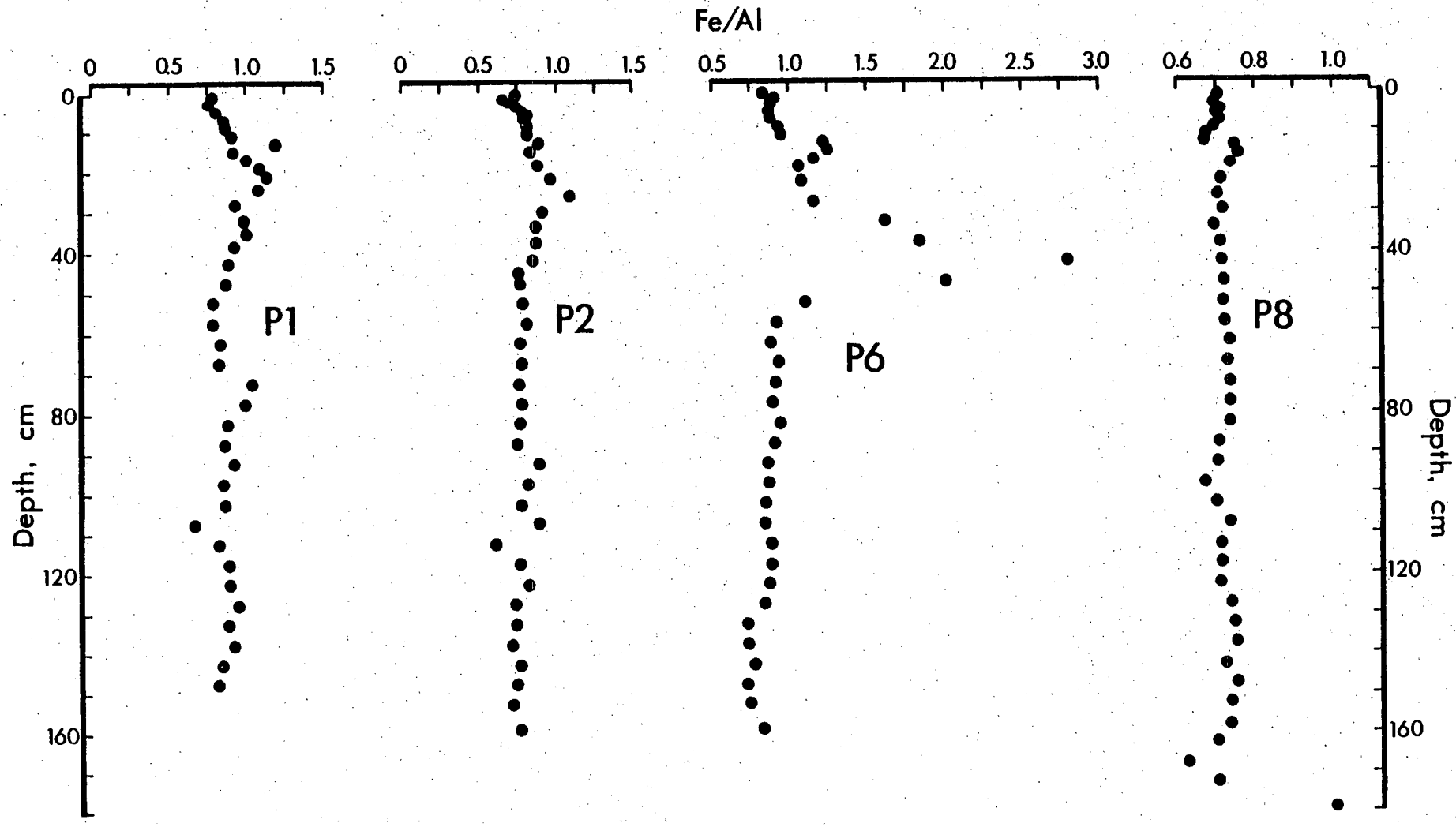

Fig. 4.11 Profiles of the Fe/Al ratio in Panama Basin area sediments. Note the different scale for core P8.

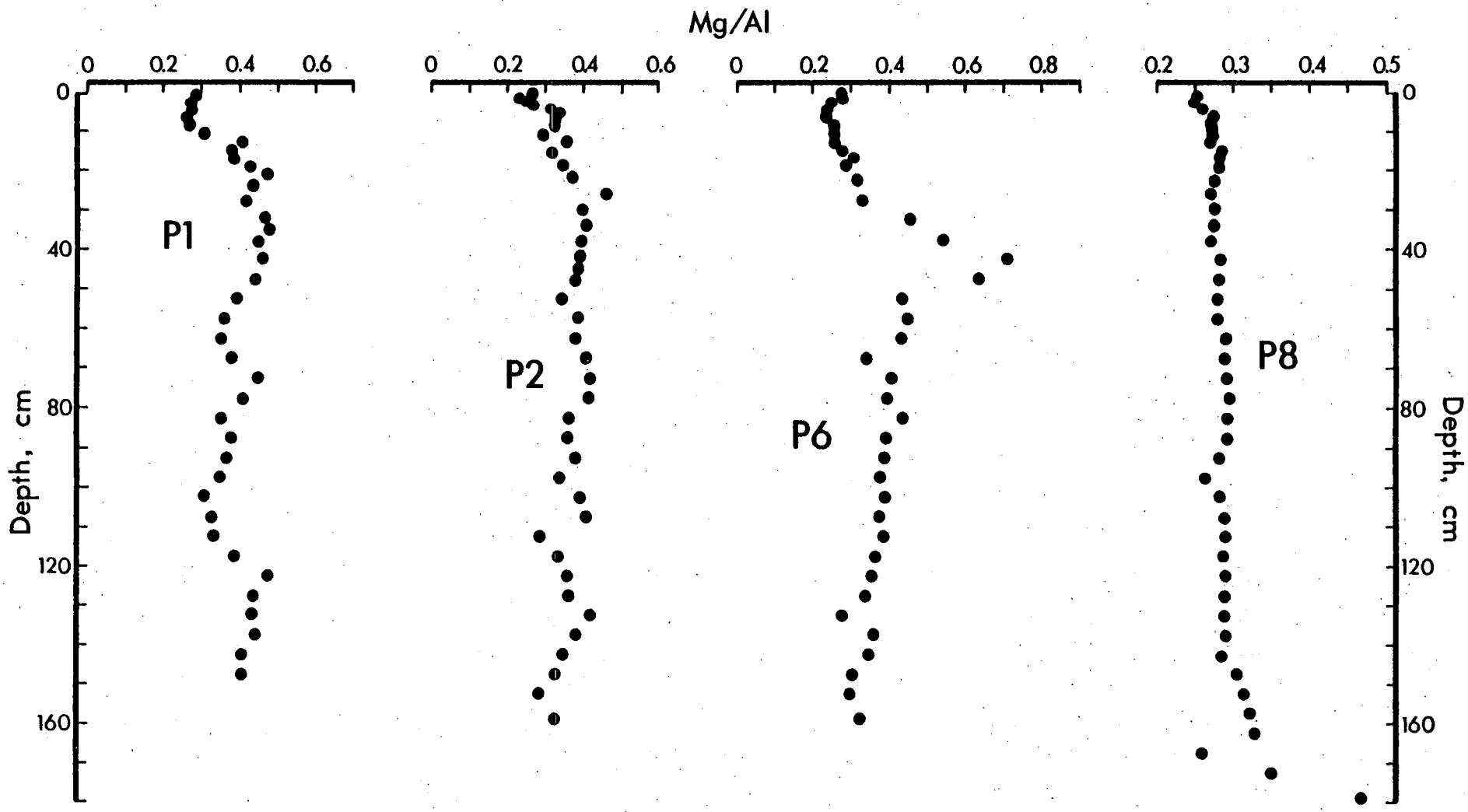

Fig. 4.12 Profiles of the salt-free Mg/Al ratio in Panama Basin area sediments. Note the different scale for core P8.

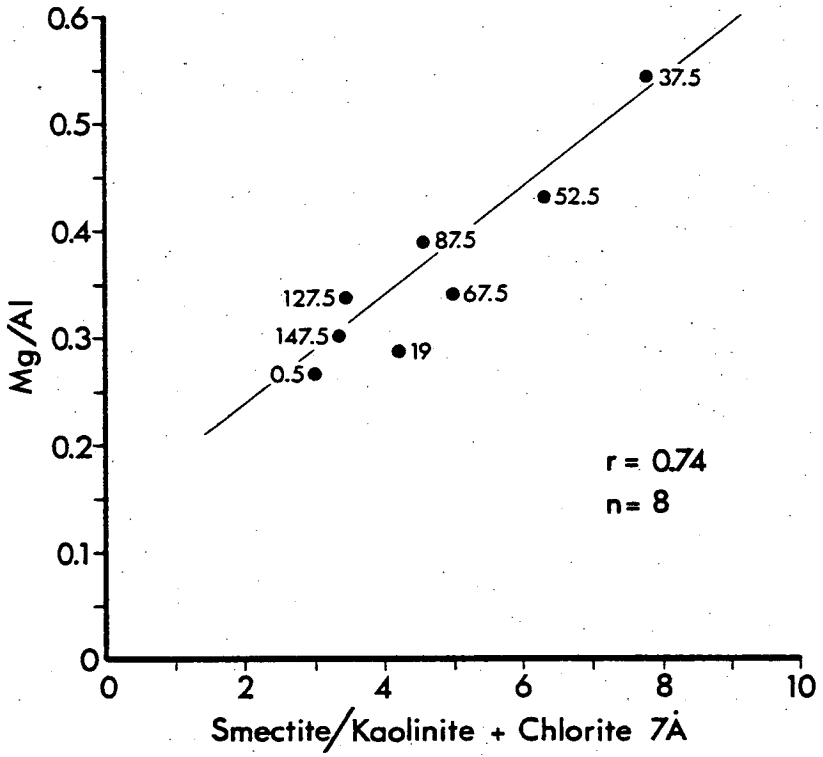

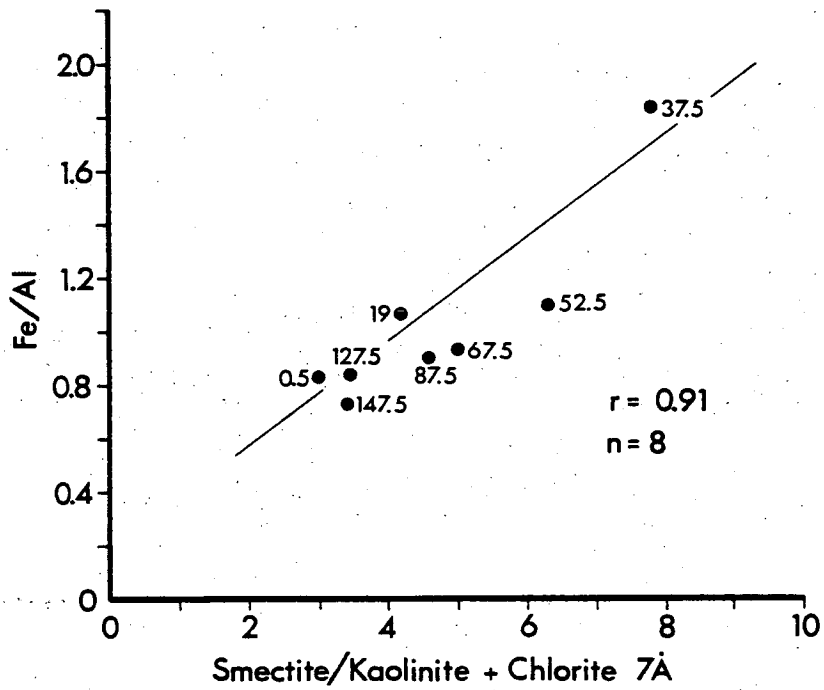

Fig. 4.13 Correlation between the smectite distribution (normalized to the kaolinite + chlorite 7Å peak height) and iron and magnesium to aluminium ratios in sediments from the Galapagos Spreading Centre area (core P6). The number beside each point is the sample depth in the core in cm. The smectite data are listed in Table 3.2 (p. 30).

convectively-circulating sea water (Bender et al, 1971; Bischoff and Rosenbauer, 1977; Cann et al, 1977).

The composition of the sediments within the iron-enriched zone of core P6 lies between that of deep-sea clays and the metalliferous sediments of the Bauer Deep and East Pacific Rise (Table 4.8). Böstrom (1973) illustrated the empirical mixing relations of pure metalliferous sediment and terrigenous material with a plot of Fe/Ti versus Al/Al + Fe + Mn. On a similar graph (Fig. 4.14), sample P6:40-45: lies at a point which suggests a metalliferous contribution of about 40%. The sample plots close to that for average heat flow areas of the East Pacific Rise and not far from that for a band of Fe-Mn enriched, Al-depleted sediment from the DOMES area south of the Clarion Fracture Zone. The latter facies has been interpreted as having a metalliferous component (Bischoff and Rosenbauer, 1977).

Like the characteristics noted for type metalliferous sediments, the band in P6 features titanium and aluminium depletions and iron, magnesium, potassium and smectite enrichments. There may, as well, be an increase in silica contributed by hydrothermal fluids since there is a significant increase in the Si/Al ratio (Table 4.8); however, in the presence of much opal this is difficult to substantiate.

The mineralogy of the metalliferous horizon is dominated by a smectite which appears to be enriched in Fe and Mg (Fig. 4.13). Other metalliferous deposits commonly contain an Fe-smectite along with poorly-crystallized ferromanganese oxides including goethite, δ-MnO_2 and todorokite (Sayles and Bischoff, 1973). It is believed that the smectite forms authigenically from reaction of the precipitated iron oxides with hydrothermal and possibly biogenic amorphous silica and sea water Mg. Sayles and Bischoff (1973) claim to have observed smectite pseudomorphs of radiolaria in Bauer Deep sediments which, if

Table 4.8 Major element compositions of selected metalliferous and non-metalliferous sediments. Concentrations in wt. % element. CSF = carbonate-and salt-free basis; SF = salt-free basis only.

	Fe	Al	Mn	Mg	Ti	Si	K	Na	P	Ca	Fe/Al	Mn/Al	Mg/Al	K/Al	Si/Al
This study, P6:40-45: Metalliferous, CSF	8.76	3.13	0.46	2.21	0.16	25.6	1.12	1.21	0.11	--	2.80	0.15	0.71	0.36	8.2
This study, P6:100-105: Non-metalliferous, CSF	3.99	4.71	0.53	1.83	0.25	27.3	1.12	1.25	0.13	--	0.85	0.11	0.39	0.24	5.8
Bauer Deep[1], Metalliferous, CSF	14.8	1.31	3.54	2.54	0.12	21	0.75	0.61	--	1.56	11.3	2.7	1.9	0.57	16.0
East Pacific Rise[2], High heat flow Metalliferous, CF	18.0	0.50	6.0	--	0.02	6.1	--	--	--	--	36.0	12.0	--	--	12.2
East Pacific Rise[3], Average heat flow Metalliferous, CF	9.5	4.7	2.4	--	0.17	13	--	--	--	--	2.02	0.51	--	--	2.9
Average deep-sea clay[4], SF	6.8	8.7	0.70	2.0	0.48	26	2.6	2.9	0.16	3.0	0.78	0.08	0.23	0.30	3.0

[1] Average composition of core 14, Sayles and Bischoff (1973).

[2] Average composition of Group (b) sediments, Böstrom and Peterson (1969).

[3] Average composition of Group (a) sediments, Böstrom and Peterson (1969).

[4] Turekian and Wedepohl (1961), salt-corrected using the listed Cl concentration.

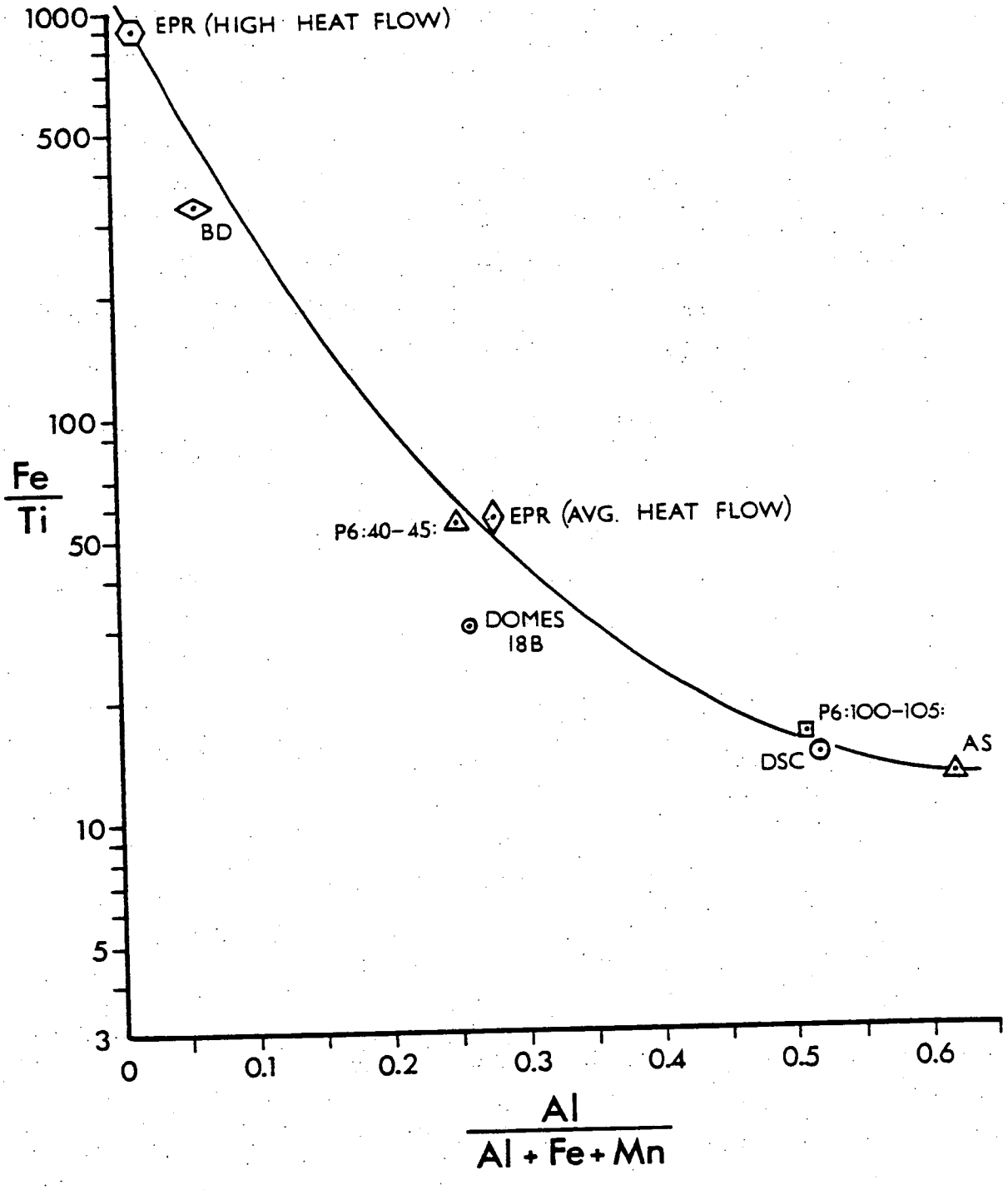

Fig. 4.14 Mixing relationships (after Böstrom, 1973) of sediment from an average heat flow area of the East Pacific Rise (EPR), the DOMES area, the Bauer Deep (BD), and metalliferous and non-metalliferous zones of core P6, with pure EPR metalliferous sediment (high heat flow), average deep-sea clay (DSC), and average shale (AS). EPR, core P6 and BD data from Table 4.8, DOMES data from Bischoff and Rosenbauer (1977), and DSC and average shale data from Turekian and Wedepohl (1961).

correct, would suggest that biogenic silica is important in the smectite formation. Recent work by Lyle (1978) indicates that biogenic opal may be the principal silica source for authigenic smectite formation. The magnesium content in the metalliferous band in P6 is considerably in excess of that which could be contributed by terrigenous detritus. Similar Mg enrichments in metalliferous sediments have been attributed to precipitation of an Mg-SiO_2 phase upon mixing of silica-rich hydrothermal fluid and bottom sea water (Bischoff and Rosenbauer, 1977). Sayles et al (1975) considered such magnesium excesses in Bauer Deep sediments to reflect the occurrence of significant amounts of magnesium in the iron smectite or in an associated mixed layer mica component.

It appears that sea water is the source of both the magnesium and potassium enrichments in the hydrothermal zone in P6. Assuming the Mg/Al and K/Al ratios in the unenriched sediments of sample P6:100-105: (Table 4.8) represent the lithogenous component in the core, the "excess" quantities of Mg and K associated with the high smectite concentration in P6:40-45: can be calculated. The Mg excess/K excess ratio is ~ 2.7 which, by virtue of its rough similarity to the Mg/K ratio in sea water (3.19), suggests that the smectite takes up both elements in approximately sea water proportions.

Although both the mineralogy and chemistry of the Fe-Mg enriched horizon in core P6 support its interpretation as a discrete layer of metalliferous sediment, there are important differences between that band and archetypal East Pacific metalliferous sediments. Cores from the latter facies lack a well-defined redox boundary and both manganese and iron oxides are well preserved to considerable depths. The metal-rich zone in P6 is situated well below the oxidation-reduction boundary in the core and is therefore subject to reduction reactions. On the

assumption that manganese was originally precipitated along with iron in the zone, this feature may explain the absence of manganese in the metalliferous horizon. Since Mn oxides dissolve well in advance of iron oxides as the Eh is lowered (Stumm and Morgan, 1970), any original manganese enrichment may have been obliterated by dissolution and diffusion. The dissolved manganese profile for the core (Fig. 7.6) clearly indicates that there is now no source of dissolving manganese in the metalliferous zone. In contrast, the interstitial iron profile for core P6 (Fig. 4.15)[1] shows a considerable increase in concentration at ~40 cm, implying that in the hydrothermal zone an iron oxide phase exists which is dissolving in response to low Eh.

4.6 The distribution and geochemistry of manganese

It is well known that the distribution of manganese in marine sediments is highly susceptible to sediment oxidation potentials (Lynn and Bonatti, 1965; Li et al, 1969; Calvert and Price, 1972). Dissolution of buried manganese oxides in sediments which are reducing at depth supports upward diffusion of dissolved Mn(II) ions and reprecipitation of Mn(IV) as oxide where higher redox potentials prevail, usually near the sediment-water interface. Some of the dissolved Mn^{2+} diffuses into sea water, precipitates, and is deposited at another location; the remainder accumulates in the oxic surface layer.

---

[1] The considerable degree of scatter in much of the dissolved iron data (Table C.3) can only partly be attributed to the analytical precision of the method used (flameless AA analysis of directly injected, acidified, undiluted pore water; see Appendix B). Some may be due to partial oxidation of samples during squeezing which was not undertaken in an inert atmosphere. The only anti-oxidation precaution taken was the use of the last several ml of pore water extracted from each sample for iron analysis; this considerably reduces but does not eliminate the problem (Troup et al, 1974). Although the data undeniably indicate dissolution in the enriched zone, it should be kept in mind that they may be subject to a variable oxidation artifact of unknown magnitude.

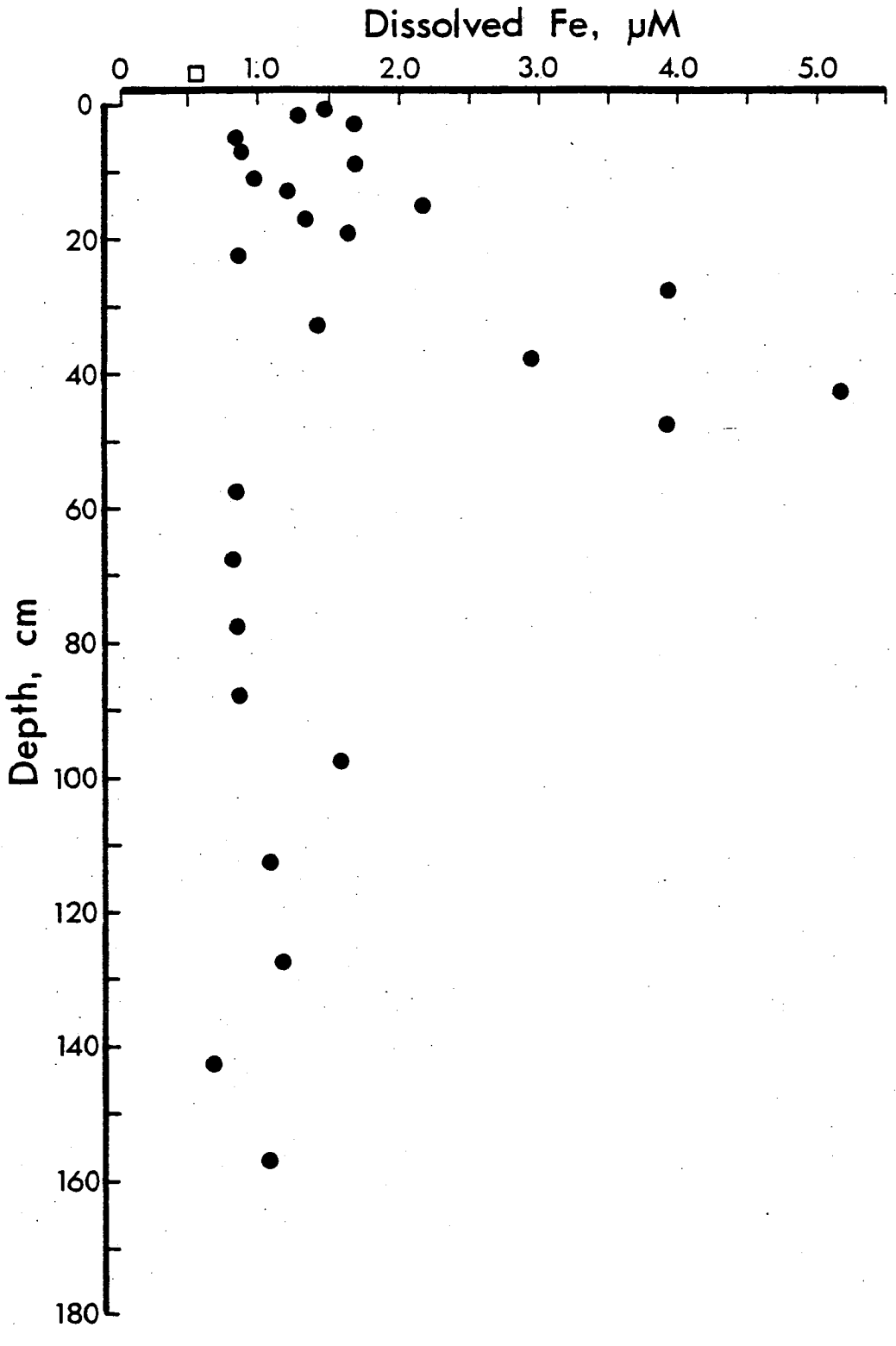

Fig. 4.15 Profile of dissolved iron in the interstitial water of core P6. □ = supernatant. The highest dissolved iron concentration at 42.5 cm depth correlates with the highest iron concentration in the solid phase. Data from Table C.3 (Appendix C).

In the Panama Basin surface sediments investigated here, salt-free manganese concentrations vary from very low (0.07%) to very high (3.91%) (Table C.1), but there are some doubts about these values. Since the manganese concentration decreases enormously within the top few centimetres of each core (Table C.1) only a coring technique which ensures full recovery of the uppermost oxidized layer, such as box coring, will provide samples suitable for studying the areal manganese distribution. The gravity cores obtained for this study may have suffered some loss of the uppermost layer (and therefore manganese) despite precautions taken during coring. Pore water data (Chapter Seven) do suggest, however, that such loss was minimal, at least in P1, P2, P6 and P8. The very low surficial concentrations in P5, P9 and P13 suggest that loss of the top may have been significant in these cores. In view of these suspicions, the areal manganese distribution will not be discussed here.

The vertical distribution of sediment manganese is similar throughout the Basin area, as is evident in the five profiles of Fig. 4.16 and in core P6702-59 described by Lynn and Bonatti (1965). The element is strikingly enriched in the oxic surface layer and its concentration decreases rapidly to background values as the oxidation potential decreases. One exception to this pattern is the increase in Mn content at the base of core P8, which occurs in association with the abundance of volcaniclastic detritus present there. With the exception of this zone, manganese distributions at depth in the cores are largely independent of lithologic variations, including fluctuations in carbonate content. Background levels range from about 0.07-0.15% for the carbonates (P1, P2 and P6) to 0.17-0.23% in the clays dominating P8.

While surface enrichments in the cores imply the presence of manganese oxide, the same reasoning cannot be invoked to explain the high

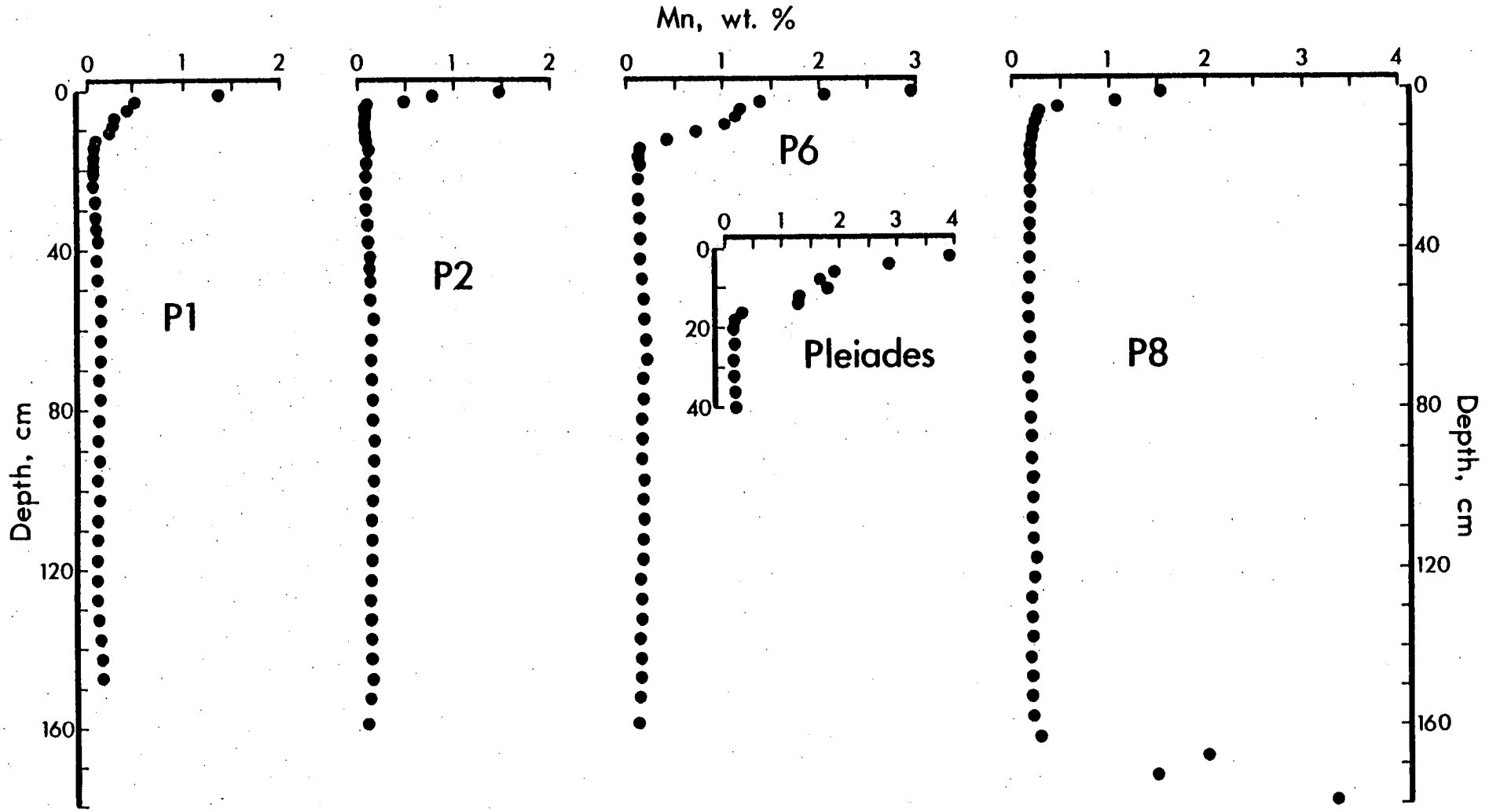

Fig. 4.16 Manganese distribution in Panama Basin area cores, on a salt-free basis. Note the different scale for the Pleiades box core.

Mn content at the base of P8 since this zone occurs in reducing sediments. Optical examination of these sediments revealed several indurated crusts of a creamy-white to grey-black material up to 1 cm^2 in size and ~1 mm in thickness. The crusts, friable in some cases, had surface textures varying from smooth to botryoidal, with botryoids typically 100 microns in diameter but ranging up to twice that size. Oxidation of some of the surfaces occurred subsequent to isolation of the fragments as indicated by a fresh fine-grained lustrous black powder which coated some botryoids and adhering clays; this alteration product appeared to be a manganese oxide.

Scanning electron microscopy and petrography were used to further examine the material and provide evidence of its origin. Plate 4.1 (a) and (b) suggest that the crusts were formed by numerous individual microspheres merging during growth. In thin-section, the spheres are seen to be composed of radiating sub-micron-sized crystallites which produce clear extinction crosses under crossed nicols. The radiating pattern indicates continuous growth subsequent to nucleation on a seed crystal having a single dislocation (Nielsen, 1964).

X-ray diffraction of a finely-ground ultrasonically-cleaned fragment shows the material to be a mixed calcium-manganese-magnesium carbonate with reflections corresponding very closely to the mineral kutnahorite, $Ca(Mn, Mg)(CO_3)_2$ (ASTM Powder Diffraction File, card 11-345). The diffractogram almost exactly matches that of manganous carbonate recovered from sediments of Loch Fyne, Scotland (Fig. 4.17), described by Calvert and Price (1970a).

Wet chemical analysis of the carbonate (Table 4.9(a)) reveals high concentrations of SiO_2, Al_2O_3, MgO, and Fe_2O_3 which are almost certainly due to adhering smectite not removed by ultrasonic washing. Calculation of the empirical composition of the carbonate, based on Mn, Ca,

Plate 4.1

Scanning electron micrographs of manganese-bearing carbonate from core P8.

(a) Botryoidal texture characteristic of many of the carbonate fragments.

(b) Higher magnification, showing merged microspheres.

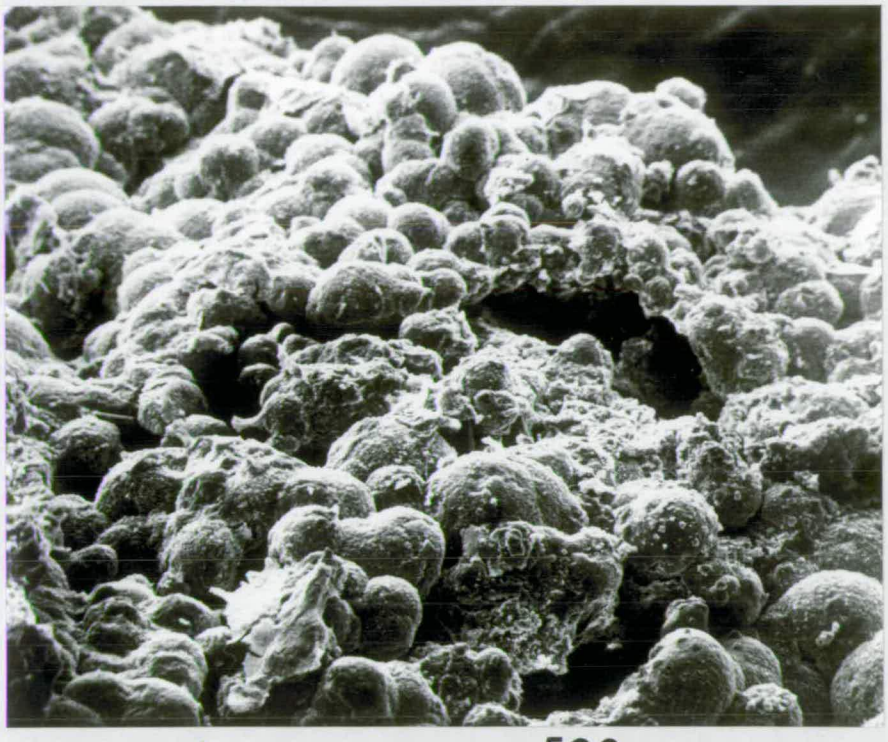

(a)

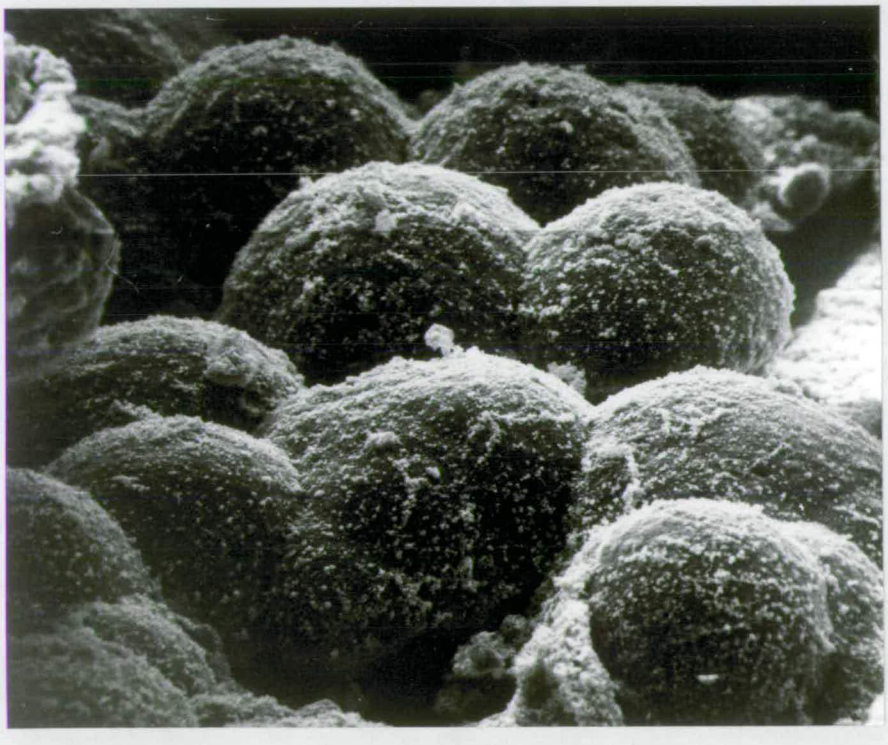

(b)

Plate 4.1

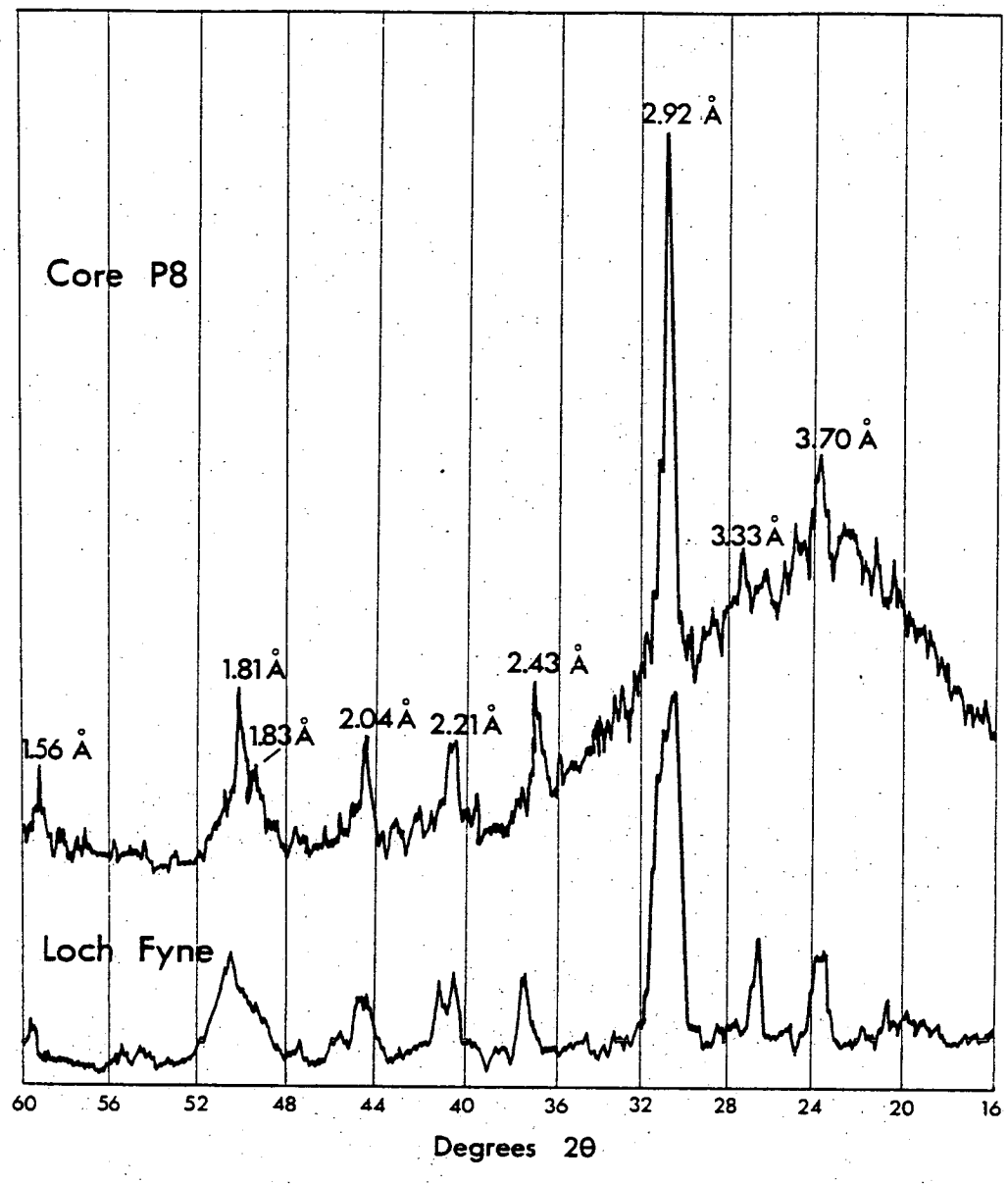

Fig. 4.17 X-ray diffractograms of manganese-bearing carbonates from Loch Fyne (after Calvert and Price, 1970a) and from sample P8:175-183: (this study). The broad hump between 16° and 38° 2θ in the core P8 diffraction pattern is due to scattered background radiation from the glass slide on which the sample was mounted.
Instrument conditions: $\frac{1}{2}^{\circ}$ 2θ min^{-1}, CuKα radiation, 36 kV, 20 mA, Ni filter, curved graphite crystal monochromator.

and CO_2 analyses and choice of a magnesium value to sum the mole fractions to 100%, yields $(Mn_{51}Ca_{45}Mg_4)CO_3$. This composition is supported by the results of two energy-dispersive microprobe analyses on clay-free material in thin-section (Table 4.9 (b), (i) and (ii)).

Thermodynamic calculations (Chapter Seven) strongly suggest that interstitial water in core P8 is supersaturated with respect to manganese carbonate at all depths below about 5 cm. The occurrence of the solid phase only in the ash layer near the base of the core is, therefore, somewhat enigmatic and requires further investigation.

Controls on manganese carbonate precipitation

Recent manganous carbonates have been recovered from several areas, principally in diagenetically-active shallow coastal sediments; their compositions and localities are listed in Table 4.10. It would appear from available descriptions that a common association exists between authigenic Mn-carbonate and coarse-grained sediments. For example, in Loch Fyne sediments, manganous carbonate is found mainly within silty bands occurring in the dominant clays (N.B. Price, personal communication). Zen (1959) identified rhodochrosite in two buried horizons in Peru Trench sediments; in both cases notable quantities of glass shards were present, implying an increase in grain size where the $MnCO_3$ was found. Lynn and Bonatti (1965) observed a high manganese content associated with an ash layer at depth in a core from the Guatemala Basin ($5^{\circ}22.5'N$, $91^{\circ}45'W$).

Strakhov (1969) noted that manganese carbonate also occurs in many ancient rock sequences and is usually found in the coarse-grained horizons of alternating coarse- and fine-grained sediments. He reasoned that its precipitation there was regulated by the carbon dioxide distribution. According to his rather arguable hypothesis, CO_2 produced by bacterial action in fine-grained organic-rich sediments migrates to

	Wt. % Oxides		
	(a)	(b)	
		(i)	(ii)
MnO	23.57	31.84	29.92
CaO	16.52	23.49	25.30
MgO	5.67	2.06	2.11
SiO_2	15.52	0.00	0.00
Fe_2O_3	4.64	0.00	0.00
Al_2O_3	4.00	0.00	0.00
CO_2	28.80	40.44*	40.72*
Total	98.72	97.83	98.05
Calculated empirical formula	$(Mn_{51}Ca_{45}Mg_4)CO_3$	$(Mn_{49}Ca_{46}Mg_5)CO_3$	$(Mn_{46}Ca_{49}Mg_5)CO_3$

Table 4.9 (a) Wet chemical analysis, Mn-bearing carbonate. Analytical methods: Mn-potentiometric titration (Lingane and Karplus, 1946) following Al removal by hydroxide absorption; Ca - complexometric titration with EDTA and Patton and Reeder's reagent (Patton and Reeder, 1956); Mg - complexometric titration with EDTA and Eriochrome Black-T to determine Ca+Mg, Mg calculated by difference; Fe, Al - atomic absorption (standard additions); Si - colourimetric (Bunting, 1944) following fusion in $LiBO_2$ and dissolution in HCl; CO_2 - gravimetric by ascarite absorption following liberation with hot H_3PO_4. The total is slightly low since Na, K etc. were not analyzed.

(b) Energy-dispersive electron microprobe analyses (Cambridge Instruments Microscan V with a Link Systems Energy Dispersive Spectrometer). Slightly low totals are due to poor polish of probe section. Analyses (i) and (ii) represent two different botryoids. Scans across a single botryoid indicated compositional homogeneity; no elements other than Mn, Ca, and Mg were indicated.

*CO_2 concentrations calculated from total cation concentrations.

Table 4.10 Locations and empirical formulae of some manganese-bearing carbonates from marine sediments.

Locality	Empirical Composition	Source
Peru Trench	$MnCO_3$*	Zen (1959)
Baltic Sea	$(Mn_{70}Ca_{30})CO_3$ to $(Mn_{60}Ca_{32}Mg_8)CO_3$	Manheim (1961)
Baltic Sea	$(Mn_{56.8}Ca_{25.5}Mg_{9.7}Fe_{8.0})CO_3$	Hartmann (1964)
Guatemala Basin	$(Mn_{50-80}Ca_{20-50})CO_3$	Lynn and Bonatti (1965)
Gulf of Riga	$(Mn_{40}Ca_{25}Mg_{35})CO_3$	Shterenberg et al (1968)
Oslo Fjord	$(Mn_{50}Ca_{50})CO_3$	Doff (1969)
Loch Fyne	$(Mn_{47.7}Ca_{45.1}Mg_{7.2})CO_3$	Calvert and Price (1970a)
Panama Basin	$(Mn_{51}Ca_{45}Mg_4)CO_3$	This study

* Optical identification of "skeletal and subhedral" rhodochrosite crystals. Qualitative analysis of the sample yielded a strong MnK line.

more porous organic-poor sandy or silty beds where it diffuses away rapidly; loss of the CO_2 from this coarse band raises the pH and induces Mn carbonate precipitation.

It seems much more likely that the general association of Mn-carbonates with coarse sediments is a function not of CO_2 migration but of precipitation on a suitable substrate. It is suggested that, despite supersaturation throughout most of P8, manganous carbonate is found only in the coarse basal sediments of the core because the larger mineral grains there catalyze nucleation of Mn-carbonate seed crystals.

Classical chemical nucleation theory states that the formation of embryonic nuclei is governed by the statistical likelihood of a sufficient number of ions colliding simultaneously to form clusters from which spontaneous growth can proceed (Nielsen, 1964). The higher porosity of coarse sediments encourages development of such clusters by providing larger intra-grain volumes in which a greater probability exists for the chance collision of the requisite number of ions. Hence, higher porosity would lower the activation energy barrier in a similar way to that of a catalyst reducing the activation energy required to initiate a chemical reaction. Manganese carbonate precipitation is therefore encouraged by the decreased critical supersaturation levels of coarser sediment horizons.

A further point emerging from this study is that organic carbon is not as directly critical to manganous carbonate generation as has been suggested, for example, by Strakhov (1969). In core P8, for instance, sufficient organic carbon exists to render the sediment anoxic at a shallow depth and to initiate rapid dissolution of manganese oxides. However, bacterial metabolic activity is insufficient to deplete much sulphate and little increase in alkalinity is thus observed (Chapter Seven). It appears in this case that there is no significant increase

over sea water levels of the concentration of inorganic dissolved carbon species in pore water, in contrast to the high interstitial manganese content.

In order to shed some additional light on the role that organic matter plays in the geochemistry of manganese carbonate, sediments were collected from the area of known Mn-carbonate occurrence in Loch Fyne and their pore waters extracted and analyzed. The pore water chemistry (Fig. 4.18) is similar to that in core P8 - the dissolved manganese concentration exceeds the solubility product of $MnCO_3$, sulphate reduction is minor, and there is a slight consumption of alkalinity resulting presumably from Mn-carbonate precipitation. The interstitial water chemistry of the Loch Fyne core concurs with the conclusion for P8 that substantial production of alkalinity (i.e. CO_3^{2-}) is not required to precipitate manganous carbonate. The critical factors instead appear to be the availability of soluble manganese oxides and a sufficient organic carbon content to reduce the pE to ~ 9, roughly the point at which MnO_2 begins to dissolve (Stumm and Morgan, 1970).

For both areas, the postulated relative unimportance of alkalinity in manganous carbonate precipitation is supported by isotopic analyses (Table 4.11). Mn-carbonate in P8 yields a δC^{13} value of -2.59 per

Table 4.11 Stable carbon isotopic analyses of manganous carbonates.

Location	Empirical composition	C^{13}/C^{12}, ‰
Panama Basin, core P8, 175-183 cm depth	$(Mn_{51}Ca_{45}Mg_4)CO_3$	-2.59(P.D.B.)[1]
Loch Fyne, 55°51.7'N, 5°21.5'W	$(Mn_{47.7}Ca_{45.1}Mg_{7.2})CO_3$	-5.75(P.D.B.)

[1] Analysis kindly provided by Dr. N. J. Shackleton.

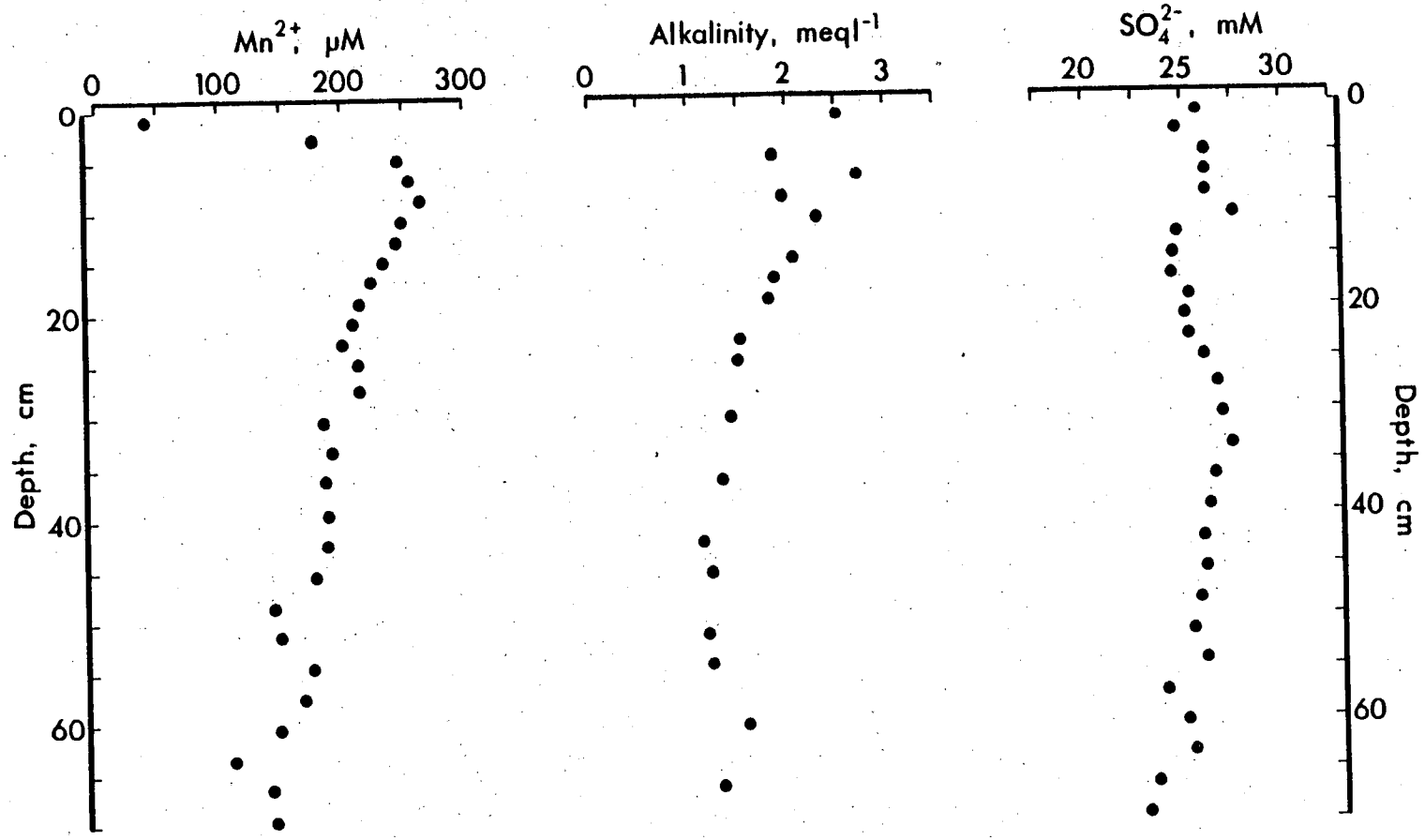

Fig. 4.18 Pore water manganese, alkalinity and sulphate profiles from a Mn-carbonate-bearing core from Loch Fyne (55°52.2'N, 5°21.0'W). Pore waters were extracted in a nitrogen atmosphere by centrifugation. Analytical methods are described in Appendix B.

mil, not very different from the calcite of benthic foraminifera in the Panama Basin which ranges typically from +1 to -1.5 per mil (N. J. Shackleton, written communication). The low depletion of C^{13} indicates that little carbon of organic origin ($\delta C^{13} \sim$ -20 per mil, Degens and Mopper, 1976) was utilized in the Mn-carbonate precipitation reaction. Instead, carbon must have been supplied either by carbon species diffusing downward from sea water or from dissolving calcite tests. The Loch Fyne carbonate has a δC^{13} of -5.75 per mil (J. N. Weber, written communication) which indicates that roughly 75% of the constituent carbon is from an inorganic source (i.e. "sea water alkalinity" or calcite carbon) and 25% is of organic origin. This reinforces the conclusion that high concentrations of decomposing organic matter are not a prerequisite for manganous carbonate formation in marine sediments.

CHAPTER FIVE

THE DISTRIBUTION OF MINOR ELEMENTS

5.1 Introduction

The interpretation of major element analyses has shown that the sediments of cores P1, P2 and P6 consist of three phases: terrigenous detritus, organic and biogenous material, and an authigenic-hydrogenous fraction, manifested principally as oxides in surface sediments and the "metalliferous" band of P6. In contrast, P8 is distinguished by its general mineralogical and chemical homogeneity excepting the chemically distinct Mn-rich ash horizon at the base of the core and the thin oxic top; opaline silica and biogenic calcite are of minor importance in this core. This spectrum of sediment types within the two facies provides an opportunity to investigate the partitioning of minor elements between different constituents.

As in Chapter Four, the distributions of certain elements are considered here on an element/Al basis in order to avoid bias introduced by biogenic dilution. The decision to discuss specific distributions as ratios is largely subjective since several elements occur in significant concentrations in both biogenic and terrigenous or authigenic fractions. Where it is felt that dilution complicates interpretation of the distribution of an element, ratios to Al are used. Elements independent of variations in $CaCO_3$ or opal concentrations are discussed solely on a salt-free basis.

Minor elements were analyzed by X-ray fluorescence spectrometry, as described in Appendix B, and all analyses and relevant inter-element ratios are listed in Appendix C.

For purposes of comparison, Table 5.1 lists the mean minor element composition of the sediments along with estimated oceanic averages and analyses compiled from a brief previous study (Bonatti et al, 1971) of sediment chemistry in the central Panama Basin. Iodine and bromine were also analyzed but their geochemistry is sufficiently dissimilar

Table 5.1 Minor element concentrations in Panama Basin sediments (in ppm).

Element	This study: Biogenic sediments[1]		This study: Terrigenous sediments[2]		Panama Basin biogenic sediments[3]		Average deep-sea clay[4]	Average deep-sea carbonate[4]
	Sfc. n=5	Depth n=92	Sfc. n=1	Depth n=29	Sfc. n=6	Depth n=6		
Ba	3650 (2434-5040)	2233 (1205-4912)	2570	2217 (1882-2970)	3460 (3250-3600)	2540 (2100-3300)	2300	190
Co	20 (15-22)	13 (5-30)	39	37 (29-60)	27 (10-40)	10 (7-13)	74	7
Cr	26 (9-65)	16 (9-33)	126	134 (81-142)	27 (21-34)	35 (23-42)	90	11
Cu	130 (96-158)	84 (48-164)	116	119 (103-223)	140 (90-155)	100 (90-110)	250	30
Ni	256 (201-318)	127 (58-357)	155	176 (145-335)	281 (190-360)	149 (130-170)	225	30
Mo	33 (11-76)	6 (1-13)	11	6 (1-13)	-	-	27	3
Rb	9 (2-22)	4 (1-10)	29	37 (35-57)	-	-	110	10
Sr	1134 (1001-1289)	1071 (846-1246)	179	187 (159-331)	-	-	180	2000
S	1495 (1340-2050)	1332 (200-4180)	400	1770 (560-2550)	3700 (3600-3800)	3500 (2600-3900)	1300	1300
Zn	219 (120-378)	172 (92-333)	313	290 (245-354)	-	-	165	35
Zr	31 (23-39)	28 (16-55)	58	67 (50-135)	47 (42-52)	31 (29-34)	150	20

[1] Surface values are averages of P1, P2, P6, Pleiades, and P7 core tops. Values at depth are the means of all analyses of P1, P2, Pleiades and P6 below 20 cm depth. Corresponding ranges are in parentheses. All concentrations are on a salt-free basis.

[2] Surface values are those for the top of core P8; concentrations at depth are the averages for sediments below 20 cm, excluding the bottom 20 cm (ash band). Ranges however include the ash-band. All concentrations are on a salt-free basis.

[3] Data compiled from Bonatti et al (1971) from the analysis of one 40 cm long core at 2°45'N, 85°20'W. Surface values are the mean of the top 8 cm; values at depth are the average concentrations below the surface oxic layer (top 8 cm). The concentrations are not salt-corrected.

[4] From Turekian and Wedepohl (1961).

to warrant separate discussion in the following chapter.

5.2 Distribution of the terrigenous elements rubidium and zirconium

Rubidium concentrations in Basin area sediments range from < 1 to 76 ppm (Table C.2, p. 192). Poor analytical precision at the 1-10 ppm level typical of the carbonate sediments (cores P1-P6) renders the Rb/Al ratio insensitive for a meaningful discussion of the element's distribution. However, the low concentrations of both Rb and Al in these sediments strongly suggest that rubidium is exclusively associated with the terrigenous fraction.

The geochemistry of rubidium classically parallels that of potassium due to the diadochous relationship of the two elements - Rb^+ has an ionic radius of 1.47 Å which is sufficiently similar to the 1.33 Å radius of K^+ to permit facile substitution into potassic micas (illite) and feldspars. The K-Rb correlation in core P8 reflects the congruent distribution of the two elements (Fig. 5.1); similar plots for the other cores are subject to spurious correlation introduced by biogenic dilutants (as well as poorer precision for Rb) and are not shown. Linear regression of the points in Fig. 5.1 yields a salt-free K/Rb ratio of 301, somewhat higher than the average ratio in deep-sea clays of 227 (Turekian and Wedepohl, 1961). The difference between the ratios may be attributable, at least in part, to the presence of clinoptilolite in the core. Although K and Rb are diadochous, potassium is likely to be enriched relative to Rb in clinoptilolite since the K/Rb ratio in sea water is considerably higher than that in the crust ($\sim$3500 vs. 267, respectively; Riley and Chester, 1971, p. 64). In addition, clinoptilolite contains a major proportion of exchangeable K (Cronan, 1974). Surface sediment K/Rb ratios from other Eastern Basin cores in which clinoptilolite was not observed range from 154-215.

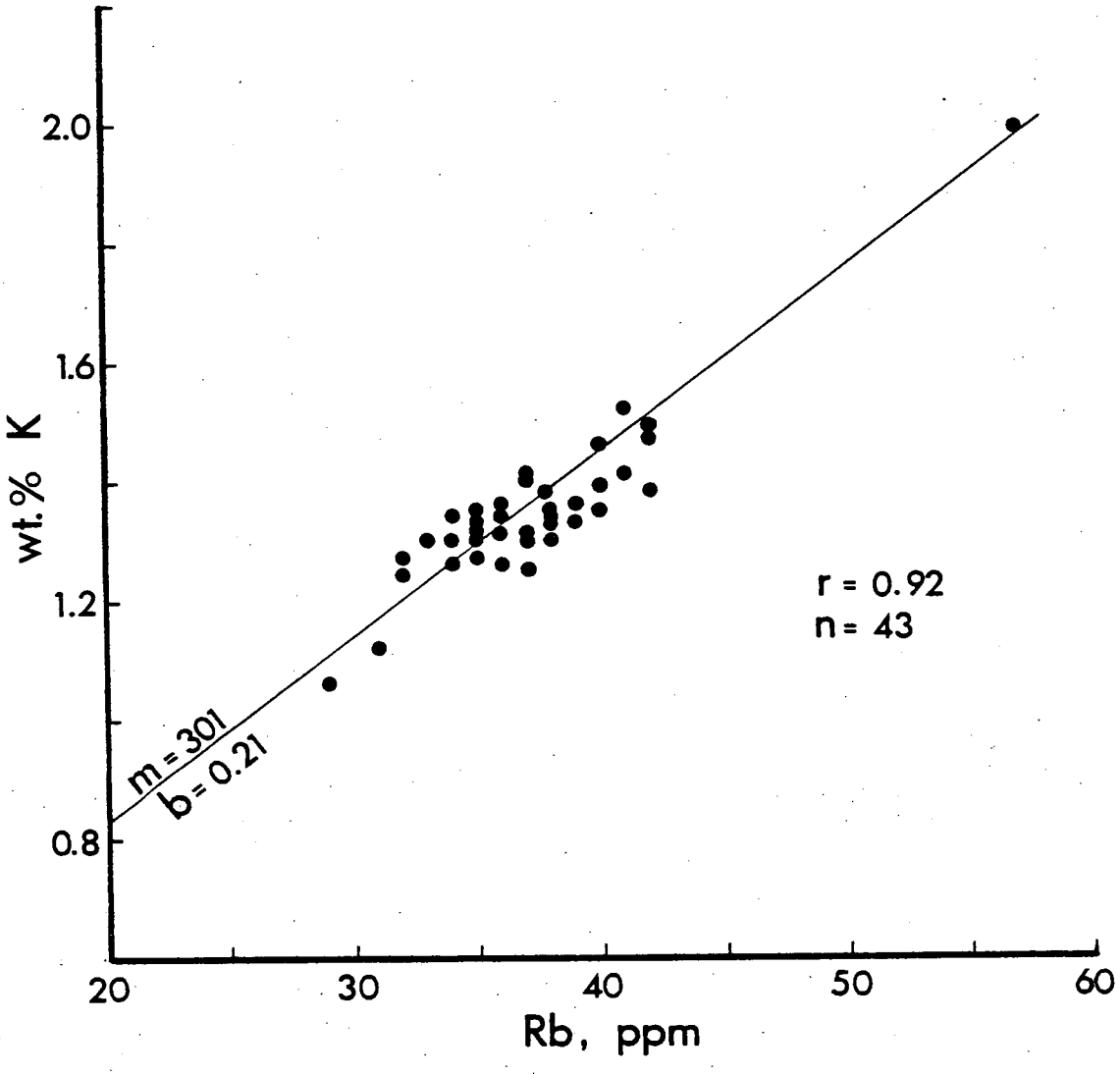

Fig. 5.1 Potassium - rubidium correlation in core P8. Concentrations are on a salt-free basis. The regression line is computer-fitted.

Zirconium concentrations range from 14-58 ppm in the surface sediments with the lowest values occurring in the carbonate oozes (Table 5.2). The Zr/Al ratio increases from about 8×10^{-4} in P8 to $> 25 \times 10^{-4}$ in P1, P2, and P5, indicating a relative zirconium enrichment in the Galapagos area sediments. The source of the enrichment is unclear, but it may be due to input of basaltic detritus from the Galapagos Islands, as was suggested for titanium. The Zr/Al profiles for cores P1 and P2 (Fig. 5.2) show a broad similarity to the Ti/Al distribution (Fig. 4.8) which is consistent with the common occurrence of both elements in the heavy mineral fraction in sediments (Rankama and Sahama, 1950).

Table 5.2 Salt-free Zr concentrations and Zr/Al ratios in Panama Basin surface sediments.

Sample	Zr, ppm[1]	Zr/Al x 10^{-4}
P1:0-2:	23	28.3
P2:0-1:	36	26.8
P5:0-1.5:	14	27.3
Pleiades (PL-2)	28	17.0
P6:0-1:	29	18.6
P7:0-2:	39	11.2
P8:0-4:	58	7.4

[1] The element was not analyzed in surface sediments from cores P9-P13.

5.3 Distribution of elements in the authigenic and biogenic fractions

Barium

High concentrations of barium, ranging from 1200 to 5200 ppm, occur throughout Panama Basin surface sediments (Table 5.3). Although Ba contents are similar in both biogenic and terrigenous sediments, the former contain an order of magnitude more barium relative to aluminium, indicating that terrigenous constituents host only a minor fraction of the total Ba content. Barium concentrations of several thousand ppm have

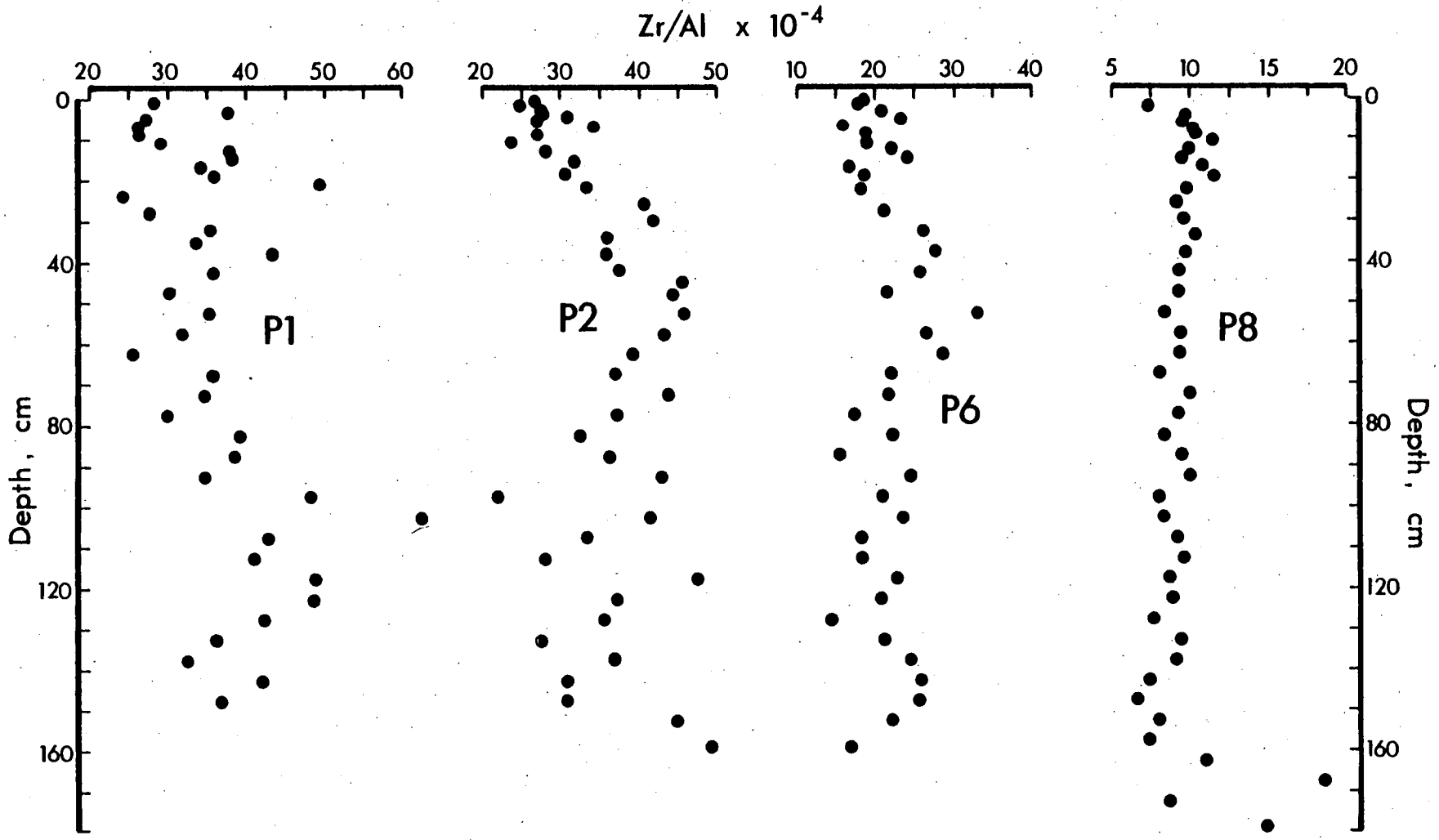

Fig. 5.2 Zr/Al profiles in Panama Basin area sediments. Note the different scale for core P8.

been observed in East Pacific sediments (Arrhenius, 1963; Arrhenius and Bonatti, 1965; Böstrom and Peterson, 1966; Church, 1970; Bonatti et al, 1971; Sayles et al, 1975) and appear to typify the entire eastern and southeastern Pacific area. The contents measured here fall toward the lower end of the reported range which reaches nearly 25,000 ppm (salt-free) in Bauer Basin sediments (Sayles et al, 1975).

Table 5.3 Salt-free barium concentrations and Ba/Al ratios in Panama Basin surface sediments.

Sample	Ba, ppm	Ba/Al	Sample	Ba, ppm	Ba/Al
P1:0-2:	3442	0.42	P8:0-4:	2572	0.033
P2:0-1:	4550	0.33	P9:0-2:	5170	0.062
P5:0-1.5:	1284	0.25	P10:0-2:	2707	0.031
Pleiades	2434	0.15	P11:0-3:	2547	0.029
P6:0-1:	2806	0.18	P12:0-1.5:	2231	0.025
P7:0-2:	5041	0.15	P13:0-2:	1215	0.014

The vertical distribution of barium in all cores is characterized by a variable but general decrease with depth which is best illustrated by the Ba/Al ratio (Fig. 5.3). The decrease is apparently consistent across the Basin, occurring in both biogenous and terrigenous facies.

A feature obscured by the Ba/Al ratio but evident in the salt-free barium data is the large increase (from 1500 to 4900 ppm) in concentration of the element near the base of core P1 (Table C.2, p. 195). This increase is not controlled by biogenic dilution since it occurs on both a carbonate-free basis (Table C.2, p. 196) and a carbonate- and biogenic silica-free basis. Equally, it cannot be due entirely to a greater lithogenous barium content since the lithogenous component can account for only a few hundred ppm of the ~3000 ppm increase. At this point, there is no evident explanation for the local (below 120 cm) increase; however, it does suggest that the distribution of barium is

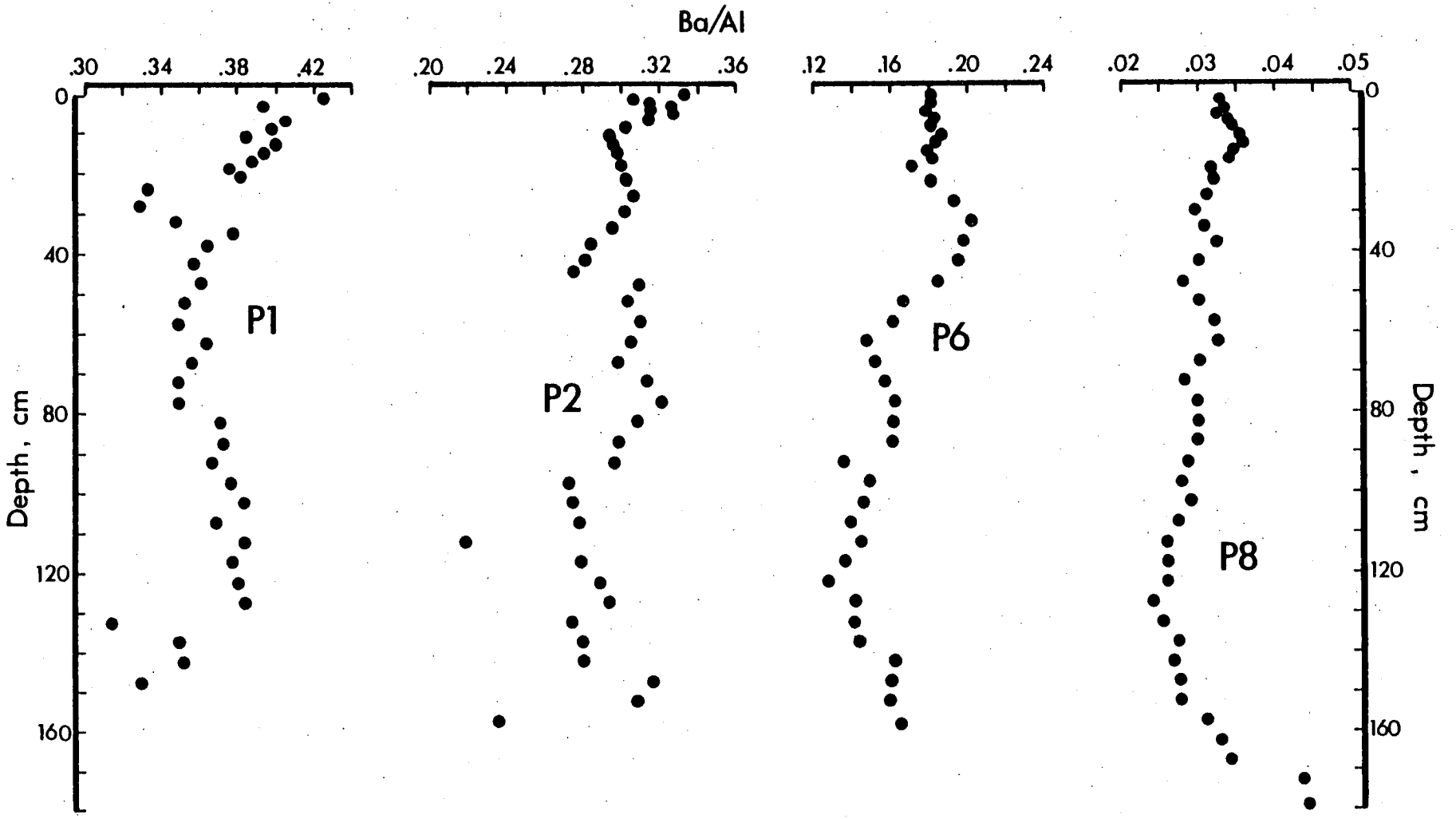

Fig. 5.3 Ba/Al profiles in Panama Basin area sediments. Note the different scale for core P8.

largely independent of both biogenic and terrigenous components.

Geochemical controls on the barium distribution

It is known that barium in east Pacific sediments exists to some degree in authigenic barite, which commonly occurs as euhedral crystals a few microns in size (Church, 1970). However, barium also occurs in two other phases of interest here: manganese (IV) oxides and detrital silicates (there is no evidence to suggest that the Ba-bearing zeolite harmotome occurs in Panama Basin sediments). The large ionic radius of the Ba^{2+} ion (1.35 Å) facilitates its substitution into cavities of those manganese oxides which have a framework of edge-shared (MnO_6) octahedra, such as psilomelane, hollandite, and probably todorokite (Burns and Burns, 1977) and the similarity of the ionic radius to that of potassium (1.33 Å) permits direct substitution of Ba in K-feldspars. Available data can be applied to estimate the proportion of barium occurring in these phases. The highest Ba/Mn ratio in todorokite-rich crusts from hydrothermal mounds near the Galapagos Rift, analyzed by Corliss et al (1978), is 0.0063; by extension, the maximum contribution of barium to Basin surface sediments if all Mn oxides are todorokite is unlikely to exceed about 100-250 ppm, or roughly 10% of the total. In detrital sediments the Ba/Al ratio ranges from about 0.0045 (Gulf of Paria clay; Hirst, 1962) to 0.013 (Barents Sea silt; Wright, 1972). Therefore, the terrigenous clay-rich sediments of the Eastern Basin probably contain about 500-700 ppm of lithogenous barium, equivalent to up to one-half of the total concentration - the remainder may be present in barite. Further calculations show that in the biogenic sediments (cores P1-P7), non-lithogenous barium accounts for upwards of 80% of the total barium content, but it has not been proven that such excesses are held exclusively in barite (see for example, Chan et al, 1977).

Despite considerable research, both the chemical form of barium in East Pacific sediments and the mechanism of its incorporation remain enigmatic. High concentrations predominate in a north-south trending belt associated roughly with the East Pacific Rise and in a broad westward-waning equatorial belt which underlies the zone of high biological productivity (Böstrom et al, 1973). The latter zone correlates reasonably well with the concentration of biogenous material and organic carbon in the sediments (Revelle et al, 1955; Goldberg and Arrhenius, 1958; Church, 1970) but the barite concentration along the East Pacific Rise (which lies mainly above the carbonate compensation depth and therefore has a high $CaCO_3$ content anyway) is probably closely related to spreading ridge hydrothermal activity (Arrhenius and Bonatti, 1965). Recent analyses of Galapagos Spreading Centre hydrothermal vent waters by Corliss et al (1979) have revealed very high dissolved barium concentrations which lend strong support to the hydrothermal origin hypothesis.

While a hydrothermal source for at least a portion of barite barium now seems incontrovertible, the mode of incorporation of the element into the sediments is still unknown. Hanor (1969) demonstrated theoretically that deep ocean waters are undersaturated relative to pure barite but are supersaturated with respect to a binary solid solution of barite and celestite. The theory is supported to some extent by analyses of marine barite which show solid solution of Sr up to several mole percent (Arrhenius and Bonatti, 1965; Church, 1970). Despite the fact that the Galapagos hydrothermal fluids are highly supersaturated and effuse into a strontium-rich environment, Corliss (personal communication, 1978) has been unable to find crystalline barite in particulate matter filtered from the hot waters. To the author's knowledge, inorganically-precipitated crystalline barite has

not been observed in any suspended oceanic particulate matter.

Since inorganic precipitation of $BaSO_4$ in the water column does not seem to be occurring, another process is probably active in transporting barium to the sea-floor. Although the element has no reported biochemical function, its depletion in surface waters and enrichment in deep and bottom waters strongly suggest that it is involved in the biogeochemical cycle (Chan et al, 1977).

Barium appears to be enriched in some marine organisms, relative to more abundant elements in sea water (Arrhenius, 1963), but the enrichments are inconsistent. Concentrations of hundreds of ppm have been reported in coccolith oozes (Thompson and Bowen, 1969) while carbonate tests contain 100 (common) to 8000 (rare) ppm barium, much of which is occluded in acid-insoluble organic aggregates (Church, 1970). In addition, barite crystals are found in the granellae of Xenophyophorid protozoans (Lowenstam, 1974). These organisms may contribute an unknown quantity of crystalline barite to pelagic sediments. Although the biota associated with barium have not been specified, on a wide scale, the close covariance of the element with silica and alkalinity in sea water (Chan et al, 1977) quite clearly supports the contention that living organisms and/or their remains have a primary responsibility in removing Ba from the sea.

The high barium concentrations typical of East Pacific sediments appear, therefore, to be a consequence of two processes: hydrothermal activity, which introduces an unknown (but at least locally important) quantity of Ba to the sea, and transport of the element to the sea-floor by biological vectors. Dissolution of the biological detritus would supersaturate pore waters with respect to $BaSO_4$ and encourage inorganic in situ precipitation of crystalline barite in the sediments.

The rough decrease in barium concentration with depth in Panama Basin cores suggests, at first glance, that barite dissolution might be operative, assuming that this mineral is the dominant barium host. Several observations, however, argue against such a process: (a) Church (1970) found no evidence of dissolution of barite crystals recovered from East Pacific cores; (b) dissolution of manganese oxides would increase the interstitial barium concentration, impeding breakdown of $BaSO_4$; (c) insufficient sulphate is reduced in these sediments to induce barite dissolution; and (d) high barite concentrations comparable to the levels found in this work have been observed in deeply-buried sediments in DSDP cores (Cronan, 1974).

Since barite dissolution does not appear to be active, on the contrary, precipitation seems likely, why does the barium content decrease with depth? There is no correlation between barium and biogenic phases (carbonate, silica or organic carbon) down the cores; so, variations in productivity are probably not responsible. It is possible that the sediment barium content may be limited by the quantity of the element available for removal from sea water. If this is the case, the Ba decrease in East Pacific sediments over the past 40,000-50,000 years may be reflecting historical variation in the rate of hydrothermal introduction of the element to the sea. However, in the absence of a sound description of the role diagenesis plays in affecting barium in sediments, this hypothesis cannot be evaluated. There is obviously a great amount of work yet required to determine how biogeochemical processes govern barium distribution in East Pacific sediments.

Strontium

The vertical distribution of Sr in Panama Basin area sediments is shown in Fig. 5.4. Calcite controls the distribution in the carbonate cores while the much lower levels in core P8 primarily reflect

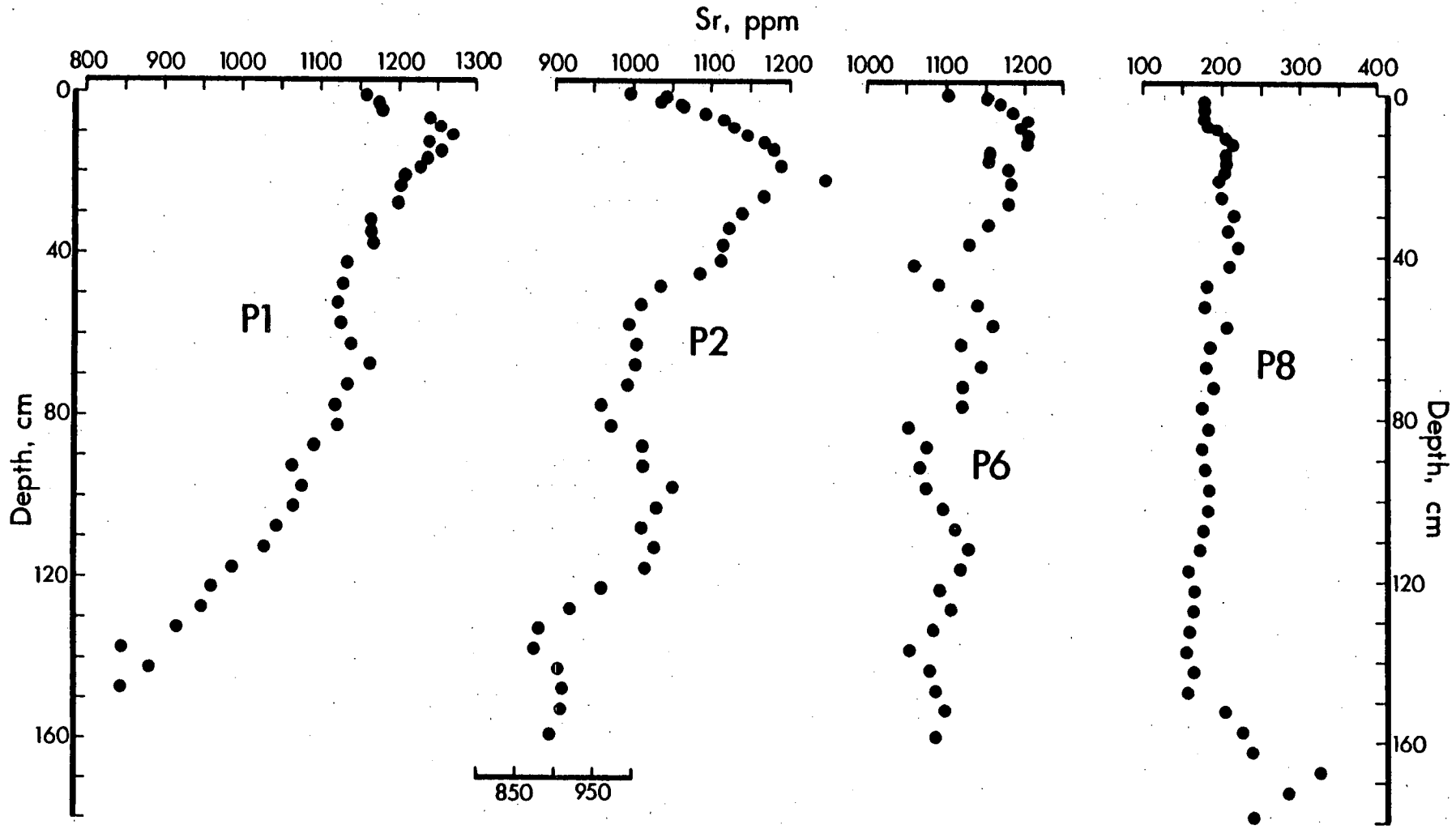

Fig. 5.4 Salt-free strontium distributions in Panama Basin area cores. Note the different scale for core P8.

the concentration in terrigenous detritus. Fig. 5.5 shows the Sr-Ca correlation for cores P1, P2 and P6. The intercept at zero carbonate is 220 ppm Sr and at 100% $CaCO_3$ (40% Ca) is 1600 ppm. These are similar to levels in average deep-sea clay (180 ppm, Turekian and Wedepohl, 1961) and carbonates (1400 ppm in pure foram ooze, Turekian, 1964, cited in Calvert, 1976; 1470 ppm in coccolith ooze, Thompson and Bowen, 1969; 2000 ppm in average pelagic carbonate, Turekian and Wedepohl, 1961). In addition to carbonates and terrigenous detritus, barite may contribute a little strontium to the sediments. Arrhenius and Bonatti, (1965) and Church (1970) report a range of Sr substitution in $BaSO_4$ of 1-5 mole percent which could therefore contribute about 30-150 ppm of the total strontium content. Sediments from core P6 fall slightly above the Sr-Ca line formed by P1 and P2 (Fig. 5.5); this is possibly due to a lower average barium concentration, i.e. less barite, in P6 which may result in lower Sr levels for a given Ca concentration in this core.

In core P8 the increases in strontium and barium near the base of the core probably reflect the higher feldspar concentrations present in the ash band. The manganous carbonate occurring there contains 380 ppm Sr and $\ll$ 100 ppm Ba (analyses by atomic absorption spectrophotometry) indicating that this phase may be a minor contributor to the local Sr increase but not to that of barium.

Sulphur

A plot of the concentration of Ba versus S in Fig. 5.6 shows sulphur to be present in Panama Basin area sediments at a level equal to or greatly in excess of that required to account for the postulated barite content. What this excess represents is unclear, although the presence of sulphides and possibly elemental sulphur could be responsible. The high quantities of sulphur in P6 and P8 where organic matter

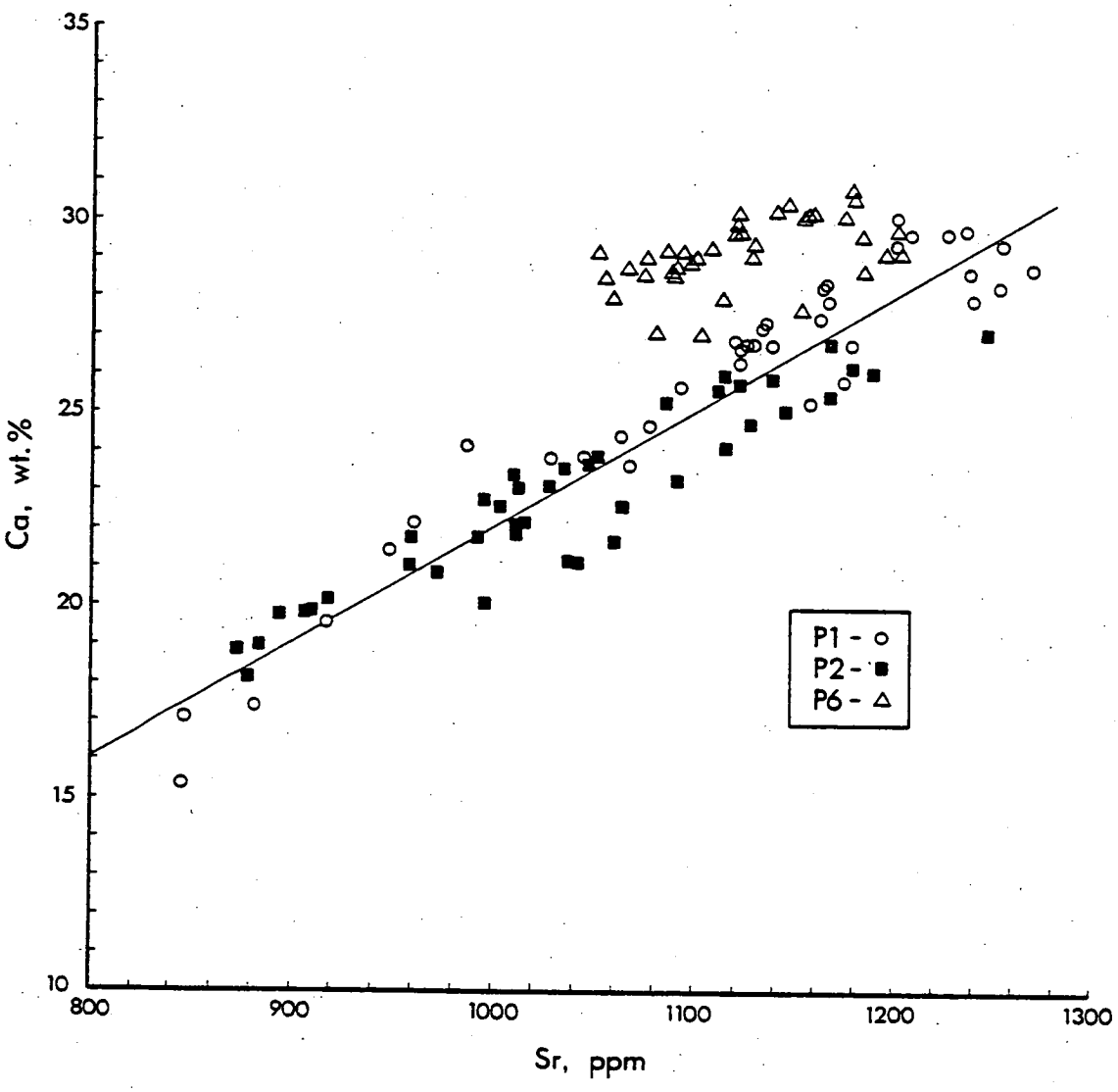

Fig. 5.5 Calcium versus strontium in the biogenic sediments, on a salt-free basis. The intercepts of the solid regression line are 220 ppm at 0 % $CaCO_3$ (0 % Ca) and 1600 ppm at 100 % $CaCO_3$ (40 % Ca).

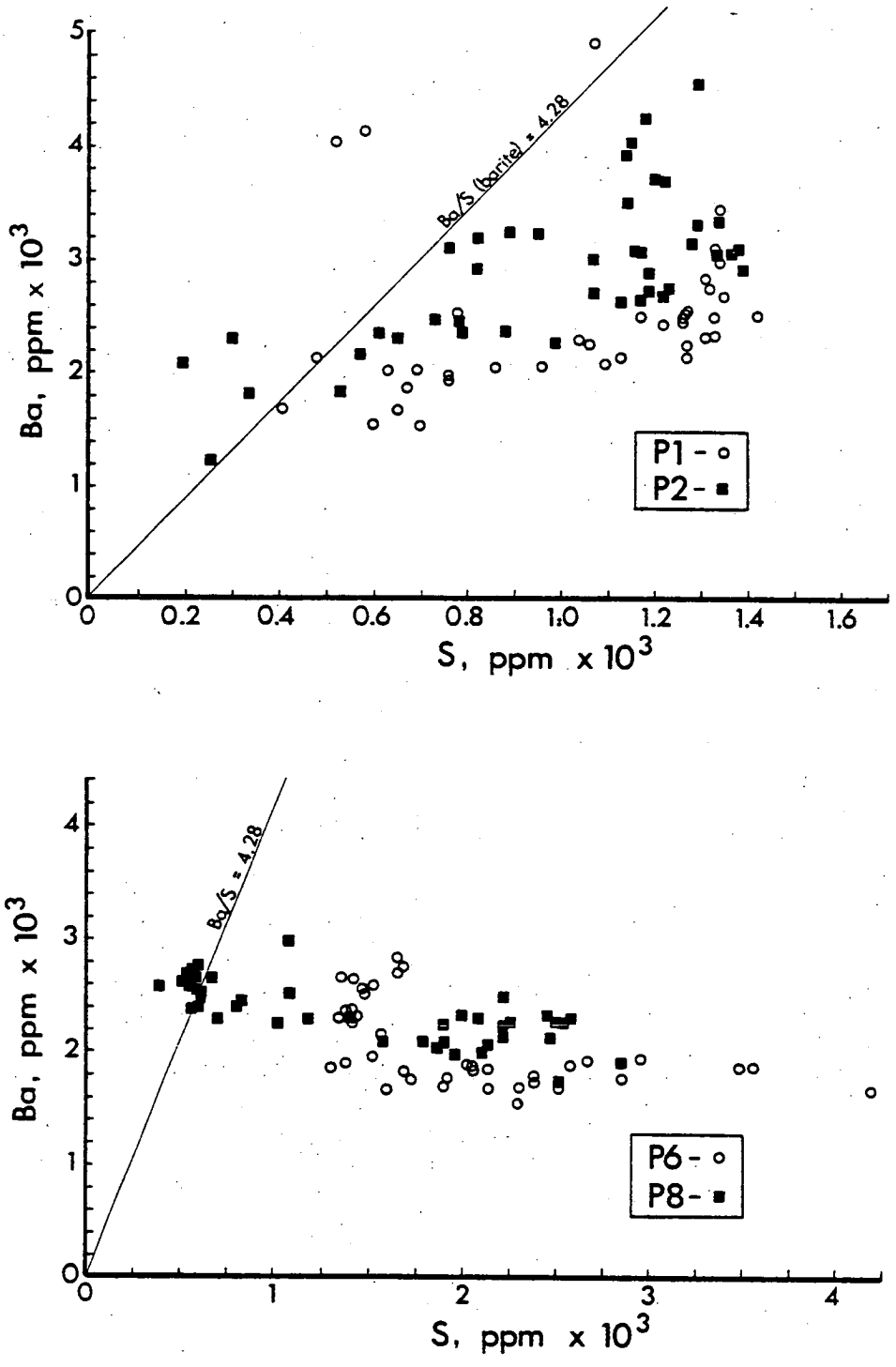

Fig. 5.6 Total Ba versus total S in Panama Basin area cores, on a salt-free basis. The solid line in both graphs represents the empirical Ba/S ratio in pure barite. Note that core P8 contains an estimated 500-700 ppm of lithogenous barium.

is more prevalent and where the reducing nature of the sediment has been well established support this suggestion.

The distribution of salt-free total sulphur in the cores is profiled in Fig. 5.7. The variable concentrations at depth in P6 and P8 indicate that sulphides are non-homogeneously distributed in these sediments. As the S/C weight ratio in non-degraded marine organic matter is about 0.02 (Kaplan et al, 1963) and since diagenetic processes will probably reduce this ratio in Basin sediments, organic sulphur is quantitatively unimportant to this discussion.

Iron sulphides are a common minor constituent of coastal and hemipelagic sediments, both oxidizing and reducing. If it is assumed that all the excess sulphur (over barite) in cores P1 and P2 (about 400-600 ppm) occurs as FeS and FeS_2, then only about 0.1-0.15% of iron sulphide minerals need be present. Such a minor concentration may well be produced in reducing microenvironments in oxidized surface sediments, for example within foraminiferal tests (Emery and Rittenberg, 1952; Kaplan et al, 1963). In the underlying reduced sediments sulphides probably occur as finely-dispersed aggregates.

The organic carbon peak at 60-80 cm depth in P6 (Fig. 4.2) must act as a locus of sulphate reduction since the "excess" sulphur concentration in this horizon is distinctly higher than elsewhere (Fig. 5.7). The absence of local depletion in the interstitial sulphate profile within this zone (Fig. 7.4) indicates that the rate of sulphate reduction must be less than the rate of diffusion.

Purely on the basis of the olive-green colour of the reduced sediment of all cores (Appendix A), pyrite may be the principal sulphide phase since dispersed iron monosulphide imparts a jet-black colour to sediments (Berner, 1970). Pyrite framboids were observed in clusters between botryoids and within cavities of manganous carbonate recovered

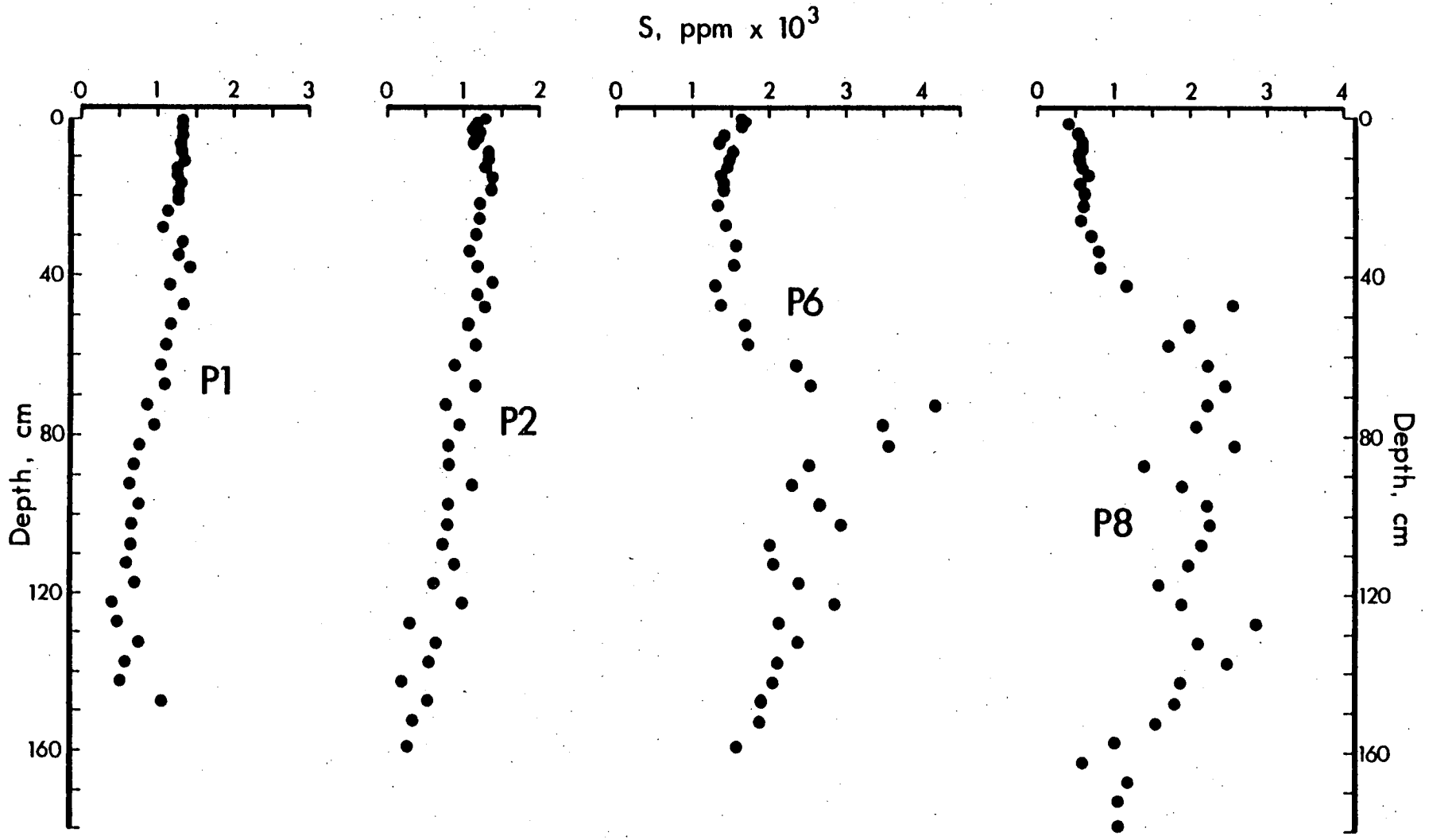

Fig. 5.7 Salt-free sulphur distributions in Panama Basin area cores.

from the ash horizon of core P8 (Plate 5.1(a).). The framboids are spheroid to ovoid and range in size from 5-20 μm (Plate 5.1(b).). High magnification scanning electron microscopy reveals that the framboids are typically composed of closely-packed euhedral octahedra about 0.5 μm in size (Plate 5.1(c).); in some spheroids tetrahedra(?) occur, as do individual crystals that appear to be obliquely-cut cubes.

Framboids are a common mode of occurrence of pyrite in both recent sediments and sedimentary rocks (Vallentyne, 1963; Love, 1967; Berner, 1971). They appear to develop from a number of centres of crystallization within a blob of monosulphide (Love, 1967); the crystals remain distinct as growth proceeds and may merge to a homogeneous whole at a later stage.

Energy-dispersive microprobe analyses of two framboids are listed in Table 5.4; iron and sulphur concentrations in both are stoichiometric with respect to FeS_2. In addition, cobalt, copper, zinc and manganese occur in detectable quantities. Although a calcium peak was observed in a qualitative scan, the element does not appear in the analysis since the EDS computer program which resolves the sulphide composition discriminates against lithophile elements. The presence of both calcium and manganese may well be due to the manganous carbonate substrate on which the framboids rest rather than the pyrite itself. The chalcophile elements Co, Cu and Zn have divalent ionic radii closely similar to that of divalent iron (0.72, 0.72, 0.74 and 0.74 Å respectively; Mason, 1966). Facile substitution of these elements for iron in the pyrite lattice probably produces the observed concentrations.

Plate 5.1

Scanning electron micrographs of pyrite framboids found with manganese-bearing carbonate in core P8.

(a) Framboid "colony" occurring on a botryoidal Mn-carbonate substrate.

(b) Higher magnification, showing framboidal aggregates of individual pyrite crystals.

(c) Detail of a single framboid showing closely-packed euhedral octahedra.

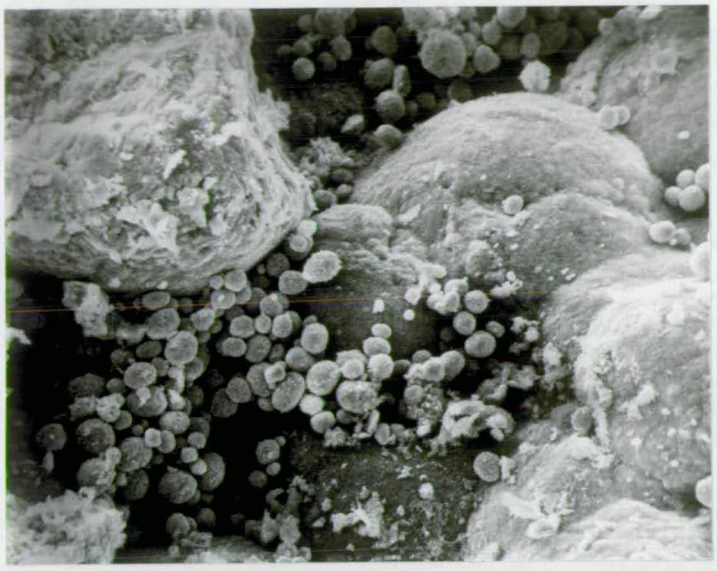

(a)

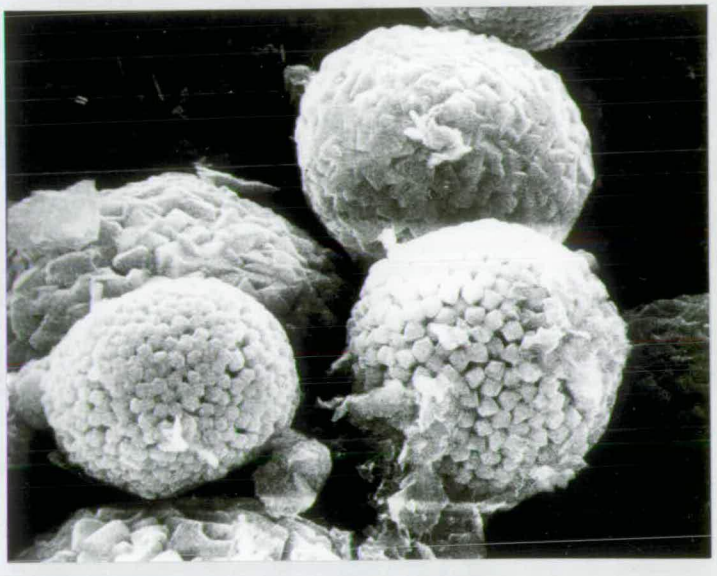

(b)

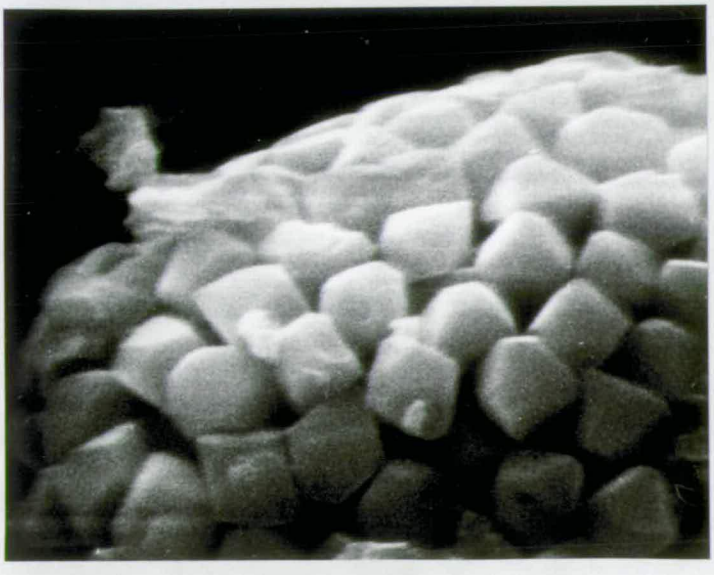

(c)

Plate 5.1

Table 5.4 EDS electron microprobe analyses of pyrite framboids in core P8, using a Cambridge Instruments Stereoscan IV Microprobe with a Link Systems energy-dispersive analyzer. Low totals are due to a poorly polished section. Fe and S in wt. %; other elements, ppm. At a detection limit of about 700 ppm, no nickel was found.

	(a)	(b)	Estimated Detection Limit
Fe	41.9	43.3	0.06
S	48.1	47.9	-
Mn	8400	6900	700
Co	4100	4500	700
Cu	1900	1600	900
Zn	3300	2500	1200
Total	91.8	92.75	

5.4 Molybdenum

Among the trace constituents investigated in this work, molybdenum alone is consistently and strikingly enriched in the surface layer of Basin area sediments with salt-free concentrations reaching almost 80 ppm (Table C.2). The directly-underlying reduced sediments have values of from several times to an order of magnitude lower, as can be seen in the profiles of Fig. 5.8. In the oxic surface layers molybdenum enrichments closely parallel the distribution of manganese (compare Fig. 5.8 with Fig. 4.16); at depth, however, while manganese is present only in evenly-distributed background quantities, Mo occurs in variable but significant concentrations. Mo/Mn ratios range from 0.8 to 3.0 [1] (average 1.6) x 10^{-3} in Basin surface sediments which is greater than manganese-rich East Pacific Rise sediments (Mo/Mn = 0.5 x 10^{-3}; Elderfield, 1977) but which brackets the Mo/Mn ratio in nodules of 2.55 x 10^{-3} (world average, Cronan, 1977).

The association of Mo and Mn is well known in oxic marine sediments

[1] Neglecting cores P5, P9, and P13 for which loss of the top of the core during coring is suspected.

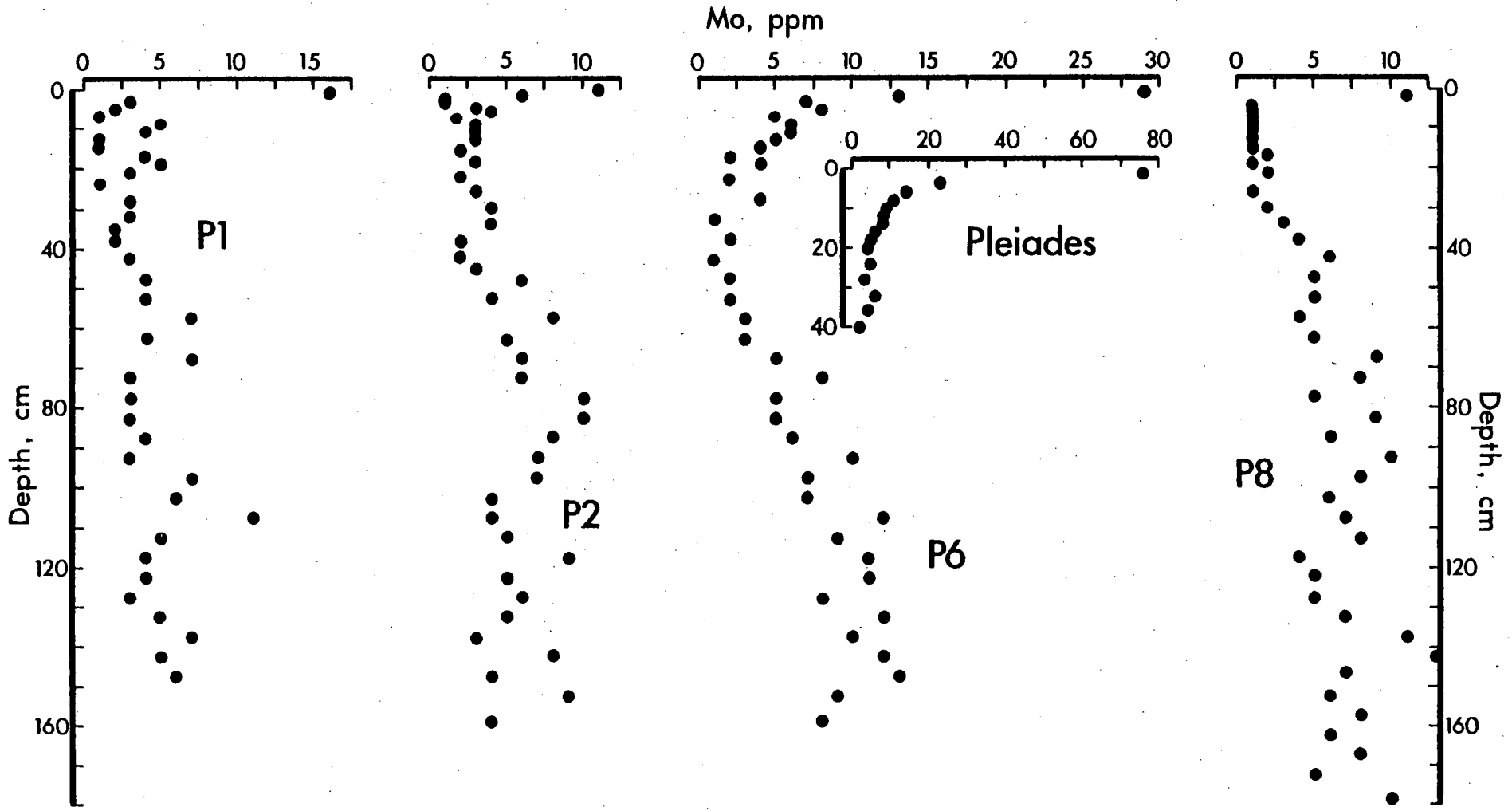

Fig. 5.8 Molybdenum distributions in Panama Basin area cores, on a salt-free basis. Note the different scale for the Pleiades box core insert.

from coastal to pelagic environments. Molybdenum is clearly adsorbed from sea water by hydrous manganese oxides (Krauskopf, 1956; Berrang and Grill, 1974) although the mechanism of adsorption of the typical molybdenum species, MoO_4^{2-}, by negatively-charged Mn oxides is difficult to explain (Murray and Brewer, 1977). In addition to anion adsorption, some of the molybdenum may occur as tetravalent cations substituting for Mn^{4+} in linked MnO_6 octahedra (Burns and Burns, 1977).

The molybdenum concentrations observed in the reducing zones of cores investigated here are obviously not due to the occurrence of oxides at depth - another phase must be controlling the distribution. It is known that anoxic sediments commonly incorporate molybdenum from sea water, primarily through coprecipitation of a thiooxymolybdate with iron monosulphide according to the reaction (Bertine, 1972):

$$FeS_{amorphous} + MoO_2S_2^{2-} + H_2S + 2H^+ = FeS \cdot MoS_3\ amorphous + 2H_2O. \quad (1)$$

With aging, the amorphous solid solution dissociates:

$$FeS \cdot MoS_3\ amorphous = FeS_{tetrag.} + MoS_3.$$

The variable but significant increase in molybdenum concentration with depth in all cores, coupled with the excess sulphur (over barite) content, suggest that reaction (1) above is active within all Panama Basin area sediments. Only very minor sulphide contents would be required to produce the observed Mo concentrations.

In a series of experiments, Bertine (1972) noted some dissolution with time of freshly precipitated MoS_3; hence it is possible that this phase may not be stable in sediments. Pilipchuk and Volkov (1968) suggested that molybdenum ousted from iron sulphides during aging was adsorbed by organic matter. However, the absence of such a Mo-organic carbon association in Panama Basin sediments is well demonstrated by

the sharp mid-depth carbon peaks of cores P1, P2 and P6 which have no correlative molybdenum enrichments. If MoS_3 is coprecipitated and then partly dissolved, the solubilized molybdenum may well be retained by sorption onto solid phases other than organic matter. This process would be enhanced by the reduction of Mo(VI) to cationic Mo(V) which occurs in the presence of humic acids (Szilagyi, 1967); Mo(V) has a very high susceptibility to sorption by almost any solid substrate.

The geochemical behaviour of molybdenum in all Panama Basin sediments can be explained by a simple qualitative model based on analogy with the distribution of solid and dissolved manganese in core P8. Initially, a surficial molybdenum enrichment is produced by sorption of the element from sea water onto manganese oxides. As the oxidizing Mo-enriched surface sediments are subsequently buried and reduced, Mo^{6+} and Mn^{2+} are released to pore water. Dissolution occurs rapidly within the top 20 cm of the sediment column. Concurrent minor reduction of sulphate below the oxic layer produces hydrogen sulphide in quantities sufficient to locally exceed the solubility product of FeS, and coprecipitation of Mo occurs with iron monosulphides as in reaction (1).

The model predicts that the pore water profile of dissolved molybdenum would resemble that of Mn^{2+} in core P8 where manganous carbonate precipitates at depth following dissolution of surficial oxides. Diffusion gradients for Mo^{6+} (or $MoO_2S_2^{2-}$) would be established in both positive (upward) and negative directions with the net result of upward recycling and reabsorption onto Mn oxides of a portion of the molybdenum; the remainder would diffuse downward and be sorbed or precipitated as sulphides at depth. The salient features of this system are summarized in Fig. 5.9.

An important implication of this hypothetical model is that it can explain the molybdenum enrichment observed in the bottom of marine

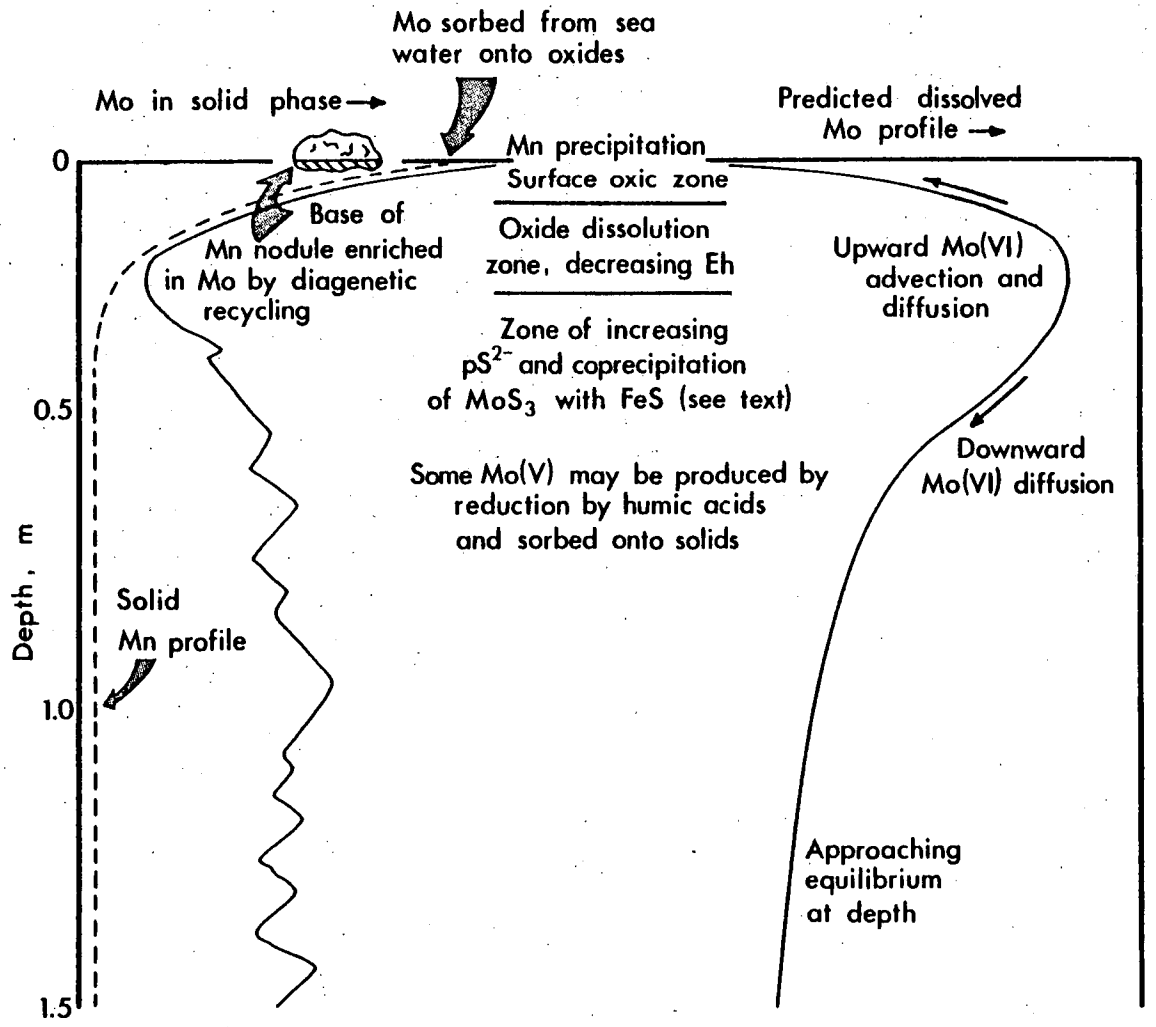

Fig. 5.9 Qualitative model hypothesized to explain the observed vertical molybdenum distribution in Panama Basin sediments.

manganese nodules (Raab, 1972) as being due to a diagenetic recycling process. It is quite plausible that other elements which are enriched on the underside of pelagic nodules may be subject in varying degree to similar diagenetic reactions as suggested by Calvert and Price (1977), especially in sediments proximal to the equatorial productivity belt.

5.5 Distribution of zinc and the transition metals Cr, Co, Ni and Cu

Geochemical diversity exists among zinc and the four minor transition metals investigated in this section. Manganese and iron oxides, biogenic detritus, terrigenous material, sulphides and organic matter have varying degrees of association with each element. Since some of the elements are strongly affected by post-depositional reactions and since their concentrations are often higher in the biogenic sediments, it is incorrect to examine the distributions on a carbonate-free basis. Consequently, element distributions discussed in this section are considered either on a salt-free basis or ratioed to aluminium; the latter ensures independence from dilution artifacts.

Cobalt, nickel, copper and zinc concentrations in all facies of the sediments studied here (Table 5.1) are up to several times higher than "average" contents in marine deposits. Although there is a paucity of comparative data available (especially for Zn), high concentrations of these transition metals appear to be characteristic of eastern equatorial Pacific sediments. For example, Bonatti et al (1971) found high concentrations of Ni, Co and Cu in biogenic Panama Basin sediments (Table 5.1) and Greenslate et al (1973) reported $CaCO_3$-free Ni and Cu concentrations averaging 450 (n = 13) and 380 (n = 12) ppm, respectively, in equatorial sediments west of the Galapagos Islands (100-120°W).

Average element : aluminium ratios for Co, Ni, Cu and Zn (Table C.2, p. 193) are substantially higher in the biogenic sediments of P1, P2 and P6 than in the clays of core P8, indicating that these elements are largely of non-lithogenous origin in the former sediments. In contrast, average Cr/Al ratios are of similar magnitude in all Basin sediments, suggesting that chromium is associated primarily with the terrigenous fraction (with one exception, discussed below). The distribution of each element in the four cores studied is displayed in the profiles of Fig. 5.10 to 5.14. Chromium alone is normalized to aluminium to avoid dilution effects.

Distribution in near-surface sediments

On a more detailed level, cobalt and nickel are similarly distributed in all cores. Both elements are enriched in the oxide layer of the biogenic sediments and both show roughly parallel variable concentrations at depth.

The decreases with depth of Ni and, to a lesser extent, cobalt in the upper 20 cm of the carbonate sediments apparently follow the ubiquitous decrease in manganese concentration (Chapter Four). Such a distribution points to the well known association of nickel and cobalt with manganese in sediments (Turekian and Imbrie, 1966; Carvajal and Landergren, 1969) and nodules (Aumento et al, 1968; Calvert and Price, 1970a). Copper and zinc also appear to be enriched in the biogenic surface sediments (Figs. 5.12 and 5.13) although not to the same extent as cobalt and especially nickel. In contrast to the other cores, the surficial sediments of P8 show no transition metal enrichments (with the possible exception of cobalt).

In order to clarify these distributions, it is necessary to examine three processes which bear on transition metal geochemistry: metal release at or near the sediment-water interface by dissolving

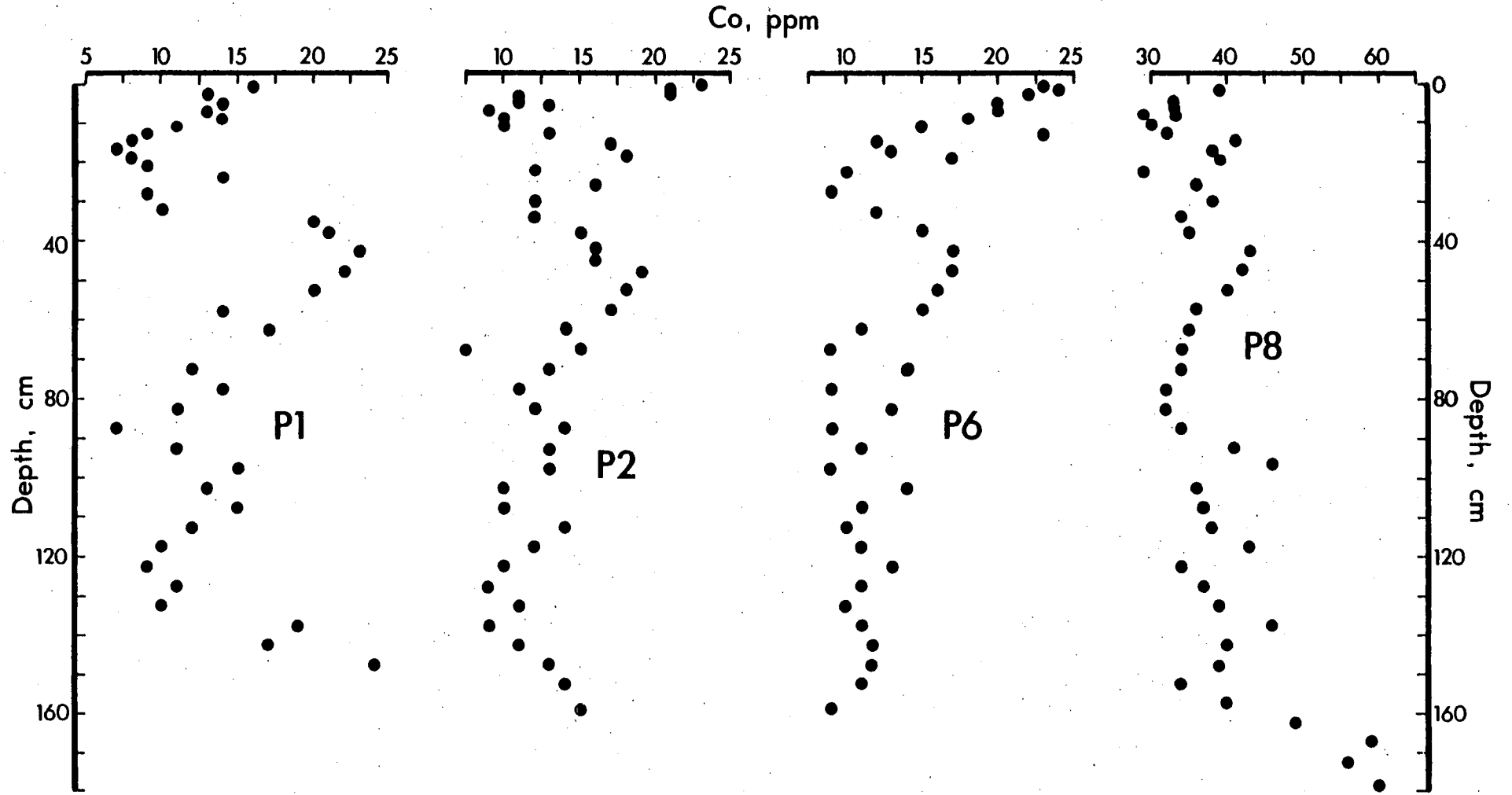

Fig. 5.10 Cobalt distributions in Panama Basin area cores, on a salt-free basis.

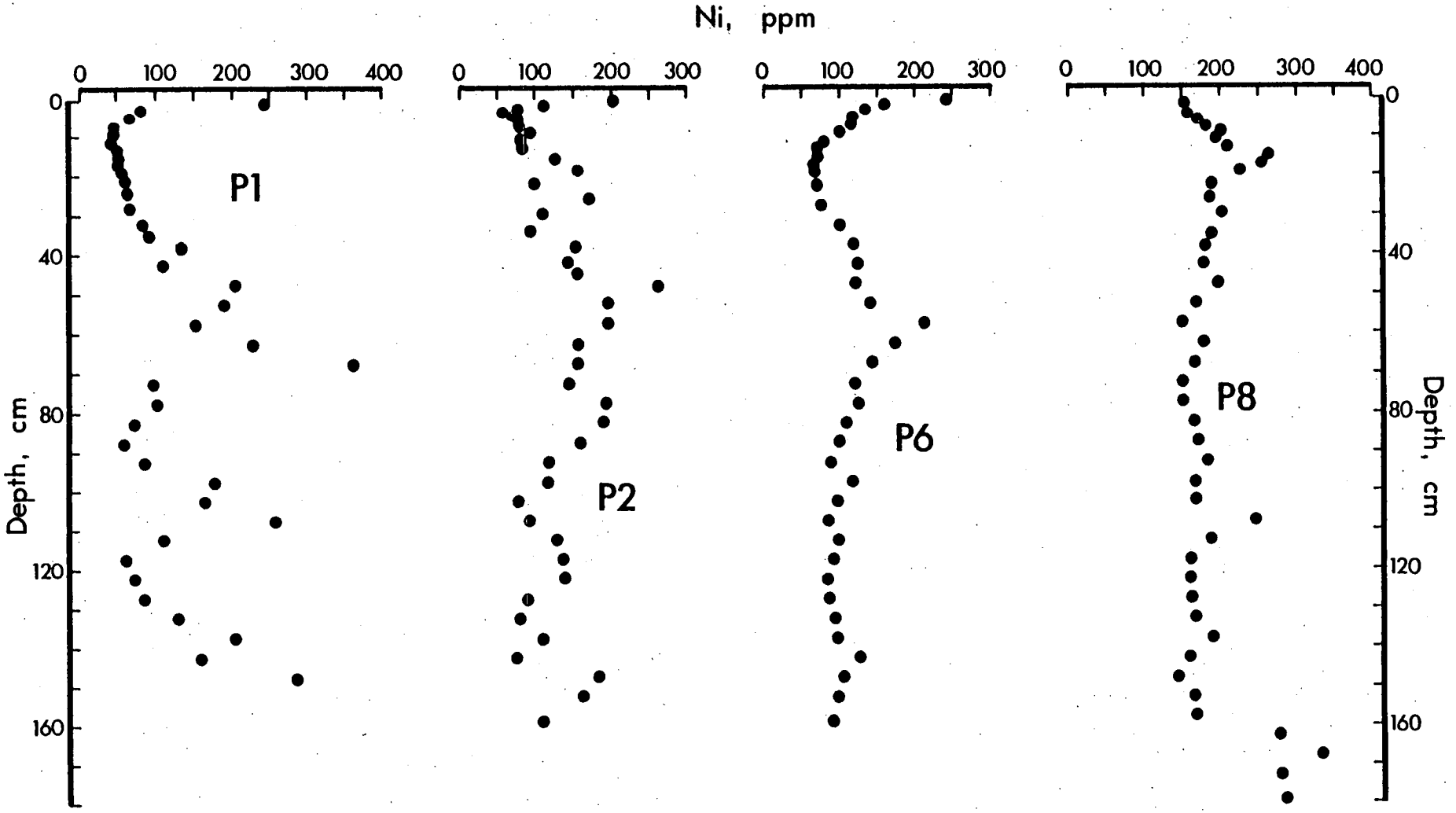

Fig. 5.11 Nickel distributions in Panama Basin area cores, on a salt-free basis.

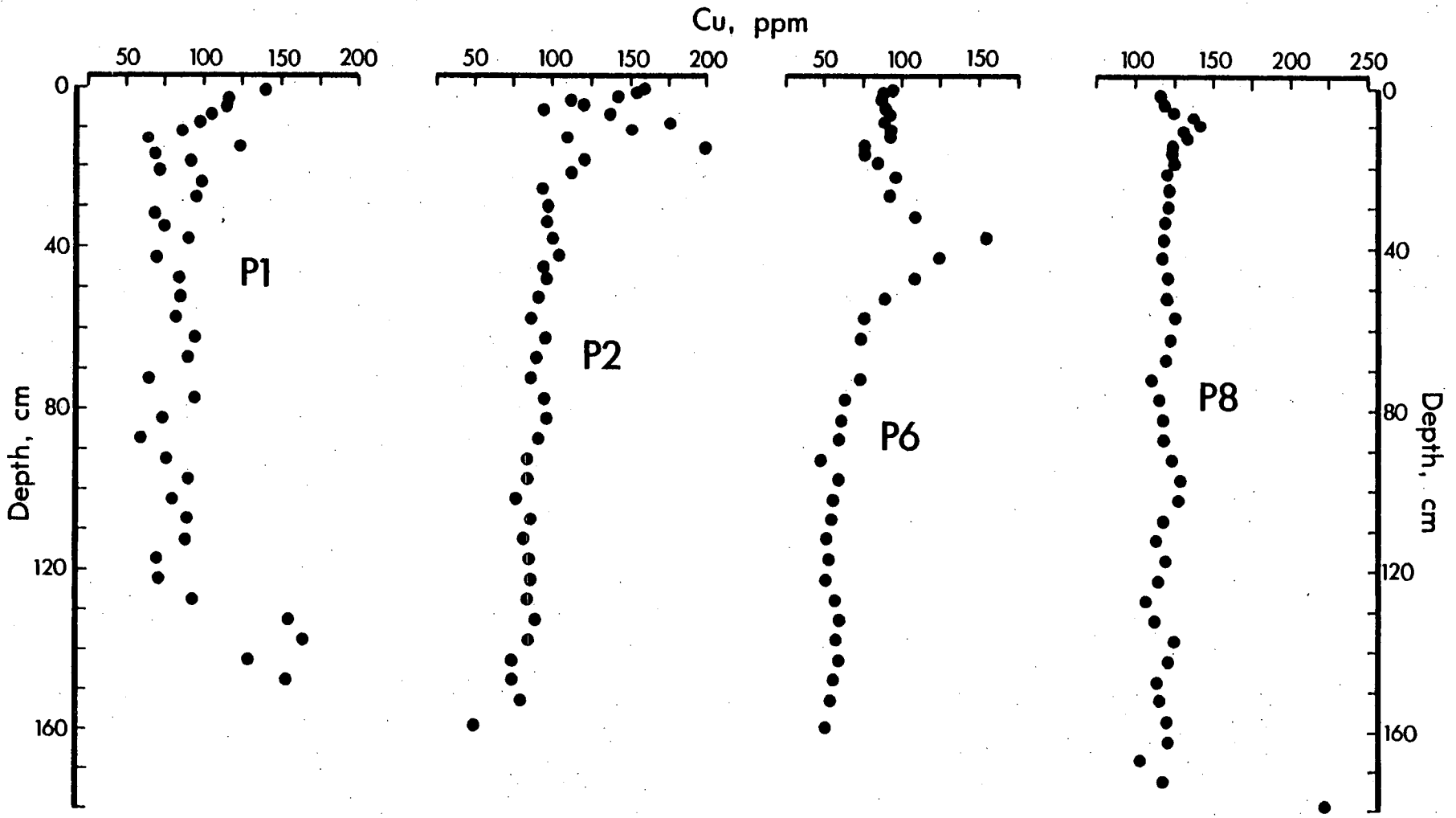

Fig. 5.12 Copper distributions in Panama Basin area cores, on a salt-free basis.

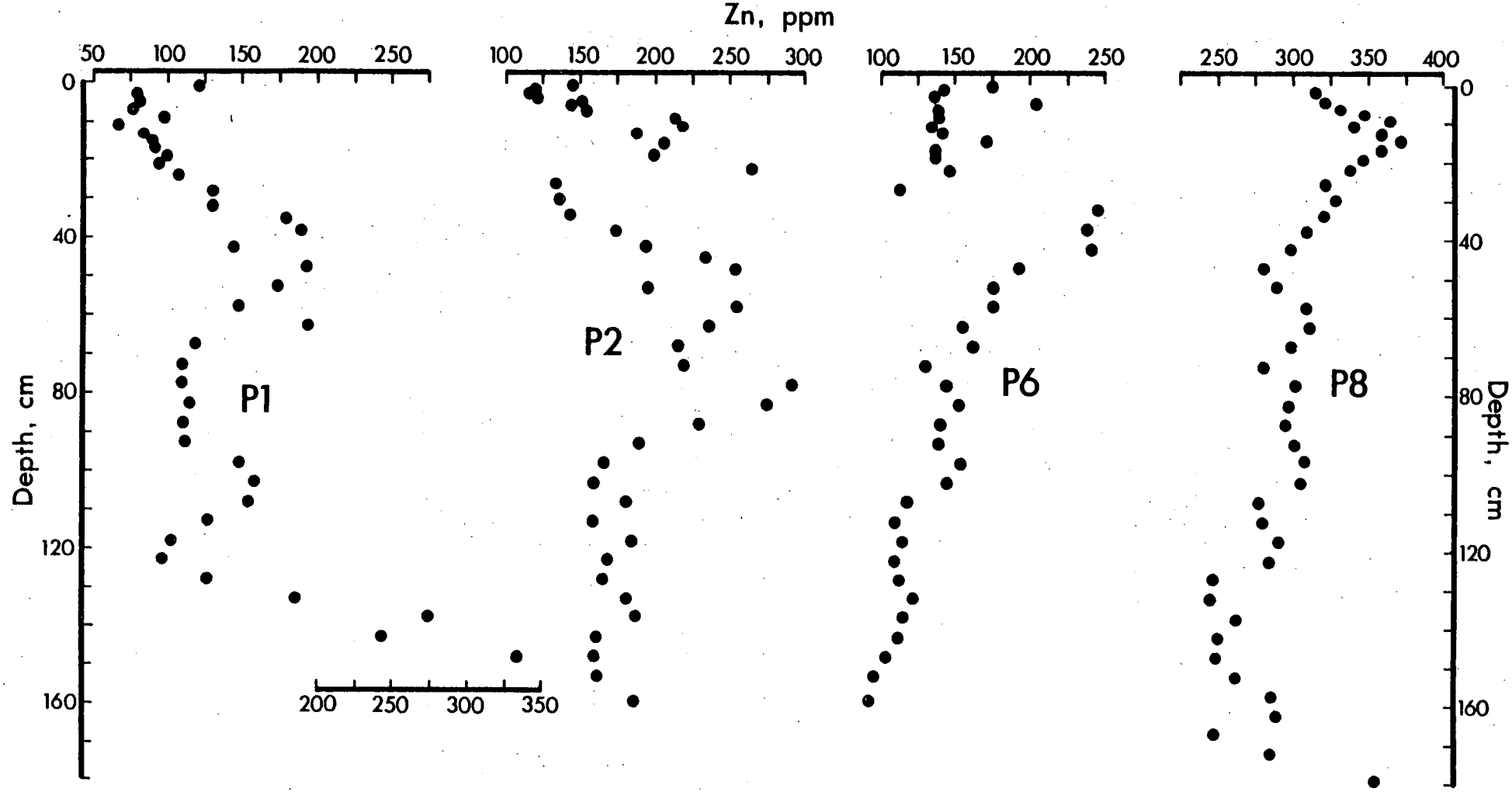

Fig. 5.13 Zinc distributions in Panama Basin area cores, on a salt-free basis.

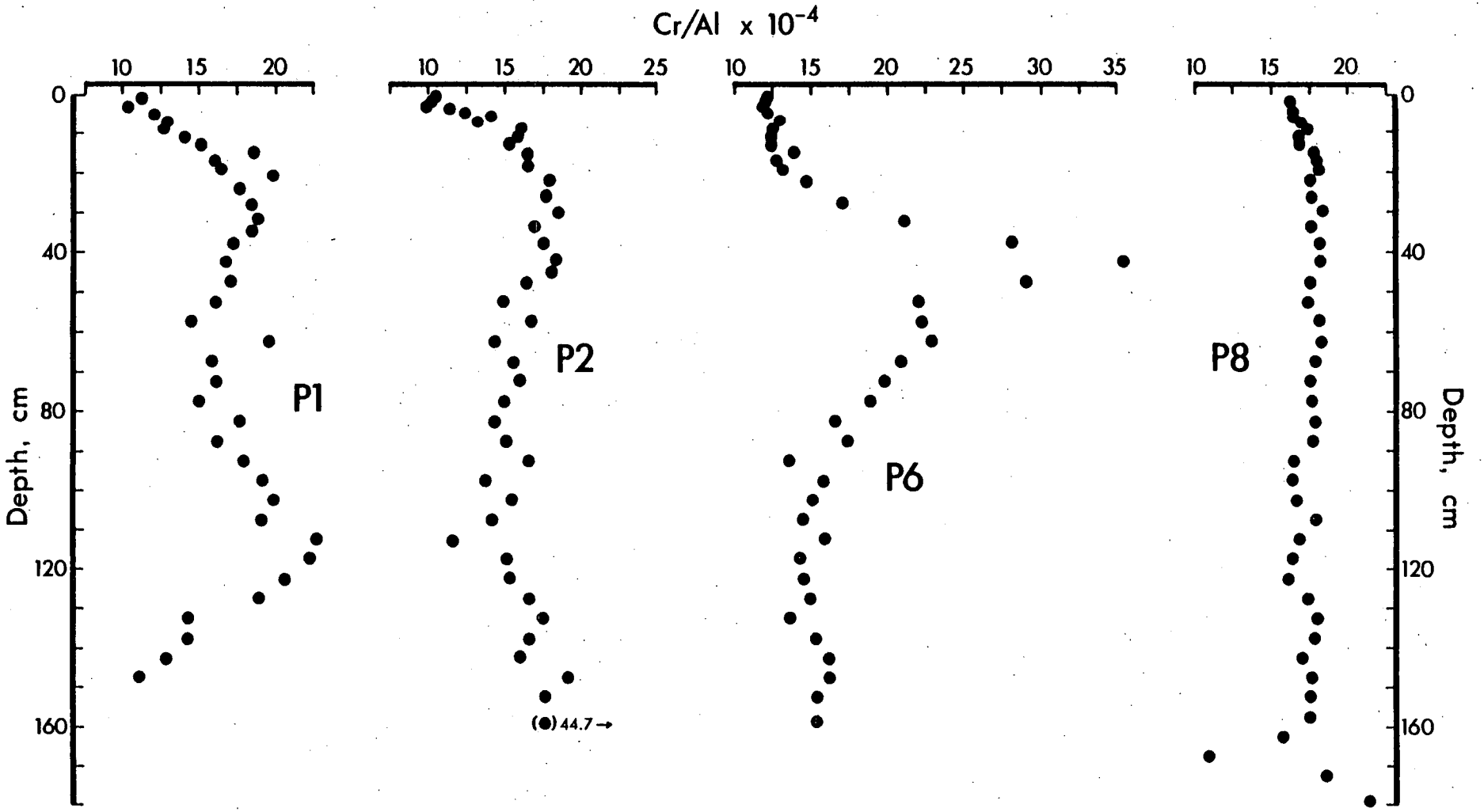

Fig. 5.14 Cr/Al profiles in Panama Basin area sediments.

particles, manganese oxide absorption and chelation by organic ligands. These will be outlined in turn.

Recent work has provided increasing evidence that biological vectors play an important role in transporting certain elements to the sea-floor. Sclater et al (1976) and Bruland et al (1978) have respectively demonstrated that Ni and Zn distributions in the open ocean water column follow that of Si. Boyle et al (1977) have shown that Cu is actively removed in the mixed layer, scavenged by particles in deep water and apparently released at or just below the sediment surface. Their observations are supported by sharp increases in dissolved Cu in pore waters of the upper centimetre of oxic pelagic Pacific sediments (Callender, 1976). Cobalt is enriched in phytoplankton (Bowen, 1966) and is probably released throughout the water column and on or near the sediment surface in a similar manner to the other metals. It should be noted that other sources of transition metals and zinc may exist in addition to biota, e.g. iron and manganese oxide colloids and coatings on particles. The important point here, however, is that unlike metals sorbed onto oxides which are released only in the presence of low Eh, release from biological materials occurs under typical oxidizing potentials.

Negatively-charged hydrous manganese oxides have a known absorptive affinity for divalent cations. The selectivity sequence (in manganese nodules, relative to sea water) is apparently Co $\geqslant$ Mn > Fe >Ni > Cu > Zn (Murray and Brewer, 1977) although Murray (1975) experimentally determined the sequence Co $\geqslant$ Mn > Zn > Ni. Oxic, biogenic Panama Basin sediments conform most closely to the former order.

The third feature to be considered is the chelation of trace metals by organic matter, which is of demonstrable importance in some sediments (Volkov and Fomina, 1974; Calvert and Price, 1970b). The stability

sequence which governs such associations is widely regarded to follow the order Mn < Fe < Co < Ni < Cu > Zn for all organic ligands (Irving and Williams, 1953).

In attempting to understand the metal distributions observed in the near-surface sediments, it is necessary to consider the MnO_2 selectivity sequence and the Irving-Williams order in concert. Metals released at the sediment surface by decomposing biota may be either adsorbed by the oxide component or chelated by organic matter depending on the relative affinity (at present unknown) of the two phases. In the Galapagos area surface sediments (P1, P2 and P6), the oxide phase appears to be more important than organic matter as a zinc and transition metal host. This statement is supported by the low metal concentrations observed in the oxide-free sample P5:0-1.5: (Table C.2, p.192). In contrast, oxides appear to have little importance in incorporating transition elements into near-surface sediments of the Eastern Basin. Since organic carbon concentrations are considerably higher in these sediments it is possible that chelation of metals by the organic phase may be significant here. This is very difficult to evaluate, however, as the proportion of Co, Ni, Cu and Zn in the lithogenous fraction is unknown. The concentrations of these elements are very high which suggests that enrichment has occurred but, equally, the smectites which dominate the sediments may host substantially greater metal contents than does, for example, "average" shale.

Two additional factors pertain to the contrast in transition metal distributions between the two sediment facies. Firstly, it is well known that coastal marine ferromanganese nodules contain lower transition metal concentrations than their pelagic counterparts. The difference has been ascribed to the relatively rapid accretion of the former nodules which kinetically inhibits metal adsorption (Price, 1967). In

the Panama Basin, surficial manganese oxides in the rapidly-accumulating terrigenous sediments must have a much shorter "residence time" than oxides in the Galapagos area; this may bear on the apparent lack of association with adsorbed transition elements in the former facies.

Secondly, the higher C_{org} content of Eastern Basin sediments probably produces a higher dissolved organic carbon (DOC) concentration in pore waters. Metals released from biological sources near the surface may be complexed by organic ligands in solution, inhibiting element adsorption by the oxide component. The Galapagos area sediments probably contain less DOC since their lower sediment accumulation rate allows a greater oxidative loss, especially of the labile fractions, near the sediment surface.

Distribution below the oxic surface layer

One of the most pronounced features at depth in the sediments is the association of transition metals with the metalliferous horizon in core P6. Each of the five elements (Co, Ni, Cu, Zn and Cr) is enriched to some degree in the zone (Figs. 5.10 to 5.14). It is not directly possible to determine whether metals were coprecipitated with iron (and Mn ?) during the hydrothermal event which produced the Fe-rich horizon (Chapter Four) or were subsequently scavenged. The chromium distribution gives some clue, however.

It is known that chromium, unlike the other elements, is not enriched in ferromanganese nodules (Cronan, 1977) but it does occur in high concentrations in crestal sediments of the East Pacific Rise (Böstrom and Peterson, 1966). This fractionation suggests that the EPR chromium is of hydrothermal rather than sorptive origin and implies that the high Cr content in the iron-rich band of P6 resulted from coprecipitation with iron from hydrothermal solutions. It follows that the other metal enrichments may have had a similar source, albeit

post-precipitation adsorption may also have been important. Although iron hydroxides are less effective than MnO_2 in scavenging transition metals at sea water pH (Murray and Brewer, 1977), cobalt, for example, may be adsorbed from solution if a very high oxidizing potential exists. In such conditions Co(II) will oxidize to Co(III) which may substitute for Fe(III) in the $FeOOH \cdot 2H_2O$ phase (Burns, 1965).

The nickel profile for core P6 suggests that, unlike any of the other metals, a portion of the nickel may be associated with the organic carbon peak at 60 cm depth (Fig. 4.2), i.e. immediately underlying the metalliferous horizon. The salt-free Ni concentration increases by about 90 ppm from 47.5 to 57.5 cm depth and is accompanied by a 1% increase in organic carbon. It is doubtful that sulphides are significant as a host phase for nickel in this stratum since the sulphur concentration in excess of barite requirements is only 1300 ppm. If this occurred entirely in pyrite an implausible concentration in the sulphide of 35000 ppm Ni would be required to account for the nickel increase whereas recent sedimentary sulphides contain little more than 3000 ppm Ni (see, for example, Calvert, 1976, p. 212; Volkov and Fomina, 1974, p. 470; and Table 5.4 where Ni < 700 ppm). The nickel enrichment is more likely to be directly related to the organic carbon increase. Since fresh marine plankton contains an average of only ~10 ppm Ni (Presley et al, 1972; Martin and Knauer, 1973) the 90 ppm excess must have been sorbed from solution onto the organic phase. Humic material is known to have a very large sorption capacity for metals, including nickel (Swanson et al, 1966; Szilagyi, 1967).

There is no apparent explanation why nickel should be singularly associated with the organic horizon in the core. The absence of other metal enrichments in the band is especially puzzling considering that the Ni-organic complex is less stable than those for Cu and Zn.

The partitioning and inter-element relationships of Co, Ni, Cu, Zn and Cr in cores P1 and P2 are less well defined than in P6 and are accordingly more difficult to explain. Comparison of Fig. 4.2 with the profiles of P1 and P2 in Figs. 5.10 to 5.14 suggests that at depth, Co, Ni and Zn concentrations may be positively related to the organic carbon content. Chromium and copper, in contrast, are apparently unassociated with organic matter and show little covariance with the other metals. The independent distribution of Cr is expected since it occurs almost entirely in the terrigenous fraction as demonstrated earlier (p. 75). Unlike similarly constrained minor elements such as Rb, however, it apparently has no strong association with a major lithogenous element.

A major feature evident in core P1 is the large increase in transition metal concentrations below 120 cm depth. At the base of the core, nickel, cobalt and copper contents reach levels similar to their respective maxima in overlying horizons whereas zinc is enriched to an even greater degree than elsewhere in the core. Only a minor proportion of these basal increases can be attributed to a greater contribution from the lithogenous component (indicated by the sharp rise in aluminium content below 120 cm, Table C.2, p. 195). Since the organic carbon content is also greater in this zone (Fig. 4.2), there may be a metal-organic association which can account for much of the "excess" transition element content, even though the carbon increase is proportionately less than those of the metals. This interpretation, however, is hampered by the termination of the core within the metal-rich horizon rather than below it.

If organic matter is a major host for transition metals in both P1 and P2, a special post-depositional enrichment process must have been operative to produce the unusually high metal/C_{org} ratios. Such

a mechanism can be postulated by analogy to the molybdenum model discussed earlier. This theory has three important features: (a) the transition elements Co, Ni, Cu and Zn are transported to the sea-floor by biological vectors; (b) resolution of much of the biologic detritus at or near the sediment surface creates an environment conducive to substantial uptake of metals by manganese oxides in the upper few centimetres of the sediments; and (c) subsequent dissolution of the manganese phase upon burial releases large quantities of the four elements to interstitial water which drives the reaction,

$$\text{Metal}^{2+}(aq) + 2RCOO^{-}(\text{reactive organic matter})(s) \rightarrow \text{Organometallic complex}(s)$$

(where R is a carbon chain) to the right. Sediment horizons rich in organic matter can therefore become enriched in certain metals as a consequence of post-depositional activity.

It is important to note that this proposed enrichment process is entirely contingent upon the initial concentration of metals by MnO_2 and their subsequent release to interstitial solution where lower oxidizing potentials prevail. In wholly anoxic sediments, therefore, lower metal/C_{org} ratios should be expected since the surficial manganese phase ultimately responsible for creating high dissolved metal concentrations in pore water is absent.

The apparent lack of association of copper with organic material in P1 and P2 is not inconsistent with the hypothesized model since CuS is by far the least soluble of the transition metal monosulphides ($K_{sp} \simeq 10^{-45}$); dissolved uncomplexed copper would therefore be most susceptible to rapid removal from pore water in the presence of even small quantities of HS^{-}.

CHAPTER SIX

HALOGEN DISTRIBUTION

6.1 Introduction

Sediments are known to play an active role in determining the concentrations in the sea of a great number of elements, but for many of these the geochemical processes involved are poorly known. The geochemistry of iodine and bromine, for example, has been investigated in some shelf and marginal sea deposits but little is known about the behaviour or distribution of either element in hemipelagic facies.

The occurrence of high concentrations of iodine in near-shore and continental margin sediments has been reported in several studies (e.g. Vinogradov, 1939; Shishkina and Pavlova, 1965; Price et al, 1970; Pavlova and Shishkina, 1973; Price and Calvert, 1973). In oxidized surface sediments the concentration of this element has been found to be directly proportional to the organic carbon content. Thus, oxic sediments underlying areas of high primary productivity are characteristically enriched in iodine.

Similar enrichments for bromine associated with organic carbon have been noted in Barents Sea (Vinogradov, 1939; Price et al, 1970) and Namibian Shelf surface sediments (Price and Calvert, 1977). Unlike iodine, however, the relationship $[Br] = k\,[C_{org}]$ appears to be independent of the surface sediment redox potential.

Iodine and bromine concentrations have been shown to generally decrease with increasing depth of burial in sediments undergoing early diagenesis (Shishkina and Pavlova, 1965; Pavlova and Shishkina, 1973; Price and Calvert, 1977). The iodine decrease is accompanied by a more gradual fall in the organic carbon content and by an increasing iodine concentration in interstitial water (Pavlova and Shishkina, 1973). A similar increase might be expected for bromide in pore water; however the screening effect of the relatively high concentration of sea water bromide would render it difficult to detect such an enrichment.

In this chapter the distributions of iodine and bromine in hemipelagic Panama Basin area sediments and iodine distribution in the pore waters of two Basin cores are discussed. In addition, the historical variations in organic carbon input described in Chapter Four are used to assist in resolving contrasts in the post-depositional behaviours of the two elements. Analytical methods are fully described in Appendix B and the results of all analyses are listed in Appendix C.

6.2 Iodine and bromine distribution in Panama Basin area sediments

Iodine concentrations vary considerably in Panama Basin area surface sediments, ranging from 76 to 861 ppm while bromine values range from 11 to 287 ppm. The concentrations of both elements are plotted against organic carbon in Fig. 6.1. Of the two well-segregated clusters of points on the graphs, one corresponds to the biogenic sediments of the Galapagos Platform area and Western Basin, which are relatively depleted in halogens and organic carbon, while the other represents the organic carbon and halogen-enriched sediments of the Eastern Basin. As explained in Chapter Four, the sediment accumulation rate in the Eastern Basin is high, thereby preserving a greater fraction of the carbon input which, in turn, appears to be associated with higher halogen contents in the sediments. Unfortunately, the lack of data points in the 1-2% C_{org} range in Fig. 6.1 reduces, to some extent, confidence in the halogen-C_{org} correlations. Even so, regression lines for both elements have slopes which are very similar to those for Barents Sea surface sediments (Price *et al*, 1970): Panama Basin, $I/C_{org} = 395$, $Br/C_{org} = 146$; Barents Sea, $I/C_{org} = 380$, $Br/C_{org} = 120$ (all x 10^{-4}). This consistency demonstrates that the relationships previously observed for shelf sediments probably apply equally to hemipelagic areas.

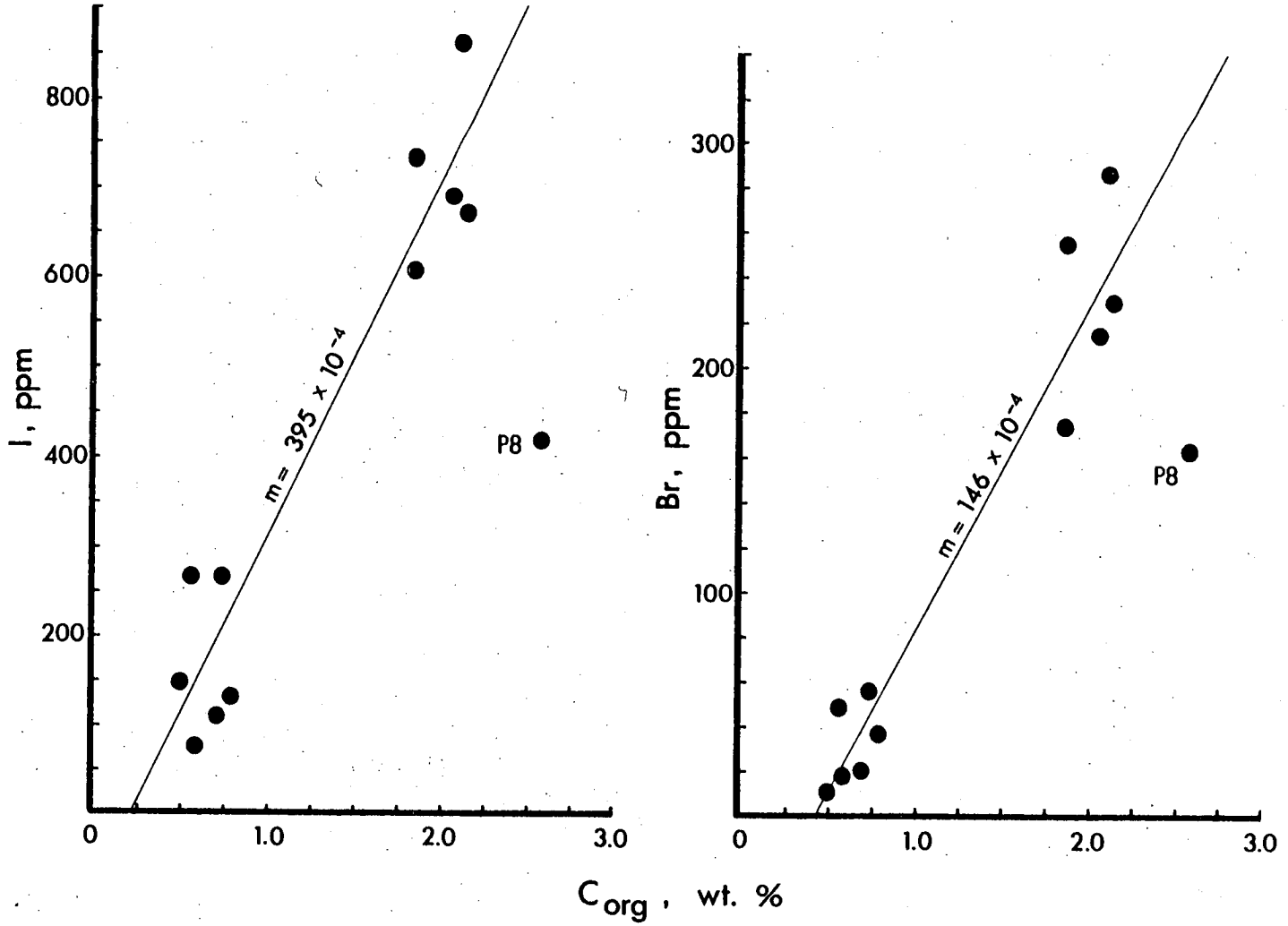

Fig. 6.1 The relationship between salt-free iodine, bromine and organic carbon in Panama Basin area surface sediments. Sample P8:0-4: was omitted from the regression calculations since it deviates strongly from linearity. This deviation may be due to the presence of reworked, relatively refractory carbon in the core (Chapter Four).

Profiles of salt-free iodine and bromine distributions with depth are displayed in Fig. 6.2 and 6.3 respectively. Both elements are enriched in the surface sediments of all cores, although the magnitude of the iodine enrichment is considerably greater. The extent of the iodine enrichment relative to bromine can be gauged by comparing the I/Br ratio in surface sediments (~3) with that in sea water (8.5×10^{-4}). On this basis the addition of iodine to the sediments from sea water is favoured over bromine by a factor of 3.5×10^{3}.

A striking feature common to the three carbonate cores (P1, P2 and P6) is the sharp three-fold increase in iodine and the nearly six-fold increase in bromine contents at 40-80 cm depths in the sediments, relative to the minima seen at ~20 cm in each case. Less obvious increases in the iodine content occur lower in the cores at depths of 110-145 cm. Iodine peaks here are subtle, but the opposite is true for bromine; concentrations of this element in the lower horizons (110-145 cm) are nearly equal to those seen between 40 and 80 cm in each core. In all three instances, variations in the concentrations of both elements broadly parallel the organic carbon profiles (Fig. 4.2).

Core P8 differs from the others in lacking well-defined carbon, iodine and bromine maxima at depth. Nevertheless, a minor iodine increase at ~30 cm is associated with a similar increase in carbon content. Variations in bromine concentrations in this core are clouded by some scattering of the data which has been mainly introduced by the large interstitial salt correction.

6.3 Dissolved iodine distribution

Iodine in sea water exists almost entirely as iodate and iodine (Sugawara and Terada, 1957). Thermodynamic calculations show that iodate is the stable ion at the pE (~12.5) of normal oxygenated

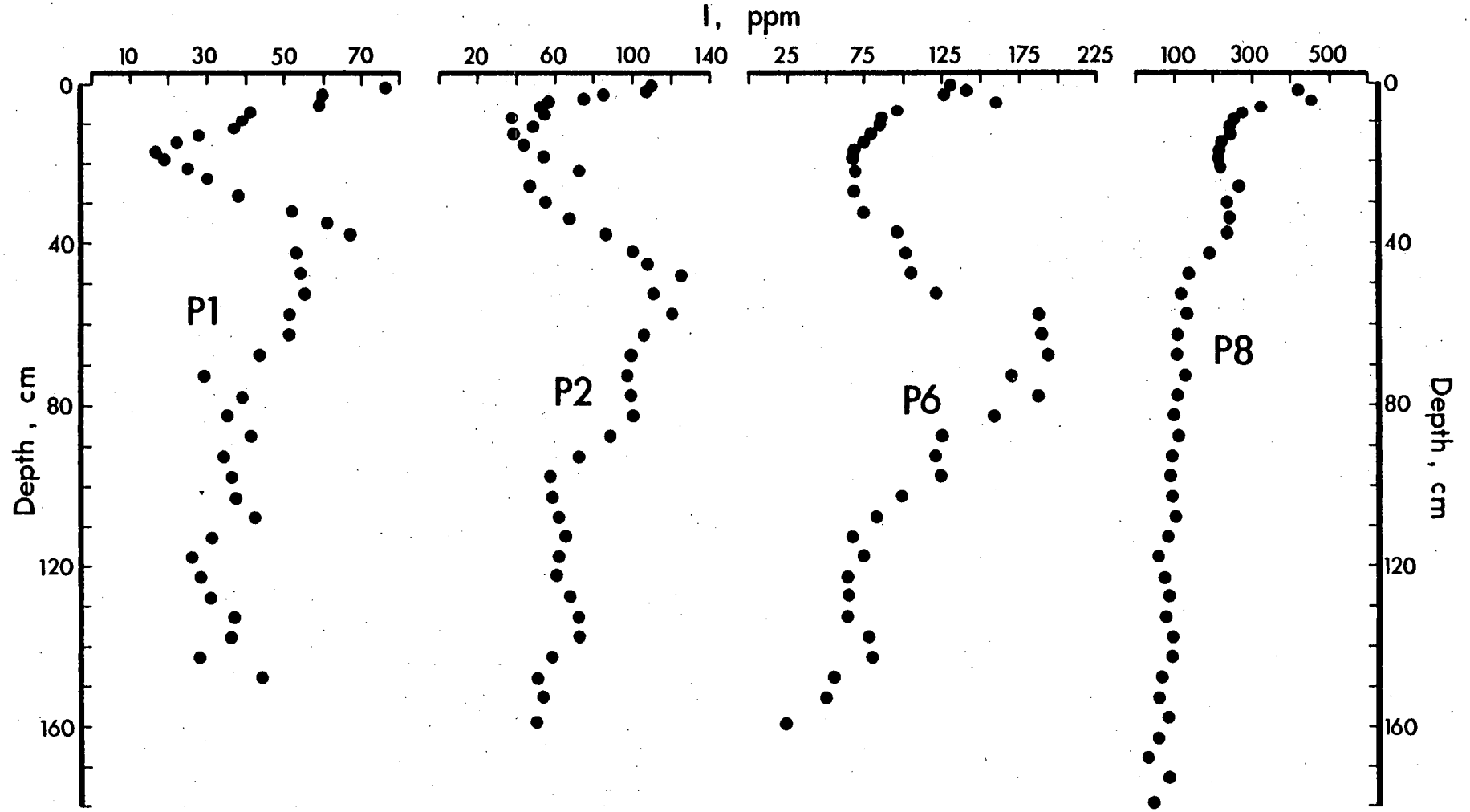

Fig. 6.2 Iodine distributions with depth in Panama Basin area sediments, on a salt-free basis. Note the differing scales on the abscissae.

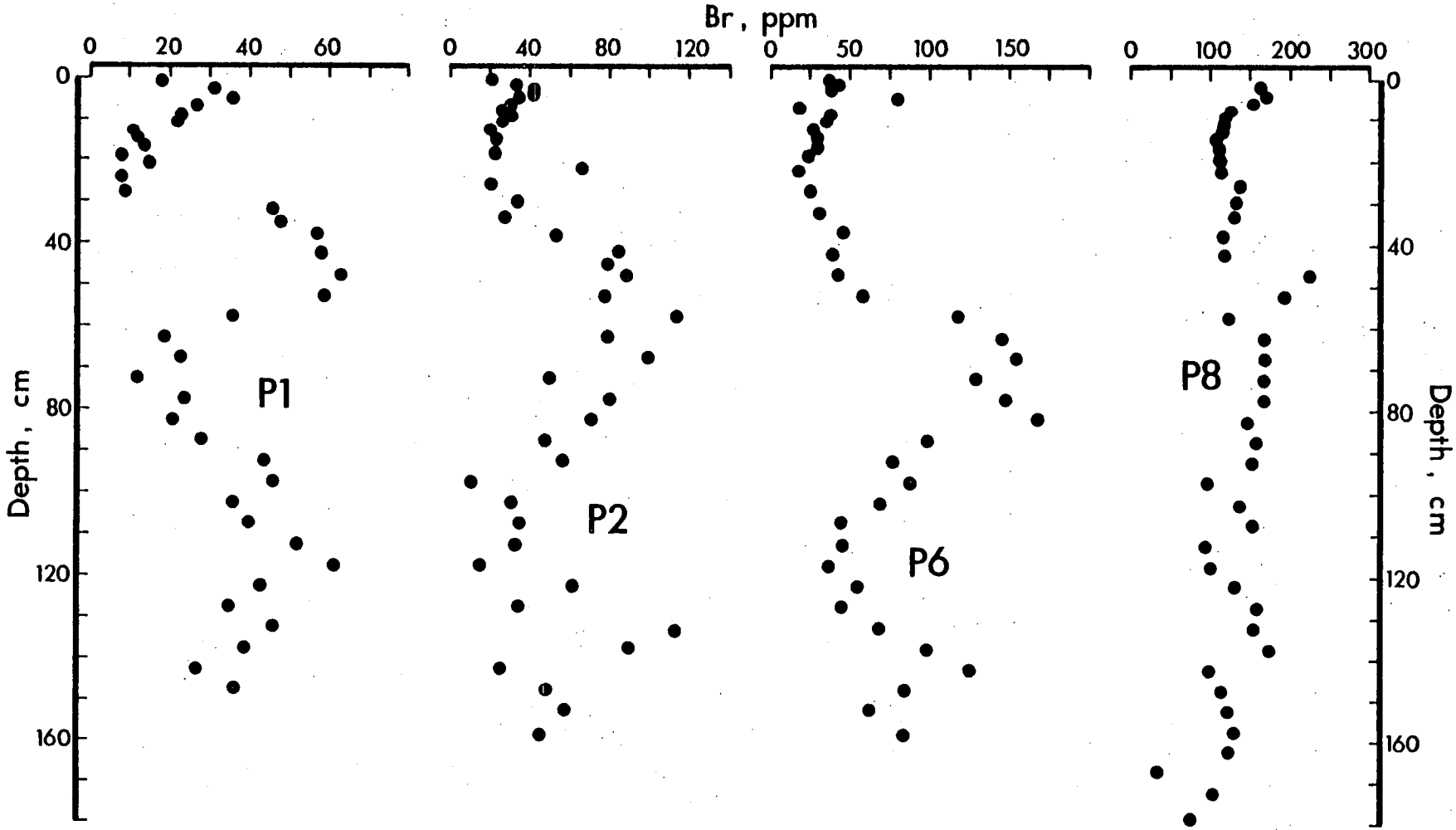

Fig. 6.3 Bromine distributions in Panama Basin area sediments. Note the differing scales on the abscissae. The increased scatter compared to the iodine profiles is probably due to the large corrections applied for salt bromine.

sea water (Sillén, 1961) but recent work has demonstrated that iodide predominates in anoxic conditions (Wong and Brewer, 1977).

In this study, the pore waters of two cores (P6 and P8) were analyzed for both iodine species. At a detection limit of ~0.06 μM IO_3^-, no iodate was found in either core, even in the core top interstitial water samples. Hence, "total dissolved iodine" as used here denotes the analyzed iodide concentration. The analyses are plotted in Fig. 6.4 and listed in Appendix C (Table C.3).

Interstitial waters of both cores are enriched over the average deep ocean total iodine concentration of 0.44 μM (Tsunogai, 1977; Wong and Brewer, 1974) by a maximum factor of ~20 for core P6 and ~3.6 for P8.

The profiles differ sharply. Core P6 is characterized by a broad linear increase in total iodine concentration to a maximum 9.2 μM between 60 and 80 cm depth followed by an exponential decrease to the bottom of the core. In contrast, the dissolved iodine concentration in P8 increases rapidly in the upper 20 cm and appears to gradually approach an equilibrium value with increasing depth. A maximum concentration of 1.58 μM is reached at the base of the core.

6.4 Uptake and diagenesis of the halogens

A possible mechanism of iodine uptake by organic matter has been outlined by Price and Calvert (1977), but little is known about bromine absorption. It is well known that marine organisms concentrate iodine and bromine from sea water often to levels of 200-300 ppm (e.g. 300 ppm I in diatoms; Bowen, 1966). Some algae such as Laminaria sp. contain up to 10,000 ppm I. The concensus of most workers is that iodine is absorbed as iodide and the degree of uptake is limited by the available iodide concentration (Shaw, 1962; Tsunogai and Sase, 1969). The reaction

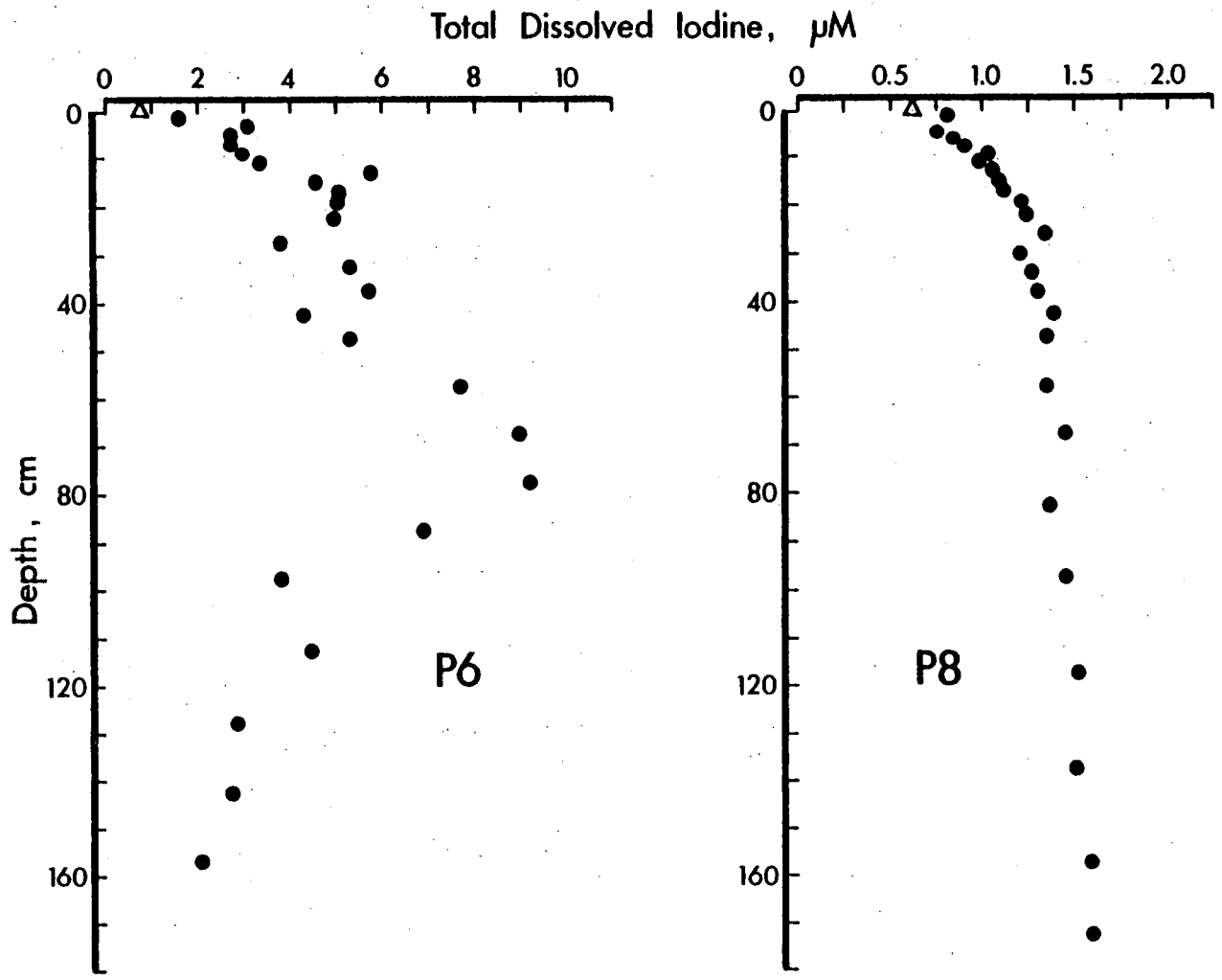

Fig. 6.4 Total dissolved iodine profiles for two Panama Basin cores. △ = supernatant water. Precision: P6 = ± 8% (1σ, n = 6); P8 = ± 2% (1σ, n = 9).

appears to be mediated by a soluble enzyme, "iodide-oxidase" (Kylin, 1930, cited in Price and Calvert, 1977). According to Shaw (1962), iodide, possibly produced by the reducing action on iodate of nitrate-reducing organisms (Tsunogai and Sase, 1969), is oxidized to I_2 by the enzyme which is present on the surface of many algae. The molecular iodine is hydrolyzed to HOI which diffuses through the cell wall and is subsequently reduced back to iodide. This reaction apparently occurs only in the presence of free oxygen; it is strongly inhibited in anoxic conditions (Shaw, 1959; Price and Calvert, 1977).

Comparative studies of the iodine and bromine concentrations in oxic and anoxic sediments of the Namibian shelf led Price and Calvert (1977) to postulate that uptake occurs to a much higher degree on plankton seston on the seabed rather than by incorporation into living organisms. They suggested that as much as 80% of the total iodine in oxidized sediments is adsorbed by seston.

The detailed pore water profiles of P6 and P8 show clearly that sorbed iodine is subject to diagenesis during burial. From this data and several previously published analyses (Table 6.1), it is apparent that the magnitude of the pore water iodine enrichment in marine sediments is broadly a function of the organic matter content in the sediments. As a general rule, coastal and continental margin sediments are considerably more enriched in dissolved iodine than organic carbon-poor pelagic clays; interstitial waters in hemipelagic sediments fall between these end-members.

The dissolved iodine distribution in core P8 implies that much of the iodine is released near the sediment-water interface and that an equilibrium level is approached at depth. In contrast, the carbon and iodine-enriched horizon at about 60-80 cm depth in P6 acts as the dominant locus of dissolved iodide production in the core so that iodide

Table 6.1 Summary of some published interstitial iodine concentrations in marine sediments.

Reference	Locality and Sediment Description	Interstitial Iodine Concentration	Comments
Vinogradov (1939)	Sea of Okhotsk, green mud	4.7 μM	Range of seven analyses from various localities. The Barents Sea concentration would appear to be unacceptably high.
	Barents Sea, grey-green mud, 300 m depth	to 873 μM	
Shishkina and Pavlova (1965)	Mediterranean carbonate clayey mud	0.94 μM	Range of reported values for Indian Ocean, Mediterranean and Black Seas. Authors noted a general increase in dissolved iodine content with depth in sediments.
	Black Sea sulphide-bearing clay	to 63 μM	
Bojanawski and Paslawska (1970)	Southern Baltic Sea, sandy muds	29-150 μM	Sediments mainly anoxic with high C_{org} contents.
Pavlova and Shishkina (1973)	Northwest Pacific	1.26-180 μM	Highest concentrations found in sulphate-depleted oozes of the northern Japan Trench, lowest in oxic (?) brown clays. A regular increase of dissolved iodine with depth was noted where C_{org} in the sediments exceeded 1%.
	Peruvian continental margin	1.6-7.3 μM	
Wakefield (1978)	Bauer Basin, East Pacific Rise, metalliferous clays	0.5-2.5 μM	Range of several profiles. Very little increase over sea water concentration in highly oxidized clays.
This study	Panama Basin	0.72-9.2 μM	Range of analyses from two cores.

diffuses along concentration gradients both upward and downward from that band.

Variations in halogen/C_{org} ratios in the sediments can also provide evidence of the mechanism of halogen diagenesis at depth. Unlike the elemental distributions, the I/C_{org} (Fig. 6.5) and Br/C_{org} (Fig. 6.6) ratios differ markedly in the sediments. I/C_{org} ratios decrease exponentially in all four cores to values less than 100×10^{-4}.

The absence of I/C_{org} peaks at depth, irrespective of the iodine and organic matter-enriched horizons in the biogenic cores, indicates that, relative to carbon, the rate of loss of iodine is independent of the concentration at any point in the sediment column. Where organic matter oxidation is most severe near the sediment-sea water interface, the relative rate of loss of iodine is greatest. The rate decreases exponentially upon burial, presumably because bacterial destruction of organic matter becomes progressively less efficient at depth and the remaining iodine becomes increasingly less labile. The first-order decrease in the I/C_{org} ratio is consistent with the observations of Price et al, (1970) for shelf sediments.

In contrast to the I/C_{org} ratio, Br/C_{org} profiles (Fig. 6.6) show considerable variation with depth; subsurface peaks in the Br/C_{org} ratio roughly reflect the sediment Br distribution.

The absence of a regular decrease in the Br/C_{org} ratio is the most important indicator of the markedly different post-depositional behaviour of bromine compared to iodine. In fact the overall increase with depth suggests that during diagenesis organically-bound bromine is released at an apparently slower rate than that at which the bulk of organic matter itself is mineralized. This clearly contrasts with the preferential rate of loss of iodine relative to organic carbon. Of the two halogens bromine must be bound much more strongly to organic

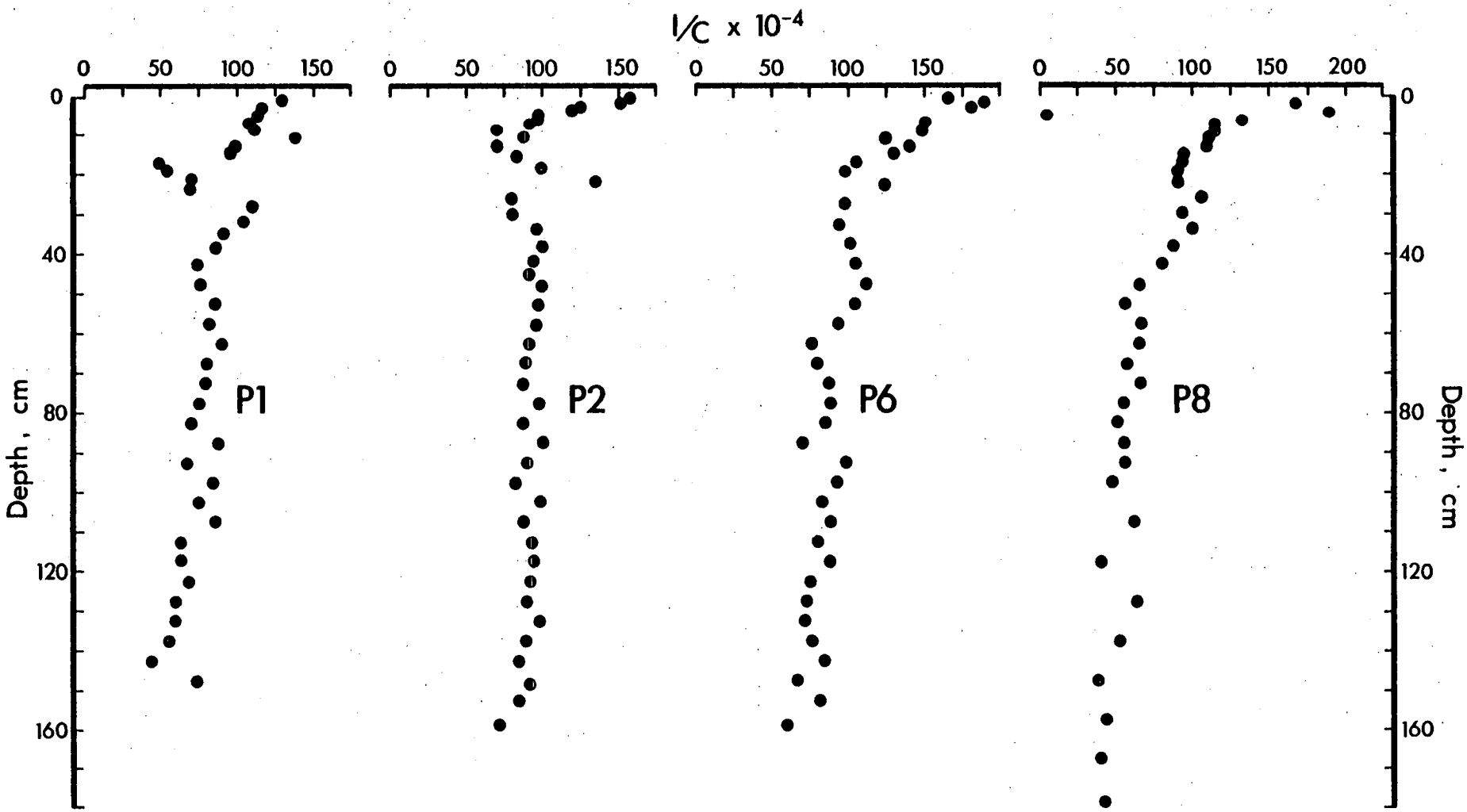

Fig. 6.5 I/C_{org} ratios in Panama Basin area cores. All four surface samples lie considerably below the regression line calculated in Fig. 6.1 and therefore have surface I/C ratios considerably lower than the mean for the Basin.

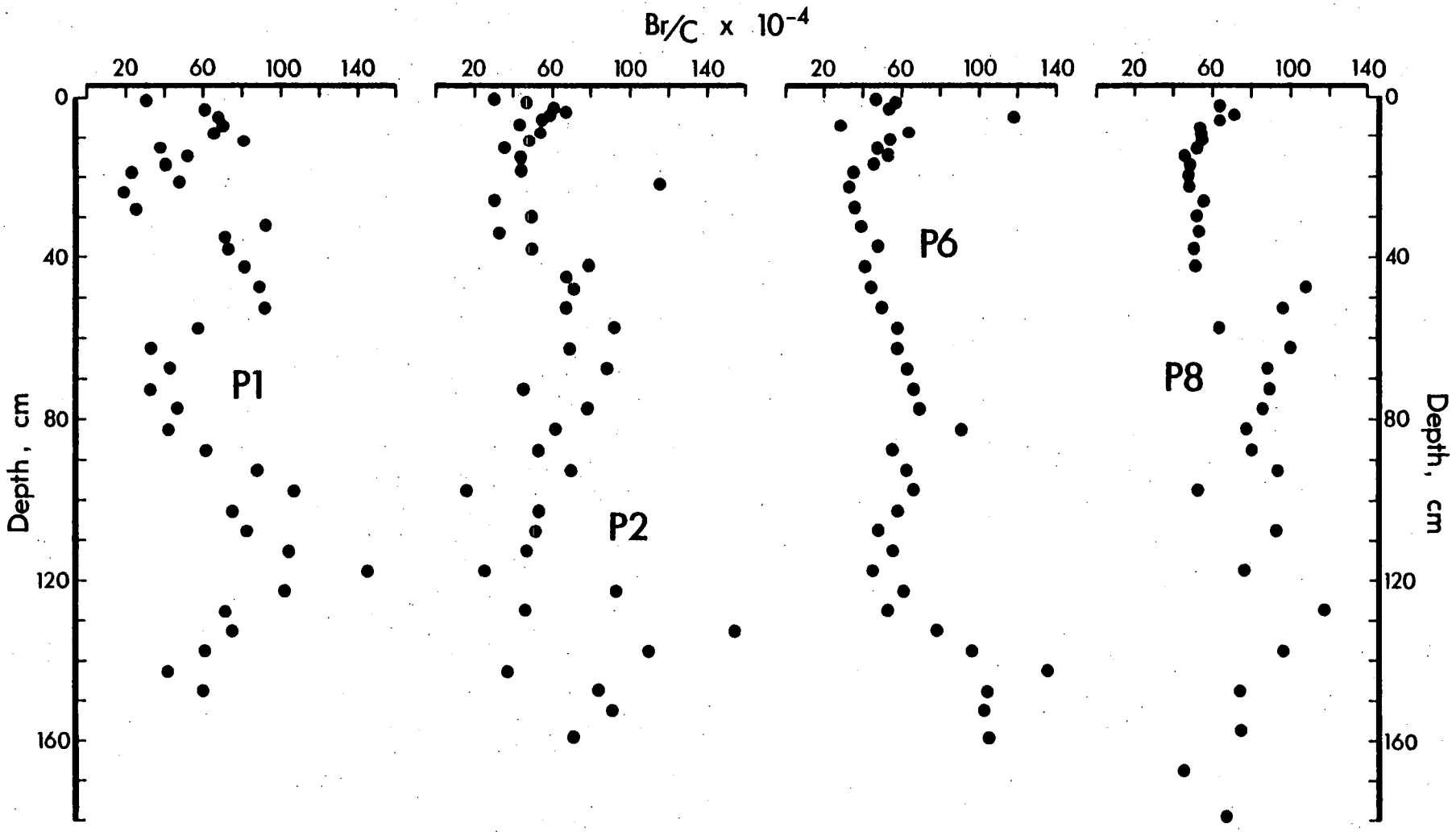

Fig. 6.6 Br/C_{org} ratios in Panama Basin area cores. As for I/C, surface Br/C ratios in these four cores are all less than the mean for Basin surface sediments.

material.

Some insight into the possible halogen binding sites can be gained by using pore water chemistry to compare the relative reactivities of nitrogenous organic substances and iodine within the sediments. The dissolved ammonium profile for core P6 (Fig. 6.7) shows, in contrast to dissolved iodine, little evidence of increased ammonia production at the 60-80 cm deep halogen and organic carbon-rich horizon. Since iodide and ammonium ions have nearly identical diffusion coefficients (Li and Gregory, 1974), the absence of ammonium enrichment here cannot be due to physical factors. Instead, the contrasting NH_4^+ and I profiles in this core suggest that iodine is much more labile than organic nitrogen during diagenesis. This apparent greater lability of iodine relative to nitrogen suggests that iodine may not be associated with the proteinaceous fraction of organic matter as has been previously postulated (e.g. Price and Calvert, 1973). In addition the contrast between the postdepositional behaviour of iodine and bromine discussed above implies that different binding sites for the two elements exist. It is possible, for example, that iodine may react principally with unsaturated carbon to produce such forms as labile halohydrins (March, 1968) whereas bromine may become bonded to a more refractory carbohydrate phase.

Implications of sediment diagenesis to the halogen balance in the ocean

The evidence presented here demonstrates that organically-bound iodine is more susceptible to diagenetic remobilization in hemipelagic sediments than the more refractory bromine. The data can also be used to assess the influence that uptake and sediment diagenesis of iodine have on the distribution of the element in the overlying sea water.

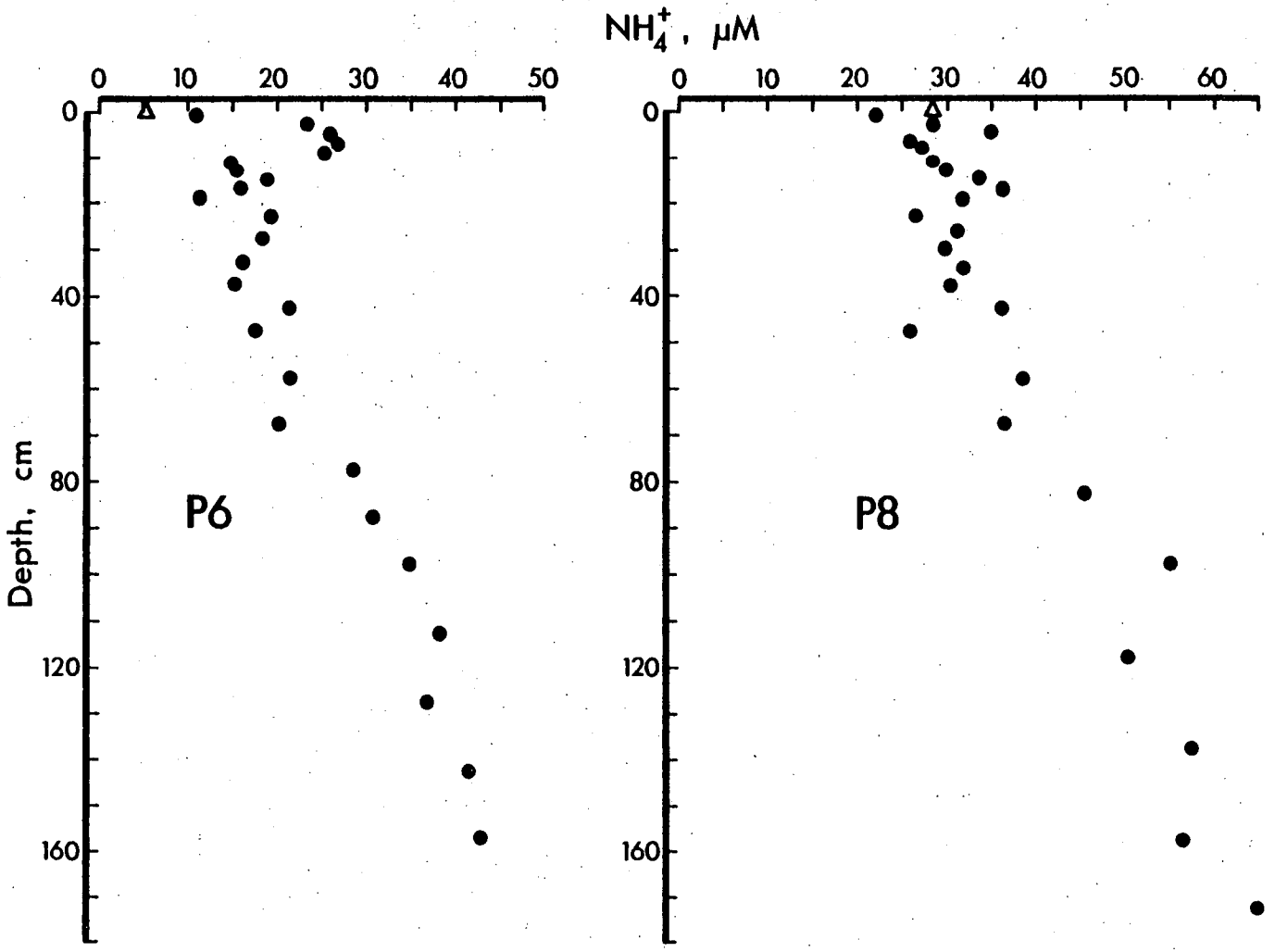

Fig. 6.7 Dissolved ammonium profiles for cores P6 and P8. $\Delta = NH_4^+$ concentration in supernatant water.

In the foraminiferal oozes of the equatorial Pacific (represented in this work by cores P1, P2, and P6) iodine is enriched in historic horizons of high organic carbon content which are believed to be a result of enhanced surface biological productivity during glacial maxima (Chapter Eight). As explained in Chapter Eight, the carbon peak found at depths of 40-70 cm in P1, P2 and P6 corresponds very closely to the period of maximum advance of the Wisconsin glaciation in the northern hemisphere, about 18,000 years ago. In the central Panama Basin, represented by core P6, the rate of removal of iodine from sea water during the Wisconsin maximum must have been at least twice as high as at present, assuming an invariant I/C_{org} ratio in surface sediments during the past 20,000 years. Simple calculations summarized in Table 6.2 suggest that if climatically-induced increased production occurred over the entire equatorial productivity belt of the Pacific for a period of several thousand years, about 0.3 per cent of the Pacific iodine reservoir could be removed to the sediments by organic matter sorption. This quantity has some significance, especially considering that the assumed organic carbon concentration and sedimentation rate used in the calculations may well be minimum estimates. The calculations suggest that climatic fluctuations may well have a measureable importance in regulating the iodine balance in the oceans on a time scale of several mixing cycles.

An additional factor of possible importance to iodine distribution in the sea, especially in an area of restricted bottom water circulation such as the Panama Basin, is diffusion from sediments of diagenetically-remobilized iodine. The diffusive flux to Panama Basin Bottom Water can be estimated from the pore water profiles and sediment properties. Core P6, collected on the north flank of the Galapagos Spreading Centre, is almost identical in composition to the Pleiades

Table 6.2 Estimate of the proportion of the Pacific iodine reservoir removed by equatorial Pacific sediments during the height of the Wisconsin glacial stage.

Assume:

i) Area of equatorial Pacific productivity belt $= 1.5 \times 10^7$ km^2.

ii) Avg. C_{org} content of sediment accumulating during Wisconsin maximum was 1% (dry wt.).

iii) I/C_{org} in surface sediments $= 350 \times 10^{-4}$

Therefore $[I] = 350$ ppm.

iv) Avg. thickness of I-enriched sediments $= 5$ cm.

v) Avg. $CaCO_3$ content = 50%. Then avg. bulk density = 0.43 (calculated from equations of Lyle and Dymond, 1976).

Therefore volume of enriched sediment is 7.5×10^{11} m^3 containing 11×10^{13}g iodine.

vi) Pacific Ocean vol. $= 7.24 \times 10^{20}$l (Riley & Chester, 1971).

Avg. iodine concentration = 0.44 μM

Therefore Pacific contains 4×10^{16}g I.

Hence during the Wisconsin maximum, about

$$\frac{11 \times 10^{13}}{4 \times 10^{16}} = 0.3\%$$

of the Pacific iodine reservoir could have been removed to the sediments.

---

box core raised from the nearby Mounds Hydrothermal Field and is assumed to have similar physical characteristics. These are: (a) an average porosity[1] $\phi = 0.80$ in the upper sediment horizons and (b) an average formation factor[2] $F = 1.5$.

The diffusion coefficient, D_j^o, of iodide at 0^o C in sea water is 10.3×10^{-6} cm^2 sec^{-1} (Li and Gregory, 1974). The in situ diffusion coefficient, D_s, is then 6.9×10^{-6} cm^2 sec^{-1}, calculated from the equation $D_s = D_j^o/F$ (Manheim, 1970). If linearity is assumed for the pore water iodine distribution of the upper half of core P6, then the concentration gradient, dC/dZ, is about 1×10^{-4} μmole cm^{-4} and the flux can be calculated from Ficks First Law (Berner, 1971):

$$J_Z = D_s \phi \frac{dC}{dZ}$$

$$= 5.5 \times 10^{-10} \text{ μmole cm}^2 \text{ sec}^{-1}.$$

The flux can be similarly estimated for core P8. The upper several centimetres of the core, where the concentration gradient is approximately linear, are assumed to have a porosity of 0.85 (higher than P6 since the sediments are mainly clays) and a formation factor of 1.4. These parameters are unlikely to be more than 5% in error. The concentration gradient is 2.8×10^{-5} μmole cm^{-4} which yields a flux of 1.8×10^{-10} μmole cm^{-2} sec^{-1}. Clearly, the diffusive iodine loss from core P8 is only one-third of that for P6 (which contains the sharp mid-depth halogen-carbon enrichment).

The volume of Panama Basin Bottom Water (PBBW) which lies below the ~2200 m "sill depth" of the enclosing Carnegie and Cocos Ridges is 4.4×10^{14} m^3; the underlying sediments occupy 6.5×10^{11} m^2

---

1. Resistivity and porosity data supplied by Dr. J. M. Geiskes, SIO.
2. The formation factor, F, is defined by Manheim (1970) as "the ratio of bulk electrical resistivity of the sediment to the resistivity of the pore fluid alone".

(Lonsdale, 1977b). Since the average total iodine concentration of PBBW is 0.45 μM (H. Elderfield, personal communication) the water mass contains about 2×10^{11} moles of the element. It is estimated that the flux from core P6 represents $\frac{2}{3}$ of the sediment area and that from P8 the remainder (i.e. the rapidly accumulating detrital sediments of the Eastern Basin). During the 42-year renewal period of PBBW (Lonsdale, 1977) the diffusive iodine contribution is therefore about 4×10^{9} moles, which accounts for 2% of the calculated total PBBW iodine content.

This figure may be an over-estimate of the quantity of iodine recycled to the PBBW since no attempt has been made to quantify the fraction of upward-diffusing iodine which may be reabsorbed by organic debris at or near the sediment-water interface. Furthermore, since the largest proportion of the iodine flux is contributed by solubilized iodine probably deposited during the Wisconsin maximum, the flux will decrease with time.

Conclusions

(a) The distribution of iodine and bromine in hemipelagic sediments of the Panama Basin broadly parallels that of organic carbon. This congruence is especially well illustrated in the biogenic sediments by sharp mid-depth maxima of all three elements.

(b) Pore water analyses show increased dissolved iodine concentrations at depth in the sediments.

(c) The iodine-rich band at mid-depth in core P6 is the major contributor of dissolved iodine in the core.

(d) Smooth exponential decreases of the I/C_{org} ratio with depth in all sediments are independent of concentration and indicate a regular preferential loss of iodine relative to carbon during diagenesis.

(e) In considerable contrast to iodine, peaks at depth in Br/C_{org} profiles suggests that bromine is relatively refractory during post-depositional alteration of organic matter. The dissimilar behaviour of the two halogens implies bonding by different organic ligands.

(f) Mass balance estimates suggest that a small fraction of the Pacific iodine inventory could be removed to equatorial Pacific sediments during glacial maxima. Climatic fluctuations may therefore be of some importance in regulating the iodine balance in the sea.

(g) Flux calculations for iodine suggest that up to 2% of the iodine in Panama Basin Bottom Water is contributed by upward-diffusing iodine remobilized from the sediments during organic matter diagenesis. The source for most of the flux is the iodine enrichment in the equatorial sediments associated with the high organic carbon concentration thought to have resulted from deposition during the Wisconsin glacial maximum.

CHAPTER SEVEN

INTERSTITIAL WATER CHEMISTRY

7.1 Introduction

Variations in the composition of interstitial water are the most sensitive indicators of net chemical diagenetic reactions occurring in marine sediments. Since progressive bacterial metabolization of organic material is the principal diagenetic driving force, sediments receiving large inputs of organic matter, such as those in the Panama Basin, are most likely to exhibit significant changes in pore water chemistry.

In order to investigate the imprint of a high organic matter flux on two contrasting hemipelagic sediment facies, pore water was squeezed from four cores collected from foram ooze southwest of the Galapagos Islands (P1 and P2) and near the Galapagos Spreading Centre (P6), and from terrigenous clays in the Coiba Gap area (P8).

Pore waters were extracted in air at in situ temperatures. Minor precautions were taken to reduce oxidation effects during squeezing; these are discussed in the description of extraction methodology in Appendix B. In addition to dissolved iron (Chapter Four) and iodine (Chapter Six), pore water samples were analyzed for silicate, phosphate, ammonia, sulphate, alkalinity and manganese. Analytical methods are described in Appendix B and all results are listed in Table C.3 (Appendix C).

7.2 Distribution of reactive silicate

Interstitial water profiles for reactive silicate (monomeric silicic acid, H_4SiO_4 or $Si(OH)_4$) are shown in Fig. 7.1. Each profile is characterized by an initial sharp increase in dissolved silicate in the upper few cm followed by rapid attainment of an approximately constant or marginally increasing concentration. The pore waters are enriched over the average Panama Basin Bottom Water concentration of

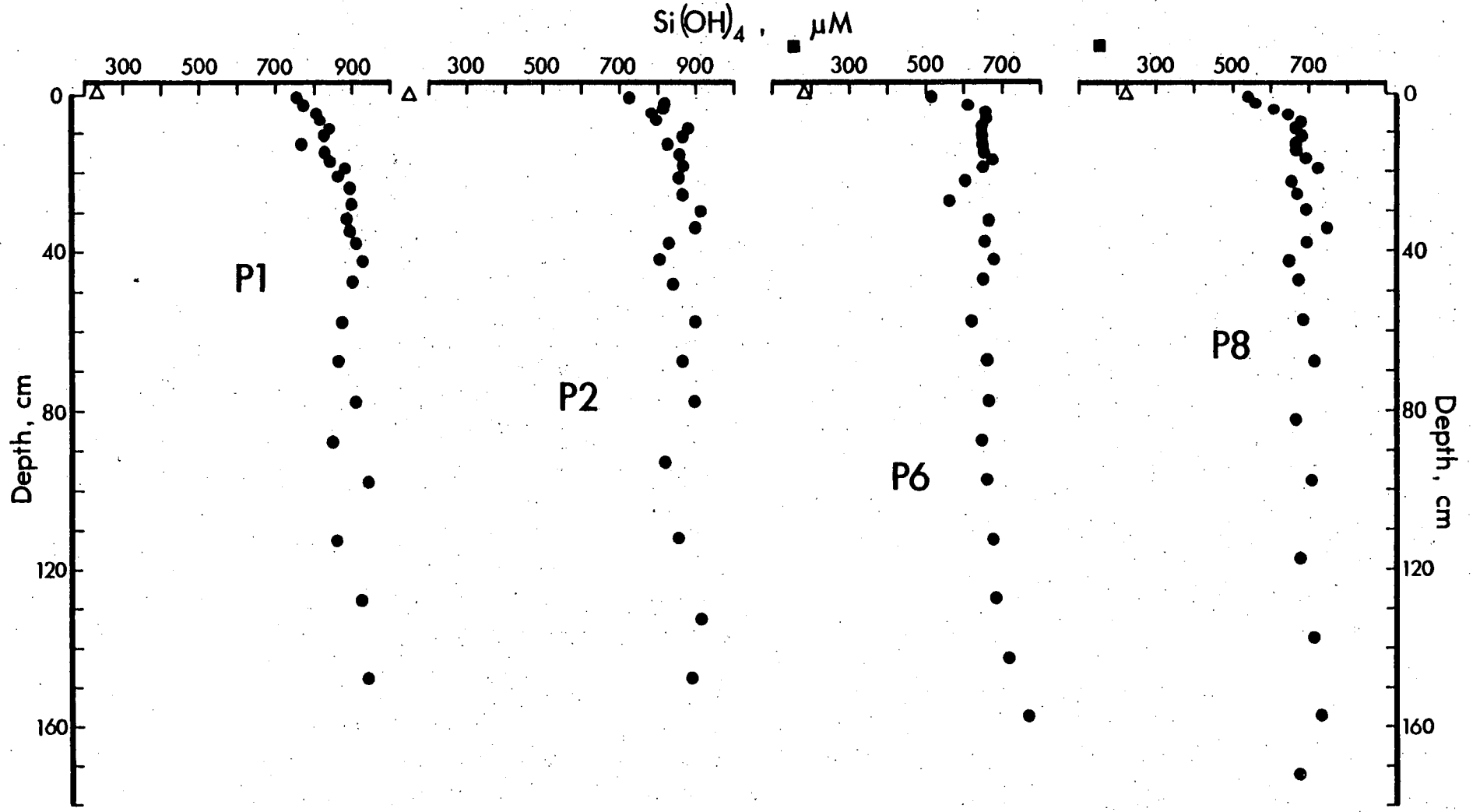

Fig. 7.1 Interstitial silicate profiles, Panama Basin area. △ = supernatant concentration, just above the sediment-water interface; ■ = bottom water concentration. Analytical precision = ± 3% (1σ , n = 15).

152 μM (based on data in unpublished Cruise Reports Shackleton 2/1976 and Pleiades Leg II/1976) by a factor of 3.4 to 6.3. Mean concentrations at depth (i.e. 20 cm - 180 cm) range from 658-894 μM $Si(OH)_4$, similar to the 300-950 μM found in Bauer Basin - East Pacific Rise pore waters (Bischoff and Sayles, 1972; Wakefield, written communication, 1978).

Many workers (Fanning and Schink, 1969; Fanning and Pilson, 1974; Schink et al, 1974; Schink et al, 1975) have suggested that dissolution of amorphous biogenic silica is responsible for the apparently ubiquitous silicate enrichments in marine pore waters. It also appears that the sharp initial increase in dissolved silicate in the upper few centimetres is characteristic of marine sediments (Schink et al, 1974) and results from rapid dissolution of certain highly soluble diatom and radiolarian species. However, it is not yet clear how the deeper equilibrium concentrations are established.

It is apparent that both opal dissolution and equilibration of silica with clay minerals are active in regulating equilibrium concentrations. The solubility of opal ranges from 1035 μM at 2°C and 500 atm (Jones and Pytkowicz, 1973) to about 1200 μM (Krauskopf, 1959) whereas Garrels (in Bischoff and Ku, 1970) calculated an equilibrium $Si(OH)_4$ concentration of ~500 μM in instances where clays were taking up excess silicate. Resolution of opaline material commonly dominates the dissolved silicate distribution in marine sediments (Schink et al, 1974), but in some opal-poor deposits $Si(OH)_4$-clay equilibria appear to exert the primary control (Bischoff and Ku, 1970).

In Panama Basin area pore waters, the $Si(OH)_4$ concentration greatly exceeds the level expected for equilibrium with clay minerals; opal dissolution therefore appears to be paramount. Consequently, the higher mean dissolved silicate values in cores P1 and P2 may reflect

the higher content of SiO_2 in these sediments (Table 4.1) where sufficient soluble silica would be available to shift the equilibrium toward opal saturation. Lower average concentrations in P6 and P8 are consistent with the smaller proportion of opal in these sediments. The mean silicate concentrations in the four cores are thus roughly related to euphotic zone productivity. On a much more comprehensive scale, such an areal relationship has been observed in the central and northern Atlantic (Schink et al, 1974).

7.3 Distribution of PO_4^{3-}, NH_4^+, SO_4^{2-} and alkalinity

The results of interstitial phosphate, ammonia, sulphate and titration alkalinity analyses are listed in Table C.3 (p.213) and displayed in Figs. 7.2-7.5 respectively.

Phosphate concentrations are enriched up to one order of magnitude over the average Panama Basin Bottom Water value of 2.74 μM (mean of 12 analyses from unpublished Cruise Reports Shackleton 2/1976 and Pleiades Leg II/1976). Concentrations in cores P1 and P2 increase linearly from near bottom water values at the surface of the core to 25-30 μM at ~40 cm depth and then remain essentially constant (Fig. 7.2). In contrast, P6 and P8 interstitial phosphate concentrations are characterized by a sharp five or six-fold increase in the top few centimetres of each core followed by marginal increases to maxima of ~20 μM and ~25 μM respectively.

Ammonia (protonated to NH_4^+ in pore water) profiles are shown in Fig. 7.3. Concentrations increase with depth in all cores although in P1 and P2 they are only slightly greater than the analytical detection limit (~5 μM) in the lower half of each. In P6 and P8, concentrations increase approximately linearly with depth, reaching much higher levels of >40 μM and >60 μM, respectively.

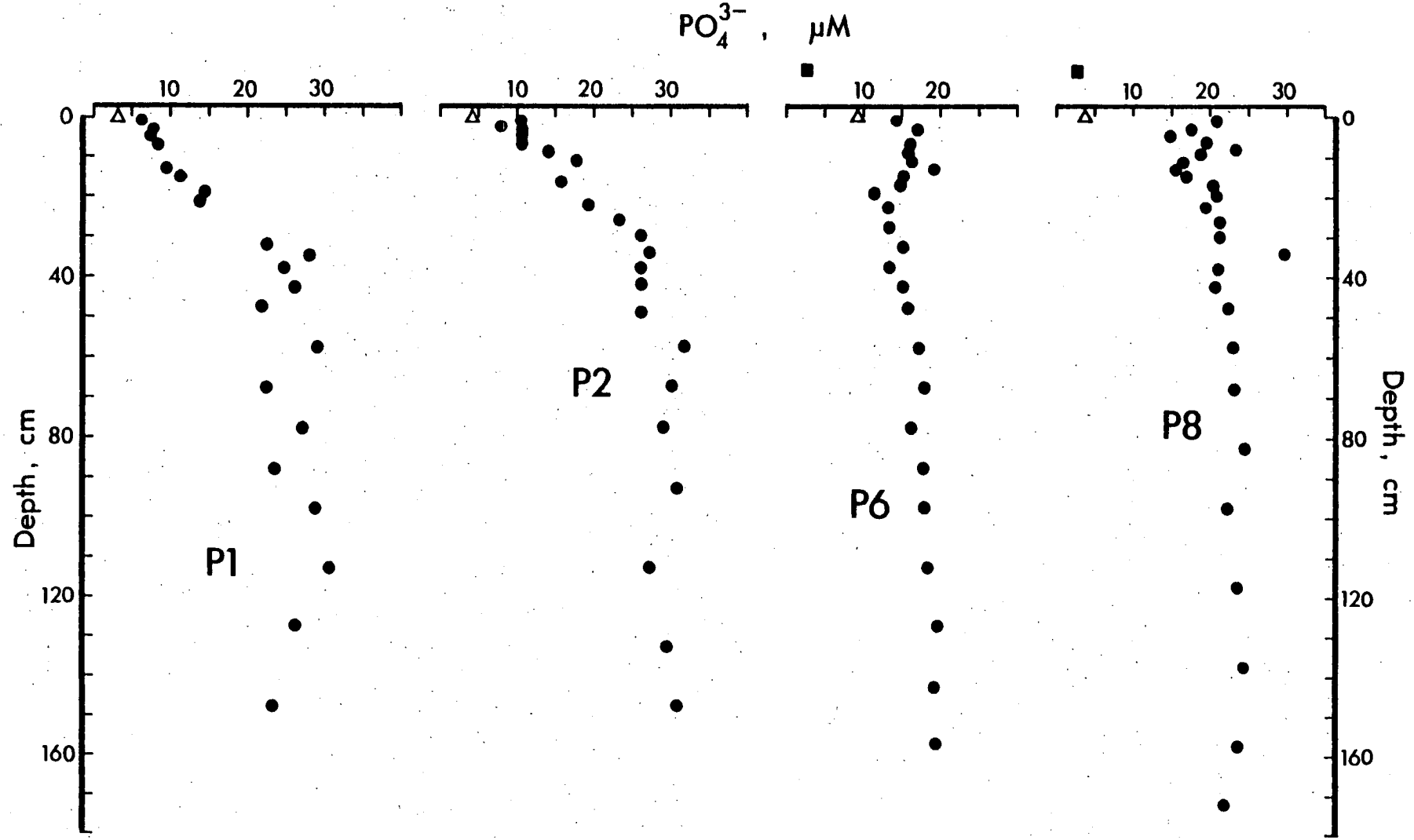

Fig. 7.2 Interstitial phosphate profiles, Panama Basin area. △ = supernatant concentration; ■ = bottom water concentration. Analytical precision = ± 5% (1σ, n = 15).

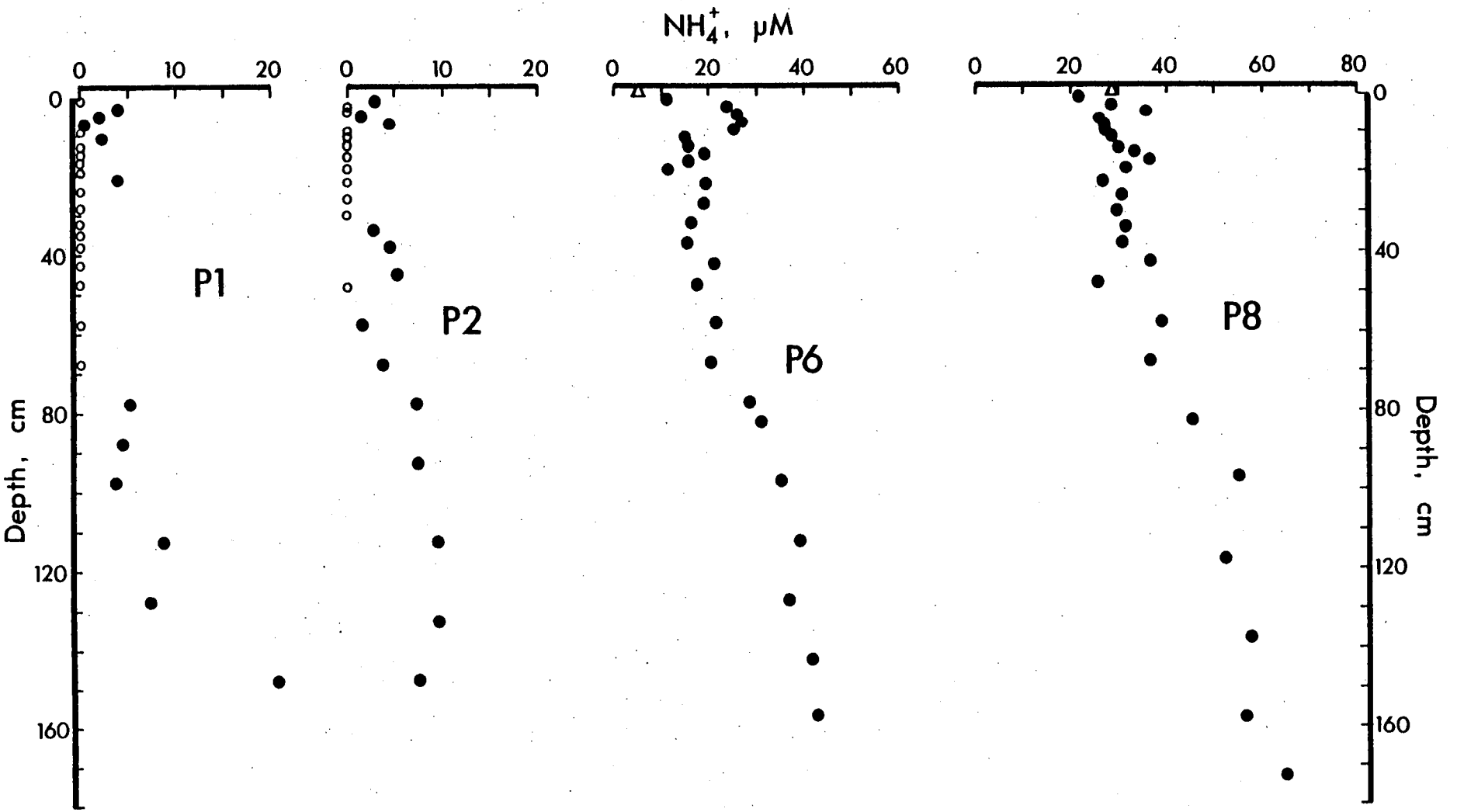

Fig. 7.3 Interstitial ammonia profiles, Panama Basin area. △ = supernatant concentration; o = below detection limit. Analytical precision = ± 8% (1σ , n = 9). Values <5 μM are suspect.

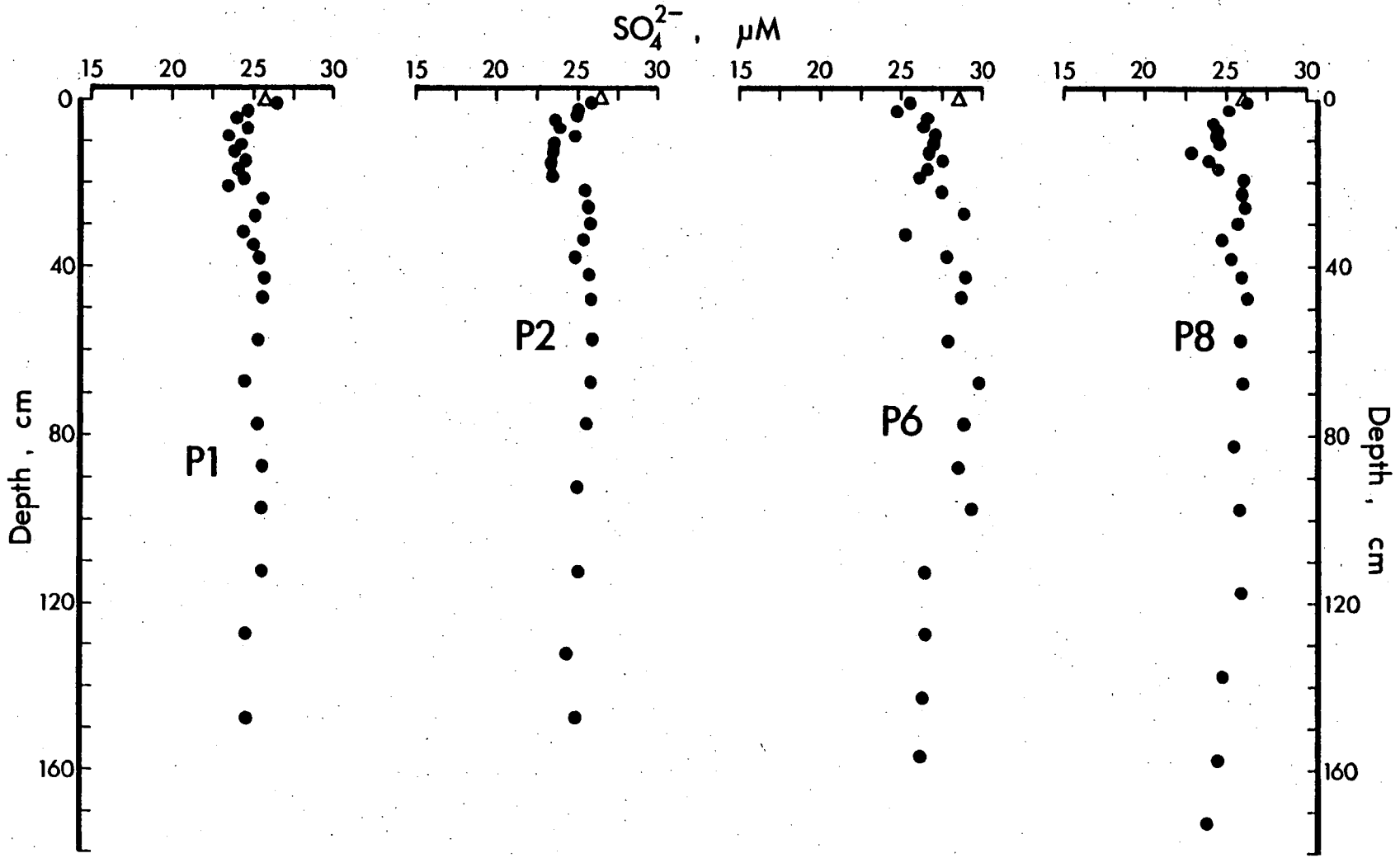

Fig. 7.4 Interstitial sulphate profiles, Panama Basin area. △ = supernatant concentration. Analytical precision = ± 4% (1σ, n = 4).

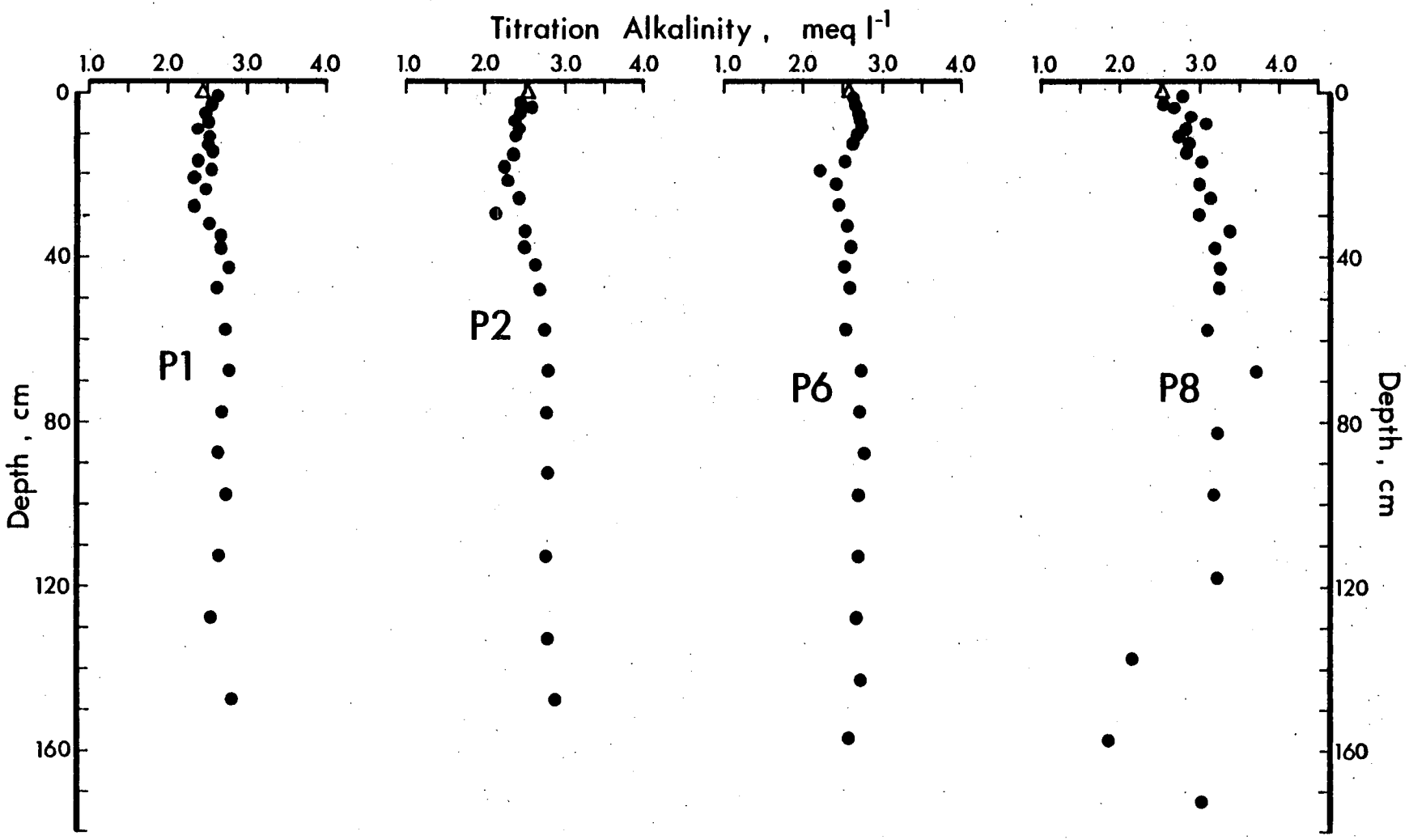

Fig. 7.5 Interstitial alkalinity profiles, Panama Basin area. △ = supernatant concentration. Analytical precision = ± 1.3% (1 σ, n = 5).

The increasing NH_4^+ concentrations contrast sharply with the relatively stable interstitial sulphate (Fig. 7.4) and titration alkalinity (Fig. 7.5) distributions. Sulphate concentrations throughout all cores are within several millimoles litre^{-1} of the overlying sea water concentration of 28.0 mM (calculated from the measured salinity of 34.665 per mil). Slight depletions apparent at depth in P1 and P2 are less than analytical precision ($\pm$ 1 mM at 25 mM SO_4^{2-}), while those in P6 and P8 are marginally greater. With the exception of core P8, alkalinity concentrations do not exceed 3.0 meql^{-1}, varying only slightly between ~2.2 and 2.8 meq/l [1]. A maximum enrichment of ~1 meql^{-1} occurs at mid-depth in P8, followed by a significant decrease of ~1.5 meql^{-1} toward the bottom of the core. No significant increases at depth are observed in P1, P2 or P6, but in all three a slight depletion of ~0.3 meql^{-1} occurs above 40 cm.

The principal control on the distributions described above is the bacterially-mediated oxidation of organic matter. This process is constrained by a series of oxidation-reduction reactions which follow the order of decreasing free energy available to organisms (Stumm and Morgan, 1970, p. 334). Those reactions pertinent to the sediments studied here are listed in Table 7.1. Although thermodynamic theory suggests that adherence to this sequence should develop a clear vertical zonation in sediments, in practice, the boundaries between the different reduction zones are typically diffuse and may be strongly altered by such processes as bioturbation and irrigation. Several

---

[1] Recent work by Murray et al (1979) has revealed that the large pressure decrease accompanying sediment retrieval from deep water (~4000 m) produces an alkalinity decrease in the interstitial water of 80-90 μeq kg^{-1}, presumably because $CaCO_3$ precipitates as hydrostatic pressure lessens. This sampling artifact has probably affected the results in this work to a similar degree but since it is so small (roughly equal to analytical precision) it is not of concern here.

Table 7.1 Oxidation-reduction reactions applicable to Panama Basin area sediments, in order of decreasing free energy availability. Since the stoichiometric C:N:P ratio of the organic matter is not known and is probably variable (see text, p.104), a generalized C:N:P ratio is used in the manner of Sholkovitz (1973).

(1) Aerobic respiration

$$(CH_2O)_C(NH_3)_N(H_3PO_4)_P + (O_2)_{C+2N} + (CaCO_3)_{C+N}$$
$$= (NO_3^-)_N + (H_3PO_4)_P + (Ca^{2+})_{C+N} + (HCO_3^-)_{2C+N} + (H_2O)_N$$

(2) Denitrification

$$(CH_2O)_C(NH_3)_N(H_3PO_4)_P + 0.8(NO_3^-)_C + 0.2(CaCO_3)_C$$
$$= (NH_3)_N + (H_3PO_4)_P + 0.2(Ca^{2+})_C + 0.4(N_2)_C + 1.2(HCO_3^-)_C + 0.4(H_2O)_C$$

(3) Manganese reduction

$$(CH_2O)_C(NH_3)_N(H_3PO_4)_P + 2(MnO_2)_C + 3(Ca^{2+})_C + 2(HCO_3^-)_C$$
$$= (NH_3)_N + (H_3PO_4)_P + 2(Mn^{2+})_C + 3(CaCO_3)_C + 2(H_2O)_C$$

(4) Iron reduction

$$(CH_2O)_C(NH_3)_N(H_3PO_4)_P + 4(FeOOH)_C + 7(Ca^{2+})_C + 6(HCO_3^-)_C$$
$$= (NH_3)_N + (H_3PO_4)_P + 4(Fe^{2+})_C + 7(CaCO_3)_C + 6(H_2O)_C$$

(5) Sulphate reduction

$$(CH_2O)_C(NH_3)_N(H_3PO_4)_P + 0.5(SO_4^{2-})_C + 0.5(CaCO_3)_C$$
$$= (NH_3)_N + (H_3PO_4)_P + 1.5(HCO_3^-) + 0.5(HS^-)_C + 0.5(Ca^{2+})_C$$

investigators have considered the effects of these processes on diagenesis and pore water composition (e.g. Goldhaber et al, 1977; Grundmanis and Murray, 1977; Schink and Guinasso, 1977; Vanderborght et al, 1977a and 1977b). In addition, ionic diffusion and advection act to blur diagenetic boundaries as, for example, in the (hypothetical ?) case where NH_3 produced at depth might diffuse upward into the free-O_2 zone and be oxidized to nitrate, thus producing a nitrate maximum which is not a direct result of aerobic diagenesis (Bender et al, 1977).

Biological or physical mixing is evinced by depth-independent pore water profiles in sediments in which organic matter decomposition and/or silica dissolution are occurring. Further indications are provided by visual observations of sediment disruption or the recovery from cores of burrowing organisms.

The Panama Basin pore water profiles studied here show no evidence of a mixed layer. The rapidly generated increases in dissolved silicate, manganese (p.111), and to some extent ammonia and phosphate argue against significant bioturbation. Additional evidence for the apparent absence of mixing is furnished by the existence of a sharp, undisturbed contact between the dark brown surface oxic layer and underlying olive-green sediments in the four cores studied. Chemical analyses of the sediments (Chapters Four and Five) also show no evidence of physical or biological disruption. If mixing does occur, it is at such a slow rate that it cannot counter the natural readjustment of redox conditions and nutrient profiles in the cores.

Diffusion accompanies advection (burial of bottom water by accumulating particles) in the sediments to provide communication with the overlying sea water. Since bioturbation is effectively absent it is assumed in the following discussion that a steady state is established

wherein the rate of production of metabolites by organic matter diagenesis is balanced by diffusion-advection processes (neglecting, for the moment, ion-exchange, adsorption, and solution-precipitation reactions).

Nutrient regeneration and organic diagenesis

Denitrification (Table 7.1) can commence when small quantities of dissolved O_2 are still present in interstitial waters (Cline and Richards, 1972; Wilson, 1978); however, NH_3 produced from the organic component of this reaction will be oxidized to NO_3^- as long as O_2 is available. In cores P1 and P2 the near absence of ammonia in the upper 70 cm suggests that the rate of depletion of oxygen must be slower than in sediments within the Basin (P6 and P8) where ammonium ions begin accumulating very near the sediment-water interface (Fig. 7.3). This ammonia distribution is consistent with the higher organic carbon content of cores P6 and, especially, P8.

Very little sulphate is reduced in the upper 1.5 m of most of the sediments (Fig. 7.4). However, in core P8 the presence of a distinct H_2S odour (noticed during core extrusion) suggested that $SO_4^=$ reduction occurred to a greater degree in this core than in P1, P2 or P6. Since sulphate reduction does not become the dominant microbiological process until nitrate is completely consumed (Grundmanis and Murray, 1977), it appears that nitrate is the principal oxidant in the sediments studied here.

Using the diagenetic equations of Table 7.1, including that for Mn oxidation/reduction, some assessment can be made of the oxidants used and the metabolites produced during diagenesis, providing that the stoichiometric C : N : P ratio of the mineralizing organic matter is known or at least constrained by certain limits. Knowledge of this ratio is essential in diagenetic modelling, but it is known to

vary widely. The Redfield molar ratio (106 : 16 : 1) is the most widely quoted and was determined from analysis of living marine plankton (Redfield et al, 1963). However, prior to deposition and burial in sediments, organic matter is subjected to some oxidation in the water column which can modify the C : N : P stoichiometry. Gordon (1971) has shown that the C : N ratio in suspended particulate organic matter in the sea increases with depth from near the Redfield value at the surface to twice that value at 3-4 km depth. The increase is due to greater bacterial utilization of protein relative to carbohydrate during fallout (Holm-Hansen, 1969). The data of Copin-Montegut and Copin-Montegut (1972) show a pronounced two to three times increase in the C_{org}: P_{total} molar ratio with water depth in the northeast Atlantic; this relationship was also noted for Gulf of Maine particulate organic matter (Ketchum et al, quoted in Sholkovitz, 1973) and must be caused by a preferential loss of organically-bound phosphorus as oxidation proceeds. Furthermore, Price (personal communication) has determined an average C : N : P molar ratio of 106 : 12 : 0.07 for suspended organic particulate matter in Panama Basin Bottom Water.

The C : N : P ratio of organic matter in hemipelagic sediments also differs from the Redfield ratio. For example, Sholkovitz (1973) used pore water nutrient concentrations to establish a C : N : P ratio of 106 : 8 : 0.5 and Hartmann et al (1976), from the measurement of organic C, N and P in hemipelagic sediments, found a compositional range of 106 : 10.9-12.2 : 0.2-0.5. Diagenetic equations applying this spectrum of C : N : P molar ratios are listed in Table 7.2 and the calculated concentrations for each diagenetic zone are summarized in Table 7.3. Two assumptions are implicit in these calculations. Firstly, no allowance is made for a change in C : N : P with depth in the sediments (however, the ranges reported by Hartmann et al (1976)

Table 7.2 Diagenetic equations for calculating nutrient generation from organic matter of different C:N:P ratios. Equations are based on redox reactions of Table 7.1.

	C:N:P Ratio		
	106:16:1 [1]	106:12:0.07 [2]	106:10.9-12.2:0.2-0.5 [3]
Aerobic respiration	$138(O_2) = 16NO_3^- + H_3PO_4$	$130(O_2) = 12(NO_3^-) + 0.07(H_3PO_4)$	$127.8\text{-}130.4(O_2) = 10.9\text{-}12.2(NO_3^-) + 0.2\text{-}0.5(H_3PO_4)$
Denitrification	$84.8(NO_3^-) = 16(NH_3) + H_3PO_4$	$84.8(NO_3^-) = 12(NH_3) + 0.07(H_3PO_4)$	$84.8(NO_3^-) = 10.9\text{-}12.2(NH_3) + 0.2\text{-}0.5(H_3PO_4)$
Manganese reduction	$212(MnO_2) = 16(NH_3) + H_3PO_4$	$212(MnO_2) = 12(NH_3) + 0.07(H_3PO_4)$	$212(MnO_2) = 10.9\text{-}12.2(NH_3) + 0.2\text{-}0.5(H_3PO_4)$
Iron reduction	$424(FeOOH) = 16(NH_3) + H_3PO_4$	$424(FeOOH) = 12(NH_3) + 0.07(H_3PO_4)$	$424(FeOOH) = 10.9\text{-}12.2(NH_3) + 0.2\text{-}0.5(H_3PO_4)$
Sulphate reduction	$53(SO_4^{2-}) = 16(NH_3) + H_3PO_4$	$53(SO_4^{2-}) = 12(NH_3) + 0.07(H_3PO_4)$	$53(SO_4^{2-}) = 10.9\text{-}12.2(NH_3) + 0.2\text{-}0.5(H_3PO_4)$

[1] Average composition of living marine plankton (Redfield et al, 1963).

[2] Average composition of suspended particulate organic matter, Panama Basin Bottom Water (N.B. Price, pers. comm.).

[3] Compositional range of organic matter, hemipelagic sediments, NW African continental margin (Hartmann et al, 1976).

Footnotes for Table 7.3 (facing)

[1] See footnotes, Table 7.2, for sources of ratios.

[2] The average Panama Basin Bottom Water (PBBW) dissolved oxygen concentration of 130 μM O_2 is assumed to be entirely consumed prior to denitrification.

[3] The sum of the average PBBW dissolved nitrate concentration of 40 μM plus nitrate produced by aerobic respiration is used as total nitrate available for reduction.

[4] Calculated using the maximum dissolved manganese concentration reached in each core. It is assumed that no Mn^{2+} is precipitated as carbonate.

[5] Since the dissolved iron concentration in all cores ranges from 1.8-5 μM (Table C.3), insignificant quantities of NH_3 ($\ll 1$ μM) and H_3PO_4 ($\ll 0.1$ μM) are produced.

Table 7.3 Concentrations of dissolved ammonia and phosphate produced by each diagenetic stage, calculated from equations of Table 7.2. For simplicity, diffusional exchange of components is neglected.

	C:N:P Ratio[1]					
	106:16:1		106:12:0.07		106:10.9-12.2:0.2-0.5	
Aerobic respiration[2]	ΔNO_3^- = 15 μM ΔNH_3 = 0 μM	ΔH_3PO_4 = 1.0 μM	ΔNO_3^- = 12 μM ΔNH_3 = 0 μM	ΔH_3PO_4 = 0.07 μM	ΔNO_3^- = 10.9-12.4 μM ΔNH_3 = 0 μM	ΔH_3PO_4 = 0.2-0.5 μM
Denitrification[3]	ΔNH_3 = 10.4 μM	ΔH_3PO_4 = 0.6 μM	ΔNH_3 = 7.4 μM	ΔH_3PO_4 = 0.04 μM	ΔNH_3 = 6.1-8.0 μM	ΔH_3PO_4 = 0.1-0.3 μM
Manganese reduction[4]	ΔNH_3 (μM)	ΔH_3PO_4 (μM)	ΔNH_3 (μM)	ΔH_3PO_4 (μM)	ΔNH_3 (μM)	ΔH_3PO_4 (μM)
	P1 = 3 P2 = 4.5 P6 = 5.3 P8 = 14	P1 = 0.2 P2 = 0.3 P6 = 0.4 P8 = 0.9	P1 = 2.3 P2 = 3.4 P6 = 4.0 P8 =10.5	P1 = 0.01 P2 = 0.02 P6 = 0.02 P8 = 0.06	P1 = 2.0-2.3 P2 = 3.1-3.5 P6 = 3.6-4.0 P8 = 9.5-10.6	P1 = 0.04-0.1 P2 = 0.06-0.1 P6 = 0.07-0.2 P8 = 0.2-0.4
Iron reduction[5]	-		-		-	
Cumulative Totals	ΣNH_3 (μM)	ΣH_3PO_4 (μM)	ΣNH_3 (μM)	ΣH_3PO_4 (μM)	ΣNH_3 (μM)	ΣH_3PO_4 (μM)
	P1 = 13.4 P2 = 14.9 P6 = 15.7 P8 = 24.8	P1 = 1.8 P2 = 1.9 P6 = 2.0 P8 = 2.5	P1 = 9.7 P2 = 10.8 P6 = 11.8 P8 = 17.9	P1 = 0.12 P2 = 0.13 P6 = 0.13 P8 = 0.17	P1 = 8.1-10.3 P2 = 9.2-11.5 P6 = 9.7-12.0 P8 = 15.6-18.6	P1 = 0.34-0.9 P2 = 0.36-0.9 P6 = 0.37-1.0 P8 = 0.5-1.2
Sulphate reduction	If 0.5 mM SO_4^{2-} reduced: ΔNH_3 = 151 μM,	ΔH_3PO_4 = 9.4 μM	If 0.5 mM SO_4^{2-} reduced: ΔNH_3 = 113 μM,	ΔH_3PO_4 = 0.7 μM	If 0.5 mM SO_4^{2-} reduced: ΔNH_3 = 103-115 μM,	ΔH_3PO_4 = 1.9-4.7 μM
	If 1.0 mM SO_4^{2-} reduced: ΔNH_3 = 302 μM	ΔH_3PO_4 = 18.8 μM	If 1.0 mM SO_4^{2-} reduced: ΔNH_3 = 226 μM	ΔH_3PO_4 = 0.7 μM	If 1.0 mM SO_4^{2-} reduced: ΔNH_3 = 206-230 μM	ΔH_3PO_4 = 3.8-9.4 μM

probably cover such variations). Secondly, diffusion is ignored since allowance for it here would introduce complications unnecessary to this discussion.

It is clear from Table 7.3 (Cumulative Totals) that, whichever C : N : P ratio is used, very little dissolved phosphate is produced relative to ammonia. It would appear that only the phosphate levels in cores P1 and P2 could have been produced by aerobic respiration since ammonia is practically absent. However, the presence of dissolved manganese in the pore waters (p.111) argues against this since manganese oxides are reduced subsequent to the effective completion of aerobic respiration.

Considerable quantities of ammonium can be bound to clay minerals, both in fixed and exchangeable sites (Stevenson and Cheng, 1972; Müller, 1977), and adsorption of pore water ammonia by clays is probably important in regulating the dissolved NH_3 concentration where quantities produced by diagenesis are small. Taking the cumulative totals for P1 and P2 in Table 7.3, calculated using the 106 : 10.9-12.2 : 0.2-0.5 ratios (considered the most reasonable), it is apparent that the production of $\sim$25 µM of phosphate (roughly the "equilibrium" value in both cores) would produce $\sim$250-800 µM of ammonia, nearly two orders of magnitude more than is observed. Unfortunately, no data are known which would permit estimation of the quantity of ammonia taken up by clays in these sediments.

In cores P6 and P8 higher dissolved ammonia concentrations accompany lower levels of dissolved phosphate. The ammonia can be accounted for by the reduction of < 0.5 mM SO_4^{2-} (Table 7.3); the phosphate concentrations are then approximately an order of magnitude higher than predicted.

It appears that the production and distribution of dissolved

phosphate in all cores are independent of all diagenetic models which account for the ammonia concentrations. It is possible, therefore, that an additional source of dissolvable phosphorus is present which contributes considerably more phosphate to interstitial water than does oxidation of organic matter. Two phases are potential candidates: poorly-ordered ferriphosphate compounds and skeletal hydroxyapatite derived from marine vertebrates. It was suggested previously (Chapter Four) that ferriphosphates are quantitatively unimportant in Panama Basin sediments. In pore waters, the improbability of ferriphosphate dissolution contributing significant dissolved phosphate is indicated by the low concentrations of dissolved iron (generally < 2 μM, Table C.3, Appendix C) observed in all cores. The other possible phosphate source, skeletal debris of fishes, appears to occur in significant quantities in the sediments (Chapter Four), mainly as hydroxyapatite (Lowenstam, 1974). Carbonate fluorapatite (francolite), which is the principal component of authigenic phosphorites and some animal hard parts (mainly teeth), is of little importance here.

In order to evaluate the probability that hydroxyapatite is a source of dissolved phosphate, the solubility of the mineral in sea water must be clarified. Most workers agree that sea water is supersaturated with respect to carbonate fluorapatite (Gulbrandsen, 1969) but this condition does not apply to hydroxyapatite. Kramer (1964) has pointed out that $Ca_2 \cdot HPO_4 \cdot CO_3^{\circ}$ and $Ca_2 \cdot PO_4 \cdot CO_3^{-}$ ion-pairs greatly reduce phosphate activity in sea water. If allowance for these ligands is made in rigorous solubility calculations, sea water appears to be considerably undersaturated with respect to hydroxyapatite ($pK'^{\circ}_{2C} \simeq 122$ compared to $pK^{\circ}_{2C} \simeq 112$). The calculations are supported by the observation of Arrhenius (1963) that skeletal fish debris recovered from pelagic sediments shows serious signs of corrosion.

Pore waters may be in equilibrium with hydroxyapatite at depth in the four cores studied here. However, considering that dissolved phosphate increases only one order of magnitude, the degree of saturation is difficult to evaluate for the following reasons: (a) a definitive K_{sp} value for hydroxyapatite is unavailable (published values range widely and depend on the degree of substitution of CO_3^{2-} ion); (b) dissociation constants for ion-pairs and complexes involving orthophosphate are available for 20-30°C only (Sillén and Martell, 1964), not for *in situ* temperatures (~2°C); and (c) uncertainty in estimation of an activity coefficient for PO_4^{3-} produces considerable error in the resulting computed pK'_{sp} value.

Two other factors may influence pore water phosphate distributions by extracting PO_4^{3-} from solution: these are adsorption by clays and precipitation of authigenic iron phosphate minerals. Weaver and Wampler (1972) suggest that clays act as a buffer on pore water phosphate concentrations by adsorbing phosphate when concentrations exceed an (undefined) "critical value". However, Stumm and Morgan (1970) state that orthophosphate adsorption by clays is favoured at lower pH values (e.g. pH = 5-6 for montmorillonite; pH = 3 for kaolinite). By implication, adsorption is probably relatively low at the pH of pore water in Panama Basin sediments (~7.8, Bonatti *et al*, 1971).

Iron phosphate minerals, such as vivianite, $Fe_3(PO_4)_2 \cdot H_2O$, have been found in some anoxic marine sediments (Troup *et al*, 1974; Bricker and Troup, 1975) and therefore the likelihood of their occurence in Panama Basin sediments should be investigated. Rosenqvist (1970) reported that at an ionic strength of I = 0.03, the minimum interstitial water activities required for the precipitation of vivianite in the sediments of a Norwegian lake were 10^{-5} M for Fe^{2+} (10 μM) and $10^{-4.5}$ M for "hydroxyapatite" (~190 μM PO_4^{3-} if the accepted

stoichiometry is the unit-cell composition, $Ca_{10}(PO_4)_6(OH)_2$). From the iron phosphates-hydroxides stability field diagram of Nriagu (1972), it can be estimated that in the absence of H_2S and with $a_{Fe^{2+}}$ = 100 μM, a minimum $a_{HPO_4^{2-}} = 10^{-4}$ M (100 μM) is required at pH = 8 for vivianite to be stable. If hydrogen sulphide is present, a much higher phosphate concentration is required. Concentrations of 0.5-5 μM Fe^{2+} (Table C.3, Appendix C) and ~3-30 μM PO_4^{3-} were measured in this study. Considering that in sea water Fe^{2+} is significantly complexed as $Fe.Cl^+$ and PO_4^{3-} highly complexed as HPO_4^{2-} (Garrels and Christ, 1965), only fractions of the analytical concentrations are present as free ions. Therefore, the iron and phosphate concentrations in Panama Basin pore waters are at least two and probably three orders of magnitude less than that required for vivianite precipitation. Equilibrium with hydroxyapatite is far more likely to be the main control on interstitial phosphate distributions.

It is not clear why a significant difference exists between the apparent equilibrium phosphate concentrations of ~28-30 μM in P1 and P2 and ~20-24 μM in P6 and P8 (Fig. 7.2). The lower skeletal phosphate content of the latter cores, especially P8 (Table 4.3), may be insufficient to produce phosphate concentrations of the same level as those in P1 and P2. Previous calculations (Table 4.3) indicated that the surface sediments of core P8 contain a considerably higher level of organic phosphorus than do the foram oozes. Oxidation of this component may contribute a major proportion of the interstitial phosphate, but this cannot be properly evaluated using the equations of Table 7.3 since the quantity of ammonia extracted from solution by the dominant clay fraction is not known.

In summary, it seems likely that dissolution of skeletal apatite is of primary significance in maintaining the dissolved phosphate

concentrations in cores P1, P2 and P6 and of lesser significance in P8 where mineralization of organic phosphorus could be important. The key to a better understanding of these processes lies in future elucidation of the reactions between ammonia and clay minerals. Knowledge of ammonia-clay equilibria will remove an impediment to the use of diagenetic models in explaining the dissolved phosphate distributions in hemipelagic sediments.

A slight alkalinity minimum of 0.2-0.3 $meql^{-1}$ is developed at ~20 cm depth in cores P1, P2 and P6 (Fig. 7.5) which suggests minor consumption. Table 7.1 shows that manganese and iron oxide reduction are the only diagenetic processes which consume an alkalinity component, in this case HCO_3^-. Production of one mole of dissolved manganese and one mole of iron consumes 1.0 and 1.5 equivalents of bicarbonate iron, respectively. The dissolved manganese and iron data of Table C.3 (Appendix C) indicate that a consumption of ~40-70 μeq of HCO_3^- can be acccunted for, about one-quarter of the observed depletion. No other processes are known which could further explain the alkalinity minima in the three cores. In core P8, the higher rate of organic matter oxidation produces a distinct alkalinity increase in the top metre followed by an equally distinct decrease. The consumption of alkalinity at depth in this core is discussed below.

7.4 Distribution of Mn^{2+}

Dissolved interstitial manganese profiles are displayed in Fig. 7.6 and the concentrations listed in Table C.3 (Appendix C). The distribution of Mn^{2+} is generally similar in all four cores - an initial rapid rise in Mn^{2+} concentration is followed by the attainment of apparent equilibrium at depth as in P1, or a maximum in the top metre, as in P2, P6 and P8, below which a nearly steady decrease prevails.

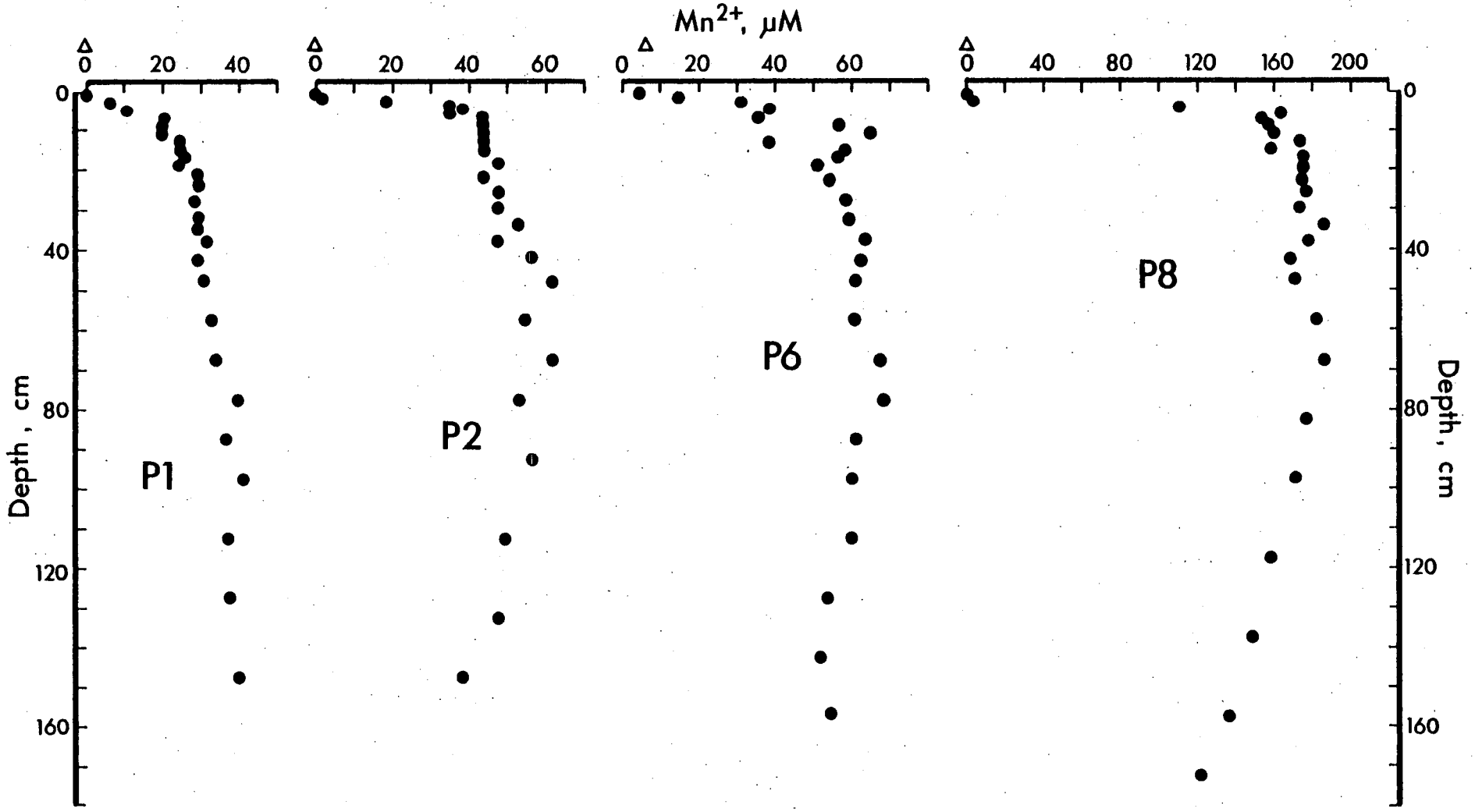

Fig. 7.6 Dissolved manganese profiles, Panama Basin area. Δ = supernatant. Analytical precision = ± 4.5% (1σ, n = 6).

Two well-documented reactions control these distributions: firstly, consumption of oxygen during the bacterial decomposition of organic matter decreases the oxidation potential, initiating dissolution of Mn oxides at Eh values less than about + 330 mV (Hartmann et al, 1976); secondly, as the dissolved manganese concentration increases, a manganese-bearing carbonate may be precipitated if supersaturation is reached (Lynn and Bonatti, 1965; Li, Bischoff and Mathieu, 1969; Calvert and Price, 1972; Robbins and Callender, 1975).

Several workers have applied standard thermodynamic calculations to the problem of Mn^{2+} - $MnCO_3$ equilibria in marine (Li, Bischoff and Mathieu, 1969), estuarine (Holdren et al, 1975), and lacustrine (Robbins and Callender, 1975) interstitial waters. It was concluded in each particular case that supersaturation with respect to rhodochrosite occurred in the upper few metres of the sediments. One feature common to these studies was that, due to very low concentrations, no manganous carbonate could be isolated from the sediments from which interstitial waters were obtained, although Holdren et al (1975) were just able to identify $(Mn,Ca)CO_3$ in some Chesapeake Bay sediments by X-ray diffraction.

In the following section the degree of saturation with respect to $MnCO_3$ at in situ conditions is examined for each of the Panama Basin cores studied. The pertinent reaction is:

$$MnCO_3 \rightleftharpoons Mn^{2+}\ (aq) + CO_3^{2-}\ (aq) \qquad (1)$$

K_{sp} at 25°C and 1 atm is 3.82×10^{-11}, based on equilibrium with precipitated rhodochrosite in water (Morgan, 1967). This value varies as a function of absolute temperature (°K) and pressure (bars) and is thus different for each core. The equation used for determining the in situ K_{sp} is (Edmond and Geiskes, 1970):

$$K_{sp}(T,P) = K_{sp}(298^{\circ}K,\ 1\ bar) \times 10^{-\frac{\Delta V(P-1)}{2.303RT}} \qquad (2)$$

where R = gas constant = 83.15 cm^3 bar deg^{-1} $mole^{-1}$

T = *in situ* temperature, $^{\circ}K$

P = *in situ* pressure, bars

ΔV reaction = change in partial molal volume from reaction (1).

The change in partial molal volume is:

$$\Delta V_{reaction} = V^{\circ}_{Mn^{2+}} + V^{\circ}_{CO_3^{2-}} - V_{MnCO_3} \qquad (3)$$

where $V^{\circ}_{Mn^{2+}}$ = standard state partial molal volume for dissolved manganese, given as -15.5 cm^3 $mole^{-1}$ (Li, Bischoff and Mathieu, 1969).

$V^{\circ}_{CO_3^{2-}}$ = -3.7 cm^3 $mole^{-1}$ (Stumm and Morgan, 1970; Berner, 1971).

V_{MnCO_3} = partial molal volume of pure crystalline rhodochrosite, given as 31.3 cm^3 $mole^{-1}$ (Robie and Waldbaum, 1968).

It is assumed that the temperature dependence of $\Delta V_{reaction}$ is the same as that for aragonite, 0.23 cm^3 deg^{-1} (Edmond and Geiskes, 1970). Then $\Delta V_{reaction(298^{\circ}K)}$ = -50.5 cm^3 $mole^{-1}$ and $\Delta V_{reaction(275^{\circ}K)}$ = -55.8 cm^3 $mole^{-1}$. Using this latter value and equation (2), the *in situ* K_{sp} values for each core have been calculated and are summarized in Table 7.4.

Table 7.4 *In situ* manganese carbonate solubility products for Panama Basin cores.

Core	T($^{\circ}$C)	T($^{\circ}$K)	P(bars)	$K_{sp(in\ situ)} \times 10^{-11}$
P1	2.1	275.3	346	9.1
P2	2.1	275.3	356	9.3
P6	2.4	275.6	275	7.6
P8	2.4	275.6	414	10.7

It is clear from the *in situ* K_{sp} values that $MnCO_3$ solubility increases with increasing pressure, as does calcite.

The calculated thermodynamic solubility product constants ($K_{sp(\underline{in\ situ})}$) are independent of compositional variation in solution (Ben-Yaakov and Goldhaber, 1973). However, their application in sea water requires knowledge of all ion-pairing equilibria and activity coefficients of all ions at the temperature and pressure of interest. Sufficient information exists in the literature to enable reasonable estimation of these quantities; an ion activity product for each sample may then be calculated and compared to the $K_{sp(\underline{in\ situ})}$ to determine the local degree of saturation.

The ion activity product (K'_{sp}) for each sample is defined as follows:

$$K'_{sp(T,P)} = a_{Mn^{2+}(T,P)} \cdot a_{CO_3^{2-}(T,P)}$$

$$= \gamma^T_{Mn^{2+}(T,P)} [Mn^{2+}]^T \cdot \gamma^T_{CO_3^{2-}(T,P)} [CO_3^{2-}]^T \qquad (4)$$

where a = activity

γ^T = total activity coefficient of the species designated by the subscript, at *in situ* temperature and pressure

$[Mn^{2+}]^T$ and $[CO_3^{2-}]^T$ are the total analytical concentrations of each ion, including free and complexed forms. Also, $\gamma^T_{Mn^{2+}(T,P)} = \gamma_{Mn^{2+}(T,P)} \cdot$ (% Mn as free ion) and $\gamma^T_{CO_3^{2-}(T,P)} = \gamma_{CO_3^{2-}(T,P)} \cdot$ (% CO_3^{2-} as free ion).

The degree of Mn^{2+} complexation in sea water is principally a function of HCO_3^- and SO_4^{2-} activities, manganese-chloride complexes being insignificant (Hem, 1963). Using the sea water model of Garrels and Thompson (1962), at 19‰ Cl^-, 25°C and 1 atm, $a_{SO_4^{2-}}$ = 174 ppm. Unfortunately, no dissociation constant data for determination of

$\gamma^T_{SO_4^{2-}}$ at 2°C and high pressures are available. However, $\gamma^T_{HCO_3^-}$ can be determined for *in situ* conditions, using the equations (Berner, 1971):

$$\gamma^T_{HCO_3^-(T)} = 0.55 - 0.003\ (298 - T_{^oK}) \qquad (5)$$

and

$$\log\left(\frac{\gamma^T_P}{\gamma^T_{1atm}}\right) = 1.13 \times 10^{-4}\ (P_{atm} - 1) \qquad (6)$$

Hence, *in situ* $\gamma^T_{HCO_3^-}$ for the four cores is 0.52 ± 0.01 and since $[HCO_3^-]_{\text{Deep Pacific}} = 2.35$ moles m^{-3} (Broecker, 1974), $a_{HCO_3^-}$ (*in situ*) $\simeq$75 ppm. With $a_{SO_4^{2-}} \simeq 174$ ppm and $a_{HCO_3^-} \simeq 75$ ppm, Mn^{2+} is ~32% complexed (Hem, 1963, p. A44), i.e. 68% is available as free ion. Since $\gamma_{Ca^{2+}} = 0.28$ (Garrels and Thompson, 1962) and Ca^{2+} and Mn^{2+} have the same effective diameter in solution (Garrels and Christ, 1965) it can be assumed that $\gamma_{Ca^{2+}} = \gamma_{Mn^{2+}} = 0.28$ and it follows that

$$\gamma^T_{Mn} = (0.68)(0.28) = 0.19.$$

Berner (1971) states that $\gamma^T_{CO_3^{2-}}$ is negligibly affected by ΔT in the oceans. However, pressure does have an effect which can be allowed for using the following equation (Berner, 1971):

$$\log\left(\frac{\gamma^T_P}{\gamma^T_{1atm}}\right)_{CO_3^{2-}} = 3.76 \times 10^{-4}\ (P_{atm} - 1) \qquad (7)$$

$\gamma^T_{CO_3^{2-}}$ at 1atm and 25°C is 0.031 (Li, 1967, quoted *in* Berner, 1971). Therefore $\gamma^T_{CO_3^{2-}}$(*in situ*) is 0.042 for P1 and P2, 0.039 for P6 and 0.044 for P8.

The carbonate ion concentration can be calculated from alkalinity and pH data using the equation (Riley and Chester, 1971):

$$\left[CO_3^{2-}\right]_{\text{m moles } l^{-1}} = A_c \left[\frac{K_2'}{a_{H^+} + 2K_2'}\right] \qquad (8)$$

where A_c = carbonate alkalinity (in units of m moles l^{-1} of H^+ required for titration)

K_2' = second dissociation constant of the carbonic acid system in sea water

a_{H^+} = hydrogen ion activity = antilog (-pH)

Since total alkalinity (= titration alkalinity) = $A_T = \left[HCO_3^-\right] + 2\left[CO_3^{2-}\right] + \left[B(OH)_4^-\right]$, and $B(OH)_4^-$ concentration is only about 3% of A_T, then $A_T \simeq A_c$ where $A_c = \left[HCO_3^-\right] + 2\left[CO_3^{2-}\right]$. The second dissociation constant K_2' at 2°C can be estimated from the tables of Lyman (1956), reproduced by Riley and Chester (1971, p. 133), to be $10^{-9.28}$. Correcting K_2' for *in situ* pressure using the data of Culberson and Pytkowicz (1968) gives $K_2' = 10^{-9.27}$ for P1 and P2, $10^{-9.29}$ for P6 and $10^{-9.25}$ for P8.

Although interstitial pH was not measured in the four cores studied, Bonatti *et al* (1971) determined, by direct electrode insertion, a pH of 7.8 for the upper metre of a core collected from the central Panama Basin (2°45'N, 85°20'W). It is reasonable to assume that this pH is typical for Panama Basin sediments where sulphate reduction is negligible. Since Bonatti *et al* (1971) measured the pH on board ship, corrections for temperature (assumed to be 20°C ± 5°C) and pressure must be applied, according to the equations:

$$pH_P = pH_{1atm} - 4.0 \times 10^{-4} P \text{ (Berner, 1971)}$$

and

$$pH_T = pH_{T(\text{surface})} + 0.011 \left[T_{\text{surface}} - T_{\textit{in situ}}\right] \text{ (Li, Broecker, and Takahashi, 1969).}$$

Hence, corrected pH is ~7.9 for cores P1, P2 and P6 and ~7.8 for P8.

Using these and the T,P-corrected K_2' values, the carbonate concentration equations reduce in each case to:

$$CO_3^{2-} = 0.039\ A_T \quad \text{(P1 and P2)}$$

$$CO_3^{2-} = 0.038\ A_T \quad \text{(P6)}$$

$$CO_3^{2-} = 0.033\ A_T \quad \text{(P8)}$$

Substituting the <u>in situ</u> activity coefficient values and the equations above in (4), the K_{sp}' equations for each core become:

$$K_{sp}' \text{ (P1 and P2)} = 3.1 \times 10^{-4} \left[Mn^{2+}\right] A_T$$

$$K_{sp}' \text{ (P6 and P8)} = 2.8 \times 10^{-4} \left[Mn^{2+}\right] A_T$$

Using the titration alkalinity and dissolved manganese data from Table C.3 (Appendix C), K_{sp}' values have been calculated for each sample and are summarized in Table 7.5 along with the calculated saturation index (see footnote, Table 7.5). It is apparent from these calculations that only the interstitial waters of core P8 are supersaturated with respect to $MnCO_3$. Not surprisingly, this was the core from which a manganese carbonate phase was isolated.

In order to facilitate the saturation calculations, only precipitation of a pure $MnCO_3$ phase was considered. Solid solution of other components can considerably complicate solubility product determination. In a binary system it is reasonably safe to assume ideal behaviour for the solid solution component which has a mole fraction of N = 0.9 (Garrels and Christ, 1965). In such a case, the major component activity (and therefore the major component solubility) decreases in proportion to its mole fraction. However, the precipitated carbonate in core P8 has the composition $(Mn_{49}\ Ca_{46}\ Mg_5)CO_3$ (Table 4.10) which disallows the assumption of ideal behaviour. In the absence of experimental data on the solid solution system, the effective solubility of

Table 7.5 Saturation levels with respect to $MnCO_3$ in Panama Basin area interstitial waters.

Sample Depth (cm)	Mn^{2+} (10^{-6}M)	Alkalinity (10^{-3}M)	$K'_{sp} \times 10^{-11}$	S.I.[1]	Sample Depth (cm)	Mn^{2+} (10^{-6}M)	Alkalinity (10^{-3}M)	$K'_{sp} \times 10^{-11}$	S.I.
	C O R E P 1					C O R E P 2			
0-2	Not detected	2.64	-	-	0-1	Not detected	2.59	-	-
2-4	6.4	2.55	0.52	0.057	1-2	1.8		0.14	0.015
4-6	10.9	2.50	0.84	0.092	2-3	18	2.44	1.4	0.15
6-8	20.9	2.53	1.6	0.18	3-4	35	2.59	2.8	0.30
8-10	20.0	2.36	1.5	0.16	4-5	38	2.44	2.9	0.31
10-12	20.0	2.53	1.6	0.18	5-6	35		2.6	0.28
12-14	24.6	2.51	1.9	0.21	6-8	44	2.37	3.2	0.34
14-16	24.6	2.58	2.0	0.22	8-10	44	2.44	3.3	0.35
16-18	25.5	2.38	1.9	0.21	10-12	44	2.39	3.3	0.35
18-20	24.6	2.56	2.0	0.22	12-14	44	-	-	-
20-22	29.1	2.32	2.1	0.23	14-17	44	2.35	3.2	0.34
22-26	29.1	2.49	2.2	0.24	17-20	47	2.22	3.2	0.34
26-30	28.2	2.31	2.0	0.22	20-24	44	2.28	3.1	0.33
30-34	29.1	2.51	2.3	0.25	24-28	47	2.44	3.6	0.39
34-36	29.1	2.69	2.4	0.26	28-32	47	2.12	3.1	0.33
36-40	31.9	2.68	2.7	0.30	32-36	53	2.50	4.1	0.44
40-45	29.1	2.76	2.5	0.27	36-40	47	2.49	3.6	0.39
45-50	30.9	2.62	2.5	0.27	40-44	56	2.62	4.5	0.48
55-60	32.8	2.73	2.8	0.31	46-50	62	2.69	5.2	0.56
65-70	33.7	2.76	2.9	0.32	55-60	55	2.75	4.7	0.51
75-80	40.0	2.69	3.3	0.36	65-70	62	2.78	5.3	0.57
85-90	36.4	2.64	3.0	0.33	75-80	53	2.76	4.5	0.48
95-100	41.0	2.73	3.5	0.38	90-95	56	2.79	4.8	0.52
110-115	37.3	2.64	3.1	0.34	110-115	49	2.76	4.2	0.45
125-130	37.3	2.55	2.9	0.32	130-135	47	2.77	4.0	0.43
145-150	40.0	2.80	3.5	0.38	145-150	38	2.87	3.4	0.37
	C O R E P 6					C O R E P 8			
0-1	4.6	2.63	0.34	0.045	0-2	Not detected	2.76	-	-
1-2	15	2.65	1.1	0.14	2-4	1.8	2.52	0.13	0.012
2-4	31		2.3	0.30	4-5.5	111	2.68	8.3	0.76
4-6	38	2.70	2.9	0.38	5.5-7	164	2.89	13.3	1.24
6-8	36	2.70	2.7	0.36	7-8.5	153	3.06	13.1	1.22
8-10	56	2.73	4.3	0.57	8.5-10	157	2.82	12.4	1.16
10-12	65	2.69	4.9	0.64	10-12	160	2.73	12.2	1.14
12-14	38	2.63	2.8	0.37	12-14	173	2.84	13.8	1.29
14-16	58	2.95	4.8	0.63	14-16	158	2.82	12.5	1.17
16-18	56	2.54	4.0	0.53	16-18	175	3.02	14.8	1.38
18-20	51	2.20	3.1	0.41	18-21	175	-	-	-
20-25	55	2.41	3.7	0.49	21-24	171	2.99	14.3	1.34
25-30	58	2.45	4.0	0.53	24-28	177	3.13	15.5	1.45
30-35	59	2.56	4.2	0.55	28-32	173	2.98	14.4	1.35
35-40	64	2.60	4.7	0.62	32-36	186	3.39	17.7	1.65
40-45	63	2.51	4.4	0.58	36-40	178	3.17	15.8	1.48
45-50	61	2.59	4.4	0.58	40-45	169	3.25	15.4	1.44
55-60	61	2.54	4.3	0.57	45-50	171	3.23	15.5	1.45
65-70	67	2.75	5.2	0.68	55-60	182	3.09	15.8	1.48
75-80	68	2.71	5.2	0.68	65-70	186	3.70	19.3	1.80
85-90	61	2.77	4.7	0.62	80-85	177	3.21	15.9	1.49
95-100	60	2.70	4.5	0.59	95-100	171	3.17	15.2	1.42
110-115	60	2.70	4.5	0.59	115-120	158	3.21	14.2	1.33
125-130	54	2.67	4.0	0.53	135-140	149	2.15	8.9	0.83
140-145	52	2.73	4.0	0.53	155-160	137	1.83	7.0	0.65
155-159	55	2.57	4.0	0.53	170-175	122	3.01	10.3	0.96

[1] S.I. = Saturation Index = $\frac{K'_{sp}}{K_{sp(\underline{in\ situ})}}$. If: <1, pore water undersaturated; = 1, saturated; >1, supersaturated.

the $MnCO_3$ fraction cannot be calculated but since it is known that solid solution in most compounds reduces effective solubility (Bodine *et al*, 1965; Stumm and Morgan, 1970, p. 207) it is likely that the $MnCO_3$ in the authigenic phase studied here is less soluble than indicated by the pertinent $K_{sp(in\ situ)}$ value. It follows that the computed saturation indices may be low, i.e., the pore waters in P8 may be more saturated with respect to manganese-calcium carbonate than is shown in Table 7.5. Likewise, the pore waters at depth in the other cores, although apparently undersaturated with respect to pure $MnCO_3$, may be supersaturated with respect to the mixed phase. This may apply especially to P2 and P6 where the decrease in Mn^{2+} concentration toward the base of the cores indicates removal of dissolved manganese by a solid phase. No enrichment in the sediment-manganese concentration for P2 and P6 is evident at depth in Fig. 4.16. Hence, if a manganese-bearing carbonate is precipitating in these sediments, it would appear that the loci of precipitation are at depths greater than those sampled.

CHAPTER EIGHT

THE EFFECT OF CLIMATIC VARIATION ON SEDIMENT COMPOSITION

8.1 Introduction

During the Quaternary period, global climate has been in a state of continual change. In the past 100,000 years alone, the termination of one interglaciation (67,000 years ago), a complete glaciation (the Wisconsin) and the beginning 11,000 years ago of the present interglaciation (the Holocene epoch) have occurred. Radiocarbon dating and correlation with another dated core in the eastern equatorial Pacific have shown (Chapter Four) that the three biogenic cores studied in this work encompass the record of sedimentation in the Galapagos Islands area over the past 50,000 years. Variations in sediment composition in these cores can therefore be used to study the effect of the Wisconsin-Holocene climatic cycle on deposition in the eastern equatorial Pacific.

Previous research on climate-sediment interaction has concentrated on the accumulation of biogenic components, especially calcium carbonate. Many investigators have remarked on the positive correlation in eastern Pacific sediments between glacial stages and increases in the $CaCO_3$ concentration (e.g. Arrhenius, 1952, 1963; Hays *et al*, 1969; Thompson and Saito, 1974; Luz and Shackleton, 1975; Pisias, 1976). In fact it is now recognized that carbonate stratigraphy provides a consistent paleoclimatic framework over the entire equatorial Pacific for the past 700,000 years (Valencia, 1977).

In contrast to the major collective investigation of carbonate stratigraphy which has been carried out over the past three decades, the relationship between climatic variations and the vertical distribution of other sediment components has received only cursory attention. In this chapter, therefore, consideration of the effects of climatic change on sediment deposition in the eastern equatorial Pacific will be briefly extended to also include organic carbon and some terrigenous components.

8.2 Oceanographic and sediment responses to climatic fluctuations

The prevailing theory of how changes in atmospheric and oceanic circulation have affected sediment deposition in the equatorial Pacific during the Quaternary period is based largely on the work of Arrhenius (1952, 1963). Briefly, Arrhenius suggests that periodic equatorward advances of polar ice-sheets cause compression of the atmospheric sub-tropical high-pressure cells. Extreme temperature gradients between the equator and the polar ice margins would develop which, in turn, would cause intensification of the major wind systems. In the tropical zone of the Pacific, faster trade-winds would generate increased equatorial current velocities, consequently giving rise to more pronounced upwelling along the equatorial divergence. Biological productivity would thus be enhanced and, according to Arrhenius, would produce a higher net carbonate accumulation rate in equatorial sediments.

Considerable support exists for the trade-wind-upwelling hypothesis. Parkin and Shackleton (1973), for example, found a clear positive correlation between wind intensity increases and Pleistocene cold periods by comparing the size distribution of quartz grains with the $^{18}O/^{16}O$ ratio in benthic foraminifera in an eastern equatorial Atlantic core. Similar conclusions concerning greater global trade-wind intensity during glacials have been reached in studies by Hays *et al* (1969), Hays and Puruzza (1972), Damuth (1975), Gardner and Hays (1976) and Prell *et al* (1976), and most of these authors noted that the rate of upwelling must have been increased concurrently.

There are also indications that deep-water circulation rates were enhanced during glacial periods, as initially suggested by Arrhenius (1952). For example, Damuth (1975) observed increased dissolution of radiolaria in Antarctic Ocean sediments deposited during periods of maximum ice advance; he attributed this feature to faster circulation

of contemporaneous, rapidly-formed, highly corrosive Antarctic Bottom Water. Arrhenius (1952) indicated that faster deep-water circulation would heighten carbonate dissolution. He found it necessary to postulate further that the productivity increase outweighed dissolution effects so that glacial periods in equatorial Pacific sediments would be characterized by a net increase in $CaCO_3$ concentration. The latter association was unquestionably confirmed by Hays et al (1969) but the process producing the correlation has not yet been satisfactorily resolved.

Although glacial stages are probably accompanied by enhanced productivity in upwelling zones, some confusion exists about fluctuations with time in the rate of carbonate dissolution and how these may have affected sediment composition. In contrast to Arrhenius' (1952, 1963) theory, Berger (1973) showed that dissolution effects were greatest during interglacial periods and suggested that the $CaCO_3$ cycles observed in Pacific sediments resulted from fluctuations in dissolution intensity rather than from productivity changes. Subsequent work by Thompson and Saito (1974) and Luz and Shackleton (1975) supported Berger's conclusion to some extent. However, the latter authors also noted that the intensified dissolution hypothesis strictly applies only to sediments at or below the lysocline, and they clearly demonstrated that dissolution was minor in supralysoclinal sediments in the east Pacific. As well as considering dissolution effects, Luz and Shackleton (1975) implied that insufficient evidence exists to support Arrhenius' theory of productivity cycles.

Despite these reservations, some sediments do appear to reflect periodic increases in the rate of supply of calcite. Recent work by Adelseck and Anderson (1978) on a core collected from 3675 m depth, 1500 km west of the Galapagos Islands, has shown that, although carbonate

cycles follow glacial-interglacial variations, the degree of preservation of calcite remains fairly constant with depth and therefore is not correlative with the pattern of climatic change. These authors conclude that, at least in supralysoclinal sediments, cyclic fluctuations in productivity are primarily responsible for variations in the carbonate content.

8.3 Investigation of the Galapagos area sediments

According to the map developed by Parker and Berger (1971), the lysocline in the Galapagos area lies at a depth slightly less than 3000 m. If this is indeed correct then cores P1 and P2, collected from depths of 3422 m and 3510 m respectively, should be subject to cyclical dissolution effects while P6 (raised from a depth of 2712 m) should be affected to a lesser degree. This hypothesis is borne out to some extent by the fact that, in the past 50,000 years, the difference between the maximum and minimum $CaCO_3$ concentrations in the cores is considerably greater in P1 and P2 than in P6 (37, 22.5 and 9.5 wt. %, respectively, Fig. 4.5). However, it should be kept in mind that processes other than dissolution, such as winnowing and increased calcite production, may be important.

It can be seen in Fig. 8.1 that, on a very detailed stratigraphic basis, increased calcite contents are not as directly associated with climatic extremes as has been indicated by most other investigators, who invariably work on a scale of several climatic cycles. The highest carbonate levels in both cores P2 and P6 occur after the Wisconsin termination 11,000 years ago (Termination I, Broecker, 1971) which suggests that, at least in the sublysoclinal core P2, dissolution may have been more intense during the maximum of the Wisconsin glaciation 19,000 to 14,000 years ago (Broecker, 1971). Intensified dissolution may have

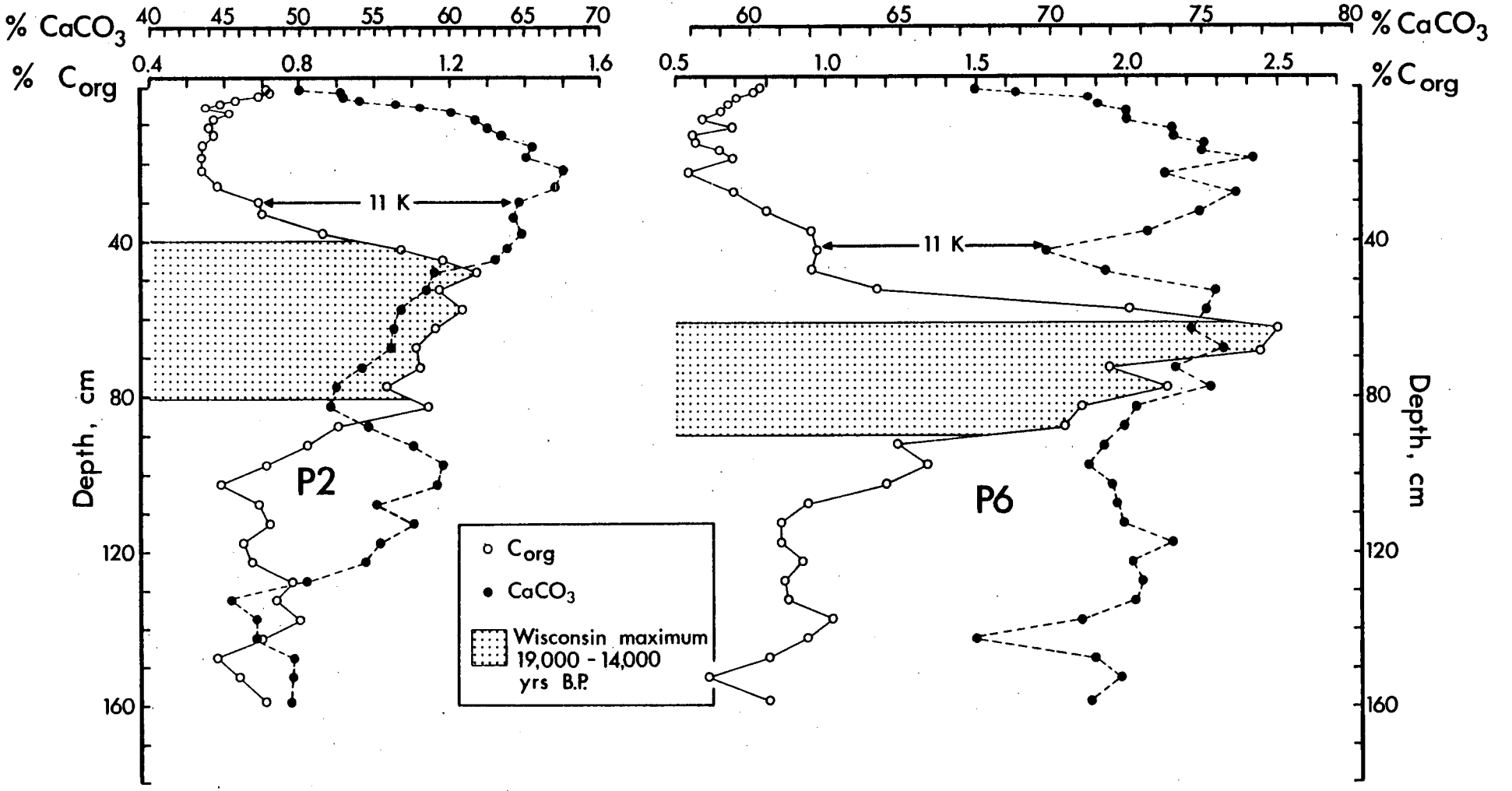

Fig. 8.1 Organic carbon and calcium carbonate distributions in Galapagos area cores P2 and P6 and their association with climatic stages determined by radiocarbon dating (Chapter Four).

been caused on a local scale by greater productivity if the increase in production of foraminiferal and coccolithophorid calcite had been insufficient to balance the increase in the corrosiveness of bottom water - the latter condition would have resulted from the oxidation of greater quantities of tissue carbon. As production waned toward the end of the Wisconsin stage, less calcite may have been dissolved which would be reflected in the profiles by the increase in $CaCO_3$ content after Termination I. This suggestion fits loosely with Arrhenius' (1952, 1963) theory and is given some support by the strong association between organic carbon at depth in the cores and the 19,000-14,000 yr BP period of maximum ice advance (Fig. 8.1).

Although it is likely that these carbon peaks directly reflect enhanced productivity during the climatic extreme, such an association cannot be properly evaluated at this point for the following reasons. Firstly, it is possible that the distribution of organic carbon with depth is a result of a varying degree of post-depositional decomposition. However, the smooth decrease of the I/C_{org} ratios down the cores (Chapter Six) argues against this - a change in the degree of decomposition would be indicated by a deviation of the I/C_{org} profile from a first-order relationship. Secondly, it could be argued that the carbon trends are a function of fluctuations in the total sediment accumulation rate which can directly affect the content of organic matter in sediments. In order to clarify the relative importance of the latter point, it is necessary to investigate variations in total sediment and individual component accumulation rates in the Galapagos area cores.

8.4 Accumulation rates

Since the water content and wet bulk density of the samples were not measured, the bulk sediment and component accumulation rates have been calculated using the equations developed by Lyle and Dymond (1976) for carbonate- and smectite-rich southeast Pacific sediments.[1]

The bulk accumulation rates have been calculated for radiocarbon-dated intervals (Table 4.4) by subtracting the ages of adjacent dated samples and dividing this difference into the sediment thickness between the mid-points of the samples. The range of dated sediments was extended by assuming an age of 0 yr for the tops of the cores and by assuming, somewhat arbitrarily, that the 35,000 yr horizon marked in Fig. 4.5 falls at 132 cm depth in P2 and 142 cm depth in P6.

$CaCO_3$, SiO_2, C_{org}, Al and Ti accumulation rates (A_E) were calculated for each interval using the equation:

$$A_E(gcm^{-2}\ 10^{-3}\ yr^{-1}) = C_E A_B$$

where C_E is the average weight fraction of the element or component in question. The calculations were applied to the two well-dated cores, P2 and P6. All data are listed in Table 8.1.

The data clearly show that net sedimentation rates (in cm $10^{-3} yr^{-1}$) on both the southwest (core P2) and northeast (core P6) sides of the Galapagos Archipelago were higher during the late Wisconsin (Fig. 8.2a). Fastest sediment deposition occurred during the glacial maximum in P2 and slightly later in P6. It should be noted that in both cores

---

[1] Water content (X_W) and wet bulk density (ρ_T) were determined from the respective equations:

$$X_W = 0.83 - 0.36C$$

and

$$1/\rho_T = 0.91 - 0.21C - 0.03C^2$$

where C = the weight fraction of $CaCO_3$ in the dried sample. The bulk sediment accumulation rate (A_B) is then given by:

$$A_B = S\rho_T (1 - X_W)$$

where S is the net sedimentation rate (in cm 10^{-3} yr^{-1})

Table 8.1 Sedimentation rates and accumulation rates of selected components in Galapagos area cores.

	Interval (cm)	Interval (yr)	Net Sedimentation Rate ($cm10^{-3}yr^{-1}$)	Bulk Sediment Accumulation Rate ($gcm^{-2}10^{-3}yr^{-1}$)	Component Accumulation Rates ($gcm^{-2}10^{-3}yr^{-1}$)					Accumulation Rate Ratios		
					$CaCO_3$	C_{org}*	Al*	Ti*	SiO_2	$\frac{CaCO_3}{Al}$	$\frac{Ti}{Al}$	$\frac{CaCO_3}{SiO_2}$
P2	0-4	0-4005	1.0?	0.46?	0.24?	3.2?	6.0?	0.39?	0.16?	40?	0.065?	1.5?
	4-34	4005-12310	3.6	1.87	1.20	11	18	1.4	0.50	67	0.078	2.4
	34-48	12310-16970	3.0	1.56	0.98	17	16	1.3	0.44	61	0.081	2.2
	48-77.5	16970-18840	15.8	7.48	4.2	85	76	5.7	2.8	55	0.075	1.5
	77.5-97.5	18840-24450	3.6	1.70	0.95	15	16	1.1	0.60	59	0.069	1.6
	97.5-132	24450-35000?	3.2?	1.46?	0.79?	10?	13?	0.85?	0.55?	61?	0.065?	1.4?
P6	0-4	0-3575	1.0?	0.56?	0.39?	4.1?	8.5?	0.40?	0.09?	46?	0.047?	4.3?
	4-22.5	3575-6190	7.1	4.27	3.2	26	57	2.6	0.63	56	0.046	5.1
	22.5-47.5	6190-11890	4.4	3.39	2.5	29	35	1.7	0.51	71	0.049	4.9
	47.5-57.5	11890-12730	11.9	7.17	5.4	114	77	3.9	0.99	70	0.051	5.5
	57.5-77.5	12730-15870	6.4	3.86	2.9	87	42	2.2	0.50	69	0.052	5.8
	77.5-102.5	15870-24660	2.8	1.63	1.2	24	20	1.1	0.26	60	0.055	4.6
	102.5-142	24660-35000?	3.8?	2.20?	1.6?	20?	27?	1.6?	0.37?	59?	0.059?	4.3?

* ($mgcm^{-2}10^{-3}yr^{-1}$)

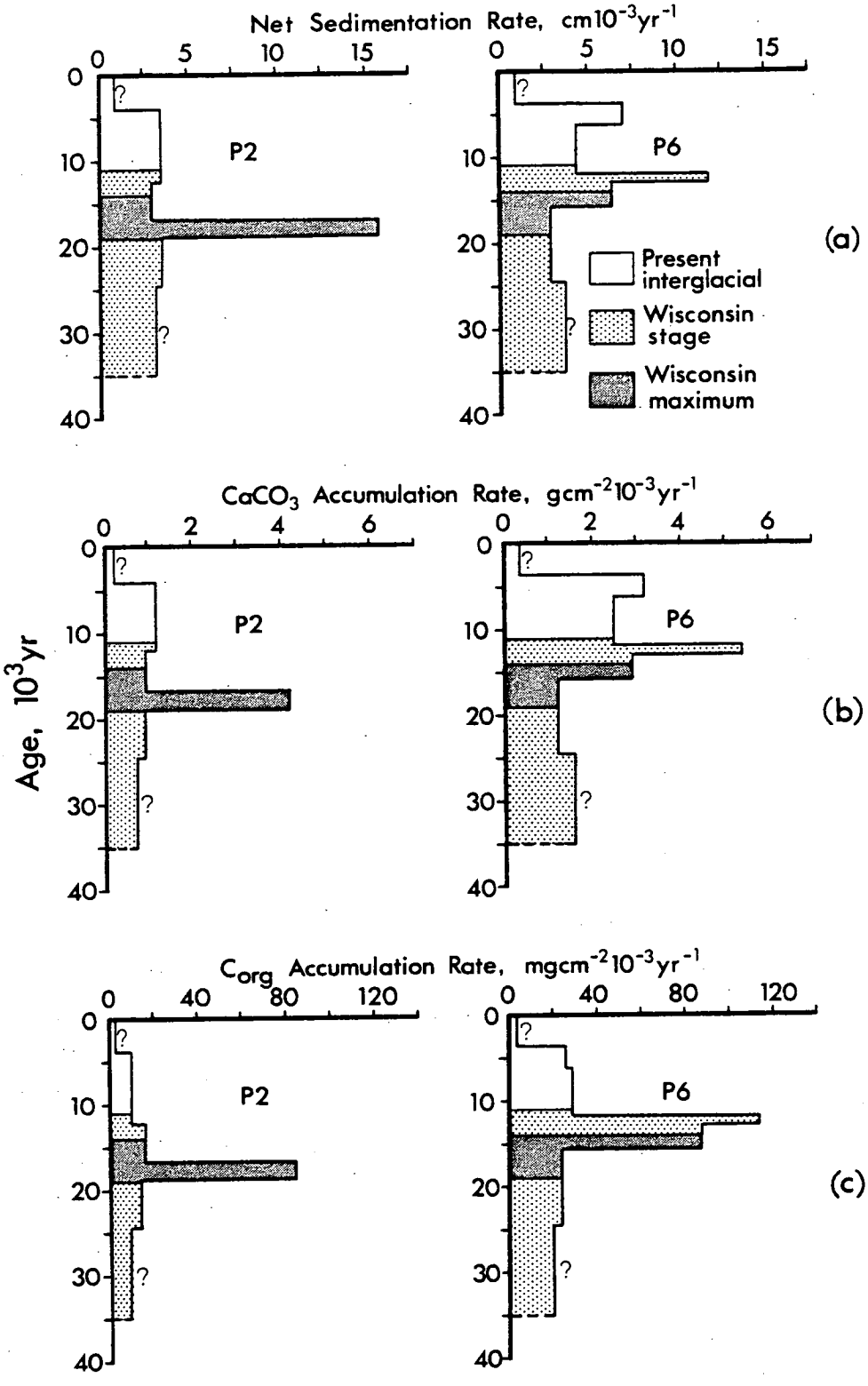

Fig. 8.2 Variations with time in cores P2 and P6 of
(a) the net sedimentation rate;
(b) the carbonate accumulation rate; and
(c) the organic carbon accumulation rate.

sedimentation rates calculated for intervals defined by similar dates are highly subject to the error inherent in determining the difference (in years) between radiocarbon ages. Hence, the net sedimentation rates calculated for both the 16970-18840 yr BP and the 11890-12730 yr BP intervals in P2 and P6 could both be high by a factor of nearly two.

Down-core fluctuations in the total accumulation rate of the bulk sediment dominate variations in the accumulation rates of specific components (except, perhaps, organic carbon) and, as a result, profiles of the latter approximately parallel those of the bulk sediment (Figs. 8.2b, 8.2c and 8.3). These profiles indicate that the rates of accumulation of all the sediment components investigated here were higher near the Wisconsin peak. Given the limited data available, this consistency is difficult to explain. It is possible that the concurrent accumulation rate increases of all components arose from faster deposition of sediments eroded from ridge and slope deposits. However, this process should produce anomalously old radiocarbon dates as have been seen in core P8 (p. 40). Such anomalies are not observed in either P2 or P6. It is likely that two other processes are important: biological productivity variations and eustatic changes in sea level.

Since differential diagenetic effects on the carbon distribution have been ruled out by the smooth I/C_{org} profiles, the increased carbon accumulation rate during the Wisconsin maximum can only be due to increased productivity or the preserving effect of the higher sedimentation rate. However, since the net sedimentation rate must have been increased mainly as a result of a greater flux to the sediments of biogenic detritus, the rate of production of organic carbon must have been enhanced concurrently - it can be concluded that the carbon peaks coincident with the Wisconsin maximum (Fig. 8.1) do indicate exceptionally high biological productivity during that period.

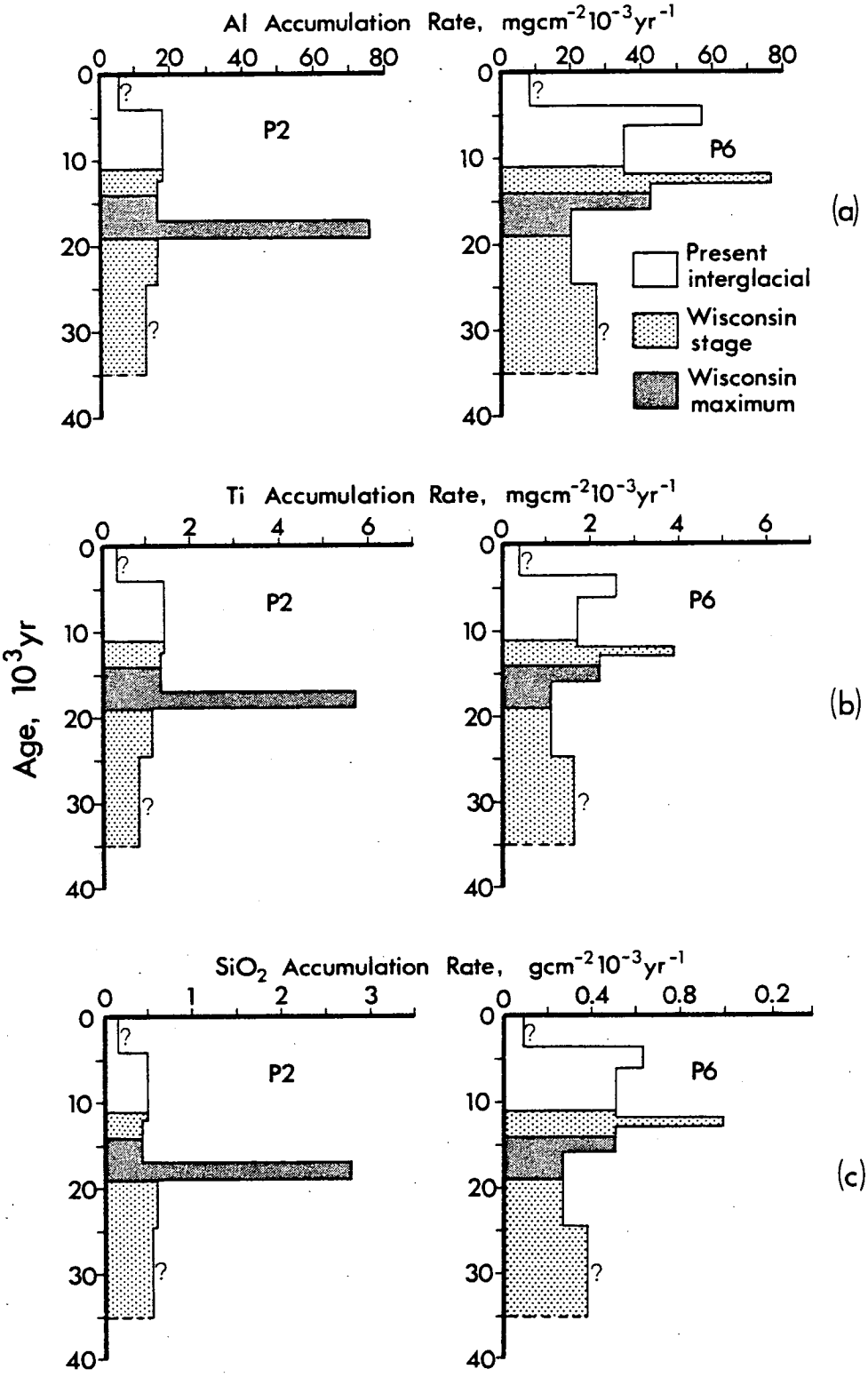

Fig. 8.3 Accumulation rate variations in cores P2 and P6 of:
(a) aluminium;
(b) titantium; and
(c) silica.

The high $CaCO_3$ and SiO_2 accumulation rates during the Wisconsin peak are also a reflection of exceptional productivity. Arrhenius (1952) found similar increased accumulation rates of these components during glacial maxima but noted that, in contrast to $CaCO_3$, the SiO_2 concentration in the sediments tended to be highest during interglacials. He attributed this distribution to increased dilution by $CaCO_3$ during circulation minima. Acceptance of this hypothesis implies that during cold periods either greater silica dissolution or less $CaCO_3$ dissolution occurred, or $CaCO_3$ production was increased to a proportionately higher degree than SiO_2. There is no evidence to indicate that the first alternative (silica dissolution) is correct (see Dinkelman, 1974). In supralysoclinal core P6, there is a distinct increase in the $CaCO_3$/SiO_2 accumulation rate ratio during the Wisconsin maximum (Fig. 8.4a) which supports the latter suggestion that the relative increase in calcite production exceeded the proportionate increase in silica production during glacial periods. The reason for this difference is unknown.

The probable influence of eustatic sea level changes on accumulation rates is quite clear. At the height of the Wisconsin, sea level stood about 120 m lower than at present (Curray and Moore, 1964) and a considerable area of the Galapagos Platform and the continental shelves bordering the Panama Basin would have been exposed. Fluvially-transported continental material would therefore have been discharged nearer the continental margins rather than sedimenting-out on the shelves. Such direct input of sediment to the open sea, coupled with erosion of the exposed shelves and transport by the intensified currents thought to have been characteristic of the period, probably produced the net increase in the accumulation rate of the terrigenous fraction observed in P2 and P6 during the last major cold interval.

The sedimentological regime active in the Galapagos area during the Wisconsin maximum therefore appears to have been characterized both by greater terrigenous input and by higher production of carbonate, silica and organic carbon. This situation can be considered to be broadly analogous to contemporaneous deposition on the Californian continental margin. In that area, carbonate accumulation rates increased at least twofold during the period 12,000-17,000 yr BP, ostensibly as a direct result of increased upwelling (Gorsline and Prensky, 1975). At the same time, the accumulation rate of terrigenous detritus was about an order of magnitude higher since the lower sea level assisted delivery of sediments to distal areas of the borderland.

In core P6, the rise in the $CaCO_3$/Al accumulation rate ratio (in essence, the ratio of the absolute concentration of the two components averaged over each dated interval) near the climatic extreme (Fig. 8.4b) suggests that the productivity increase was proportionately larger at the time than the terrigenous input to these supralysoclinal sediments. In contrast, sublysoclinal core P2 has a minimum in the $CaCO_3$/Al accumulation rate ratio at the glacial extreme which may have resulted from concurrent greater carbonate dissolution, as discussed earlier.

The high-titanium basalts of the Galapagos Platform probably had increased importance as a source of terrigenous detritus during the Wisconsin maximum. The combination of increased physical erosion resulting from stronger easterly trade-winds and greater dispersion of detritus by the intensified westward-flowing Peru Current - South Equatorial Current (Chapter Two, Fig. 2.3) should have led to a higher rate of deposition of basaltic debris in sediments on the "downstream" side of the Archipelago. Support for this hypothesis is given by the Ti/Al accumulation rate ratio in core P2 which shows a maximum approximately

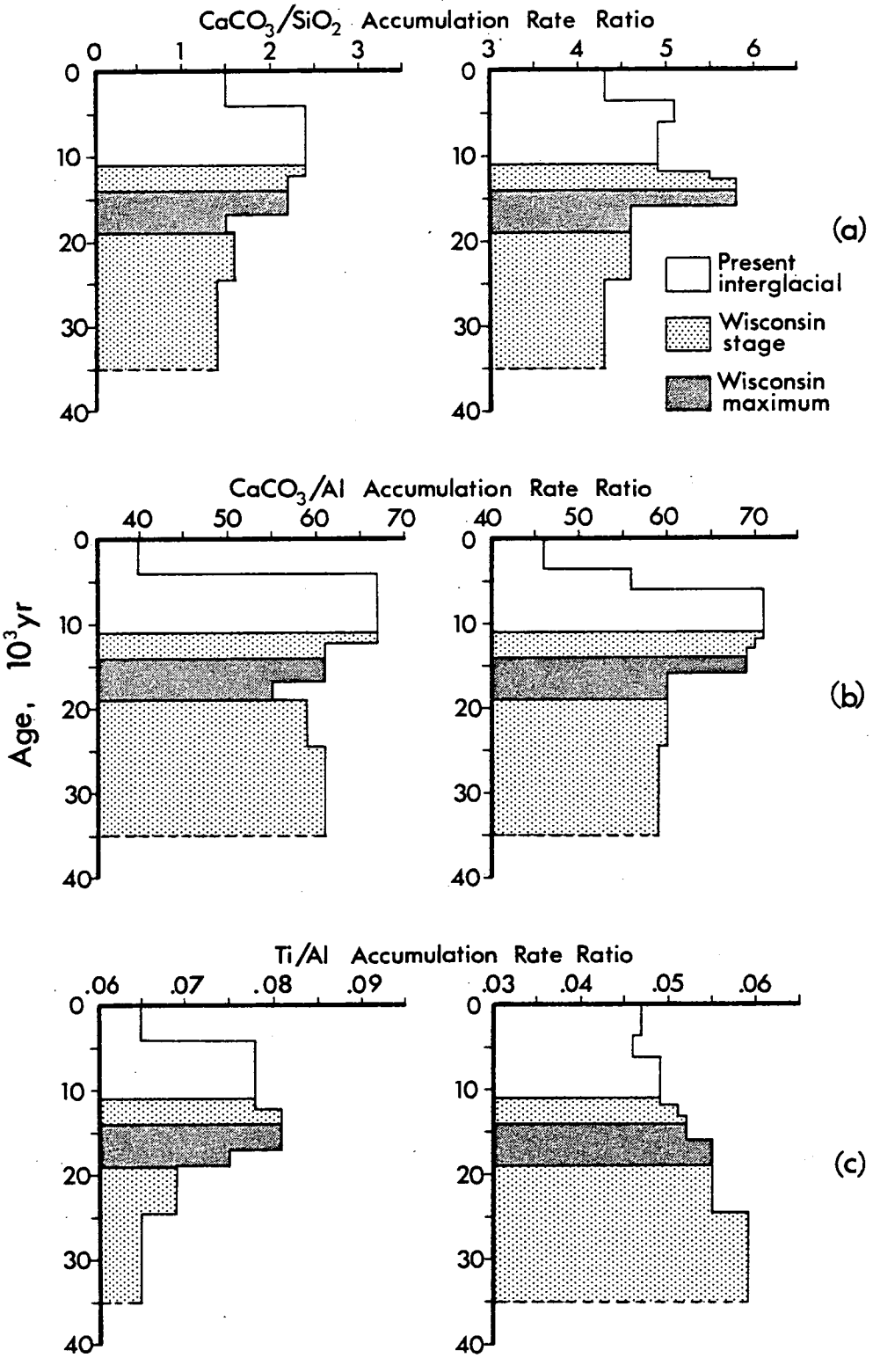

Fig. 8.4 Variations of accumulation rate ratios with time in cores P2 and P6:
(a) $CaCO_3/SiO_2$; (b) $CaCO_3$/Al; and (c) Ti/Al.
The ratios are, in essence, the absolute concentration ratios of each pair of components, averaged over each dated interval.

coincident with the Wisconsin peak (Fig. 8.4c). In core P6, the Ti/Al rate ratio increases with age (depth), in contrast to the pattern established in P2, and is apparently unrelated to the Wisconsin-Holocene climatic sequence. In the absence of additional data, the process(es) controlling this distribution cannot be clarified.

CHAPTER NINE

SUMMARY AND CONCLUSIONS

This thesis has investigated some of the many factors which collectively govern the composition of hemipelagic sediments in the oceans. Emphasis has been placed on the importance of diagenetic processes which have been shown to have a major effect on the eventual composition of buried eastern equatorial Pacific sediments.

Surface circulation in the eastern equatorial Pacific is complex. The combination of upwelling associated with the equatorial divergence, the Peru and Colombia currents, and the Cromwell Current (which breaks surface around the Galapagos Islands) produces rapid nutrient recycling over large areas of the Panama Basin, thereby giving rise to some of the most productive surface waters in the oceans.

The sediments in the Panama Basin are conveniently divided into two major facies: dominantly terrigenous clays, confined mainly to the area east of the Coiba-Malpelo Ridge system, and highly calcareous oozes which occupy most of the remainder of the Western Basin and Galapagos Platform areas. The mineralogy of the non-biogenic fraction is broadly similar across the Panama Basin, consisting largely of smectite with subordinate quantities of chlorite, kaolinite, illite, quartz and feldspars. The zeolite, clinoptilolite, occurs in only one core and is probably derived from reworked Pleistocene sediments proximal to the Coiba Gap region.

An integral part of this study has been the detailed investigation of the major and minor element compositions and interstitial water chemistry of four cores collected from both sediment facies in the Panama Basin area. These data have been supplemented by elemental analyses of a short box-core raised from the Galapagos Spreading Centre and the tops of seven additional cores. A number of the most important findings will be highlighted here.

Phosphorus is partitioned amongst detrital, organic and biogenous phases in the sediments. Limited evidence suggests that a fourth phase, ferriphosphate, may be quantitatively unimportant. In the carbonate ooze, the biogenous phase, in the form of marine vertebrate skeletal debris, apparently predominates. This material is composed of hydroxyapatite which, on the basis of thermodynamic considerations, appears to be soluble in the deep-sea. Dissolution of this phase with time may be responsible for the decreasing phosphorus concentrations observed at depth in these sediments. In the terrigenous clays, organic matter is thought to be the principal phosphorus host. Bacterially-mediated metabolization of this material could be responsible for the P decrease at depth in this facies.

Diagenetic modelling of the interstitial water composition reveals a large excess of dissolved phosphate relative to organically-derived ammonia in all of the sediments. In the calcareous oozes this can be reasonably explained by skeletal apatite dissolution, while in the clay facies, decomposing organic matter appears to be the major dissolved phosphate source. In the latter sediments uncertainty about the degree of uptake of dissolved ammonia by clays inhibits resolution of the relative importance of skeletal apatite and organic material as contributors of dissolvable phosphorus.

In a core collected from the north flank of the Galapagos Spreading Centre, a band of sediment occurs which has an anomalously high Fe, Mg, Si and K content (relative to aluminium) and a high smectite/kaolinite + chlorite ratio. These chemical and mineralogical characteristics suggest that about 40% of the non-biogenic fraction in the horizon is of hydrothermal origin. The "excess" smectite possibly formed authigenically from the reaction of iron oxides, sea water Mg (and K?) and/or biogenic silica. Interstitial iron analyses indicate that some iron

oxides may still be present in the zone and are dissolving under the influence of the low oxidizing potential present below shallow depths in the sediments. The absence of a manganese association with the horizon is thought to result from dissolution subsequent to burial of the hydrothermal precipitates. Minor metals, notably chromium, cobalt, copper and zinc are enriched in the metalliferous band. Since Cr is not enriched in ferromanganese nodules, its presence in this zone implies a hydrothermal/volcanic source for the element. It follows that the other metals may have been similarly supplied although post-precipitation adsorption onto iron oxides cannot be ruled out.

High surficial manganese concentrations which decrease rapidly with depth to very low levels are characteristic of Panama Basin sediments. This distribution can be attributed to a well-documented diagenetic recycling process which is contingent upon a lowering of the sediment oxidation potential as bacterial decomposition of reactive organic matter consumes free oxygen. Dissolution of surficial manganese oxides upon burial increases the dissolved manganese concentration in pore waters. Thermodynamic calculations indicate that the interstitial manganese concentration is limited by precipitation of a manganese-bearing carbonate. An authigenic mineral of this type, having the composition $(Mn_{51}Ca_{45}Mg_4)CO_3$, is found in an ash-rich horizon in one core. It is suggested that the ash-carbonate association is a result of the larger mean grain size in the ash layer which encourages spontaneous nucleation of carbonate seed crystals. This interpretation disagrees with at least one previously published hypothesis (Strakhov, 1969) which was developed to account for the frequently-observed association of manganese-bearing carbonates with coarser horizons in sediments and sedimentary rocks.

Investigation of the stable carbon isotopic composition of the Panama Basin Mn-carbonate and a similar authigenic phase recovered from manganese nodule-bearing sediments in Loch Fyne, Scotland, indicates that little carbon of organic origin is involved in the carbonate precipitation reaction. The data suggest that an increase in organically-derived dissolved carbonate is not necessarily a prerequisite for Mn-carbonate formation. Rather, the quantity of MnO_2 available for dissolution appears to be the major chemical factor governing Mn-carbonate precipitation, at least in the sediments studied.

The molybdenum distribution in Panama Basin sediments can be broadly likened to that of manganese. High Mo concentrations in surface sediments, reaching nearly 80 ppm, result from adsorption of the element from sea water onto manganese oxides. It is postulated that subsequent reduction of the oxides upon burial releases Mo^{6+} to pore water. Concurrent minor reduction of interstitial sulphate produces hydrogen sulphide in quantities sufficient to locally exceed the solubility product of FeS and some of the dissolved molybdenum coprecipitates with iron monosulphides; the remainder is thought to diffuse upward and be readsorbed by the oxides or lost to sea water. This hypothesis can account for the variable Mo concentrations seen at depth in the sediments and provides an explanation for previously observed (Raab, 1972) Mo enrichments on the bottom surfaces of ferromanganese nodules.

The partitioning and chemistry of zinc and the transition metals Co, Cu and Ni is highly complex in the sediments investigated in this work. In the surficial biogenic sediments all four elements appear to be associated with manganese oxides, in the order $Ni \geq Co > Cu > Zn$. These surface enrichments are not observed in the organic-rich terrigenous clays, possibly because metal adsorption by oxides is inhibited

chemically by complexation with organic ligands in interstitial solution and kinetically by relatively rapid sedimentation. In the Galapagos area cores, Ni, Co and Zn appear to be associated with organic carbon at depth in the sediments. This relationship can be explained by a hypothetical, qualitative diagenetic model based upon three main factors. The model suggests that the high biological productivity characteristic of Panama Basin surface waters is important in maintaining a substantial flux of metals to the sea floor. Resolution of the biologic detritus at or near the sediment-water interface creates an environment conducive to uptake of metals by surficial oxides. Subsequent dissolution of the oxide phase upon burial greatly increases the concentration of metal ions in solution which drive the reaction

$$\text{Metal}^{2+}(aq) + 2RCOO^{-}(s) \longrightarrow \text{Organometallic complex}$$

to the right. It is important to recognize that, although biological productivity is clearly important in this sequence, the model is most strongly contingent upon the initial concentration of metals by the oxide phase. In the absence of oxides, for example in wholly anoxic sediments, lower metal/C_{org} ratios should occur since the mechanism for producing metal enrichments in pore waters is absent.

Iodine and bromine are strongly associated with organic matter throughout Panama Basin sediments. Both elements appear to be adsorbed from sea water at the sediment-water interface but the process involved is not yet clearly known. The post-depositional behaviours of the two halogens are dissimilar. I/C_{org} ratios decrease smoothly with depth, following a first-order relation. The I/C_{org} profiles indicate that the progressive loss of iodine relative to carbon is independent of the greatly increased iodine concentration in zones of high carbon content. In complete contrast Br/C_{org} ratios approximately

parallel the vertical bromine distribution, implying that bromine is refractory during diagenesis, relative to both iodine and most of the carbon. It is suggested that this difference between the two elements is due to sorption by different sites in the host organic matter.

Total dissolved iodine analyses in interstitial water indicate that the carbon peak coincident with the Wisconsin glacial maximum is, at present, the major source of dissolved iodine in central Panama Basin pore waters. Flux calculations suggest that upward-diffusing dissolved iodine, diagenetically remobilized from the sediments, may contribute up to 2% of the dissolved iodine content of Panama Basin Bottom Water.

Investigation of the effects of the Wisconsin-Holocene climatic transition on sediment composition in the Galapagos Islands area indicates that climate has directly influenced sedimentary processes during the past 50,000 years. The striking correlation of the peak of the Wisconsin glacial stage (19,000-14,000 yr BP) with high organic carbon concentrations in the biogenic sediments is attributed to increased biological productivity in surface waters caused by enhanced upwelling during the climatic extreme. During this period the high flux of carbon to bottom water may locally increase the total CO_2 concentration causing greater $CaCO_3$ dissolution in sublysoclinal sediments. Detailed radiocarbon dating permits calculation of bulk sediment and component accumulation rates. During the Wisconsin maximum the rate of sediment accumulation was considerably higher than at any other time during the past 40,000 years. It is suggested that the sharp rise in all component accumulation rates during the extreme can be explained by a eustatic lowering of sea level coupled with very high biological productivity. A well-defined maximum in the Ti/Al accumulation rate ratio in a core collected 250 km southwest of the Galapagos Islands coincides with the

Wisconsin peak, indicating that the high-titanium Galapagos basalts contributed a proportionately larger quantity of basaltic debris to "downstream" sediments when extreme climatic conditions prevailed.

In this thesis, the integrated examination of the mineralogy, major and minor element composition and interstitial water chemistry of Panama Basin sediments has been invaluable in assessing influences on sediment chemistry. Diagenetic processes have been shown to widely affect eastern equatorial Pacific sediments and it is hoped that this research may stimulate a fuller appreciation of their significance.

APPENDICES

APPENDIX A

SAMPLE COLLECTION AND CORE DESCRIPTION

Samples were collected during cruise 2/1976 of the R.R.S. Shackleton (April 30 - May 25, 1976) in the eastern equatorial Pacific Ocean. A suite of thirteen 6 cm-diameter cores were recovered with a stainless steel gravity-corer lined with butyl acetate. In order to minimize disruption during coring of the thin oxic surface layer characteristic of Panama Basin sediments, a greatly reduced rate of entry of the corer into the sediments ($\sim$0.25 m sec^{-1}) was employed. In addition, the fingers of the sphincter-type Cu-Mo alloy core catcher were opened and trimmed well back prior to use.

Following the recovery of each core, the "supernatant" water was carefully removed with 50ml disposable syringes, thus avoiding disturbance of the sediment surface, and the core was capped, labelled and logged on deck. Cores intended for pore water squeezing were cut into 30 cm sections with a clean hacksaw, all cut sediment surfaces scraped with a plastic spatula and the sections capped and refrigerated until they could be squeezed. One-to-five cm-thick samples were removed for squeezing by extruding the sediment sections with a vinyl-coated brass plunger and slicing off the required thickness with a clean plastic spatula. The core "slices" were placed directly in the squeezing apparatus and the pore water was expressed as described in Appendix B. After squeezing, the considerably drier sediments were placed in plastic bags, sealed and frozen.

The unsqueezed cores were frozen for transport to Edinburgh. Tops of these cores were removed in the Grant Institute by cutting off the upper several centimetres with a hacksaw. These sections were sawn in half while still frozen. One half was wrapped in polyethylene and returned to the freezer and the other thawed and subsampled for analysis.

All core and surface sediment samples were oven-dried at 50°C in

clean plastic jars; portions of the dry samples were subsequently ground to a fine (< 200 mesh) powder in a tungsten carbide Tema disc mill. Sample numbers consist of the core number and the depth range (in cm) of the sample in the core. For example, P2:8-10: refers to a 2 cm-thick sample collected from Core P2 at 8-10 cm depth.

The sediments are briefly described in Table A.1. Samples from the Pleiades box core were not examined visually but are probably very similar to core P6.

Table A.1 Description of sediment cores investigated in this study (with the exception of the Pleiades box core collected by the Scripps Institution of Oceanography).

Core Number	Length (cm)	Log Description	Microscopic Description
P1	150	Foram ooze; 10 cm-thick creamy-brown oxidized layer grading quickly at 10-12 cm to gray-green reduced sediment. Irregular lighter-coloured carbonate-rich patches at depth. No H_2S odour.	Whole sand-sized foraminifera and foram fragments predominate with infrequent whole radiolaria and occasional diatoms and siliceous spicules. Surface sediments contain abundant fine-grained ($\ll 50$ μm) black micronodules. No glass shards noted.
P2	163	Foram ooze; 4 cm-thick brown oxic top overlying gray-green to creamy-olive sediment. No H_2S.	Similar to P1.
P5	263	A few mm of light brown highly-foraminiferal sediment mantling pale gray-green homogeneous foram sand. No H_2S.	Mostly whole forams in a fine-grained matrix consisting largely of comminuted carbonate fragments. Occasional radiolaria; very rare micronodules in surface sample.
P6	159	Foram ooze; oxic-anoxic (brown-green) boundary at about 14 cm. Sediment becomes darker green with increasing depth. Possible trace of H_2S near base?	Whole and fragmented forams predominate. Fine-grained (typically ~ 5 μm) disseminated micronodules common in surface sediments. Some spicules and occasional whole radiolaria.
P7	190	Foram ooze; 1 cm-thick brown oxic top grading to olive-green. Some evidence of bioturbation just below the sediment surface is furnished by brown meandering stripes surrounded by green reduced sediment. Trace H_2S at base?	Abundant foram fragments and less abundant whole tests with common micronodules (surface sample only); some radiolaria, spicules, and rare diatoms.
P8	183	About 5 cm dark chocolate brown oxic clay overlying homogeneous stiff very dark green clay. Very rare forams visible as white specks. Slight H_2S odour in lower half of core. Significant quantities of creamy-brown to black friable crusts noticed in bottom 20 cm.	0-5 cm: clay, common black micronodules, very rare forams. 5-160 cm: occasional clear glass shards in homogeneous clay matrix. Very few forams, some spicules and very rare radiolaria. 160-bottom: abundant clear glass shards ($\sim 25\%$?) ranging from 10-400 μm in size. Subhedral creamy-white to gray crystals up to 800 μm long and having two cleavages are probably feldspars. Clear subhedral to anhedral quartz grains are present along with some biotite flakes, amphibole, and rarer brown subhedral crystals with high R.I. (zircon ?). Some spicules and rare forams present. Creamy-white to brown (occasionally pinkish) friable, often botryoidal crusts are a major component.
P9	168	Thin (few mm) dark-brown surface layer overlying dark-green clay. H_2S present below 80 cm depth.	Predominantly homogeneous clay; rare forams and diatoms.
P10	150	4 cm-thick very dark brown surface layer overlying homogenous non-gritty olive-green clay. Distinct H_2S odour at base.	Clay with rare glass shards, forams and diatoms. In surface sample, micronodules abundant. Frequent ovoid pellets 100-200 μm in size appear to be clay-micronodule aggregates and may be faecal pellets produced by benthic organisms.
P11	190	1 cm-thick brown top overlying homogeneous non-gritty olive-green clay. Distinct H_2S odour at base.	Clay; no glass shards visible, very rare forams. Very few ovoid pellets.
P12	225	4 mm brown oxic top sharply overlying dark-green clay. Intense H_2S generation at base of core.	Clay; no shards, little coarse detritus.
P13	150	1 mm-thick brown layer mantling gray-green clay. No H_2S noticed.	Surface: clay with abundant quartz, feldspar, amphibole, pyroxene(?) and possibly epidote-group minerals. Few siliceous spicules, rare forams, rare very fine-grained glass shards. Ovoid to near-spherical bright green to black friable pellets (~ 100 μm long) may be glauconitic.

APPENDIX B

ANALYTICAL METHODS

B.1 Mineralogy : X-ray diffractometry

Approximately 1.5g samples, ground in a WC Tema disc mill to pass 200 mesh, were prepared for X-ray diffraction analysis using the following procedure. To remove $CaCO_3$, samples were placed in 80 ml polyethylene centrifuge tubes with 40 ml of 14% acetic acid; this treatment does not harm clay minerals (Carroll and Starkey, 1971). The tubes were shaken occasionally in a 70°C water bath until effervescence ceased (usually 5-10 min). No calcite peaks were observed in subsequent diffractograms. The suspension was centrifuged at 200-2400 rpm for 10 min, the supernatant decanted off, and the sample resuspended in distilled deionized water, centrifuged and decanted again.

Amorphous Fe-Mn oxides were removed by the dithionate-citrate method of Mehra and Jackson (1959) as follows: 40 ml of 0.3 M Na-citrate and 5 ml of 1 M $NaHCO_3$ solutions were added, the suspension warmed to 70°C and approximately 1g of $Na_2S_2O_4$ added. The tubes were capped, shaken vigorously for at least 30 sec and occasionally during the next 15 min. The samples were again centrifuged and the supernatant decanted. Resuspension in warm Na-citrate followed by centrifugation and a distilled water wash ensured suitable extraction of oxides. After centrifugation and decantation of the wash liquid, the sediment was resuspended in several ml of distilled water and poured into 100 ml polycarbonate beakers. To remove amorphous silica 50 ml of 2% Na_2CO_3 solution was added and the suspension boiled for 1 hr. Unfortunately this treatment removed only a portion of the opal from the highly opaline sediments of the Galapagos Platform area, possibly because the solution became saturated. Otherwise, the procedure was generally effective. Hot (80°C) 0.5 N NaOH was briefly investigated as an alternative removal agent for opal. Although the opal background on diffractograms was lowered by a 5 min suspension in 0.5 N NaOH, clay

mineral peak intensities were reduced and the peaks suffered general loss of sharpness. Hence, the less severe Na_2CO_3 treatment was adopted in preference. Finally, the treated sediment was twice centrifuged and washed with distilled water and redispersed in sufficient water (usually ~20ml) to produce an opaque suspension when held up to a fluorescent light. If flocculation occurred, a very small quantity of sodium hexametaphosphate was added and the sediment thoroughly deflocculated in a Mettler ultrasonic bath.

The sediment was mounted on 2 x 3 cm unglazed ceramic tiles, cut from bulk tile supplied by H. & R. Johnson Ltd., Tunstall, Stoke-on-Trent. The tiles were placed on a hot-plate, warmed to ~60°C, and drops of the well-shaken suspension were dispensed onto them with a Pasteur pipette and quickly evaporated. Rapid evaporation avoids differential settling which can enhance X-ray response of finer components (Archer, 1969).

The tendency of the sediment layer to crack and curl prevented build-up of a thickness sufficient to mask the diffraction spectrum (quartz, cristobalite, and anorthite) of the tile. Therefore unoriented powder mounts of selected samples were prepared for examination of quartz, feldspar, and "total" clay distributions. Untreated ground sediment was poured into aluminium planchets and lightly compressed with a gear-type mechanical press. The planchets were presented directly to the X-ray beam.

Analytical conditions used for all diffraction runs were as follows: CuKα radiation at 36 kV, 20mA; Ni filter; curved graphite crystal monochromator; variable dispersion slits from $\frac{1}{4}^\circ$ 2θ to 1° 2θ; chart speed $\frac{1}{8}^\circ$ 2θ min^{-1} to 1° 2θ min^{-1}.

B.2 Pore water extraction and analysis

Extraction methodology

Approximately 25 samples from each core, varying in thickness from 0.5 or 1 cm near the top of the core to 5 cm at depth, were squeezed within 18 hr of collection in a simple hydraulic press. The outer 1-2 mm of each refrigerated sample slice was removed with a polyethylene spatula to avoid possible core liner contamination and the sediment placed in a 6 cm diameter PVC sleeve. End-plugs for the sleeve consisted of a removable finely perforated teflon disc set in a cylindrical PVC block. The seal between the end-plugs and the sleeve wall was provided by black neoprene O-rings; single Whatman #41 filter papers separated the sediment from the teflon discs. Pressure was applied to the sleeve and end-plug assembly by a small hydraulic jack set in an aluminium and steel frame. Pore water was expressed through a few cm of tygon tubing (attached to a port on each end-plug) into 20 ml disposable syringes and subsequently expelled from the syringes through 13 mm diameter, 0.4 μm Nuclepore filters into acid-cleaned polyethylene-capped 10 and 30 ml glass vials. Two vials for each sample were used: an aliquot for metals analysis (Mn^{2+}, Fe^{2+}) was placed in a 10 ml vial which contained sufficient previously added Aristar conc. HCl to reduce the pH to ~2; the remainder was expressed into a pre-weighed 30 ml vial, untreated, and used for alkalinity, silicate, phosphate, ammonia, sulphate and iodine determinations.

In order to avoid the "temperature-of-squeezing" effect (Mangelsdorf et al, 1969; Bischoff et al, 1970; Fanning and Pilson, 1971), the PVC assembly was surrounded by a water-jacket through which a 3°C water-alcohol solution was circulated. No precautions were applied to prevent oxidation of anoxic sediment during squeezing except that the aliquot for oxidation-prone dissolved metals was taken

only after at least 10 and usually 15 ml of pore water had been expressed. Results of a study of oxidation effects on pore water iron by Troup et al (1974) suggest that pore water obtained by this procedure contains >80% of the in situ Fe^{2+} concentration; the remainder is probably oxidized to $Fe(OH)_3$ and retained by the sediment within the squeezer. Since Panama Basin sediments have a much lower dissolved iron content than those in Chesapeake Bay studied by Troup et al (1974), the extent of oxidation may be proportionately more severe in this study. A related problem may arise with interstitial phosphate which is scavenged from solution by freshly-precipitated Fe oxide (Bray et al, 1973). This is thought to be unimportant in this work, however, since phosphate concentrations are very high relative to iron.

Between sample squeezes, which often took 15-20 min, the PVC-Teflon-tygon tube assembly was dismantled, washed in sea water and thoroughly rinsed in distilled, deionized water.

Alkalinity analysis

Titration alkalinity, A_T, was determined in pore waters by direct potentiometric titration, based on the method detailed by Edmond (1970). Briefly, aliquots of a strong acid were added to the stirred sample and the EMF monitored with a pH electrode. The volume of acid required to reach the second endpoint of the carbonic acid system (the bicarbonate endpoint) was determined by extrapolating the linear portion of a Gran function (defined below) versus volume of acid added (ml) curve.

Titrations were performed open to the atmosphere in the original pre-weighed glass sample vials in order to include any $CaCO_3$ which might have precipitated during storage. A Teflon-coated magnetic stirring bar was added to each vial and each sample stirred throughout titration. BDH volumetric HCl (0.1 N) was added using a 2 ml capacity Gilmont micrometer burette; the pH (in mV) was measured after each acid

addition with a Corning Digital 112 pH meter coupled to a Corning combination semi-micro pH electrode, calibrated against Analar tris buffers. At least 12 readings were recorded, predominantly in the pH zone 3.5-2.5 where the Gran plot is linear.

The Gran function, F_2, was calculated using the following equation:

$$F_2 = \frac{10\ (V_o + V_i)}{V_o}\ e^{\frac{E_i - E_o}{A}}$$

where V_o = original sample volume (ml)

V_i = ml acid added

E_o = arbitrary EMF, ~20 mV higher than the measured maximum

E_i = EMF at V_i (mV)

$A = \frac{1000RT}{F}$ where $R = 1.9872$, $F = 23061$, $T = 273.15 + T\ (^oC)$.

Alkalinity was calculated from the equation:

$$A_T\ (\text{meq}\ l^{-1}) = \frac{(V_2)\ (N_a)}{V_o} \cdot 1000\ \text{ml}\ l^{-1}$$

where V_2 = vol. acid required to reach the bicarbonate endpoint (ml). This is determined by extrapolating the linear portion of an F_2 (Gran function) versus volume of acid added curve to the intercept (V_2) on the abscissa.

V_o = original sample volume (ml).

N_a = acid normality (eq l^{-1}).

All calculations were performed by computer using a program very similar to that described by Edmond (1970). The relative standard deviation of 5 replicate analyses of Copenhagen Sea Water was $\pm$ 1.3%.

Nutrient analyses

Dissolved silicate, phosphate, and ammonia were measured on board ship by colourimetric techniques using 1 cm optical glass cells in a Unicam SP 600 Series 2 spectrophotometer. Analyses of silicate and phosphate were based on the methods detailed in Strickland and Parsons (1968) as modified for very small sample volumes by B. J. Presley (Techniques For Analyzing Interstitial Water Samples : Part I - Determination of selected minor and major inorganic constituents, Publ. No. 869, Inst. of Geophys. and Planet. Phys., Univ. of Calif., mimeographed manuscript). Ammonia analyses were performed using Presley's (op. cit.) adaptation of the method of Solorzano (1969).

Sample volumes for silicate and ammonia analyses ranged from 0.5-1.5 ml. The smaller volumes were required when the concentrations were too high to obey Beer's Law; in these cases, the volume was brought to 1.5 ml with distilled, deionized water. Phosphate was determined on 3.0 ml samples. Using Eppendorf pipettes, reagents were added directly to pore water samples in 1 cm disposable plastic curettes (W. Sarstedt (U.K.) Ltd.). Colour development was carried out in the curettes but the solutions were transferred to 1 cm Unicam glass cells for measurement of absorbances since the plastic cells lacked acceptable optical consistency.

Replicate analyses gave an overall precision of $\pm$ 3.1% ($n = 15$, 1σ) for silicate, $\pm$ 4.9% ($n = 15$, 1σ) for phosphate and $\pm$ 8.0% ($n = 9$, 1σ) for ammonia. Ammonia analyses were less precise than expected due to both low concentrations and a high reagent blank. Reasons for the latter are obscure. Two commercial hypochlorite solutions were used (a Peruvian household bleach and standard British Domestos®) but neither had any effect in reducing the blank. Liddicoat et al (1975) had similar blank problems and found that

substitution of potassium ferrocyanide in place of sodium nitroprusside as the catalyst gave stable reproducible blanks. In addition, they indicated that the use of sodium dichloroisocyanurate as a hypochlorite donor is preferable to unstable commercial hypochlorite solutions. Unfortunately, substitution of these reagents on board ship was not possible.

Sulphate

Sulphate was determined gravimetrically. 4.00 ml of each pore water sample plus 0.4 ml of 1 N HCl were added to 50 ml Erlenmeyer flasks and heated on a hot-plate to near boiling. 2 ml of warm 10% w/v $BaCl_2$ solution were added slowly to each flask while agitating the acidified samples, and $BaSO_4$ was precipitated. The solutions were cooled, covered, and left overnight. Following resuspension, the precipitates were vacuum-filtered onto pre-weighed 0.4 um, 37 mm Nuclepore filters; each flask was washed several times with distilled water and the washings filtered to ensure 100% collection of precipitate. The filters were dried for several days in a dessicator and reweighed on a Perkin-Elmer AD-2 Autobalance. Sulphate concentration was then calculated from the weight of $BaSO_4$ precipitated from a known sample volume. The $BaCl_2$ addition is sufficient to provide a very large excess of barium. Precision of four replicate analyses of Copenhagen Sea Water was ± 4.0% (1 σ).

Iodine

Different methods were employed for total iodine determinations in pore waters for the two cores analyzed (P6 and P8). Interstitial iodine was determined by autoanalysis using Dr. V. W. Truesdale's Technicon Auto-Analyzer II facility at the Institute of Hydrology, Wallingford. The ceric ammonium sulphate-arsenious acid catalytic method described by Truesdale and Chapman (1976) was followed exactly

except that pore waters were diluted by varying factors with iodine-free artificial sea water to bring the total iodine concentrations within the operative range of the method (30-80 $\mu g\ l^{-1}$ I). Analytical precision determined from nine replicate diluted pore water analyses was $\pm$ 2.0% (1σ). Core P6 pore waters gave wildly inconsistent results using this method; results of replicate analyses of the same sample varied over an enormous range. No reasons to account for this behaviour were found. Further work is clearly required to investigate this problem.

Total iodine was determined in Core P6 by an alternative technique suggested to the author by A. Leonard (Dept. of Oceanography, Liverpool University), based partly on the method of Truesdale and Spenser (1974).

500 µl of sample were diluted to 3.0 ml by the addition of iodine-free sea water. 20 µl of 1.5% Analar H_2SO_4 and 40 µl of bromine water (made from Analar reagents) were added and the solution gently heated on a hot-plate for about five minutes; this step oxidizes all iodide to iodate. 40 µl of neat BDH formic acid was then added to discharge the yellow bromine colour, followed by 30 µl of 10% Analar KI solution and 500 µl of 1% BDH sulphamic acid. The excess iodide reacts with IO_3^- under acid conditions to form I_2 which is measured colourimetrically. The addition of sulphamic acid aids in suppressing any interference from nitrite (Chapman and Liss, 1977). Using a Unicam SP-200 spectrophotometer, absorbances were measured at 3550 Å in 1 cm cells 3 min ($\pm$ 5 sec) after addition of the 10% KI solution and were calibrated against standards made by dissolving Analar KI in iodine-free artificial sea water. Beer's Law was obeyed for the range 0-2.0 µmoles $I^-\ l^{-1}$. Precision of 6 replicate analyses of a diluted sample was $\pm$ 8% (1σ).

Dissolved manganese and iron

Manganese and iron were determined by flameless atomic absorption spectrophotometry using an Instrumentation Laboratories IL 455 flameless programmer unit with an IL 151 spectrophotometer.

Manganese was analyzed using direct injections of acidified (pH = 2), 1000-times diluted pore water samples. Dilution was carried out in 150 ml polyethylene bottles fitted with polyethylene screw tops. 99.8 ml of membrane-filtered distilled deionized water (ddw) was added by weight to 100 µl of sample and 100 µl of concentrated Aristar HCl, both dispensed by calibrated Eppendorf pipettes. Standards were prepared in a similar manner to cover the range 0-10 $\mu g l^{-1}$ Mn: 100 µl conc. HCl, 100 µl of filtered sea water (to ensure similar salt content), and the required volumes of secondary manganese standard and ddw were added to yield a total volume of 100.0 ml. A ddw- conc. HCl blank was also prepared. Working curves prepared from the standards were linear in the range 0-7 µg/l (abs. range 0-0.5). Where pore water manganese concentrations were low, a smaller dilution factor was used and standards made up accordingly. Non-atomic absorption due to volatilization of dissolved salts was corrected for by use of a deuterium lamp.

Analytical precision of replicate 1000x dilutions of samples averaged 4.3% (n = 12, 1 σ). Full analytical conditions are listed in Table B.1.

Direct injection of 10 µl aliquots of acidified, undiluted pore water was employed for dissolved iron analyses. A special graphite furnace heating program was developed which allowed selective volatilization of salt prior to atomization. The program dries the sample, heats it slowly to the minimum temperature at which most of the sodium chloride and other sea salts will volatilize, holds this temperature for a long period to allow the vaporized matrix components to be fully

cleared from the cell, and then atomizes the sample. Any slight non-atomic absorption during atomization is corrected for using a deuterium lamp. Figure B.1 illustrates the use of the selective volatilization program for determining dissolved iron concentration in a pore water sample.

Standards were prepared by spiking filtered sea water with an Fe secondary standard and taking the pH to 2 with Aristar HCl. Precision of the direct injection method was $\pm$ 9.8% (n = 21, 1 σ). Full analytical conditions for analysis with the IL instrument are listed in Table B.1.

Table B.1 Instrument conditions for flameless atomic absorption analysis of Mn and Fe using an IL 151 spectrophotometer and IL 455 flameless atomizer.

	Manganese	Iron
151:		
λ (nm)	279.5	371.9 (or the more sensitive 248.3nm)
H.V. (volts)	700	800
Slit width (μm)	320	160
Analysis mode	A-B (SB)	A (A-B if using 248.3 nm)
H.C. A lamp	2 mA	4.5 mA
B lamp	20 mA	~20 mA
Intensity	4.0 v.	4.0 v.
Integration	1/16	1/16
mA/count	1.0	1.0
Readout	Pk. ht. or chart	Pk. ht. or chart
455:		
Program Power	10 25 25 25 60 60	10 30 30 30 60 60
Program Time	4 3 3 2 0 2	5 5 7 4 0 2
Clean	On	On
Mode	Auto	Auto
Purge gas	Ar	Ar
Flow rate	15 scfh	15 scfh
Ar pressure	20 psi	20 psi
Air pressure	30 psi	30 psi

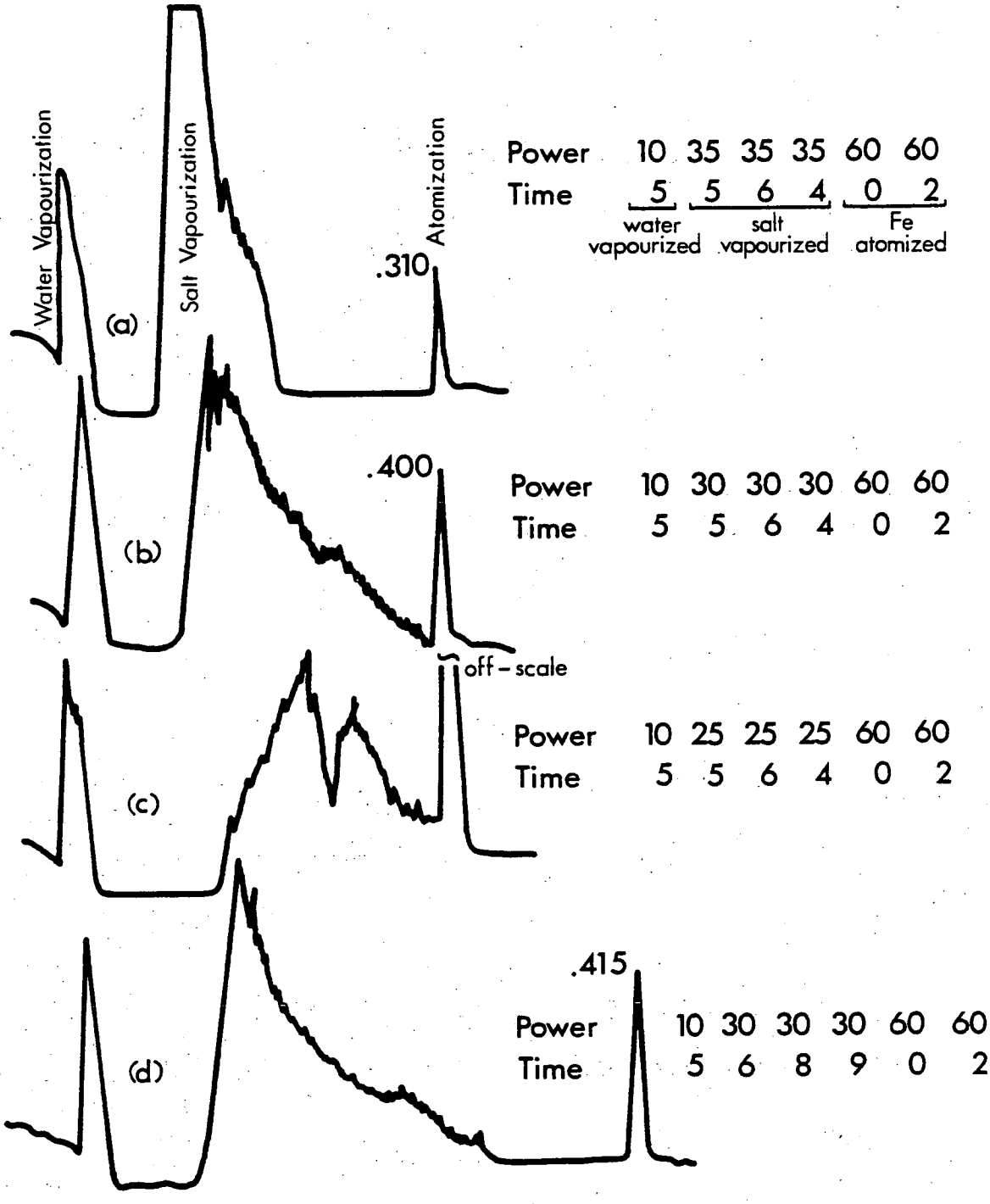

Fig. B.1 Responses to varying selective volatilization programs during flameless AA analysis of Fe in acidified, undiluted pore water. (Power in %, 60% = 2750°C; time at each power setting in units of 5 sec, i.e. 5 = 25 sec, 2 = 10 sec).

(a) "Burn-off" or salt vapourization temperature too high (35% power). Salt vapourizes very rapidly, taking some Fe with it. Anomalously low (and highly variable) absorbances result.

(b) A full 50 seconds at 30% power is just sufficient to allow nearly complete salt vapourization, and atomization of Fe proceeds properly.

(c) If the vapourization temperature is lowered below that which will "burn-off" all the salt (30% power), a severe interference occurs during atomization, completely screening the iron peak as the remaining salts are suddenly vapourized.

(d) Correct results, with salt vapourized at 30% power. In this cycle, the vapourization time was greatly lengthened to allow wide, clear separation of the atomization peak.

B.3 Sediment analysis : X-ray fluorescence spectrometry

Major elements

Fused 46 mm diameter glass discs were prepared by a method similar to that of Norrish and Hutton (1969). About 10g of each sediment sample were ground for several minutes in a Tema WC disc mill, and dried overnight at 60°C. Approximately 0.8-1.0 g of the ground sample was accurately weighed into a 95% Pt/5% Au crucible, an alloy chosen for its excellent resistance to wetting. An ultra-pure flux, Spectroflux 105 (Johnson-Matthey Chemicals Ltd.), was added in the ratio 6.000:1 (by weight, flux:sample), the crucible covered with a Pt foil lid and placed in a muffle furnace at 1100°C for 20 min. All weighings were to $\pm$ 0.001g. The flux, which consists of $Li_2B_4O_7$, La_2O_3 and Li_2CO_3, was pre-ignited at 400°C for 24 hr to drive off adsorbed H_2O. After removal and cooling, weight loss was made up with Spectroflux 100 (pure $Li_2B_4O_7$ only) so that the La:element ratio would not be altered. This consideration arose from the large weight losses inherent in fusing carbonate-rich sediments. Up to 40% of the sample weight was lost during fusion. Replacement of such a loss with La-bearing flux would considerably increase the heavy absorber (La):element ratio. Incorrectly low analyses, relative to a sample with a lower volatile content, would therefore result.

The crucible was then placed over a Meker burner and the contents (glass plus $Li_2B_4O_7$) fused once more. On a hot-plate at 220°C a disc-shaped slightly concave graphite mould was placed inside a brass sleeve and the molten glass poured onto the centre of the mould. An aluminium plunger, also at 220°C, was used to press the glass into a 1 mm thick disc which would later be presented directly to the X-ray beam.

The large quantities of La-bearing flux added to the sample make

a very large contribution to, and hence buffer, the total mass absorption of the glass discs produced after fusion. This procedure practically eliminates matrix absorption effects between samples and standards of varying composition.

Since the compositions of available international rock standards did not span the expected compositional range of Panama Basin sediments, a series of five synthetic standards were prepared by adding varying quantities of $CaCO_3$, SiO_2, KH_2PO_4, MnO_2, Fe_2O_3, NaCl, and MgO (all Johnson-Matthey Specpure chemicals) to USGS standard granodiorite GSP-1 (which approximated the composition of the terrigenous fraction). Glass discs were prepared as outlined above. The standards generated excellent linear calibration curves for all elements except Ti, for which very small deviations from linearity were observed at low Ti (high Ca) concentrations. At the titanium fluorescence energy, La has a minimum in its mass absorption coefficient while Ca has a maximum, hence samples with high calcium contents will have a relatively higher matrix absorption and will yield low inaccurate Ti analyses. This can produce a systematic error of 10% in the titanium determination of an unknown containing nearly 100% $CaCO_3$, if the unknown is compared to a standard containing little calcium (E. A. Boyle, written communication). The synthetic standards, however, take the effect largely into account since high Ca concentrations are accompanied by low Ti concentrations; the least squares linear regression therefore "averages out" the systematic error between low Ca, high Ti-bearing samples and those with high calcium and low titanium to $<2.5\%$ at a level of 0.040% Ti (with $>80\%$ $CaCO_3$).

Minor elements

Pressed powder discs, 46 mm in diameter, were used for minor element analysis and were made in the following manner: a minimum of

7g of sediment, ground to pass 200 mesh in a Tema WC disc mill, was placed in a stainless steel sleeve, sitting on a highly-polished WC disc. Both sleeve and disc sat within a larger stainless cylinder. A leucite plunger was placed within the inner cylinder and the sediment flattened by hand pressure into a semi-competent powder disc. Following removal of the leucite rod and the inner sleeve, two teaspoonsful of boric acid powder were added, and a large stainless plunger lowered onto the powder. A hydraulic ram was then used to press the sample at 10 tons. This load was held for one minute and gently released over a further half minute.

Matrix absorption coefficients (μ) for all samples were determined by the method of Reynolds (1963) in which the time taken to reach a specified number of counts on the Mo Compton scatter peak is directly proportional to μ. The matrix absorption coefficients of standard rocks were calculated at the wavelength of SrKα radiation and used for calibration. The Reynolds method does not apply to elements whose Kα lines are of longer wavelength than the iron absorption edge, which in this study include Cr and S. Standards for Cr analysis were chosen from standard rock powders which had matrix absorption coefficients that closely bracketed those of the samples. Synthetic standards were made up for S analysis in carbonate-rich samples by adding varying quantities of Analar K_2SO_4 to a bulk sediment collected in Loch Fyne, which has a very similar matrix absorption coefficient to the high-$CaCO_3$ samples. Sulphur standards for the lower matrix absorption clay-rich samples were made by adding Na_2SO_4 to a bulk sample from core P8. By using such standards, mass absorption corrections are not required; however, precision ($\pm$ 4%) is poorer than that for the Reynolds method ($\pm$ 2%).

Iodine, molybdenum, and bromine were calibrated using synthetic

standards. Varying quantities of $Ba(IO_3)_2$, which is insensitive to degradation by X-rays, (N. B. Price, personal communication), MoO_3, and KBr were added to a Mo, Br, and I-free base (a Grant Institute standard ferrogabbro) and mixed by prolonged grinding in a Tema WC disc mill. Duplicate pressed discs of each standard were made; these indicated full homogeneity of the standard mixtures.

The remaining elements (Ba, Co, Cu, Ni, Rb, Sr, Zn, and Zr) were analyzed using standard international rock powders for calibration.

The analytical conditions used for both major and minor elements and for MoKα Compton scatter determinations are listed in Table B.2; estimated precision of the analyses is presented in Table B.3.

The chlorine problem

Suspicions that chlorine might be volatile during fusion were investigated using an organic-poor sediment (0.75% C_{org}) taken from near the base of core P6, and an organic-rich sediment ($\sim$6% C_{org}) collected from Loch Etive by S. J. Malcolm. Samples of both were heated at various temperatures for 30 minutes in covered and uncovered vitreosil crucibles; the Cl concentration was monitored by subsequent leaching of the samples with distilled water and measuring Cl^- in the leachate by standard Mohr titration. Results are listed in Table B.4.

Table B.4 Variation in chlorine concentration during sediment heating.

Ignition Temp. °C	LOCH ETIVE		CORE P6	
	% Cl[1]	%wt. loss	% Cl[1]	%wt. loss
60	2.79	0	3.19	0
110	2.95	3.44	3.20	2.19
400 (with lid)	1.23	14.69	3.23	9.10
400 (without lid)	0.63	15.42	2.63	10.55
900 (with lid)	0.03	18.79	3.25	32.91
900 (without lid)	not detected	18.92	0.91, 2.55	36.06, 33.85

[1] Weight loss adjusted.

Table B.2 Analytical conditions used for XRF analysis of major and minor elements.

F = flow, S = scintillation, LL = lower level, P.D. = pressed powder disc.

Element and line	Tube	kV	mA	Crystal	Peak $^{o}_{2\theta}$	Background $^{o}_{2\theta}$	Counter	Pulse Height LL	Pulse Height Window	Count time (sec)	Collimator	Vacuum	Sample Prep.	Al Filter	Notes
AlKα	Cr	50	45	PE	145.13	139.00	F	250	600	40	Coarse	Yes	Fusion	out	
BaLβ_2	W	80	20	LiF 200	73.33	74.00	F	150	700	40	Coarse	Yes	P.D.	out	IKβ_1(10.94) interferes with BaKα(11.02); TiKα(86.14 interferes with BaLα_1, and Lα_2
BrKα	W	70	30	LiF 200	29.97	30.30	FS	250	600	40	Fine	Yes	P.D.	out	Avoid AsKβ_2(30.08)
CaKα	Cr	50	30	LiF 200	113.09	110.40	F	200	600	10	Fine	Yes	Fusion	out	
ClKα	Cr	50	45	PE	65.49	66.60	F	250	600	20	Coarse	Yes	Fusion	out	
CoKα	W	70	30	LiF 200	52.80	53.20 and 52.40	F	200	500	100	Fine	Yes	P.D.	out	Two backgrounds required since CoKα sits near shoulder of FeKβ_1(51.73)
CrKα	W	70	30	LiF 200	69.36	70.00	F	100	700	40	Fine	Yes	P.D.	out	Avoid VKβ_1(69.13)
CuKα	W	70	30	LiF 200	45.03	44.65	F	200	500	40	Fine	Yes	P.D.	out	
FeKα	Cr	50	45	LiF 200	57.52	56.00	F	150	700	10	Fine	Yes	Fusion	out	
IKα	W	70	30	LiF 200	12.40	12.00 and 12.70	S	250	600	40	Fine	Yes	P.D.	out	
K Kα	Cr	50	45	LiF 200	136.69	132.15	F	200	600	10	Fine	Yes	Fusion	out	
MgKα	Cr	50	45	TLAP	45.17	44.00	F	200	600	100	Coarse	Yes	Fusion	out	
MnKα	Cr	50	45	LiF 200	62.97	61.80	F	150	600	20	Fine	Yes	Fusion	in	Al filter used to eliminate CrKβ_1 tube line (62.36)
MoKα	W	70	30	LiF 220	28.90	28.65 and 29.15	S	200	600	100	Fine	Yes	P.D.	out	Avoid ZrKβ_1 (28.53)
NaKα	Cr	50	45	TLAP	55.10	53.30	F	250	500	100	Coarse	Yes	Fusion	out	
NiKα	W	70	30	LiF 200	48.67	48.20	F	200	500	40	Fine	Yes	P.D.	out	
PKα	Cr	50	45	GE	141.04	144.20	F	375	500	20	Coarse	Yes	Fusion	out	Discriminate against CaK escape peak with pulse height selection.
RbKα	W	90	30	LiF 220	37.99	39.06 and 36.90	FS	200	600	100	Coarse	Yes	P.D.	out	Avoid BrKβ_1 (38.24)
SKα	W	70	30	PE	75.85	75.00	F	250	600	40	Coarse	Yes	P.D.	out	Avoid ZrL$\mathfrak{N}_1$ (76.04)
SiKα	Cr	50	45	PE	109.21	113.30	F	250	600	20	Coarse	Yes	Fusion	out	
SrKα	W	70	30	LiF 220	35.85	34.74 and 36.90	FS	150	700	40	Fine	Yes	P.D.	out	
TiKα	Cr	50	45	LiF 200	86.14	91.00	F	250	600	20	Fine	Yes	Fusion	out	
ZnKα	W	70	30	LiF 200	41.80	42.30	FS	250	600	40	Fine	Yes	P.D.	out	
ZrKβ_1	W	70	30	LiF 220	28.53	28.35 and 28.65	S	200	600	100	Fine	Yes	P.D.	out	Avoid MoKα at 28.90; SrKβ_1(31.91) interferes with ZrKα(32.10)
Compton Scatter (MoKα)	Mo	60	30	LiF 200	21.13	None	S	250	600	10^5 counts	Fine	Yes	P.D.	out	Time taken to reach 10^5 counts = K(mass absorption); $\mu_{stds.}$ calculated at SrKα wavelength

Table B.3 XRF analytical precision for major and minor elements in Panama Basin sediments.

Element	Estimated total precision[1] (as % relative std. deviation, 1σ)
Al	0.6
Ba	2.5
Br	4.0
Ca	0.7
Cl	2.0
Co	4.0
Cr	6.0
Cu	2.5
Fe	0.5
I	4.0
K	0.8
Mg	1.2
Mn	2.0
Mo	6.0[2]
Na	3.2
Ni	3.0
P	2.5
Rb	25[3]
S	4.0
Si	0.5
Sr	2.5
Ti	3.0
Zn	3.0
Zr	20[4]

[1] Includes counting error, disc reproducibility, error in choice and slope of each regression line, and error in mass absorption determinations (minor elements). Major element precision is based mainly on analyses by J. G. Fitton of three duplicate discs of a wet chemically-analyzed sample.

[2] Increasing to ~30% for $[Mo] \leq 5$ ppm.

[3] Precision for carbonate-rich cores with $[Rb] \simeq 3$ ppm; decreases to ~2.5% for clay cores with $[Rb] \geq 50$ ppm.

[4] Precision for carbonate-rich cores with $[Zr] \simeq 20$ ppm; decreases to ~6% for clay cores with $[Zr] \simeq 60$ ppm.

The experiments indicated that heating the Loch Etive organic-rich sediment to 900°C resulted in almost total loss of Cl whether the samples were covered or uncovered. In contrast, the covered carbonate-rich organic-poor P6 sediment lost no Cl at 900°C, but the uncovered samples lost considerable and variable quantities. Two processes appear responsible. Firstly, during heating of salt in the presence of large quantities of reactive organic matter, sodium and magnesium chlorides are probably hydrolyzed and the Cl lost as volatile HCl, along with CO_2 from the organic material; the experiments indicated that such loss of Cl was initiated at temperatures $< 400°C$. Secondly, CO_2 is produced from decomposition of $CaCO_3$ at a temperature $\ll 900°C$. Judging by the appearance of the crucibles after heating to 900°C, evolution of carbon dioxide was violent for the carbonate-rich sediment of the core P6 sample and material was likely lost by spattering. In addition to the loss of sediment and salt by spattering, NaCl melts at 801°C and may be lost by evaporation at temperatures higher than the melting point.

To check the behaviour of Na during the loss of Cl by hydrolysis, pressed powder discs of several ignited Loch Etive sediment samples were made and checked by XRF for the comparative loss of Cl and Na relative to Al. These results are presented in Table B.5.

While Cl was almost entirely lost, no significant loss of Na occurred; as previously observed, considerable chlorine (roughly half) was lost at temperatures $\leqslant 400°C$. Clearly this poses problems for Cl analyses by XRF fusion in organic-rich sediments, which includes most coastal sediments. It is suggested that water content data be used for salt correction in such sediments. Alternatively, Cl can be determined on pressed powder discs by calibrating against a well-mixed internal standard or against standards having the same matrix absorption

as the samples.

Table B.5 Cl/Al and Na/Al count ratios determined by XRF for ignited Loch Etive sediment samples.

Ignition Temp °C	COUNT RATIOS Cl/Al	Na/Al x 10^{-2}
100	.959	3.74
400 (with lid)	.522	3.64
400 (without lid)	.359	3.67
900 (with lid)	.039	3.64
900 (without lid)	.054	3.55

Salt vapourization and spattering were avoided during fusion by using Spectroflux 105 rather than a La_2O_3-$Li_2B_4O_7$ mixture. Spectroflux 105 is a finely-ground glass, made by fusing Li_2CO_3, La_2O_3 and $Li_2B_4O_7$; it has a Li_2O:B_2O_3 ratio of 3:2 which yields the lowest eutectic point, about 700°C (Norrish and Hutton, 1969). During the fusion disc preparation the sample was blanketed by the flux, ensuring full solution of the sediment at the lowest possible temperature.

Since some Panama Basin sediments have relatively high organic carbon contents, it was possible that some Cl was lost during fusion. To check this, several samples of varying C_{org} contents were analyzed for Cl using both pressed powder discs, calibrated by adding known amounts of NaCl to sediment of similar mass absorption, and fusion discs. The results are shown in Table B.6. Within analytical precision ($\pm$ 20% for fusion, $\pm$ 5% for pressed discs) it is evident that no chlorine was lost during fusion. This could be due to insufficient quantities of organic matter or possibly a more refractory behaviour of organic compounds in Basin sediments as compared to those from Loch Etive. In any event, Cl analyses obtained with fusion discs

were used for salt corrections in this thesis.

Table B.6 Comparison between XRF-determined Cl concentrations using fusion discs and pressed powder discs.

Sample	$\%C_{org}$ (salt-free)	% Cl (fusion)	% Cl (pressed disc)
P6:50-55:	1.17	3.54	3.41
P6:60-65:	2.50	4.57	4.43
P1:30-34:	0.50	1.77	1.80
P8: 0-4:	2.52[1]	1.52[1]	1.52
P8:175-183:	1.14	2.08	2.19
P7: 0-2:	0.74	5.13	4.86

[1]Average of concentrations in P8:0-2: and P8:2-4: To obtain 7.0g of sample for the pressed disc, it was necessary to combine the two samples.

Calculation of totals

As a rough check on the overall quality of the major element analyses, the weight per cent oxide equivalents of the elements have been summed, along with percentage weight loss on fusion, for three samples, and are listed in Table B.7. Several other samples were checked and the totals ranged from 99.5% to 102.5%, with the great majority >101.0%. They are believed to be slightly high due to loss of a volatile component (probably adsorbed water) from the flux during fusion. Although the flux was pre-ignited at 400°C, not all water may have been driven off, and some may have been readsorbed subsequent to ignition. In view of the large volatiles loss, the totals are reasonable.

Table B.7 Representative totals for XRF analysis of Panama Basin sediments.

	P6:10-12:	P2:3-4:	P8:175-183:
SiO_2	14.09	32.69	43.95
Al_2O_3	2.48	2.19	10.13
CaO	40.54	29.24	5.25
TiO_2	0.10	0.13	0.55
P_2O_5	0.12	0.10	0.14
Fe_2O_3 (tot)	1.79	1.23	7.79
MnO	0.92	0.11	4.34
Na_2O	1.97	2.18	3.91
MgO	0.70	0.75	4.38
K_2O	0.36	0.36	1.81
BaO	0.27	0.42	0.27
SrO	0.14	0.12	-
SO_3[1]	0.50	0.50	0.47
Cl	1.28	2.05	2.08
% Loss on fusion	36.53	29.87	15.81
Less O = Cl	0.28	0.45	0.46
TOTAL	101.51	101.49	100.42

[1] All S was assumed to be present as sulphate-S (from salt and barite). No allowance for sulphides was made.

Accuracy of synthetic standards

The accuracy of the synthetic standards used in major element analyses was checked by analyzing two USGS standard rock powders as unknowns and comparing the elemental concentration determined by XRF with recommended values. The results are listed in Table B.8. Agreement between the two sets of data is good for all elements except manganese where a systematic error of 0.03% MnO is evident. Although this is negligible where high concentrations of manganese prevail, it is significant at low concentrations. Manganese concentrations discussed in this thesis may therefore be systematically high by about 0.02% Mn.

Table B.8 Check on the accuracy of the synthetic standards used for XRF major element analysis in this thesis. The USGS rocks were analyzed using the synthetic standards for calibration.

Element	AGV-1		GSP-1	
	Analyzed	Recommended[1]	Analyzed	Recommended
SiO_2	59.98	59.72	67.40	67.31
Al_2O_3	17.25	17.22	15.21	15.19
Fe_2O_3	6.92	6.84	4.32	4.33
MgO	1.59	1.55	0.96	0.96
CaO	5.08	5.00	2.03	2.02
Na_2O	4.32	4.31	2.83	2.80
K_2O	3.01	2.93	5.61	5.53
TiO_2	1.07	1.05	0.67	0.66
MnO	0.13	0.10	0.07	0.04
P_2O_5	0.49	0.50	0.27	0.28

[1] Usable values from Abbey (1977).

Corrections for dilution by salt and carbonate

Allowance must be made for the diluting effect of residual sea-salt when reporting elemental concentrations in marine sediments. Salt interferes both as a direct diluent and as a contributor of certain elements to the sediment.

To correct for salt, two assumptions were made: first, that interstitial water salinity was 35 per mil and second, that the chlorine in the sediments occurred entirely in salt and not in any other components. Individual corrections were applied first, using the following equations which utilize the XRF-determined Cl concentrations:

$$(\text{wt. \% Na})_{sed} = (\text{wt. \% Na})_{sed + salt} - 0.556^{1}\ (\text{wt. \% Cl})$$

$$(\text{wt. \% Mg})_{sed} = (\text{wt. \% Mg})_{sed + salt} - 0.067\ (\text{wt. \% Cl})$$

$$(\text{wt. \% Ca})_{sed} = (\text{wt. \% Ca})_{sed + salt} - 0.021\ (\text{wt. \% Cl})$$

$$(\text{wt. \% K})_{sed} = (\text{wt. \% K})_{sed + salt} - 0.020\ (\text{wt. \% Cl})$$

$$(\text{ppm S})_{sed} = (\text{ppm S})_{sed + salt} - 16.6\ (\text{wt. \% Cl})(\text{mM } SO_4^{2-})_{\text{pore water}}{}^{2}$$

$$(\text{ppm Br})_{sed} = (\text{ppm Br})_{sed + salt} - 34.6\ (\text{wt. \% Cl})$$

$$(\text{ppm Sr})_{sed} = (\text{ppm Sr})_{sed + salt} - 4.13\ (\text{wt. \% Cl})$$

All elemental concentrations were subsequently corrected for dilution using the equation:

$$(\text{Element concentration})_{\text{salt-free}} = (\text{Element conc.})_{sed} \times \left(\frac{100}{100 - 1.82(\text{wt.\%Cl})}\right)$$

In addition to salt, terrigenous components can be diluted by biogenic $CaCO_3$ and, to a lesser extent, opal. Opal was not quantitatively analyzed and therefore no corrections have been applied for dilution by this phase. The concentrations of $CaCO_3$ in cores P1-P7 were calculated

1. Factors calculated using the composition of sea water tabulated by Horne (1969, p.151).
2. Sulphur was corrected using measured interstitial sulphate concentrations since SO_4^{2-} is not conservative in these sediments.

from the salt-free Ca concentrations by assuming all the calcium was contributed by biogenic carbonate. Negligible error is introduced in the corrections by this technique since the concentration of non-biogenic calcium in the carbonate-rich samples is, in all cases, less than analytical precision for total Ca. Core P8 and the tops of P9-P13 generally contain < 2.5% $CaCO_3$; therefore, no correction for carbonate dilution was applied to these samples. The dilution equation used is:

$$(\text{Element concentration})_{\text{salt-and } CaCO_3\text{-free}} = (\text{Element concentration})_{\text{salt-free}} \times \frac{100}{100 - 2.497\ (\text{wt. \% Ca})_{\text{salt-free}}}$$

B.4 Organic carbon analysis

Two methods were required for the determination of organic carbon in Panama Basin sediments, one for biogenic carbonate-ooze sediments and the other for predominantly clay samples. The former will be described first.

A major problem in analysis of organic carbon in $CaCO_3$-rich sediments is the removal of carbonate without removing C_{org}. Organic carbon may be lost by hydrolysis if the sediments are washed following acid removal of carbonate carbon. To avoid this problem, samples were acid-treated directly in Leco ceramic crucibles. As these are porous, care was taken to ensure that the sample was dampened, not wetted, so that no acid would percolate through the crucible wall, carrying with it soluble C_{org}.

Organic carbon was determined on the carbonate-free samples by ignition in an induction furnace in a stream of CO_2-free oxygen followed by potassium hydroxide absorption of the CO_2 produced. A Leco 521-200

induction furnace equipped with dust trap, sulphur trap (SO_2 absorption by MnO_2 powder) and catalyst furnace was used for combustion; a Leco 572-100 carbon analyzer employed a gas burette to measure the change in volume which resulted when the O_2-CO_2 mixture from the combustion furnace was flushed through CO_2-absorbing KOH.

About 500 mg samples of ground sediment were weighed into Leco crucibles and placed on asbestos sheets on a 60°C hot-plate. After 15 min. warming, 10% BDH H_3PO_4 was added drop-wise, very slowly, so that violent effervescence and over-dampening were avoided. Acid was added three more times after cessation of effervescence to ensure full removal of carbonate carbon. Without wetting the samples, several hours were required to remove the carbonate-C by this method. Orthophosphoric acid was used rather than HCl since it was found that the strongly hydroscopic $CaCl_2$ formed during HCl addition produced HCl fumes during combustion. The HCl vapour was oxidized by MnO_2 in the sulphur trap to chlorine gas which interfered with the KOH absorption, producing spuriously high results. Analytical precision was $\pm 4\%$ (1σ, n = 11) at 1% C_{org} and about $\pm$ 10% for C_{org} concentrations less than $\sim 0.5\%$.

For sediments with low carbonate contents, organic carbon concentrations were calculated from the difference between total carbon and carbonate carbon analyses. Total carbon was determined by induction furnace combustion and hydroxide absorption of CO_2, as described above. Carbonate carbon was ascertained by measuring the CO_2 evolved from acid addition to a known sample weight. About 0.4g of accurately-weighed sediment and 3 ml distilled water were placed in a 10 ml Quickfit reaction flask. 3 ml of CO_2-free 25% H_3PO_4 was added from a burette and the mixture brought to incipient boiling three times with a small Bunsen burner. Evolved CO_2 was carried in a stream of

CO_2-free N_2 through a condenser-tube and water trap (conc. H_2SO_4) into the Leco gas burette system. CO_2 was then determined volumetrically by hydroxide absorption. Nitrogen was used as the carrier gas to inhibit oxidation of organic carbon during the reaction. Orthophosphoric acid was used in preference to HCl since addition of the latter to manganese-rich sediments produced interfering chlorine gas. The accuracy of the method was monitored occasionally by using a weighed aliquot of dried Analar $CaCO_3$ in place of the sample. Recovery ranged from 94-100% and was typically about 96%. Analytical precision was $\pm$ 5% (1σ, n = 6).

APPENDIX C

DATA

Sample names are of the form P1:45-50: which refers to the interval at 45 to 50 cm depth in core P1.

Elemental analyses for surface samples and each core (including the Pleiades Box Core) are listed on a salt-free and salt-and carbonate-free basis. Elemental ratios have been corrected for contributions from salt.

Note that analyses for cores P8-P13 inclusive have not been corrected for dilution by carbonate since the $CaCO_3$ content in these sediments is insignificant.

Table C.1

Major element analyses, all in dry wt. %, and ratios to aluminium.

SURFACE SEDIMENTS, UNCORRECTED DATA, WT. % ELEMENT

AL	CA	CL	FE	K	MG	MN	NA	P	SI	TI	ORG-C	NAME
0.78	24.28	2.24	0.60	0.23	0.37	1.30	1.67	0.046	11.16	0.045	0.57	P1:0-2:
1.31	19.27	2.20	0.97	0.30	0.49	1.43	1.85	0.059	15.75	0.086	0.68	P2:0-1:
0.48	33.95	3.60	0.42	0.12	0.36	0.07	2.17	0.033	3.55	0.034	0.52	P5:0-1.5:
1.59	24.20	1.90	1.32	0.37	0.57	3.77	1.60	0.059	8.36	0.070	0.49	PL-2
1.51	26.26	1.57	1.26	0.33	0.52	2.87	1.75	0.058	7.41	0.072	0.76	P6:0-1:
3.12	18.47	5.13	2.36	0.64	1.07	1.61	3.40	0.061	12.41	0.134	0.67	P7:0-2:
7.51	1.62	1.70	5.33	1.06	2.00	1.54	2.49	0.072	23.14	0.440	2.50	P8:0-2:
7.81	1.15	3.40	5.33	1.17	1.92	0.19	3.30	0.059	23.95	0.447	1.77	P9:0-2:
8.11	1.05	4.60	6.24	1.12	2.24	3.37	3.57	0.087	21.28	0.485	1.71	P10:0-2:
8.04	1.02	4.04	6.29	1.05	2.19	1.75	3.42	0.076	21.22	0.501	1.91	P11:0-3:
8.09	1.10	4.96	6.35	1.09	2.17	2.71	3.73	0.073	21.24	0.514	1.95	P12:0-1.5:
8.20	2.23	3.39	6.95	1.10	2.29	0.08	3.32	0.093	24.91	0.581	1.98	P13:0-2:

SURFACE SEDIMENTS, SALT-FREE DATA, WT. % ELEMENT

AL	CA	CL	FE	K	MG	MN	NA	P	SI	TI	ORG-C	NAME
0.81	25.26	2.24	0.63	0.19	0.23	1.36	0.44	0.047	11.63	0.047	0.59	P1:0-2:
1.36	20.03	2.20	1.01	0.27	0.36	1.49	0.65	0.062	16.41	0.090	0.71	P2:0-1:
0.51	36.25	3.60	0.45	0.08	0.13	0.07	0.18	0.035	3.80	0.037	0.56	P5:0-1.5:
1.65	25.03	1.90	1.37	0.34	0.46	3.91	0.56	0.061	8.66	0.073	0.50	PL-2
1.55	27.00	1.57	1.30	0.31	0.43	2.95	0.90	0.060	7.63	0.074	0.78	P6:0-1:
3.44	20.25	5.13	2.60	0.59	0.80	1.78	0.60	0.067	13.69	0.147	0.74	P7:0-2:
7.75	1.63	1.70	5.50	1.06	1.95	1.59	1.59	0.074	23.88	0.454	2.58	P8:0-2:
8.33	1.15	3.40	5.68	1.17	1.80	0.20	1.50	0.063	25.53	0.476	1.87	P9:0-2:
8.85	1.04	4.60	6.81	1.12	2.11	3.68	1.10	0.095	23.22	0.529	1.87	P10:0-2:
8.68	1.01	4.04	6.79	1.05	2.07	1.81	1.27	0.082	22.90	0.541	2.06	P11:0-3:
8.89	1.09	4.96	6.98	1.09	2.02	2.98	1.07	0.080	23.35	0.566	2.14	P12:0-1.5:
8.74	2.30	3.39	7.41	1.10	2.20	0.09	1.53	0.099	26.55	0.619	2.11	P13:0-2:

SURFACE SEDIMENTS, SALT-AND-CARBONATE-FREE DATA, WT. % ELEMENT

AL	CA	CL	FE	K	MG	MN	NA	P	SI	TI	ORG-C	NAME
2.19	25.26	6.07	1.71	0.51	0.62	3.68	1.19	0.128	31.50	0.128	1.60	P1:0-2:
2.72	20.03	4.40	2.02	0.53	0.72	2.98	1.30	0.123	32.83	0.179	1.42	P2:0-1:
5.38	36.25	37.96	4.74	0.84	1.37	0.74	1.90	0.367	40.07	0.385	5.90	P5:0-1.5:
4.40	25.03	5.07	3.65	0.91	1.23	10.43	1.49	0.163	23.09	0.193	1.33	PL-2
4.76	27.00	4.82	3.99	0.95	1.32	9.05	2.76	0.184	23.42	0.228	2.39	P6:0-1:
6.96	20.25	10.38	5.26	1.19	1.62	3.60	1.21	0.135	27.69	0.298	1.50	P7:0-2:
7.75	1.63	1.70	5.50	1.06	1.95	1.59	1.59	0.074	23.88	0.454	2.58	P8:0-2:
8.33	1.15	3.40	5.68	1.17	1.80	0.20	1.50	0.063	25.53	0.476	1.87	P9:0-2:
8.85	1.04	4.60	6.81	1.12	2.11	3.68	1.10	0.095	23.22	0.529	1.87	P10:0-2:
8.68	1.01	4.04	6.79	1.05	2.07	1.81	1.27	0.082	22.90	0.541	2.06	P11:0-3:
8.89	1.09	4.96	6.98	1.09	2.02	2.98	1.07	0.080	23.35	0.566	2.14	P12:0-1.5:
8.74	2.30	3.39	7.41	1.10	2.20	0.09	1.53	0.099	26.55	0.619	2.11	P13:0-2:

SURFACE SEDIMENTS, RATIOS TO ALUMINIUM (SALT-FREE)

CA/AL	FE/AL	K/AL	MG/AL	MN/AL	NA/AL	P/AL	SI/AL	TI/AL	NAME
31.185	0.778	0.235	0.284	1.679	0.543	0.059	14.358	0.058	P1:0-2:
14.728	0.743	0.195	0.265	1.096	0.478	0.045	12.066	0.066	P2:0-1:
71.078	0.882	0.157	0.255	0.137	0.353	0.068	7.451	0.072	P5:0-1.5:
15.170	0.830	0.206	0.279	2.370	0.339	0.037	5.248	0.044	PL-2
17.419	0.839	0.200	0.277	1.903	0.581	0.039	4.923	0.048	P6:0-1:
5.887	0.756	0.172	0.233	0.517	0.174	0.019	3.980	0.043	P7:0-2:
0.210	0.710	0.137	0.252	0.205	0.205	0.010	3.081	0.059	P8:0-2:
0.138	0.682	0.140	0.216	0.024	0.180	0.008	3.065	0.057	P9:0-2:
0.118	0.769	0.127	0.238	0.416	0.124	0.011	2.624	0.060	P10:0-2:
0.116	0.782	0.121	0.238	0.209	0.146	0.009	2.638	0.062	P11:0-3:
0.123	0.785	0.123	0.227	0.335	0.120	0.009	2.627	0.064	P12:0-1.5:
0.263	0.848	0.126	0.252	0.010	0.175	0.011	3.038	0.071	P13:0-2:

CORE P1, UNCORRECTED DATA, WT. % ELEMENT

AL	CA	CL	FE	K	MG	MN	NA	P	SI	TI	ORG-C	NAME
0.78	24.28	2.24	0.60	0.23	0.37	1.30	1.67	0.046	11.16	0.045	0.57	P1:0-2:
0.77	25.10	1.57	0.58	0.21	0.31	0.48	1.29	0.046	11.59	0.044	0.50	P1:2-4:
0.74	25.93	1.75	0.60	0.20	0.32	0.40	1.36	0.041	11.21	0.042	0.51	P1:4-6:
0.68	27.24	1.38	0.58	0.19	0.27	0.26	1.18	0.037	10.23	0.040	0.37	P1:6-8:
0.68	27.47	1.61	0.59	0.20	0.29	0.25	1.36	0.036	9.91	0.040	0.34	P1:8-10:
0.68	28.06	1.39	0.62	0.19	0.30	0.22	1.17	0.038	9.31	0.041	0.26	P1:10-12:
0.61	27.82	1.66	0.73	0.20	0.36	0.09	1.32	0.035	9.52	0.038	0.28	P1:12-14:
0.60	28.51	1.70	0.55	0.20	0.34	0.07	1.34	0.031	8.78	0.036	0.22	P1:14-16:
0.58	28.97	1.47	0.58	0.19	0.32	0.07	1.13	0.031	8.68	0.037	0.36	P1:16-18:
0.58	28.83	1.54	0.63	0.19	0.35	0.07	1.19	0.032	8.67	0.034	0.35	P1:18-20:
0.54	28.80	1.57	0.69	0.19	0.36	0.07	1.18	0.033	8.46	0.034	0.39	P1:20-22:
0.62	29.09	1.82	0.67	0.20	0.39	0.07	1.29	0.033	8.88	0.033	0.42	P1:22-26:
0.65	28.20	2.27	0.60	0.21	0.42	0.08	1.52	0.036	9.11	0.035	0.33	P1:26-30:
0.65	27.40	1.77	0.64	0.22	0.42	0.08	1.35	0.035	9.09	0.039	0.48	P1:30-34:
0.65	27.49	1.61	0.65	0.22	0.42	0.09	1.25	0.036	9.48	0.040	0.65	P1:34-36:
0.67	27.04	1.64	0.62	0.22	0.41	0.11	1.25	0.031	10.00	0.044	0.76	P1:36-40:
0.67	26.05	2.44	0.59	0.24	0.47	0.10	1.74	0.031	10.58	0.040	0.69	P1:40-45:
0.66	25.80	2.08	0.57	0.23	0.43	0.10	1.54	0.035	10.93	0.039	0.68	P1:45-50:
0.66	24.69	3.45	0.51	0.25	0.49	0.12	2.29	0.034	11.51	0.040	0.60	P1:50-55:
0.66	25.54	2.59	0.51	0.23	0.41	0.12	1.73	0.039	11.39	0.038	0.60	P1:55-60:
0.59	25.02	3.63	0.49	0.23	0.45	0.12	2.15	0.032	11.03	0.035	0.54	P1:60-65:
0.56	26.38	2.21	0.46	0.19	0.36	0.12	1.43	0.037	10.89	0.033	0.52	P1:65-70:
0.54	25.61	3.43	0.56	0.22	0.47	0.11	2.08	0.032	10.98	0.032	0.34	P1:70-75:
0.57	25.79	2.22	0.56	0.21	0.38	0.12	1.52	0.031	11.75	0.034	0.49	P1:75-80:
0.49	24.99	3.56	0.43	0.20	0.41	0.10	2.10	0.033	11.40	0.030	0.47	P1:80-85:
0.52	24.67	2.15	0.44	0.18	0.34	0.10	1.40	0.032	13.08	0.032	0.44	P1:85-90:
0.52	22.98	3.31	0.48	0.20	0.41	0.10	2.13	0.031	13.86	0.032	0.50	P1:90-95:
0.50	23.71	2.19	0.42	0.18	0.32	0.09	1.50	0.031	14.22	0.032	0.41	P1:95-100:
0.43	22.32	3.13	0.37	0.17	0.34	0.11	2.00	0.025	15.22	0.029	0.45	P1:100-105:
0.42	22.33	3.61	0.28	0.17	0.38	0.09	2.36	0.026	15.37	0.026	0.45	P1:105-110:
0.37	22.95	2.06	0.30	0.13	0.26	0.10	1.46	0.024	15.36	0.025	0.48	P1:110-115:
0.37	22.86	2.96	0.33	0.15	0.34	0.09	1.84	0.024	15.11	0.025	0.40	P1:115-120:
0.39	20.65	3.82	0.35	0.17	0.44	0.09	2.38	0.022	16.58	0.027	0.39	P1:120-125:
0.52	20.33	2.90	0.49	0.20	0.42	0.10	1.92	0.026	17.11	0.035	0.48	P1:125-130:
0.74	18.23	3.91	0.65	0.27	0.58	0.11	2.38	0.027	17.95	0.046	0.57	P1:130-135:
1.08	15.66	4.84	0.98	0.40	0.80	0.13	3.05	0.031	18.81	0.068	0.58	P1:135-140:
1.05	16.04	4.54	0.89	0.39	0.73	0.14	2.97	0.026	19.61	0.061	0.59	P1:140-145:
1.41	14.58	2.90	1.14	0.49	0.76	0.14	2.23	0.033	21.26	0.079	0.57	P1:145-150:

CORE P1, SALT-FREE DATA, WT. % ELEMENT

AL	CA	CL	FE	K	MG	MN	NA	P	SI	TI	ORG-C	NAME
0.81	25.26	2.24	0.63	0.19	0.23	1.36	0.44	0.047	11.63	0.047	0.59	P1:0-2:
0.79	25.80	1.57	0.60	0.18	0.21	0.49	0.43	0.047	11.93	0.045	0.51	P1:2-4:
0.76	26.75	1.75	0.62	0.17	0.21	0.41	0.40	0.042	11.58	0.044	0.53	P1:4-6:
0.70	27.91	1.38	0.59	0.17	0.18	0.27	0.42	0.039	10.49	0.041	0.38	P1:6-8:
0.70	28.26	1.61	0.61	0.17	0.19	0.26	0.48	0.037	10.21	0.041	0.35	P1:8-10:
0.70	28.76	1.39	0.64	0.17	0.21	0.23	0.41	0.039	9.55	0.042	0.27	P1:10-12:
0.63	28.65	1.66	0.75	0.17	0.26	0.09	0.41	0.036	9.82	0.039	0.29	P1:12-14:
0.62	29.38	1.70	0.57	0.17	0.23	0.07	0.41	0.032	9.06	0.037	0.23	P1:14-16:
0.60	29.73	1.47	0.60	0.17	0.23	0.07	0.32	0.032	8.92	0.038	0.37	P1:16-18:
0.60	29.63	1.54	0.65	0.16	0.25	0.07	0.34	0.033	8.92	0.035	0.36	P1:18-20:
0.56	29.61	1.57	0.71	0.16	0.26	0.07	0.32	0.034	8.71	0.035	0.40	P1:20-22:
0.64	30.05	1.82	0.69	0.17	0.28	0.07	0.29	0.034	9.18	0.034	0.43	P1:22-26:
0.68	29.37	2.27	0.63	0.17	0.28	0.08	0.27	0.037	9.50	0.037	0.34	P1:26-30:
0.67	28.27	1.77	0.66	0.19	0.31	0.08	0.38	0.036	9.39	0.040	0.50	P1:30-34:
0.67	28.28	1.61	0.67	0.19	0.32	0.09	0.37	0.037	9.77	0.042	0.67	P1:34-36:
0.69	27.84	1.64	0.64	0.19	0.31	0.11	0.35	0.031	10.31	0.045	0.78	P1:36-40:
0.70	27.21	2.44	0.62	0.20	0.32	0.10	0.40	0.032	11.07	0.042	0.72	P1:40-45:
0.69	26.77	2.08	0.59	0.20	0.30	0.10	0.40	0.036	11.36	0.040	0.71	P1:45-50:
0.70	26.27	3.45	0.54	0.19	0.28	0.13	0.40	0.037	12.28	0.042	0.64	P1:50-55:
0.69	26.75	2.59	0.54	0.19	0.25	0.13	0.30	0.041	11.95	0.040	0.63	P1:55-60:
0.63	26.71	3.63	0.52	0.17	0.22	0.13	0.14	0.034	11.81	0.037	0.58	P1:60-65:
0.58	27.44	2.21	0.48	0.15	0.22	0.13	0.21	0.039	11.35	0.034	0.54	P1:65-70:
0.58	27.24	3.43	0.60	0.16	0.26	0.12	0.18	0.034	11.71	0.034	0.36	P1:70-75:
0.59	26.83	2.22	0.58	0.17	0.24	0.13	0.30	0.033	12.24	0.035	0.51	P1:75-80:
0.52	26.64	3.56	0.46	0.14	0.18	0.11	0.13	0.036	12.19	0.032	0.50	P1:80-85:
0.54	25.63	2.15	0.46	0.14	0.20	0.10	0.21	0.033	13.61	0.034	0.46	P1:85-90:
0.55	24.38	3.31	0.51	0.14	0.20	0.11	0.31	0.033	14.75	0.034	0.53	P1:90-95:
0.52	24.65	2.19	0.44	0.14	0.18	0.09	0.29	0.032	14.81	0.033	0.43	P1:95-100:
0.46	23.60	3.13	0.39	0.11	0.14	0.12	0.28	0.027	16.14	0.030	0.48	P1:100-105:
0.45	23.82	3.61	0.30	0.10	0.15	0.10	0.38	0.028	16.45	0.027	0.48	P1:105-110:
0.38	23.80	2.06	0.31	0.09	0.13	0.10	0.33	0.025	15.96	0.026	0.50	P1:110-115:
0.39	24.10	2.96	0.35	0.10	0.15	0.10	0.21	0.026	15.97	0.026	0.42	P1:115-120:
0.42	22.11	3.82	0.38	0.10	0.20	0.10	0.28	0.024	17.82	0.029	0.42	P1:120-125:
0.55	21.40	2.90	0.52	0.15	0.24	0.11	0.32	0.028	18.06	0.037	0.51	P1:125-130:
0.80	19.54	3.91	0.70	0.21	0.34	0.12	0.22	0.029	19.33	0.050	0.61	P1:130-135:
1.18	17.06	4.84	1.07	0.33	0.52	0.14	0.39	0.034	20.63	0.074	0.64	P1:135-140:
1.14	17.38	4.54	0.97	0.33	0.46	0.15	0.49	0.029	21.38	0.066	0.64	P1:140-145:
1.49	15.33	2.90	1.20	0.46	0.60	0.15	0.65	0.035	22.44	0.083	0.60	P1:145-150:

CORE P1, SALT-AND-CARBONATE-FREE DATA, WT. % ELEMENT

AL	CA	CL	FE	K	MG	MN	NA	P	SI	TI	ORG-C	NAME
2.19	25.26	6.07	1.71	0.51	0.62	3.68	1.19	0.128	31.50	0.128	1.60	P1:0-2:
2.23	25.80	4.41	1.68	0.52	0.59	1.39	1.21	0.132	33.55	0.127	1.45	P1:2-4:
2.30	26.75	5.27	1.87	0.51	0.63	1.24	1.20	0.127	34.86	0.131	1.59	P1:4-6:
2.30	27.91	4.55	1.96	0.55	0.60	0.88	1.40	0.127	34.63	0.135	1.25	P1:6-8:
2.38	28.26	5.47	2.07	0.59	0.64	0.88	1.63	0.126	34.70	0.140	1.19	P1:8-10:
2.47	28.76	4.93	2.26	0.59	0.75	0.80	1.45	0.137	33.88	0.151	0.95	P1:10-12:
2.21	28.65	5.83	2.64	0.60	0.90	0.33	1.44	0.126	34.49	0.138	1.01	P1:12-14:
2.33	29.38	6.38	2.13	0.64	0.88	0.27	1.53	0.119	34.02	0.140	0.85	P1:14-16:
2.31	29.73	5.71	2.31	0.64	0.88	0.28	1.25	0.125	34.63	0.147	1.44	P1:16-18:
2.29	29.63	5.92	2.49	0.63	0.98	0.28	1.32	0.127	34.28	0.135	1.38	P1:18-20:
2.13	29.61	6.03	2.73	0.63	1.01	0.28	1.21	0.132	33.42	0.134	1.54	P1:20-22:
2.57	30.05	7.29	2.77	0.68	1.11	0.29	1.15	0.137	36.78	0.137	1.74	P1:22-26:
2.54	29.37	8.51	2.35	0.64	1.05	0.31	1.01	0.139	35.62	0.139	1.29	P1:26-30:
2.28	28.27	6.02	2.25	0.65	1.06	0.28	1.29	0.123	31.95	0.135	1.69	P1:30-34:
2.28	28.28	5.48	2.28	0.66	1.09	0.32	1.24	0.128	33.25	0.142	2.28	P1:34-36:
2.26	27.84	5.38	2.10	0.63	1.01	0.37	1.14	0.103	33.80	0.149	2.57	P1:36-40:
2.19	27.21	7.61	1.93	0.62	1.00	0.33	1.25	0.101	34.53	0.132	2.25	P1:40-45:
2.07	26.77	6.27	1.79	0.59	0.91	0.31	1.20	0.109	34.26	0.122	2.13	P1:45-50:
2.05	26.27	10.03	1.58	0.56	0.80	0.37	1.15	0.106	35.69	0.123	1.86	P1:50-55:
2.09	26.75	7.80	1.61	0.56	0.75	0.38	0.92	0.125	35.99	0.121	1.90	P1:55-60:
1.90	26.71	10.90	1.58	0.51	0.66	0.39	0.42	0.102	35.46	0.111	1.74	P1:60-65:
1.85	27.44	7.02	1.52	0.48	0.70	0.40	0.67	0.123	36.03	0.109	1.72	P1:65-70:
1.80	27.24	10.72	1.87	0.50	0.80	0.37	0.58	0.106	36.61	0.105	1.13	P1:70-75:
1.80	26.83	6.72	1.77	0.52	0.73	0.38	0.90	0.098	37.09	0.107	1.55	P1:75-80:
1.57	26.64	10.63	1.37	0.41	0.55	0.32	0.39	0.107	36.41	0.096	1.50	P1:80-85:
1.50	25.63	5.97	1.27	0.40	0.57	0.29	0.59	0.093	37.80	0.093	1.27	P1:85-90:
1.41	24.38	8.46	1.31	0.36	0.51	0.27	0.79	0.085	37.70	0.087	1.36	P1:90-95:
1.35	24.65	5.69	1.14	0.37	0.47	0.24	0.76	0.084	38.51	0.086	1.11	P1:95-100:
1.11	23.60	7.62	0.96	0.28	0.34	0.28	0.67	0.065	39.29	0.074	1.16	P1:100-105:
1.11	23.82	8.91	0.74	0.26	0.36	0.24	0.93	0.070	40.60	0.067	1.19	P1:105-110:
0.95	23.80	5.08	0.77	0.23	0.31	0.26	0.81	0.061	39.33	0.063	1.23	P1:110-115:
0.98	24.10	7.43	0.88	0.24	0.38	0.24	0.52	0.064	40.09	0.066	1.06	P1:115-120:
0.94	22.11	8.53	0.84	0.22	0.44	0.22	0.61	0.053	39.77	0.064	0.94	P1:120-125:
1.18	21.40	6.23	1.11	0.32	0.51	0.23	0.70	0.059	38.79	0.080	1.09	P1:125-130:
1.56	19.54	7.63	1.37	0.40	0.67	0.23	0.43	0.057	37.73	0.097	1.20	P1:130-135:
2.06	17.06	8.43	1.87	0.58	0.91	0.25	0.69	0.060	35.94	0.129	1.11	P1:135-140:
2.02	17.38	8.02	1.71	0.58	0.82	0.27	0.86	0.051	37.77	0.117	1.14	P1:140-145:
2.41	15.33	4.70	1.95	0.74	0.97	0.24	1.06	0.057	36.36	0.135	0.97	P1:145-150:

CORE P1, RATIOS TO ALUMINIUM (SALT-FREE)

FE/AL	K/AL	MG/AL	MN/AL	NA/AL	P/AL	SI/AL	TI/AL	NAME
0.778	0.235	0.284	1.679	0.543	0.059	14.358	0.058	P1:0-2:
0.753	0.232	0.266	0.623	0.542	0.059	15.052	0.057	P1:2-4:
0.811	0.223	0.274	0.541	0.523	0.055	15.149	0.057	P1:4-6:
0.853	0.239	0.261	0.382	0.607	0.055	15.044	0.059	P1:6-8:
0.868	0.247	0.268	0.368	0.684	0.053	14.574	0.059	P1:8-10:
0.912	0.239	0.304	0.324	0.584	0.055	13.691	0.061	P1:10-12:
1.197	0.273	0.408	0.148	0.651	0.057	15.607	0.062	P1:12-14:
0.917	0.277	0.377	0.117	0.658	0.051	14.633	0.060	P1:14-16:
1.000	0.277	0.382	0.121	0.539	0.054	14.966	0.064	P1:16-18:
1.086	0.274	0.426	0.121	0.575	0.055	14.948	0.059	P1:18-20:
1.278	0.294	0.472	0.130	0.569	0.062	15.667	0.063	P1:20-22:
1.081	0.264	0.432	0.113	0.449	0.053	14.323	0.053	P1:22-26:
0.923	0.253	0.412	0.123	0.397	0.055	14.015	0.055	P1:26-30:
0.985	0.284	0.464	0.123	0.563	0.054	13.985	0.059	P1:30-34:
1.000	0.289	0.480	0.138	0.546	0.056	14.585	0.062	P1:34-36:
0.925	0.279	0.448	0.164	0.505	0.046	14.925	0.066	P1:36-40:
0.881	0.285	0.457	0.149	0.572	0.046	15.791	0.060	P1:40-45:
0.864	0.285	0.440	0.152	0.581	0.053	16.561	0.059	P1:45-50:
0.773	0.274	0.392	0.182	0.563	0.052	17.439	0.060	P1:50-55:
0.773	0.270	0.358	0.182	0.439	0.060	17.258	0.058	P1:55-60:
0.831	0.267	0.350	0.203	0.223	0.054	18.695	0.059	P1:60-65:
0.821	0.260	0.378	0.214	0.359	0.066	19.446	0.059	P1:65-70:
1.037	0.280	0.445	0.204	0.320	0.059	20.333	0.059	P1:70-75:
0.982	0.291	0.406	0.211	0.501	0.055	20.614	0.060	P1:75-80:
0.878	0.263	0.350	0.204	0.246	0.068	23.265	0.061	P1:80-85:
0.846	0.263	0.377	0.192	0.393	0.062	25.154	0.062	P1:85-90:
0.923	0.257	0.362	0.192	0.557	0.060	26.654	0.061	P1:90-95:
0.840	0.272	0.347	0.180	0.565	0.062	28.440	0.064	P1:95-100:
0.860	0.250	0.303	0.256	0.604	0.058	35.395	0.067	P1:100-105:
0.667	0.233	0.329	0.214	0.840	0.063	36.595	0.061	P1:105-110:
0.811	0.240	0.330	0.270	0.850	0.064	41.514	0.066	P1:110-115:
0.892	0.245	0.383	0.243	0.525	0.065	40.838	0.068	P1:115-120:
0.897	0.240	0.472	0.231	0.657	0.057	42.513	0.068	P1:120-125:
0.942	0.273	0.434	0.192	0.592	0.050	32.904	0.068	P1:125-130:
0.878	0.259	0.430	0.149	0.278	0.036	24.257	0.062	P1:130-135:
0.907	0.281	0.440	0.120	0.332	0.029	17.417	0.063	P1:135-140:
0.848	0.285	0.406	0.133	0.425	0.025	18.676	0.058	P1:140-145:
0.809	0.306	0.401	0.099	0.438	0.024	15.078	0.056	P1:145-150:

CORE P2, UNCORRECTED DATA, WT. % ELEMENT

AL	CA	CL	FE	K	MG	MN	NA	P	SI	TI	ORG-C	NAME
1.31	19.27	2.20	0.97	0.30	0.49	1.43	1.85	0.059	15.75	0.086	0.68	P2:0-1:
1.33	20.33	2.11	0.87	0.31	0.45	0.75	1.68	0.053	15.58	0.083	0.69	P2:1-2:
1.23	20.35	2.14	0.84	0.30	0.45	0.46	1.70	0.051	15.54	0.079	0.66	P2:2-3:
1.16	20.90	2.05	0.86	0.30	0.45	0.10	1.62	0.043	15.27	0.078	0.61	P2:3-4:
1.13	21.76	1.97	0.90	0.31	0.49	0.09	1.64	0.046	14.95	0.076	0.57	P2:4-5:
1.07	22.28	2.34	0.88	0.31	0.52	0.08	1.86	0.043	14.15	0.076	0.53	P2:5-6:
1.05	23.04	2.45	0.83	0.31	0.51	0.09	1.78	0.042	13.60	0.074	0.58	P2:6-8:
1.07	24.05	1.53	0.87	0.30	0.45	0.08	1.32	0.047	12.87	0.077	0.55	P2:8-10:
1.09	24.21	1.87	0.88	0.31	0.45	0.08	1.53	0.041	12.81	0.077	0.54	P2:10-12:
1.06	24.55	1.97	0.94	0.31	0.51	0.09	1.49	0.042	12.12	0.080	0.55	P2:12-14:
1.00	25.42	1.67	0.83	0.29	0.43	0.11	1.31	0.042	11.52	0.074	0.52	P2:14-17:
0.97	25.11	2.11	0.85	0.29	0.48	0.09	1.56	0.041	11.55	0.072	0.52	P2:17-20:
0.87	26.14	1.88	0.84	0.27	0.45	0.09	1.43	0.038	10.88	0.066	0.52	P2:20-24:
0.84	25.86	2.00	0.91	0.27	0.52	0.09	1.49	0.042	11.33	0.062	0.56	P2:24-28:
0.84	24.98	2.01	0.77	0.25	0.47	0.09	1.57	0.038	11.67	0.068	0.66	P2:28-32:
0.86	24.65	2.40	0.75	0.25	0.51	0.10	1.73	0.036	11.91	0.069	0.67	P2:32-36:
0.92	25.01	2.07	0.80	0.26	0.50	0.10	1.58	0.038	11.97	0.074	0.83	P2:36-40:
0.99	24.55	2.29	0.84	0.27	0.54	0.12	1.66	0.040	12.10	0.081	1.03	P2:40-44:
0.97	23.34	4.31	0.73	0.29	0.66	0.11	2.67	0.034	11.72	0.078	1.09	P2:44-46:
0.97	22.41	2.77	0.74	0.28	0.55	0.13	1.93	0.042	13.72	0.073	1.21	P2:46-50:
0.90	21.32	5.10	0.70	0.30	0.65	0.12	2.95	0.040	13.44	0.071	1.06	P2:50-55:
0.93	21.53	3.00	0.75	0.28	0.56	0.15	1.94	0.036	14.33	0.075	1.16	P2:55-60:
0.97	20.86	4.26	0.74	0.30	0.65	0.12	2.55	0.040	14.43	0.073	1.07	P2:60-65:
0.97	21.49	2.48	0.75	0.29	0.56	0.13	1.69	0.038	14.88	0.072	1.06	P2:65-70:
0.89	19.90	5.04	0.68	0.31	0.71	0.13	2.92	0.035	14.63	0.065	1.02	P2:70-75:
0.94	19.69	3.63	0.73	0.31	0.63	0.14	2.34	0.035	16.29	0.070	0.96	P2:75-80:
0.95	19.22	4.60	0.72	0.33	0.65	0.14	2.74	0.035	16.21	0.068	1.04	P2:80-85:
0.88	20.20	4.41	0.66	0.30	0.61	0.16	2.66	0.038	15.51	0.062	0.83	P2:85-90:
0.84	21.98	2.58	0.74	0.26	0.49	0.15	1.82	0.037	14.98	0.062	0.78	P2:90-95:
0.82	22.00	4.41	0.67	0.26	0.57	0.15	2.57	0.035	14.50	0.055	0.65	P2:95-100:
0.80	22.07	3.85	0.62	0.27	0.57	0.13	2.37	0.033	14.13	0.058	0.55	P2:100-105:
0.81	20.47	4.19	0.72	0.29	0.61	0.12	2.60	0.032	15.60	0.057	0.64	P2:105-110:
1.03	21.95	2.81	0.67	0.27	0.48	0.12	1.85	0.039	15.18	0.058	0.68	P2:110-115:
0.78	20.43	4.50	0.59	0.27	0.56	0.13	2.75	0.037	15.30	0.050	0.60	P2:115-120:
0.73	20.62	3.03	0.59	0.23	0.48	0.12	1.94	0.033	16.88	0.049	0.63	P2:120-125:
0.71	18.42	5.08	0.53	0.26	0.61	0.11	3.01	0.030	17.62	0.049	0.71	P2:125-130:
0.80	17.36	2.64	0.59	0.24	0.51	0.12	1.91	0.030	20.41	0.059	0.70	P2:130-135:
0.73	17.78	3.34	0.52	0.23	0.50	0.12	2.30	0.035	19.46	0.055	0.75	P2:135-140:
0.68	17.26	5.14	0.52	0.26	0.58	0.12	2.99	0.026	19.19	0.049	0.63	P2:140-145:
0.55	18.93	2.72	0.41	0.18	0.36	0.13	1.84	0.025	19.64	0.041	0.55	P2:145-150:
0.54	18.41	4.15	0.39	0.20	0.43	0.11	2.46	0.028	18.83	0.041	0.59	P2:150-155:
0.47	18.21	4.60	0.36	0.19	0.46	0.10	2.72	0.023	18.72	0.037	0.65	P2:155-163:

CORE P2, SALT-FREE DATA, WT. % ELEMENT

AL	CA	CL	FE	K	MG	MN	NA	P	SI	TI	ORG-C	NAME
1.36	20.03	2.20	1.01	0.27	0.36	1.49	0.65	0.062	16.41	0.090	0.71	P2:0-1:
1.38	21.10	2.11	0.90	0.28	0.32	0.78	0.53	0.055	16.20	0.086	0.72	P2:1-2:
1.28	21.13	2.14	0.87	0.27	0.32	0.48	0.53	0.053	16.17	0.082	0.69	P2:2-3:
1.20	21.67	2.05	0.89	0.27	0.32	0.10	0.50	0.045	15.86	0.081	0.63	P2:3-4:
1.17	22.53	1.97	0.93	0.28	0.37	0.09	0.56	0.048	15.51	0.079	0.59	P2:4-5:
1.12	23.22	2.34	0.92	0.27	0.38	0.08	0.58	0.045	14.78	0.080	0.55	P2:5-6:
1.10	24.06	2.45	0.87	0.27	0.36	0.09	0.44	0.044	14.23	0.078	0.61	P2:6-8:
1.10	24.71	1.53	0.89	0.28	0.36	0.08	0.48	0.048	13.24	0.079	0.57	P2:8-10:
1.13	25.02	1.87	0.91	0.28	0.34	0.08	0.51	0.042	13.26	0.080	0.56	P2:10-12:
1.10	25.42	1.97	0.97	0.28	0.39	0.09	0.41	0.044	12.57	0.083	0.57	P2:12-14:
1.03	26.18	1.67	0.86	0.26	0.33	0.11	0.39	0.044	11.88	0.076	0.54	P2:14-17:
1.01	26.07	2.11	0.88	0.26	0.35	0.09	0.40	0.042	12.01	0.075	0.54	P2:17-20:
0.90	27.03	1.88	0.87	0.24	0.34	0.09	0.40	0.040	11.27	0.068	0.54	P2:20-24:
0.87	26.79	2.00	0.94	0.24	0.40	0.09	0.39	0.043	11.76	0.064	0.58	P2:24-28:
0.87	25.88	2.01	0.80	0.22	0.35	0.09	0.47	0.039	12.11	0.070	0.69	P2:28-32:
0.90	25.72	2.40	0.78	0.21	0.37	0.10	0.41	0.038	12.45	0.073	0.70	P2:32-36:
0.96	25.94	2.07	0.83	0.23	0.38	0.10	0.45	0.039	12.44	0.077	0.86	P2:36-40:
1.03	25.57	2.29	0.88	0.23	0.40	0.13	0.40	0.041	12.63	0.084	1.07	P2:40-44:
1.05	25.23	4.31	0.79	0.22	0.40	0.12	0.30	0.037	12.72	0.085	1.18	P2:44-46:
1.02	23.54	2.77	0.78	0.24	0.38	0.14	0.41	0.045	14.45	0.077	1.27	P2:46-50:
0.99	23.38	5.10	0.77	0.22	0.34	0.13	0.13	0.044	14.82	0.078	1.17	P2:50-55:
0.98	22.71	3.00	0.79	0.23	0.38	0.16	0.29	0.039	15.16	0.079	1.23	P2:55-60:
1.05	22.52	4.26	0.80	0.23	0.40	0.13	0.20	0.043	15.64	0.079	1.16	P2:60-65:
1.02	22.45	2.48	0.79	0.25	0.41	0.14	0.33	0.040	15.58	0.076	1.11	P2:65-70:
0.98	21.79	5.04	0.75	0.23	0.41	0.14	0.13	0.039	16.11	0.072	1.12	P2:70-75:
1.01	21.00	3.63	0.78	0.25	0.41	0.15	0.34	0.037	17.44	0.074	1.03	P2:75-80:
1.04	20.87	4.60	0.79	0.26	0.37	0.15	0.20	0.039	17.69	0.074	1.14	P2:80-85:
0.96	21.86	4.41	0.72	0.23	0.34	0.17	0.23	0.041	16.86	0.067	0.90	P2:85-90:
0.88	23.01	2.58	0.78	0.22	0.33	0.16	0.40	0.039	15.72	0.065	0.82	P2:90-95:
0.89	23.82	4.41	0.73	0.19	0.30	0.16	0.13	0.038	15.77	0.060	0.71	P2:95-100:
0.86	23.65	3.85	0.67	0.21	0.34	0.14	0.25	0.035	15.19	0.063	0.59	P2:100-105:
0.88	22.06	4.19	0.78	0.22	0.36	0.13	0.29	0.035	16.89	0.061	0.69	P2:105-110:
1.09	23.07	2.81	0.71	0.23	0.31	0.13	0.30	0.041	16.00	0.061	0.72	P2:110-115:
0.85	22.15	4.50	0.64	0.20	0.28	0.14	0.27	0.040	16.66	0.055	0.65	P2:115-120:
0.77	21.76	3.03	0.62	0.18	0.29	0.13	0.27	0.035	17.87	0.052	0.67	P2:120-125:
0.78	20.18	5.08	0.58	0.17	0.30	0.12	0.20	0.033	19.42	0.054	0.79	P2:125-130:
0.84	18.18	2.64	0.62	0.20	0.35	0.13	0.46	0.031	21.44	0.062	0.74	P2:130-135:
0.78	18.86	3.34	0.55	0.17	0.29	0.13	0.47	0.037	20.72	0.058	0.80	P2:135-140:
0.75	18.92	5.14	0.57	0.17	0.26	0.13	0.15	0.029	21.17	0.054	0.70	P2:140-145:
0.58	19.86	2.72	0.43	0.13	0.19	0.14	0.34	0.026	20.66	0.043	0.58	P2:145-150:
0.58	19.82	4.15	0.42	0.13	0.16	0.12	0.17	0.030	20.37	0.045	0.64	P2:150-155:
0.51	19.77	4.60	0.39	0.11	0.17	0.11	0.18	0.025	20.43	0.040	0.71	P2:155-163:

CORE P2, SALT-AND-CARBONATE-FREE DATA, WT. % ELEMENT

AL	CA	CL	FE	K	MG	MN	NA	P	SI	TI	ORG-C	NAME
2.72	20.03	4.40	2.02	0.53	0.72	2.98	1.30	0.123	32.83	0.179	1.42	P2:0-1:
2.92	21.10	4.46	1.91	0.59	0.68	1.65	1.11	0.117	34.24	0.182	1.52	P2:1-2:
2.71	21.13	4.53	1.85	0.57	0.68	1.01	1.12	0.112	34.23	0.174	1.45	P2:2-3:
2.63	21.67	4.47	1.95	0.59	0.71	0.23	1.09	0.098	34.56	0.177	1.38	P2:3-4:
2.68	22.53	4.50	2.13	0.64	0.85	0.21	1.29	0.110	35.44	0.180	1.35	P2:4-5:
2.66	23.22	5.57	2.19	0.65	0.90	0.20	1.39	0.107	35.17	0.189	1.32	P2:5-6:
2.75	24.06	6.14	2.18	0.68	0.91	0.24	1.10	0.111	35.66	0.194	1.52	P2:6-8:
2.87	24.71	3.99	2.34	0.72	0.93	0.21	1.26	0.126	34.56	0.207	1.48	P2:8-10:
3.01	25.02	4.98	2.43	0.75	0.90	0.22	1.35	0.113	35.35	0.214	1.49	P2:10-12:
3.01	25.42	5.39	2.67	0.77	1.07	0.26	1.12	0.119	34.42	0.227	1.56	P2:12-14:
2.98	26.18	4.82	2.47	0.76	0.95	0.33	1.14	0.126	34.31	0.219	1.55	P2:14-17:
2.89	26.07	6.04	2.53	0.74	1.01	0.27	1.15	0.121	34.40	0.215	1.55	P2:17-20:
2.77	27.03	5.78	2.67	0.74	1.03	0.29	1.23	0.122	34.64	0.209	1.66	P2:20-24:
2.63	26.79	6.04	2.85	0.72	1.21	0.28	1.19	0.131	35.53	0.194	1.76	P2:24-28:
2.47	25.88	5.68	2.26	0.62	0.98	0.26	1.33	0.110	34.25	0.198	1.94	P2:28-32:
2.51	25.72	6.71	2.19	0.59	1.02	0.29	1.16	0.106	34.82	0.203	1.96	P2:32-36:
2.71	25.94	5.88	2.36	0.65	1.07	0.30	1.27	0.111	35.32	0.218	2.45	P2:36-40:
2.86	25.57	6.33	2.42	0.65	1.12	0.35	1.12	0.114	34.92	0.233	2.97	P2:40-44:
2.84	25.23	11.65	2.14	0.60	1.09	0.32	0.80	0.101	34.37	0.229	3.20	P2:44-46:
2.48	23.54	6.72	1.89	0.57	0.93	0.33	1.00	0.108	35.05	0.186	3.09	P2:46-50:
2.38	23.38	12.26	1.85	0.52	0.82	0.32	0.30	0.106	35.60	0.188	2.81	P2:50-55:
2.27	22.71	6.93	1.83	0.54	0.88	0.37	0.66	0.089	35.01	0.182	2.83	P2:55-60:
2.40	22.52	9.73	1.83	0.53	0.90	0.30	0.45	0.098	35.73	0.180	2.65	P2:60-65:
2.31	22.45	5.64	1.79	0.57	0.94	0.31	0.74	0.091	35.47	0.172	2.53	P2:65-70:
2.15	21.79	11.06	1.64	0.51	0.90	0.31	0.28	0.085	35.34	0.158	2.46	P2:70-75:
2.12	21.00	7.63	1.64	0.53	0.87	0.32	0.72	0.078	36.67	0.157	2.16	P2:75-80:
2.17	20.87	9.61	1.64	0.54	0.78	0.32	0.42	0.081	36.94	0.154	2.37	P2:80-85:
2.11	21.86	9.71	1.58	0.51	0.75	0.38	0.50	0.091	37.14	0.147	1.99	P2:85-90:
2.07	23.01	6.06	1.82	0.51	0.78	0.37	0.95	0.092	36.94	0.154	1.92	P2:90-95:
2.20	23.82	10.88	1.80	0.46	0.74	0.40	0.32	0.094	38.90	0.148	1.74	P2:95-100:
2.10	23.65	9.40	1.63	0.51	0.82	0.34	0.60	0.085	37.10	0.153	1.44	P2:100-105:
1.95	22.06	9.33	1.74	0.50	0.79	0.29	0.65	0.078	37.61	0.137	1.54	P2:105-110:
2.56	23.07	6.63	1.67	0.53	0.73	0.30	0.72	0.097	37.74	0.145	1.69	P2:110-115:
1.90	22.15	10.07	1.44	0.44	0.63	0.32	0.60	0.089	37.29	0.122	1.46	P2:115-120:
1.69	21.76	6.63	1.37	0.39	0.64	0.28	0.59	0.078	39.11	0.114	1.46	P2:120-125:
1.58	20.18	10.24	1.18	0.35	0.60	0.24	0.41	0.067	39.13	0.108	1.58	P2:125-130:
1.54	18.18	4.83	1.13	0.36	0.64	0.23	0.85	0.057	39.26	0.113	1.35	P2:130-135:
1.47	18.86	6.31	1.05	0.33	0.56	0.24	0.89	0.070	39.16	0.110	1.51	P2:135-140:
1.42	18.92	9.74	1.09	0.33	0.49	0.25	0.28	0.054	40.13	0.103	1.32	P2:140-145:
1.15	19.86	5.39	0.86	0.26	0.37	0.27	0.68	0.052	40.98	0.086	1.15	P2:145-150:
1.16	19.82	8.22	0.84	0.25	0.33	0.24	0.33	0.059	40.33	0.089	1.26	P2:150-155:
1.01	19.77	9.08	0.78	0.21	0.33	0.22	0.35	0.049	40.35	0.079	1.40	P2:155-163:

CORE P2, RATIOS TO ALUMINIUM (SALT-FREE)

FE/AL	K/AL	MG/AL	MN/AL	NA/AL	P/AL	SI/AL	TI/AL	NAME
0.743	0.195	0.265	1.096	0.478	0.045	12.066	0.066	P2:0-1:
0.654	0.201	0.232	0.564	0.381	0.040	11.714	0.062	P2:1-2:
0.683	0.209	0.249	0.374	0.415	0.041	12.634	0.064	P2:2-3:
0.741	0.223	0.270	0.086	0.414	0.037	13.164	0.067	P2:3-4:
0.796	0.239	0.317	0.080	0.482	0.041	13.230	0.067	P2:4-5:
0.822	0.246	0.339	0.075	0.522	0.040	13.224	0.071	P2:5-6:
0.790	0.249	0.329	0.086	0.398	0.040	12.952	0.070	P2:6-8:
0.813	0.252	0.325	0.075	0.439	0.044	12.028	0.072	P2:8-10:
0.807	0.250	0.298	0.073	0.450	0.038	11.752	0.071	P2:10-12:
0.887	0.255	0.357	0.085	0.372	0.040	11.434	0.075	P2:12-14:
0.830	0.257	0.318	0.110	0.381	0.042	11.520	0.073	P2:14-17:
0.876	0.255	0.349	0.093	0.399	0.042	11.907	0.075	P2:17-20:
0.966	0.267	0.372	0.103	0.442	0.044	12.506	0.076	P2:20-24:
1.083	0.274	0.460	0.107	0.450	0.050	13.488	0.074	P2:24-28:
0.917	0.250	0.399	0.107	0.539	0.045	13.893	0.080	P2:28-32:
0.872	0.235	0.406	0.116	0.460	0.042	13.849	0.081	P2:32-36:
0.870	0.238	0.393	0.109	0.466	0.041	13.011	0.080	P2:36-40:
0.848	0.226	0.390	0.121	0.391	0.040	12.222	0.082	P2:40-44:
0.753	0.210	0.383	0.113	0.282	0.035	12.082	0.081	P2:44-46:
0.763	0.232	0.376	0.134	0.402	0.044	14.144	0.075	P2:46-50:
0.778	0.220	0.343	0.133	0.127	0.044	14.933	0.079	P2:50-55:
0.806	0.237	0.386	0.161	0.292	0.039	15.409	0.080	P2:55-60:
0.763	0.221	0.376	0.124	0.187	0.041	14.876	0.075	P2:60-65:
0.773	0.248	0.406	0.134	0.321	0.039	15.340	0.074	P2:65-70:
0.764	0.235	0.418	0.146	0.132	0.040	16.438	0.073	P2:70-75:
0.777	0.253	0.411	0.149	0.342	0.037	17.330	0.074	P2:75-80:
0.758	0.251	0.360	0.147	0.192	0.037	17.063	0.071	P2:80-85:
0.750	0.241	0.357	0.182	0.236	0.043	17.625	0.070	P2:85-90:
0.881	0.248	0.378	0.179	0.459	0.044	17.833	0.074	P2:90-95:
0.817	0.210	0.335	0.183	0.144	0.043	17.683	0.067	P2:95-100:
0.775	0.241	0.390	0.162	0.287	0.041	17.662	0.073	P2:100-105:
0.889	0.255	0.407	0.148	0.334	0.040	19.259	0.070	P2:105-110:
0.650	0.208	0.283	0.117	0.279	0.038	14.738	0.057	P2:110-115:
0.756	0.231	0.331	0.167	0.318	0.047	19.615	0.064	P2:115-120:
0.808	0.232	0.379	0.164	0.350	0.046	23.123	0.067	P2:120-125:
0.746	0.223	0.380	0.155	0.261	0.042	24.817	0.069	P2:125-130:
0.737	0.234	0.416	0.150	0.553	0.037	25.512	0.073	P2:130-135:
0.712	0.224	0.378	0.164	0.607	0.048	26.658	0.075	P2:135-140:
0.765	0.231	0.347	0.176	0.194	0.038	28.221	0.072	P2:140-145:
0.745	0.228	0.323	0.236	0.596	0.046	35.709	0.075	P2:145-150:
0.722	0.217	0.281	0.204	0.283	0.051	34.870	0.077	P2:150-155:
0.766	0.209	0.323	0.213	0.346	0.049	39.830	0.078	P2:155-163:

CORE P6, UNCORRECTED DATA, WT. % ELEMENT

AL	CA	CL	FE	K	MG	MN	NA	P	SI	TI	ORG-C	NAME
1.51	26.26	1.57	1.26	0.33	0.52	2.87	1.75	0.058	7.41	0.072	0.76	P6:0-1:
1.50	26.96	1.36	1.36	0.33	0.51	2.00	1.61	0.060	7.51	0.070	0.74	P6:1-2:
1.43	27.66	1.68	1.26	0.33	0.47	1.34	1.43	0.057	7.24	0.066	0.68	P6:2-4:
1.41	27.66	1.99	1.23	0.33	0.47	1.15	1.70	0.056	7.09	0.066	0.66	P6:4-6:
1.38	28.05	2.04	1.22	0.33	0.46	1.08	2.07	0.055	6.87	0.062	0.63	P6:6-8:
1.39	28.49	1.14	1.30	0.32	0.43	0.99	1.13	0.059	6.93	0.062	0.58	P6:8-10:
1.31	28.98	1.28	1.25	0.30	0.42	0.71	1.46	0.052	6.58	0.059	0.67	P6:10-12:
1.31	28.95	1.43	1.61	0.32	0.43	0.41	1.49	0.051	6.63	0.059	0.55	P6:12-14:
1.29	29.38	1.34	1.62	0.36	0.45	0.14	1.66	0.045	6.84	0.058	0.56	P6:14-16:
1.20	29.32	1.36	1.39	0.32	0.46	0.12	1.36	0.042	6.57	0.057	0.63	P6:16-18:
1.34	29.80	1.71	1.43	0.36	0.50	0.14	1.50	0.048	7.09	0.058	0.67	P6:18-20:
1.21	28.39	2.22	1.22	0.35	0.53	0.11	1.78	0.041	6.36	0.055	0.52	P6:20-25:
1.14	29.52	1.89	1.32	0.34	0.50	0.11	1.41	0.041	6.29	0.054	0.67	P6:25-30:
1.02	28.69	2.52	1.65	0.35	0.63	0.12	1.77	0.036	6.37	0.049	0.76	P6:30-35:
0.94	28.18	2.22	1.73	0.33	0.66	0.13	1.61	0.033	6.55	0.047	0.91	P6:35-40:
0.89	26.44	3.14	2.49	0.38	0.84	0.13	2.09	0.032	7.28	0.045	0.91	P6:40-45:
0.97	27.42	2.63	1.96	0.35	0.79	0.14	1.82	0.033	7.19	0.049	0.90	P6:45-50:
1.00	28.31	3.54	1.10	0.30	0.67	0.15	2.08	0.029	6.29	0.051	1.09	P6:50-55:
1.02	28.77	2.57	0.94	0.29	0.63	0.16	1.59	0.039	5.97	0.051	1.92	P6:55-60:
0.98	27.48	4.57	0.86	0.30	0.73	0.18	2.65	0.036	5.60	0.050	2.29	P6:60-65:
1.04	28.88	2.78	0.97	0.29	0.54	0.19	1.78	0.040	5.77	0.046	2.31	P6:65-70:
0.93	26.31	6.46	0.85	0.33	0.81	0.15	3.62	0.032	5.12	0.051	1.71	P6:70-75:
1.09	28.96	2.24	0.97	0.29	0.58	0.16	1.57	0.037	5.93	0.064	2.04	P6:75-80:
1.08	27.38	3.46	1.02	0.33	0.70	0.15	2.17	0.039	6.41	0.063	1.73	P6:80-85:
1.11	27.90	2.16	1.00	0.32	0.58	0.15	1.66	0.037	6.63	0.063	1.72	P6:85-90:
1.14	26.45	4.49	0.99	0.35	0.74	0.14	2.79	0.033	6.89	0.065	1.13	P6:90-95:
1.24	27.44	2.16	1.08	0.35	0.61	0.16	1.53	0.031	7.47	0.069	1.28	P6:95-100:
1.24	27.21	3.24	1.05	0.36	0.70	0.14	2.13	0.035	7.18	0.067	1.13	P6:100-105:
1.26	27.52	2.85	1.06	0.34	0.66	0.15	1.91	0.034	7.09	0.071	0.89	P6:105-110:
1.21	28.08	1.84	1.07	0.30	0.59	0.15	1.42	0.031	6.89	0.075	0.82	P6:110-115:
1.19	27.84	3.51	1.05	0.31	0.67	0.14	2.29	0.036	6.80	0.072	0.80	P6:115-120:
1.31	27.55	3.07	1.14	0.31	0.67	0.12	2.11	0.035	7.07	0.087	0.87	P6:120-125:
1.25	28.42	1.58	1.04	0.30	0.53	0.14	1.37	0.034	7.26	0.074	0.84	P6:125-130:
1.14	27.43	3.37	0.83	0.30	0.54	0.12	2.05	0.031	7.91	0.057	0.82	P6:130-135:
1.09	26.59	3.70	0.86	0.29	0.64	0.11	2.28	0.027	8.32	0.064	0.95	P6:135-140:
1.09	26.13	1.95	0.85	0.27	0.51	0.13	1.42	0.035	9.06	0.059	0.90	P6:140-145:
1.02	26.72	3.78	0.74	0.29	0.56	0.12	2.23	0.032	8.45	0.055	0.75	P6:145-150:
0.99	27.22	3.38	0.73	0.28	0.52	0.11	2.16	0.030	8.38	0.050	0.57	P6:150-155:
0.96	27.64	1.81	0.79	0.26	0.43	0.11	1.33	0.031	8.87	0.050	0.78	P6:155-163:

CORE P6, SALT-FREE DATA, WT. % ELEMENT

AL	CA	CL	FE	K	MG	MN	NA	P	SI	TI	ORG-C	NAME
1.55	27.00	1.57	1.30	0.31	0.43	2.95	0.90	0.060	7.63	0.074	0.78	P6:0-1:
1.54	27.61	1.36	1.39	0.31	0.43	2.05	0.88	0.061	7.70	0.072	0.76	P6:1-2:
1.48	28.50	1.68	1.30	0.31	0.37	1.38	0.51	0.059	7.47	0.068	0.70	P6:2-4:
1.46	28.66	1.99	1.28	0.30	0.35	1.19	0.62	0.058	7.36	0.069	0.68	P6:4-6:
1.43	29.09	2.04	1.27	0.30	0.34	1.12	0.97	0.057	7.13	0.065	0.65	P6:6-8:
1.42	29.07	1.14	1.33	0.30	0.36	1.01	0.51	0.060	7.08	0.063	0.59	P6:8-10:
1.34	29.64	1.28	1.28	0.28	0.34	0.73	0.77	0.053	6.74	0.060	0.69	P6:10-12:
1.35	29.69	1.43	1.65	0.30	0.34	0.42	0.71	0.052	6.81	0.060	0.56	P6:12-14:
1.32	30.09	1.34	1.66	0.34	0.37	0.14	0.94	0.046	7.01	0.059	0.57	P6:14-16:
1.23	30.03	1.36	1.43	0.30	0.38	0.12	0.62	0.043	6.74	0.058	0.65	P6:16-18:
1.38	30.72	1.71	1.48	0.34	0.40	0.14	0.57	0.050	7.32	0.060	0.69	P6:18-20:
1.26	29.54	2.22	1.27	0.32	0.40	0.11	0.57	0.042	6.63	0.057	0.54	P6:20-25:
1.18	30.53	1.89	1.37	0.31	0.39	0.11	0.37	0.042	6.51	0.056	0.69	P6:25-30:
1.07	30.01	2.52	1.73	0.31	0.48	0.13	0.39	0.038	6.68	0.052	0.80	P6:30-35:
0.98	29.32	2.22	1.80	0.30	0.53	0.14	0.39	0.035	6.83	0.049	0.95	P6:35-40:
0.94	27.97	3.14	2.64	0.34	0.67	0.14	0.37	0.034	7.72	0.048	0.97	P6:40-45:
1.02	28.74	2.63	2.06	0.31	0.64	0.15	0.38	0.035	7.55	0.051	0.95	P6:45-50:
1.07	30.18	3.54	1.18	0.24	0.46	0.16	0.12	0.031	6.72	0.055	1.17	P6:50-55:
1.07	30.13	2.57	0.99	0.25	0.48	0.17	0.17	0.041	6.26	0.053	2.01	P6:55-60:
1.07	29.87	4.57	0.94	0.23	0.46	0.20	0.12	0.040	6.11	0.054	2.50	P6:60-65:
1.10	30.36	2.78	1.02	0.25	0.37	0.20	0.25	0.042	6.08	0.048	2.43	P6:65-70:
1.05	29.66	6.46	0.96	0.23	0.43	0.17	0.03	0.037	5.80	0.058	1.94	P6:70-75:
1.14	30.14	2.24	1.01	0.26	0.45	0.17	0.34	0.038	6.18	0.066	2.13	P6:75-80:
1.15	29.14	3.46	1.09	0.28	0.50	0.16	0.26	0.041	6.84	0.067	1.85	P6:80-85:
1.16	28.99	2.16	1.04	0.29	0.45	0.16	0.48	0.039	6.90	0.066	1.79	P6:85-90:
1.24	28.70	4.49	1.08	0.28	0.48	0.15	0.32	0.036	7.50	0.071	1.23	P6:90-95:
1.29	28.52	2.16	1.12	0.32	0.48	0.17	0.34	0.032	7.78	0.072	1.33	P6:95-100:
1.32	28.84	3.24	1.12	0.31	0.51	0.15	0.35	0.037	7.63	0.071	1.20	P6:100-105:
1.33	28.96	2.85	1.12	0.30	0.49	0.16	0.34	0.035	7.48	0.075	0.94	P6:105-110:
1.25	29.01	1.84	1.11	0.27	0.48	0.16	0.41	0.032	7.13	0.077	0.85	P6:110-115:
1.27	29.66	3.51	1.12	0.26	0.46	0.15	0.36	0.039	7.26	0.077	0.85	P6:115-120:
1.39	29.11	3.07	1.21	0.26	0.49	0.13	0.43	0.037	7.49	0.092	0.92	P6:120-125:
1.29	29.23	1.58	1.07	0.28	0.44	0.14	0.51	0.035	7.47	0.076	0.86	P6:125-130:
1.21	29.15	3.37	0.88	0.25	0.33	0.13	0.19	0.033	8.43	0.061	0.87	P6:130-135:
1.17	28.43	3.70	0.92	0.23	0.42	0.12	0.24	0.029	8.92	0.068	1.02	P6:135-140:
1.13	27.05	1.95	0.88	0.24	0.39	0.13	0.35	0.036	9.39	0.061	0.93	P6:140-145:
1.10	28.61	3.78	0.79	0.23	0.33	0.13	0.14	0.035	9.07	0.059	0.81	P6:145-150:
1.05	28.93	3.38	0.78	0.23	0.31	0.12	0.30	0.031	8.93	0.053	0.61	P6:150-155:
0.99	28.54	1.81	0.82	0.23	0.32	0.11	0.33	0.032	9.17	0.051	0.81	P6:155-163:

CORE P6, SALT-AND-CARBONATE-FREE DATA, WT. % ELEMENT

AL	CA	CL	FE	K	MG	MN	NA	P	SI	TI	ORG-C	NAME
4.76	27.00	4.82	3.99	0.95	1.32	9.05	2.76	0.184	23.42	0.228	2.39	P6:0-1:
4.95	27.61	4.38	4.49	1.00	1.38	6.61	2.82	0.197	24.80	0.231	2.44	P6:1-2:
5.11	28.50	5.82	4.51	1.06	1.28	4.79	1.77	0.204	25.89	0.237	2.43	P6:2-4:
5.14	28.66	7.00	4.49	1.06	1.23	4.19	2.17	0.205	25.86	0.241	2.41	P6:4-6:
5.24	29.09	7.45	4.63	1.10	1.23	4.10	3.55	0.209	26.07	0.237	2.39	P6:6-8:
5.18	29.07	4.16	4.84	1.11	1.32	3.69	1.85	0.218	25.81	0.231	2.16	P6:8-10:
5.16	29.64	4.93	4.93	1.08	1.32	2.80	2.95	0.204	25.93	0.231	2.64	P6:10-12:
5.20	29.69	5.53	6.39	1.16	1.33	1.63	2.76	0.201	26.33	0.233	2.18	P6:12-14:
5.32	30.09	5.39	6.67	1.37	1.48	0.58	3.77	0.186	28.18	0.239	2.31	P6:14-16:
4.92	30.03	5.44	5.70	1.20	1.51	0.49	2.48	0.171	26.94	0.233	2.58	P6:16-18:
5.94	30.72	7.34	6.34	1.44	1.71	0.62	2.43	0.213	31.42	0.258	2.97	P6:18-20:
4.80	29.54	8.46	4.84	1.21	1.51	0.44	2.17	0.162	25.25	0.218	2.06	P6:20-25:
4.97	30.53	7.95	5.75	1.32	1.63	0.48	1.57	0.179	27.41	0.236	2.92	P6:25-30:
4.27	30.01	10.06	6.90	1.25	1.93	0.50	1.54	0.151	26.65	0.206	3.18	P6:30-35:
3.66	29.32	8.29	6.73	1.11	1.99	0.51	1.46	0.130	25.48	0.184	3.54	P6:35-40:
3.13	27.97	10.41	8.76	1.12	2.21	0.46	1.21	0.112	25.61	0.160	3.20	P6:40-45:
3.61	28.74	9.31	7.29	1.11	2.28	0.52	1.33	0.124	26.74	0.181	3.35	P6:45-50:
4.34	30.18	14.37	4.77	0.99	1.88	0.65	0.48	0.127	27.29	0.222	4.73	P6:50-55:
4.32	30.13	10.37	3.98	1.01	1.94	0.68	0.68	0.166	25.28	0.216	8.13	P6:55-60:
4.21	29.87	17.98	3.69	0.90	1.82	0.77	0.47	0.155	24.03	0.213	9.83	P6:60-65:
4.53	30.36	11.49	4.22	1.02	1.54	0.83	1.02	0.175	25.12	0.200	10.06	P6:65-70:
4.06	29.66	24.91	3.71	0.88	1.65	0.66	0.12	0.141	22.37	0.225	7.47	P6:70-75:
4.59	30.14	9.06	4.09	1.03	1.81	0.67	1.37	0.155	24.99	0.268	8.60	P6:75-80:
4.23	29.14	12.71	4.00	1.02	1.83	0.59	0.97	0.152	25.12	0.247	6.78	P6:80-85:
4.19	28.99	7.83	3.77	1.04	1.64	0.57	1.73	0.140	25.00	0.238	6.49	P6:85-90:
4.38	28.70	15.85	3.81	1.00	1.69	0.54	1.13	0.128	26.48	0.251	4.34	P6:90-95:
4.48	28.52	7.50	3.90	1.11	1.68	0.58	1.19	0.112	27.00	0.249	4.63	P6:95-100:
4.71	29.84	11.58	3.99	1.12	1.83	0.53	1.25	0.132	27.27	0.253	4.29	P6:100-105:
4.80	28.96	10.30	4.04	1.08	1.79	0.57	1.24	0.128	27.01	0.270	3.39	P6:105-110:
4.54	29.01	6.68	4.02	0.99	1.75	0.56	1.49	0.117	25.87	0.281	3.08	P6:110-115:
4.90	29.66	13.53	4.32	0.99	1.79	0.58	1.39	0.148	28.01	0.297	3.29	P6:115-120:
5.08	29.11	11.24	4.42	0.96	1.80	0.47	1.56	0.136	27.42	0.336	3.37	P6:120-125:
4.76	29.23	5.85	3.96	1.02	1.62	0.53	1.87	0.128	27.66	0.281	3.20	P6:125-130:
4.46	29.15	12.38	3.25	0.91	1.23	0.47	0.69	0.120	30.96	0.223	3.21	P6:130-135:
4.03	28.43	12.75	3.18	0.80	1.45	0.41	0.82	0.099	30.74	0.235	3.51	P6:135-140:
3.48	27.05	6.01	2.72	0.74	1.21	0.42	1.07	0.110	28.94	0.189	2.87	P6:140-145:
3.83	28.61	13.23	2.78	0.81	1.15	0.45	0.48	0.122	31.77	0.205	2.82	P6:145-150:
3.80	28.93	12.17	2.80	0.82	1.13	0.42	1.08	0.114	32.16	0.191	2.19	P6:150-155:
3.46	28.54	6.30	2.84	0.81	1.11	0.40	1.16	0.110	31.93	0.179	2.81	P6:155-163:

CORE P6, RATIOS TO ALUMINIUM (SALT-FREE)

FE/AL	K/AL	MG/AL	MN/AL	NA/AL	P/AL	SI/AL	TI/AL	NAME
0.839	0.200	0.277	1.903	0.581	0.039	4.923	0.048	P6:0-1:
0.907	0.202	0.279	1.333	0.569	0.040	5.007	0.047	P6:1-2:
0.881	0.207	0.250	0.937	0.347	0.040	5.063	0.046	P6:2-4:
0.872	0.206	0.239	0.816	0.421	0.040	5.028	0.047	P6:4-6:
0.884	0.210	0.234	0.783	0.678	0.040	4.978	0.045	P6:6-8:
0.935	0.214	0.254	0.712	0.357	0.042	4.986	0.045	P6:8-10:
0.954	0.209	0.255	0.542	0.571	0.040	5.023	0.045	P6:10-12:
1.229	0.222	0.255	0.313	0.530	0.039	5.061	0.045	P6:12-14:
1.256	0.258	0.279	0.109	0.709	0.035	5.302	0.045	P6:14-16:
1.158	0.244	0.307	0.100	0.503	0.035	5.475	0.047	P6:16-18:
1.067	0.243	0.288	0.104	0.410	0.036	5.291	0.044	P6:18-20:
1.008	0.253	0.315	0.091	0.451	0.034	5.256	0.045	P6:20-25:
1.158	0.265	0.328	0.096	0.315	0.036	5.518	0.047	P6:25-30:
1.618	0.294	0.452	0.118	0.362	0.035	6.245	0.048	P6:30-35:
1.840	0.304	0.544	0.138	0.400	0.036	6.968	0.050	P6:35-40:
2.798	0.356	0.707	0.146	0.387	0.036	8.180	0.051	P6:40-45:
2.021	0.307	0.633	0.144	0.369	0.034	7.412	0.050	P6:45-50:
1.100	0.229	0.433	0.150	0.112	0.029	6.290	0.051	P6:50-55:
0.922	0.234	0.449	0.157	0.158	0.038	5.853	0.050	P6:55-60:
0.878	0.213	0.432	0.184	0.111	0.037	5.714	0.051	P6:60-65:
0.933	0.225	0.340	0.183	0.225	0.039	5.548	0.044	P6:65-70:
0.914	0.216	0.406	0.161	0.030	0.035	5.505	0.055	P6:70-75:
0.890	0.225	0.394	0.147	0.298	0.034	5.440	0.058	P6:75-80:
0.944	0.241	0.434	0.139	0.228	0.036	5.935	0.058	P6:80-85:
0.901	0.249	0.392	0.135	0.414	0.033	5.973	0.057	P6:85-90:
0.868	0.228	0.385	0.123	0.258	0.029	6.044	0.057	P6:90-95:
0.871	0.247	0.375	0.129	0.265	0.025	6.024	0.056	P6:95-100:
0.847	0.238	0.389	0.113	0.265	0.028	5.790	0.054	P6:100-105:
0.841	0.225	0.372	0.119	0.258	0.027	5.627	0.056	P6:105-110:
0.884	0.218	0.386	0.124	0.328	0.026	5.694	0.062	P6:110-115:
0.882	0.202	0.365	0.118	0.284	0.030	5.714	0.061	P6:115-120:
0.870	0.190	0.354	0.092	0.308	0.027	5.397	0.066	P6:120-125:
0.832	0.215	0.339	0.112	0.393	0.027	5.808	0.059	P6:125-130:
0.728	0.204	0.276	0.105	0.155	0.027	6.939	0.050	P6:130-135:
0.789	0.198	0.360	0.101	0.204	0.024	7.633	0.058	P6:135-140:
0.780	0.212	0.348	0.119	0.308	0.032	8.312	0.054	P6:140-145:
0.725	0.210	0.301	0.118	0.126	0.032	8.284	0.054	P6:145-150:
0.737	0.215	0.297	0.111	0.284	0.030	8.465	0.050	P6:150-155:
0.823	0.233	0.322	0.115	0.337	0.032	9.240	0.052	P6:155-163:

CORE P8, UNCORRECTED DATA, WT. % ELEMENT

AL	CA	CL	FE	K	MG	MN	NA	P	SI	TI	ORG-C	NAME
7.51	1.62	1.70	5.33	1.06	2.00	1.54	2.49	0.072	23.14	0.440	2.50	P8:0-2:
7.69	1.71	1.32	5.37	1.07	2.00	1.07	2.24	0.070	23.37	0.447	2.40	P8:2-4:
7.58	1.86	1.08	5.42	1.12	2.04	0.47	2.05	0.068	23.67	0.448	2.35	P8:4-5.5:
7.64	1.82	1.02	5.36	1.24	2.16	0.27	2.32	0.060	23.92	0.450	2.40	P8:5.5-7:
7.64	1.85	0.90	5.43	1.27	2.14	0.25	2.19	0.063	23.74	0.450	2.36	P8:7-8.5:
7.64	2.05	0.93	5.31	1.30	2.15	0.23	2.10	0.055	23.78	0.452	2.20	P8:8.5-10:
7.51	2.26	1.08	5.10	1.26	2.13	0.21	2.17	0.052	23.50	0.444	2.13	P8:10-12:
7.51	2.41	1.07	5.04	1.30	2.10	0.20	2.26	0.059	23.39	0.441	2.21	P8:12-14:
7.44	2.56	1.09	5.55	1.34	2.19	0.19	2.26	0.057	23.48	0.441	2.32	P8:14-16:
7.40	2.47	1.26	5.62	1.34	2.18	0.18	2.35	0.054	23.09	0.441	2.28	P8:16-18:
7.64	2.59	0.85	5.63	1.34	2.20	0.18	2.00	0.057	23.46	0.462	2.34	P8:18-21:
7.61	2.34	1.14	5.43	1.33	2.17	0.18	2.26	0.055	23.25	0.455	2.35	P8:21-24:
7.40	2.56	1.48	5.25	1.29	2.10	0.19	2.40	0.053	22.60	0.441	2.46	P8:24-28:
7.51	3.00	1.26	5.39	1.32	2.15	0.19	2.27	0.059	22.97	0.453	2.50	P8:28-32:
7.38	2.73	2.23	5.16	1.31	2.18	0.19	2.97	0.057	22.52	0.434	2.33	P8:32-36:
7.25	3.22	1.67	5.19	1.29	2.07	0.18	2.54	0.059	22.22	0.432	2.29	P8:36-40:
7.21	3.10	2.68	5.17	1.29	2.21	0.17	3.31	0.054	22.03	0.428	2.25	P8:40-45:
7.81	2.13	1.46	5.63	1.40	2.29	0.17	2.46	0.046	23.76	0.468	2.02	P8:45-50:
7.34	2.15	2.98	5.30	1.35	2.25	0.16	3.43	0.045	22.59	0.440	1.91	P8:50-55:
7.49	2.48	1.65	5.41	1.30	2.20	0.16	2.62	0.049	23.11	0.451	1.92	P8:55-60:
7.25	2.37	2.30	5.35	1.32	2.26	0.17	3.06	0.044	22.56	0.434	1.63	P8:60-65:
7.43	2.27	1.90	5.44	1.34	2.26	0.19	2.97	0.043	22.91	0.450	1.84	P8:65-70:
7.11	2.41	3.06	5.23	1.29	2.27	0.16	3.80	0.047	22.01	0.430	1.76	P8:70-75:
7.37	2.23	2.17	5.43	1.35	2.31	0.19	3.04	0.046	22.88	0.444	1.86	P8:75-80:
7.36	2.37	2.10	5.36	1.38	2.29	0.17	2.93	0.043	22.82	0.443	1.83	P8:80-85:
7.19	2.24	3.28	5.08	1.36	2.32	0.19	3.77	0.043	22.35	0.429	1.85	P8:85-90:
7.43	2.26	2.54	5.23	1.45	2.26	0.19	3.22	0.042	23.22	0.435	1.55	P8:90-95:
7.84	2.27	2.67	5.28	1.44	2.25	0.20	3.37	0.043	22.96	0.436	1.77	P8:95-100:
7.33	2.27	3.04	5.14	1.39	2.27	0.21	3.54	0.042	22.66	0.428	0.00	P8:100-105:
7.13	2.45	3.13	5.25	1.34	2.26	0.19	3.53	0.044	22.23	0.419	1.57	P8:105-110:
6.97	2.14	4.45	4.99	1.25	2.32	0.20	4.37	0.042	21.43	0.418	0.00	P8:110-115:
7.74	1.98	1.69	5.50	1.34	2.33	0.24	2.61	0.047	23.66	0.467	1.29	P8:115-120:
7.59	1.95	2.12	5.39	1.34	2.33	0.22	3.14	0.044	23.23	0.462	0.00	P8:120-125:
7.46	1.94	2.43	5.51	1.33	2.31	0.19	3.21	0.046	23.00	0.450	1.30	P8:125-130:
7.35	2.12	2.64	5.48	1.37	2.30	0.19	3.23	0.046	22.94	0.439	0.00	P8:130-135:
7.42	2.18	2.08	5.59	1.39	2.29	0.20	2.97	0.043	23.86	0.436	1.77	P8:135-140:
6.86	2.09	4.98	4.99	1.24	2.30	0.18	4.92	0.039	21.52	0.395	0.00	P8:140-145:
7.11	2.08	2.77	5.34	1.32	2.35	0.19	3.42	0.039	22.54	0.424	1.50	P8:145-150:
6.84	3.19	2.83	5.05	1.26	2.34	0.20	3.27	0.042	21.68	0.406	0.00	P8:150-155:
6.91	3.57	1.90	5.08	1.30	2.35	0.21	2.59	0.046	22.59	0.411	1.91	P8:155-160:
6.82	2.72	3.29	4.79	1.47	2.46	0.28	4.01	0.051	22.62	0.414	0.00	P8:160-165:
6.75	3.30	4.09	4.22	1.92	2.03	2.02	3.84	0.042	22.73	0.412	0.71	P8:165-170:
6.62	4.32	1.70	4.67	1.26	2.43	1.49	2.56	0.057	21.06	0.404	0.00	P8:170-175:
5.36	3.75	2.08	5.42	1.50	2.64	3.36	2.90	0.060	20.53	0.329	1.13	P8:175-183:

CORE P8, SALT-FREE DATA, WT.% ELEMENT

AL	CA	CL	FE	K	MG	MN	NA	P	SI	TI	ORG-C	NAME
7.75	1.63	1.70	5.50	1.06	1.95	1.59	1.59	0.074	23.88	0.454	2.58	P8:0-2:
7.88	1.72	1.32	5.50	1.07	1.96	1.10	1.54	0.072	23.95	0.458	2.46	P8:2-4:
7.73	1.87	1.08	5.53	1.12	2.01	0.48	1.48	0.070	24.14	0.457	2.40	P8:4-5.5:
7.78	1.83	1.02	5.46	1.24	2.13	0.28	1.79	0.062	24.37	0.458	2.45	P8:5.5-7:
7.77	1.86	0.90	5.52	1.27	2.11	0.25	1.72	0.064	24.14	0.458	2.40	P8:7-8.5:
7.77	2.07	0.93	5.40	1.30	2.12	0.23	1.61	0.056	24.19	0.460	2.24	P8:8.5-10:
7.66	2.28	1.08	5.20	1.26	2.10	0.21	1.60	0.053	23.97	0.452	2.17	P8:10-12:
7.66	2.43	1.07	5.14	1.30	2.07	0.20	1.70	0.060	23.85	0.450	2.25	P8:12-14:
7.59	2.59	1.09	5.66	1.34	2.16	0.19	1.69	0.058	23.96	0.450	2.37	P8:14-16:
7.57	2.50	1.26	5.75	1.35	2.14	0.18	1.69	0.056	23.63	0.452	2.33	P8:16-18:
7.76	2.61	0.85	5.72	1.34	2.18	0.18	1.55	0.058	23.83	0.469	2.38	P8:18-21:
7.77	2.37	1.14	5.55	1.33	2.14	0.18	1.66	0.056	23.74	0.464	2.40	P8:21-24:
7.60	2.60	1.48	5.40	1.30	2.06	0.20	1.62	0.054	23.23	0.454	2.53	P8:24-28:
7.69	3.04	1.26	5.52	1.33	2.11	0.19	1.61	0.061	23.51	0.463	2.56	P8:28-32:
7.69	2.80	2.23	5.38	1.32	2.12	0.20	1.80	0.059	23.47	0.453	2.43	P8:32-36:
7.48	3.28	1.67	5.35	1.30	2.02	0.19	1.66	0.061	22.92	0.446	2.36	P8:36-40:
7.58	3.20	2.68	5.44	1.30	2.13	0.18	1.91	0.057	23.16	0.450	2.37	P8:40-45:
8.02	2.16	1.46	5.78	1.41	2.25	0.17	1.69	0.047	24.41	0.480	2.08	P8:45-50:
7.76	2.21	2.98	5.60	1.36	2.17	0.17	1.87	0.048	23.89	0.466	2.02	P8:50-55:
7.72	2.52	1.65	5.58	1.31	2.15	0.16	1.76	0.050	23.83	0.465	1.98	P8:55-60:
7.57	2.42	2.30	5.58	1.33	2.20	0.18	1.86	0.045	23.55	0.453	1.70	P8:60-65:
7.70	2.31	1.90	5.63	1.35	2.21	0.20	1.98	0.044	23.73	0.466	1.91	P8:65-70:
7.53	2.48	3.06	5.54	1.30	2.19	0.17	2.22	0.050	23.31	0.455	1.86	P8:70-75:
7.67	2.27	2.17	5.65	1.36	2.25	0.20	1.91	0.048	23.82	0.462	1.94	P8:75-80:
7.65	2.42	2.10	5.57	1.39	2.23	0.18	1.83	0.045	23.73	0.461	1.90	P8:80-85:
7.65	2.31	3.28	5.40	1.38	2.23	0.20	2.07	0.046	23.77	0.456	1.97	P8:85-90:
7.79	2.31	2.54	5.48	1.47	2.19	0.20	1.90	0.044	24.35	0.456	1.63	P8:90-95:
8.24	2.33	2.67	5.55	1.46	2.18	0.21	1.98	0.045	24.13	0.458	1.86	P8:95-100:
7.76	2.34	3.04	5.44	1.41	2.19	0.22	1.96	0.044	23.99	0.453	0.00	P8:100-105:
7.56	2.53	3.13	5.57	1.35	2.17	0.20	1.90	0.047	23.57	0.444	1.66	P8:105-110:
7.58	2.23	4.45	5.43	1.26	2.20	0.22	2.06	0.045	23.32	0.454	0.00	P8:110-115:
7.99	2.01	1.69	5.67	1.35	2.29	0.25	1.72	0.048	24.41	0.482	1.33	P8:115-120:
7.89	1.98	2.12	5.61	1.35	2.28	0.23	2.04	0.046	24.16	0.480	0.00	P8:120-125:
7.81	1.98	2.43	5.76	1.34	2.25	0.20	1.94	0.048	24.06	0.471	1.36	P8:125-130:
7.72	2.17	2.64	5.76	1.38	2.23	0.20	1.85	0.048	24.10	0.461	0.00	P8:130-135:
7.71	2.22	2.08	5.81	1.40	2.24	0.21	1.88	0.045	24.80	0.453	1.84	P8:135-140:
7.54	2.18	4.98	5.49	1.25	2.16	0.20	2.37	0.043	23.66	0.435	0.00	P8:140-145:
7.49	2.13	2.77	5.62	1.33	2.28	0.20	1.98	0.041	23.74	0.446	1.58	P8:145-150:
7.21	3.30	2.83	5.32	1.27	2.27	0.21	1.79	0.045	22.86	0.428	0.00	P8:150-155:
7.16	3.66	1.90	5.26	1.31	2.30	0.22	1.59	0.047	23.40	0.426	1.98	P8:155-160:
7.25	2.82	3.29	5.10	1.49	2.38	0.30	2.32	0.054	24.06	0.440	0.00	P8:160-165:
7.29	3.47	4.09	4.56	1.99	1.90	2.18	1.69	0.045	24.56	0.445	0.77	P8:165-170:
6.83	4.42	1.70	4.82	1.27	2.39	1.54	1.67	0.059	21.73	0.417	0.00	P8:170-175:
5.57	3.85	2.08	5.63	1.52	2.60	3.49	1.81	0.062	21.34	0.342	1.14	P8:175-183:

CORE P8, RATIOS TO ALUMINIUM (SALT-FREE)

CA/AL	FE/AL	K/AL	MG/AL	MN/AL	NA/AL	P/AL	SI/AL	TI/AL	NAME
0.210	0.710	0.137	0.252	0.205	0.205	0.010	3.081	0.059	P8:0-2:
0.219	0.698	0.136	0.249	0.139	0.196	0.009	3.039	0.058	P8:2-4:
0.242	0.715	0.145	0.260	0.062	0.191	0.009	3.123	0.059	P8:4-5.5:
0.235	0.702	0.160	0.274	0.035	0.229	0.008	3.131	0.059	P8:5.5-7:
0.240	0.711	0.164	0.272	0.033	0.221	0.008	3.107	0.059	P8:7-8.5:
0.266	0.695	0.168	0.273	0.030	0.207	0.007	3.113	0.059	P8:8.5-10:
0.298	0.679	0.165	0.274	0.028	0.209	0.007	3.129	0.059	P8:10-12:
0.318	0.671	0.170	0.270	0.027	0.222	0.008	3.115	0.059	P8:12-14:
0.341	0.746	0.177	0.285	0.026	0.222	0.008	3.156	0.059	P8:14-16:
0.330	0.759	0.178	0.283	0.024	0.223	0.007	3.120	0.060	P8:16-18:
0.337	0.737	0.173	0.281	0.024	0.200	0.007	3.071	0.060	P8:18-21:
0.304	0.714	0.172	0.275	0.024	0.214	0.007	3.055	0.060	P8:21-24:
0.342	0.709	0.170	0.270	0.026	0.213	0.007	3.054	0.060	P8:24-28:
0.396	0.718	0.172	0.275	0.025	0.209	0.008	3.059	0.060	P8:28-32:
0.364	0.699	0.171	0.275	0.026	0.234	0.008	3.051	0.059	P8:32-36:
0.439	0.716	0.173	0.270	0.025	0.222	0.008	3.065	0.060	P8:36-40:
0.422	0.717	0.171	0.282	0.024	0.252	0.008	3.055	0.059	P8:40-45:
0.269	0.721	0.176	0.281	0.022	0.211	0.006	3.042	0.060	P8:45-50:
0.284	0.722	0.176	0.279	0.022	0.242	0.006	3.078	0.060	P8:50-55:
0.326	0.722	0.169	0.279	0.021	0.227	0.007	3.085	0.060	P8:55-60:
0.320	0.738	0.176	0.290	0.023	0.246	0.006	3.112	0.060	P8:60-65:
0.300	0.732	0.175	0.287	0.026	0.258	0.006	3.083	0.061	P8:65-70:
0.330	0.736	0.173	0.290	0.023	0.295	0.007	3.096	0.060	P8:70-75:
0.296	0.737	0.177	0.294	0.026	0.249	0.006	3.104	0.060	P8:75-80:
0.316	0.728	0.182	0.292	0.023	0.239	0.006	3.101	0.060	P8:80-85:
0.302	0.707	0.180	0.292	0.026	0.271	0.006	3.108	0.060	P8:85-90:
0.297	0.704	0.188	0.281	0.026	0.243	0.006	3.125	0.059	P8:90-95:
0.282	0.673	0.177	0.264	0.026	0.240	0.005	2.929	0.056	P8:95-100:
0.301	0.701	0.181	0.282	0.029	0.252	0.006	3.091	0.058	P8:100-105:
0.334	0.736	0.179	0.288	0.027	0.251	0.006	3.118	0.059	P8:105-110:
0.294	0.716	0.167	0.290	0.029	0.272	0.006	3.075	0.060	P8:110-115:
0.251	0.711	0.169	0.286	0.031	0.216	0.006	3.057	0.060	P8:115-120:
0.251	0.710	0.171	0.288	0.029	0.258	0.006	3.061	0.061	P8:120-125:
0.253	0.739	0.172	0.288	0.025	0.249	0.006	3.083	0.060	P8:125-130:
0.281	0.746	0.179	0.289	0.026	0.240	0.006	3.121	0.060	P8:130-135:
0.288	0.753	0.182	0.290	0.027	0.244	0.006	3.216	0.059	P8:135-140:
0.289	0.727	0.166	0.287	0.026	0.314	0.006	3.137	0.058	P8:140-145:
0.284	0.751	0.178	0.304	0.027	0.264	0.005	3.170	0.060	P8:145-150:
0.458	0.738	0.176	0.314	0.029	0.248	0.006	3.170	0.059	P8:150-155:
0.511	0.735	0.183	0.322	0.030	0.222	0.007	3.269	0.059	P8:155-160:
0.389	0.702	0.206	0.328	0.041	0.320	0.007	3.317	0.061	P8:160-165:
0.476	0.625	0.272	0.260	0.299	0.232	0.006	3.367	0.061	P8:165-170:
0.647	0.705	0.185	0.350	0.225	0.244	0.009	3.181	0.061	P8:170-175:
0.691	1.011	0.272	0.467	0.627	0.325	0.011	3.830	0.061	P8:175-183:

PLEIADES BOX CORE, UNCORRECTED DATA, WT. % ELEMENT

AL	CA	CL	FE	K	MG	MN	NA	P	SI	TI	ORG-C	NAME
1.59	24.20	1.90	1.32	0.37	0.57	3.77	1.60	0.059	8.36	0.070	0.48	PL:2:
1.52	25.40	1.81	1.25	0.35	0.53	2.77	1.51	0.058	8.03	0.066	0.55	PL:4:
1.50	26.03	2.57	1.25	0.34	0.56	1.83	1.90	0.058	8.08	0.066	0.65	PL:6:
1.42	26.72	1.88	1.20	0.31	0.51	1.61	1.48	0.056	7.71	0.061	0.55	PL:8:
1.60	26.48	1.90	1.37	0.34	0.54	1.74	1.59	0.055	8.29	0.067	0.55	PL:10:
1.46	26.56	2.22	1.25	0.34	0.53	1.26	1.76	0.054	7.92	0.062	0.66	PL:12:
1.46	27.37	1.79	1.28	0.32	0.51	1.25	1.55	0.052	7.99	0.062	0.60	PL:14:
1.41	28.31	1.47	1.38	0.32	0.51	0.30	1.31	0.048	8.16	0.060	0.70	PL:16:
1.35	27.74	1.92	1.38	0.33	0.51	0.19	1.50	0.044	7.89	0.061	0.66	PL:18:
1.27	27.81	2.02	1.35	0.34	0.56	0.16	1.48	0.041	7.78	0.054	0.68	PL:20:
1.20	29.22	2.05	1.44	0.34	0.59	0.19	1.53	0.041	7.43	0.051	0.64	PL:24:
1.16	27.68	1.97	1.45	0.33	0.63	0.17	1.38	0.041	7.23	0.049	0.62	PL:28:
1.15	27.84	1.93	1.35	0.33	0.59	0.18	1.40	0.042	7.31	0.045	0.67	PL:32:
1.13	28.49	1.76	1.63	0.34	0.64	0.20	1.36	0.043	7.61	0.049	0.76	PL:36:
1.15	28.51	1.83	1.50	0.36	0.61	0.19	1.45	0.042	7.73	0.051	0.78	PL:40:

PLEIADES BOX CORE, SALT-FREE DATA, WT. % ELEMENT

AL	CA	CL	FE	K	MG	MN	NA	P	SI	TI	ORG-C	NAME
1.65	25.03	1.90	1.37	0.34	0.46	3.91	0.56	0.061	8.66	0.073	0.50	PL:2:
1.57	26.23	1.81	1.29	0.32	0.42	2.86	0.52	0.060	8.30	0.068	0.57	PL:4:
1.57	27.25	2.57	1.31	0.30	0.41	1.92	0.49	0.061	8.48	0.069	0.68	PL:6:
1.47	27.63	1.88	1.24	0.28	0.40	1.67	0.45	0.058	7.98	0.063	0.57	PL:8:
1.66	27.39	1.90	1.42	0.31	0.43	1.80	0.55	0.057	8.59	0.069	0.57	PL:10:
1.52	27.63	2.22	1.30	0.31	0.40	1.31	0.55	0.056	8.25	0.065	0.69	PL:12:
1.51	28.25	1.79	1.32	0.29	0.40	1.29	0.57	0.054	8.26	0.064	0.62	PL:14:
1.45	29.06	1.47	1.42	0.30	0.42	0.31	0.51	0.049	8.38	0.062	0.72	PL:16:
1.40	28.70	1.92	1.43	0.30	0.40	0.20	0.45	0.046	8.18	0.063	0.68	PL:18:
1.32	28.83	2.02	1.40	0.31	0.44	0.17	0.37	0.043	8.08	0.056	0.71	PL:20:
1.25	30.31	2.05	1.50	0.31	0.47	0.20	0.41	0.043	7.72	0.053	0.66	PL:24:
1.20	28.67	1.97	1.50	0.30	0.52	0.18	0.30	0.042	7.50	0.051	0.64	PL:28:
1.19	28.81	1.93	1.40	0.30	0.48	0.19	0.34	0.044	7.58	0.047	0.69	PL:32:
1.17	29.39	1.76	1.68	0.31	0.54	0.21	0.39	0.044	7.86	0.051	0.79	PL:36:
1.19	29.45	1.83	1.55	0.33	0.50	0.20	0.45	0.043	8.00	0.053	0.81	PL:40:

PLEIADES BOX CORE, SALT-AND-CARBONATE-FREE DATA, WT. % ELEMENT

AL	CA	CL	FE	K	MG	MN	NA	P	SI	TI	ORG-C	NAME
4.40	25.03	5.07	3.65	0.91	1.23	10.43	1.49	0.163	23.09	0.193	1.33	PL:2:
4.55	26.23	5.25	3.74	0.93	1.22	8.29	1.51	0.174	24.06	0.198	1.65	PL:4:
4.91	27.25	8.04	4.10	0.94	1.28	6.01	1.53	0.190	26.54	0.217	2.13	PL:6:
4.74	27.63	6.06	4.00	0.90	1.29	5.39	1.45	0.187	25.74	0.204	1.84	PL:8:
5.25	27.39	6.01	4.49	0.98	1.36	5.69	1.74	0.180	27.18	0.220	1.80	PL:10:
4.90	27.63	7.16	4.19	1.00	1.29	4.22	1.77	0.182	26.61	0.208	2.23	PL:12:
5.13	28.25	6.08	4.48	0.98	1.36	4.38	1.93	0.183	28.04	0.218	2.10	PL:14:
5.28	29.06	5.36	5.18	1.09	1.53	1.13	1.86	0.180	30.54	0.224	2.62	PL:16:
4.94	28.70	6.78	5.05	1.06	1.41	0.71	1.59	0.161	28.87	0.223	2.40	PL:18:
4.71	28.83	7.21	5.00	1.11	1.57	0.61	1.32	0.152	28.85	0.200	2.53	PL:20:
5.14	30.31	8.43	6.17	1.27	1.93	0.82	1.69	0.175	31.75	0.218	2.71	PL:24:
4.22	28.67	6.93	5.28	1.06	1.83	0.63	1.06	0.150	26.40	0.179	2.25	PL:28:
4.24	28.81	6.88	4.99	1.07	1.71	0.68	1.21	0.155	27.01	0.166	2.46	PL:32:
4.40	29.39	6.61	6.31	1.16	2.03	0.79	1.47	0.167	29.53	0.190	2.97	PL:36:
4.50	29.45	6.92	5.86	1.25	1.89	0.76	1.70	0.164	30.23	0.199	3.06	PL:40:

PLEIADES BOX CORE, RATIOS TO ALUMINIUM (SALT-FREE)

FE/AL	K/AL	MG/AL	MN/AL	NA/AL	P/AL	SI/AL	TI/AL	NAME
0.830	0.206	0.279	2.370	0.339	0.037	5.248	0.044	PL:2:
0.822	0.204	0.268	1.822	0.331	0.038	5.287	0.043	PL:4:
0.834	0.191	0.261	1.223	0.312	0.039	5.401	0.044	PL:6:
0.844	0.190	0.272	1.136	0.306	0.039	5.429	0.043	PL:8:
0.855	0.187	0.259	1.084	0.331	0.034	5.175	0.042	PL:10:
0.855	0.204	0.263	0.862	0.362	0.037	5.428	0.043	PL:12:
0.874	0.192	0.265	0.854	0.377	0.036	5.470	0.042	PL:14:
0.979	0.207	0.290	0.214	0.352	0.034	5.779	0.042	PL:16:
1.021	0.214	0.286	0.143	0.321	0.033	5.843	0.045	PL:18:
1.061	0.235	0.333	0.129	0.280	0.032	6.121	0.043	PL:20:
1.200	0.248	0.376	0.160	0.328	0.034	6.176	0.042	PL:24:
1.250	0.250	0.433	0.150	0.250	0.035	6.250	0.042	PL:28:
1.176	0.252	0.403	0.160	0.286	0.037	6.370	0.039	PL:32:
1.436	0.265	0.462	0.179	0.333	0.038	6.718	0.043	PL:36:
1.303	0.277	0.420	0.168	0.378	0.036	6.723	0.044	PL:40:

Table C.2

Minor element analyses, all in ppm, and ratios to aluminium and C_{org} (for I and Br).

SURFACE SEDIMENTS, UNCORRECTED DATA, PPM

BA	BR	CO	CR	CU	I	MO	NI	RB	S	SR	ZN	ZR	NAME
3302	95	15	9	133	73	15	231	2	2317	1120	115	22	P1:0-2:
4368	96	22	14	153	106	11	193	4	2205	965	139	35	P2:0-1:
1200	170	10	14	26	249	12	29	3	4150	1530	34	13	P5:0-1.5:
2350	76	15	20	103	140	73	307	NA	2460	1087	270	27	PL:2:
2726	90	22	18	93	126	28	234	6	2352	1077	170	28	P6:0-1:
4570	228	20	59	136	241	48	253	20	4350	1190	343	35	P7:0-2:
2499	212	38	123	113	408	11	151	28	1125	180	305	56	P8:0-4:
4850	357	NA	NA	163	686	19	203	71	2800	339	398	NA	P9:0-2:
2480	320	NA	NA	171	556	72	222	60	2730	253	343	NA	P10:0-2:
2360	339	NA	NA	170	644	40	211	58	2680	227	358	NA	P11:0-3:
2030	381	NA	125*	152	610	40	181	54	2830	221	284	NA	P12:0-1.5:
1140	387	NA	NA	94	808	13	122	48	2640	290	208	NA	P13:0-2:

* ANALYSIS BY ATOMIC ABSORPTION, FOR THIS SAMPLE ONLY

NA = NOT ANALYZED

SURFACE SEDIMENTS, SALT-FREE DATA, PPM

BA	BR	CO	CR	CU	I	MO	NI	RB	S	SR	ZN	ZR	NAME
3442	18	16	9	139	76	16	241	2	1340	1158	120	23	P1:0-2:
4550	21	23	15	159	110	11	201	4	1290	996	145	36	P2:0-1:
1284	49	11	15	28	266	13	31	3	2550	1621	36	14	P5:0-1.5:
2434	11	16	21	107	145	76	318	NA	1600	1118	280	28	PL:2:
2806	37	23	19	95	130	29	241	7	1640	1102	175	29	P6:0-1:
5041	56	22	65	150	266	53	279	22	2050	1289	378	39	P7:0-2:
2572	162	39	127	116	420	11	155	29	400	179	314	58	P8:0-4:
5170	255	NA	NA	174	731	20	216	76	1250	346	424	NA	P9:0-2:
2707	176	NA	NA	187	607	79	242	65	600	255	374	NA	P10:0-2:
2547	215	NA	NA	183	695	43	228	63	820	227	386	NA	P11:0-3:
2231	230	NA	137	167	671	44	199	59	530	220	312	NA	P12:0-1.5:
1215	287	NA	NA	100	861	14	130	51	1090	294	222	NA	P13:0-2:

NA = NOT ANALYZED

SURFACE SEDIMENTS, SALT-AND-CARBONATE-FREE DATA, PPM

BA	BR	CO	CR	CU	I	MO	NI	RB	S	SR	ZN	ZR	NAME
9321	49	42	25	375	206	42	653	5	3629	3136	325	62	P1:0-2:
9101	41	46	28	318	221	23	403	8	2581	1992	290	73	P2:0-1:
13540	513	113	158	293	2810	135	327	34	26888	17096	384	147	P5:0-1.5:
6491	28	42	55	285	387	202	848	NA	4267	2981	746	75	PL:2:
8614	113	70	58	293	398	88	739	20	5034	3382	537	88	P6:0-1:
10196	113	45	132	303	538	107	564	45	4147	2608	765	78	P7:0-2:
2572	162	39	127	116	420	11	155	29	400	179	314	58	P8:0-4:
5170	255	NA	NA	174	731	20	216	76	1250	346	424	NA	P9:0-2:
2707	176	NA	NA	187	607	79	242	65	600	255	374	NA	P10:0-2:
2547	215	NA	NA	183	695	43	228	63	820	227	386	NA	P11:0-3:
2231	230	NA	137	167	671	44	199	59	530	220	312	NA	P12:0-1.5:
1215	287	NA	NA	100	861	14	130	51	1090	294	222	NA	P13:0-2:

NA = NOT ANALYZED

SURFACE SEDIMENTS, SALT-FREE RATIOS TO ALUMINIUM (X10-4)

BA/AL	CO/AL	CR/AL	CU/AL	MO/AL	NI/AL	RB/AL	S/AL	SR/AL	ZN/AL	ZR/AL	NAME
4249.4	19.3	11.2	171.1	19.3	297.7	2.3	1654.3	1429.6	148.0	28.3	P1:0-2:
3334.4	16.8	10.4	116.4	8.4	148.1	2.9	948.5	732.2	106.5	26.8	P2:0-1:
2517.9	21.0	29.4	54.5	25.2	60.8	6.3	5000.0	3179.1	71.3	27.3	P5:0-1.5:
1475.3	9.5	12.6	64.7	45.8	192.7	NA	969.7	677.5	169.5	17.0	PL:2:
1810.6	14.6	12.1	61.5	18.6	155.4	4.3	1058.1	711.0	112.9	18.6	P6:0-1:
1465.3	6.4	18.9	43.6	15.4	81.1	6.4	595.9	374.8	110.0	11.2	P7:0-2:
328.8	5.0	16.2	14.9	1.4	19.8	3.7	51.2	22.8	40.1	7.4	P8:0-4:
620.6	NA	NA	20.9	2.4	26.0	9.1	150.1	41.6	50.9	NA	P9:0-2:
305.8	NA	NA	21.1	8.9	27.4	7.4	67.8	28.9	42.3	NA	P10:0-2:
293.5	NA	NA	21.1	5.0	26.2	7.2	94.5	26.2	44.5	NA	P11:0-3:
251.0	NA	15.4	18.8	4.9	22.4	6.7	59.6	24.8	35.1	NA	P12:0-1.5:
139.0	NA	NA	11.5	1.6	14.9	5.9	124.7	33.7	25.4	NA	P13:0-2:

NA = NOT ANALYZED

CORE P1, UNCORRECTED DATA, PPM

BA	BR	CO	CR	CU	I	MO	NI	RB	S	SR	ZN	ZR	NAME
3302	95	15	9	133	73	15	231	2	2317	1120	115	22	P1:0-2:
3014	84	13	8	114	58	3	77	3	1954	1147	77	29	P1:2-4:
2881	95	14	9	111	57	2	61	2	2016	1148	78	20	P1:4-6:
2766	74	13	9	103	40	1	42	3	1859	1214	74	18	P1:6-8:
2704	78	14	8	94	38	5	41	2	1924	1222	94	18	P1:8-10:
2620	70	11	10	84	36	4	38	NA	1888	1243	64	20	P1:10-12:
2450	68	9	9	62	27	1	48	2	1903	1206	80	23	P1:12-14:
2368	70	8	11	120	21	1	47	NA	1931	1222	86	23	P1:14-16:
2266	65	7	9	67	17	4	47	1	1877	1208	89	20	P1:16-18:
2191	61	8	10	91	18	5	51	2	1874	1198	96	21	P1:18-20:
2076	69	9	11	70	24	3	56	1	1864	1179	90	27	P1:20-22:
2060	71	14	11	96	29	1	58	2	1884	1168	104	15	P1:22-26:
2145	87	9	12	91	36	3	61	2	1983	1158	123	18	P1:26-30:
2256	106	10	12	67	50	3	77	2	2019	1133	125	23	P1:30-34:
2459	102	19	12	72	59	2	84	2	1915	1137	174	22	P1:34-36:
2434	112	20	12	88	65	2	127	3	2090	1138	182	29	P1:36-40:
2385	140	22	11	66	51	3	103	3	2186	1093	136	24	P1:40-45:
2391	133	21	11	80	52	4	195	3	2189	1094	185	20	P1:45-50:
2310	175	19	11	80	52	4	177	3	2675	1065	162	23	P1:50-55:
2300	124	13	9	78	49	7	143	3	2281	1083	139	21	P1:55-60:
2139	143	16	11	88	48	4	212	2	2500	1078	179	15	P1:60-65:
1984	99	29	9	86	41	7	343	2	1968	1124	113	20	P1:65-70:
1897	130	11	9	61	27	3	89	2	2247	1077	102	19	P1:70-75:
1974	100	13	8	89	37	3	96	2	1870	1083	104	17	P1:75-80:
1803	143	10	9	69	33	3	65	2	2236	1064	107	19	P1:80-85:
1928	101	7	8	56	39	4	54	1	1589	1058	106	20	P1:85-90:
1892	156	10	9	72	32	3	78	2	2020	1013	104	18	P1:90-95:
1876	120	14	10	87	34	7	168	2	1679	1043	141	24	P1:95-100:
1748	142	12	9	75	34	6	153	1	1974	1019	148	27	P1:100-105:
1549	162	14	8	83	39	10	238	2	2158	990	144	18	P1:105-110:
1473	121	12	8	84	30	5	104	1	1462	998	122	15	P1:110-115:
1463	160	9	8	66	25	4	55	1	1922	945	97	18	P1:115-120:
1562	172	8	8	67	26	4	65	2	1988	909	90	19	P1:120-125:
1998	134	10	10	88	29	3	77	1	1645	910	119	22	P1:125-130:
2332	178	9	11	144	34	5	118	2	2340	868	172	27	P1:130-135:
3758	203	17	16	149	33	6	183	5	2532	792	249	35	P1:135-140:
3678	182	16	13	117	26	5	144	5	2352	827	222	44	P1:140-145:
4653	134	23	16	145	42	6	269	9	2220	813	315	52	P1:145-150:

NA = NOT ANALYZED

CORE P1, SALT-FREE DATA, PPM

BA	BR	CO	CR	CU	I	MO	NI	RB	S	SR	ZN	ZR	NAME
3442	18	16	9	139	76	16	241	2	1340	1158	120	23	P1:0-2:
3102	31	13	8	117	60	3	79	3	1330	1174	79	30	P1:2-4:
2976	36	14	9	114	59	2	63	2	1340	1178	81	21	P1:4-6:
2837	27	13	9	105	41	1	43	3	1310	1239	76	18	P1:6-8:
2786	23	14	9	97	39	5	43	2	1320	1252	97	19	P1:8-10:
2688	22	11	10	86	37	4	39	NA	1350	1269	66	21	P1:10-12:
2527	11	9	10	64	28	1	49	2	1270	1237	82	24	P1:12-14:
2444	12	8	12	124	22	1	49	NA	1260	1254	89	24	P1:14-16:
2329	15	7	10	68	17	4	48	1	1310	1235	91	21	P1:16-18:
2254	8	8	10	93	19	5	53	2	1270	1226	99	22	P1:18-20:
2137	15	9	11	72	25	3	58	1	1270	1207	93	28	P1:20-22:
2131	8	14	11	99	30	1	60	2	1130	1200	108	16	P1:22-26:
2238	9	9	13	95	38	3	64	3	1060	1198	128	19	P1:26-30:
2331	46	10	13	69	52	3	80	2	1330	1163	129	24	P1:30-34:
2534	48	20	12	74	61	2	87	2	1270	1164	179	23	P1:34-36:
2508	57	21	12	90	67	2	131	3	1420	1166	188	30	P1:36-40:
2496	58	23	12	69	53	3	107	3	1170	1133	142	25	P1:40-45:
2485	63	22	12	83	54	4	202	3	1330	1128	192	21	P1:45-50:
2464	59	20	11	85	55	4	189	3	1260	1121	173	25	P1:50-55:
2414	36	14	10	82	51	7	150	3	1220	1125	146	22	P1:55-60:
2291	19	17	12	94	51	4	227	2	1037	1138	192	16	P1:60-65:
2067	23	30	9	90	43	7	357	2	1097	1162	118	21	P1:65-70:
2023	12	12	9	65	29	3	95	2	860	1134	109	20	P1:70-75:
2057	24	14	9	93	39	3	100	2	960	1119	108	18	P1:75-80:
1927	21	11	9	74	35	3	69	2	760	1122	114	20	P1:80-85:
2006	28	7	9	59	41	4	56	2	690	1092	110	21	P1:85-90:
2013	44	11	10	76	34	3	83	3	630	1063	111	19	P1:90-95:
1954	46	15	10	90	35	7	175	2	760	1077	147	25	P1:95-100:
1854	36	13	9	80	36	6	162	1	670	1067	157	29	P1:100-105:
1657	40	15	9	89	42	11	255	2	650	1044	154	19	P1:105-110:
1530	52	12	9	87	31	5	108	1	600	1028	127	16	P1:110-115:
1547	61	10	9	70	26	4	59	1	700	986	103	19	P1:115-120:
1678	43	9	9	72	28	4	70	2	410	960	97	20	P1:120-125:
2109	36	11	10	93	31	3	82	1	480	948	126	23	P1:125-130:
2511	46	10	11	155	37	5	127	2	780	917	185	29	P1:130-135:
4121	39	19	17	164	36	7	201	5	580	847	273	38	P1:135-140:
4009	27	17	15	128	28	5	157	5	520	881	242	48	P1:140-145:
4912	36	24	17	153	44	6	284	10	1070	846	333	55	P1:145-150:

NA = NOT ANALYZED

CORE P1, SALT-AND-CARBONATE-FREE-DATA, PPM

BA	BR	CO	CR	CU	I	MO	NI	RB	S	SR	ZN	ZR	NAME
9321	49	42	25	375	206	42	653	5	3629	3136	325	62	P1:0-2:
8720	86	38	23	330	168	9	222	8	3738	3300	223	84	P1:2-4:
8961	107	44	28	344	177	6	189	6	4036	3549	243	62	P1:4-6:
9361	89	44	30	348	135	3	143	10	4322	4089	250	61	P1:6-8:
9463	78	49	30	330	133	18	145	6	4484	4254	329	63	P1:8-10:
9538	80	40	35	305	131	15	138	NA	4790	4504	233	73	P1:10-12:
8877	38	33	34	223	98	4	172	8	4462	4345	290	83	P1:12-14:
9174	43	31	43	466	81	4	183	NA	4730	4707	333	89	P1:14-16:
9039	56	28	37	266	68	16	186	6	5085	4793	355	80	P1:16-18:
8665	31	32	38	359	71	20	202	9	4882	4713	380	83	P1:18-20:
8199	58	36	43	275	95	12	222	4	4873	4631	355	107	P1:20-22:
8536	33	58	45	396	120	4	242	10	4526	4808	431	62	P1:22-26:
8392	33	35	47	355	141	12	240	9	3976	4494	481	70	P1:26-30:
7926	157	35	43	236	176	11	271	7	4522	3955	439	81	P1:30-34:
8622	162	67	42	251	207	7	295	7	4322	3963	610	77	P1:34-36:
8229	187	68	39	296	220	7	430	10	4658	3825	615	98	P1:36-40:
7785	181	72	37	216	166	10	335	9	3650	3535	444	78	P1:40-45:
7495	191	66	35	250	163	13	610	9	4011	3403	580	63	P1:45-50:
7163	173	59	33	248	161	12	549	9	3662	3259	502	71	P1:50-55:
7270	109	41	30	248	155	22	452	8	3674	3389	439	66	P1:55-60:
6878	56	51	37	283	154	13	683	7	3114	3417	575	48	P1:60-65:
6565	75	96	29	285	136	23	1135	8	3484	3690	374	66	P1:65-70:
6326	38	37	29	204	90	10	297	5	2689	3545	340	63	P1:70-75:
6232	73	41	27	281	117	9	302	6	2909	3390	328	54	P1:75-80:
5757	63	32	27	221	105	10	206	7	2270	3351	342	61	P1:80-85:
5572	77	20	24	163	113	12	155	4	1917	3033	306	58	P1:85-90:
5146	113	27	25	195	87	8	213	7	1610	2718	283	49	P1:90-95:
5081	120	38	26	235	92	19	455	5	1977	2801	382	65	P1:95-100:
4514	87	31	22	195	88	15	395	3	1631	2598	382	70	P1:100-105:
4090	98	37	21	220	103	26	629	4	1604	2576	380	48	P1:105-110:
3771	127	31	21	215	77	13	266	1	1479	2534	312	38	P1:110-115:
3884	153	24	22	175	66	11	147	3	1758	2476	257	48	P1:115-120:
3747	96	19	19	162	62	10	157	4	915	2143	216	46	P1:120-125:
4529	76	23	22	200	66	7	175	3	1031	2036	270	50	P1:125-130:
4903	90	19	22	302	71	11	247	4	1523	1791	362	57	P1:130-135:
7180	68	32	30	285	63	11	350	9	1010	1475	476	67	P1:135-140:
7083	48	31	26	226	50	10	277	10	919	1557	428	85	P1:140-145:
7959	58	39	27	248	72	10	461	16	1734	1370	539	89	P1:145-150:

NA = NOT ANALYZED

CORE P1, SALT-FREE RATIOS TO ALUMINIUM (X10-4)

BA/AL	CO/AL	CR/AL	CU/AL	MO/AL	NI/AL	RB/AL	S/AL	SR/AL	ZN/AL	ZR/AL	NAME
4249.4	19.3	11.2	171.1	19.3	297.7	2.3	1654.3	1429.6	148.0	28.3	P1:0-2:
3926.9	16.9	10.4	148.4	3.9	100.2	3.7	1683.5	1486.2	100.3	37.8	P1:2-4:
3915.3	19.0	12.1	150.5	2.7	82.5	2.5	1763.2	1550.4	106.0	27.2	P1:4-6:
4053.1	19.0	12.9	150.5	1.5	61.9	4.5	1871.4	1770.6	108.4	26.4	P1:6-8:
3979.3	20.6	12.4	138.9	7.4	60.8	2.5	1885.7	1788.6	138.3	26.5	P1:8-10:
3840.6	16.1	14.1	122.7	5.9	55.5	NA	1928.6	1813.4	93.8	29.3	P1:10-12:
4010.4	14.7	15.1	100.8	1.6	77.9	3.6	2015.9	1962.7	130.9	37.7	P1:12-14:
3941.6	13.3	18.6	200.3	1.7	78.8	NA	2032.3	2022.2	143.1	38.3	P1:14-16:
3881.2	12.0	16.0	114.0	6.8	79.8	2.5	2183.3	2058.3	152.4	34.2	P1:16-18:
3757.0	13.7	16.3	155.5	8.6	87.5	4.1	2116.7	2043.3	164.6	36.0	P1:18-20:
3816.1	16.5	19.9	128.1	5.5	103.3	2.1	2267.9	2155.4	165.4	49.6	P1:20-22:
3329.7	22.6	17.7	154.4	1.6	94.3	3.8	1765.6	1875.4	168.1	24.2	P1:22-26:
3290.7	13.8	18.4	139.3	4.6	94.2	3.7	1558.8	1761.9	188.7	27.6	P1:26-30:
3479.3	15.4	19.0	103.4	4.6	118.9	3.2	1985.1	1736.1	192.8	35.5	P1:30-34:
3781.6	29.2	18.4	110.0	3.1	129.2	3.0	1895.5	1738.0	267.5	33.8	P1:34-36:
3635.3	29.9	17.3	131.0	3.0	190.2	4.2	2058.0	1689.9	271.9	43.3	P1:36-40:
3565.3	32.9	16.8	98.8	4.5	153.5	4.2	1671.4	1618.9	203.3	35.9	P1:40-45:
3601.3	31.6	17.0	120.2	6.0	293.0	4.3	1927.5	1635.0	278.7	30.1	P1:45-50:
3520.3	29.0	16.1	122.1	6.1	269.9	4.5	1800.0	1601.6	246.9	35.1	P1:50-55:
3498.5	19.8	14.4	119.2	10.7	217.6	4.0	1768.1	1630.9	211.4	31.9	P1:55-60:
3636.0	27.2	19.5	149.9	6.8	361.0	3.7	1646.0	1806.7	304.2	25.5	P1:60-65:
3563.6	52.1	15.8	154.9	12.6	616.0	4.2	1891.4	2002.7	203.0	35.9	P1:65-70:
3488.3	20.2	16.0	112.4	5.5	163.9	3.0	1482.8	1954.5	187.6	34.9	P1:70-75:
3486.5	23.0	15.0	157.2	5.3	168.8	3.4	1627.1	1896.7	183.7	30.0	P1:75-80:
3706.6	20.6	17.6	142.2	6.2	132.9	4.7	1461.5	2157.7	220.0	39.1	P1:80-85:
3715.1	13.5	16.3	108.6	7.7	103.5	2.8	1277.8	2021.9	204.3	38.5	P1:85-90:
3660.7	19.3	17.9	138.8	5.8	151.3	4.8	1145.5	1933.4	201.2	34.8	P1:90-95:
3757.2	28.0	19.2	173.6	14.0	336.7	3.6	1461.5	2070.9	282.4	48.1	P1:95-100:
4030.5	27.7	19.9	174.0	13.8	352.6	3.1	1456.5	2319.2	341.2	62.2	P1:100-105:
3683.2	33.3	19.0	198.2	23.8	566.8	4.0	1444.4	2319.2	342.5	42.8	P1:105-110:
4026.1	32.8	22.7	229.8	13.7	284.2	1.6	1578.9	2705.4	333.6	41.0	P1:110-115:
3965.5	24.4	22.3	178.8	10.8	150.0	3.2	1794.9	2527.9	262.9	48.8	P1:115-120:
3996.3	20.5	20.6	172.5	10.2	167.1	4.7	976.2	2285.6	230.3	48.6	P1:120-125:
3834.3	19.2	18.8	169.0	5.8	148.2	2.6	872.7	1723.7	228.4	42.2	P1:125-130:
3138.4	12.1	14.3	193.6	6.7	158.4	2.7	975.0	1146.4	231.5	36.3	P1:130-135:
3492.8	15.8	14.4	138.8	5.6	170.4	4.5	491.5	717.4	231.4	32.5	P1:135-140:
3516.8	15.3	12.8	112.2	4.8	137.6	4.8	456.1	772.9	212.3	42.1	P1:140-145:
3296.9	16.3	11.1	102.6	4.2	190.9	6.7	718.1	567.6	223.2	36.8	P1:145-150:

NA = NOT ANALYZED

CORE P2, UNCORRECTED DATA, PPM

BA	BR	CO	CR	CU	I	MO	NI	RB	S	SR	ZN	ZR	NAME
4368	96	22	14	153	106	11	193	4	2205	965	139	35	P2:0-1:
4075	106	20	14	148	104	6	109	4	2051	1011	115	33	P2:1-2:
3870	114	20	12	136	82	1	74	4	2014	1006	111	34	P2:2-3:
3782	111	11	13	108	73	1	55	4	1969	1029	118	32	P2:3-4:
3564	102	11	14	115	55	3	67	4	1969	1033	146	35	P2:4-5:
3495	111	12	15	89	51	4	72	5	2088	1054	138	29	P2:5-6:
3305	110	9	14	131	53	2	75	4	2083	1075	147	36	P2:6-8:
3235	83	10	17	171	38	3	88	4	1954	1102	207	29	P2:8-10:
3200	91	10	17	146	47	3	77	5	2038	1114	209	26	P2:10-12:
3137	87	13	16	106	38	3	81	4	2030	1133	178	30	P2:12-14:
2978	81	16	17	192	43	2	122	4	2001	1149	200	32	P2:14-17:
2916	95	17	16	117	52	3	148	4	2174	1151	190	30	P2:17-20:
2635	130	12	16	108	70	2	95	3	2001	1210	259	29	P2:20-24:
2576	89	15	15	90	45	3	165	4	2046	1133	128	34	P2:24-28:
2530	102	12	16	94	53	4	105	3	1996	1105	132	35	P2:28-32:
2536	110	11	14	92	65	4	88	4	2052	1082	137	31	P2:32-36:
2613	124	14	16	97	83	2	146	4	2025	1081	167	33	P2:36-40:
2778	161	15	18	100	96	2	135	4	2340	1074	186	37	P2:40-44:
2670	222	15	18	87	100	3	142	5	2972	1018	215	44	P2:44-46:
2996	180	18	16	91	120	6	248	5	2433	994	241	43	P2:46-50:
2723	247	16	13	83	101	4	177	4	3199	937	178	41	P2:50-55:
2882	212	16	16	83	113	8	184	4	2421	953	241	40	P2:55-60:
2959	221	13	14	88	98	5	144	5	2672	943	219	38	P2:60-65:
2895	181	14	15	85	95	6	147	5	2198	967	220	36	P2:65-70:
2771	220	12	14	78	89	5	131	4	2859	922	199	39	P2:70-75:
3010	200	10	14	88	93	9	181	5	2453	910	272	35	P2:75-80:
2929	224	11	14	88	92	9	172	5	2713	910	252	31	P2:80-85:
2635	197	13	13	85	81	7	144	5	2633	948	211	32	P2:85-90:
2488	144	12	14	79	69	7	110	3	2172	975	180	36	P2:90-95:
2232	163	12	11	76	53	6	106	5	2572	985	154	18	P2:95-100:
2193	162	9	12	71	54	4	71	3	2359	975	148	33	P2:100-105:
2257	178	9	11	79	56	4	86	5	2434	951	167	27	P2:105-110:
2259	130	13	12	79	62	5	120	3	2023	986	151	29	P2:110-115:
2179	170	11	12	78	56	8	122	3	2358	950	170	37	P2:115-120:
2109	163	9	11	81	57	5	128	4	2207	919	159	27	P2:120-125:
2081	208	8	12	75	62	5	80	NA	2351	854	149	25	P2:125-130:
2189	200	10	14	85	69	5	74	3	1696	847	172	22	P2:130-135:
2043	200	8	12	79	68	3	104	2	1903	834	175	27	P2:135-140:
1900	201	10	11	66	53	7	67	3	2159	841	146	21	P2:140-145:
1732	141	12	10	70	49	4	174	2	1638	876	149	17	P2:145-150:
1665	197	13	10	73	50	8	149	2	1993	856	149	24	P2:150-155:
1104	201	14	21	45	46	4	99	1	2057	838	170	23	P2:155-163:

NA = NOT ANALYZED

CORE P2, SALT-FREE DATA, PPM

BA	BR	CO	CR	CU	I	MO	NI	RB	S	SR	ZN	ZR	NAME
4550	21	23	15	159	110	11	201	4	1290	996	145	36	P2:0-1:
4238	34	21	14	154	108	6	113	4	1180	1042	120	34	P2:1-2:
4027	42	21	13	142	85	1	77	5	1150	1038	116	35	P2:2-3:
3928	42	11	14	112	76	1	57	4	1140	1060	123	33	P2:3-4:
3697	35	11	15	120	57	3	69	4	1220	1063	151	36	P2:4-5:
3650	31	13	16	93	53	4	75	5	1200	1091	144	30	P2:5-6:
3459	26	9	15	137	55	2	78	4	1140	1115	154	38	P2:6-8:
3328	31	10	18	176	39	3	91	4	1340	1127	213	30	P2:8-10:
3312	27	10	18	151	49	3	80	5	1330	1145	216	27	P2:10-12:
3254	20	13	17	110	39	3	84	4	1290	1167	185	31	P2:12-14:
3072	24	17	17	198	44	2	125	4	1380	1178	206	33	P2:14-17:
3033	23	18	16	122	54	3	154	5	1370	1188	198	31	P2:17-20:
2729	67	12	16	112	72	2	98	3	1230	1246	268	30	P2:20-24:
2673	21	16	15	93	47	3	172	5	1220	1167	133	35	P2:24-28:
2626	34	12	16	97	55	4	109	3	1170	1138	137	36	P2:28-32:
2652	28	12	15	96	68	4	92	4	1070	1121	143	32	P2:32-36:
2715	54	15	17	100	86	2	152	4	1190	1114	174	34	P2:36-40:
2899	85	16	19	104	100	2	141	4	1390	1111	194	39	P2:40-44:
2897	79	16	19	94	109	3	154	5	1190	1085	233	48	P2:44-46:
3155	89	19	17	96	126	6	262	5	1280	1035	254	45	P2:46-50:
3002	78	18	15	91	111	4	195	4	1070	1010	196	45	P2:50-55:
3049	114	17	16	87	120	8	195	4	1170	995	255	42	P2:55-60:
3208	80	14	15	95	106	5	156	5	890	1003	237	41	P2:60-65:
3032	100	15	16	89	99	6	154	5	1160	1002	230	38	P2:65-70:
3051	50	13	15	86	98	6	144	4	760	992	219	43	P2:70-75:
3223	80	11	15	94	100	10	193	5	950	958	291	37	P2:75-80:
3196	71	12	15	96	100	10	188	6	820	972	275	34	P2:80-85:
2865	48	14	14	92	88	8	157	5	820	1011	229	35	P2:85-90:
2610	57	13	15	83	72	7	116	3	1130	1012	189	38	P2:90-95:
2427	11	13	12	83	58	7	115	5	780	1051	167	20	P2:95-100:
2358	31	10	13	77	58	4	76	3	790	1031	159	35	P2:100-105:
2444	36	10	12	86	61	4	93	5	730	1011	181	29	P2:105-110:
2380	35	14	13	83	65	5	126	3	880	1027	159	31	P2:110-115:
2374	16	12	13	85	61	9	133	4	610	1015	185	40	P2:115-120:
2232	62	10	12	86	60	5	136	4	990	959	168	29	P2:120-125:
2293	36	9	13	83	68	6	88	NA	300	918	164	28	P2:125-130:
2300	114	11	15	89	72	5	78	3	650	878	181	23	P2:130-135:
2175	90	9	13	84	72	3	110	2	570	873	186	29	P2:135-140:
2097	26	11	12	73	58	8	74	3	200	904	161	23	P2:140-145:
1823	49	13	11	73	52	4	183	2	530	910	157	18	P2:145-150:
1801	58	14	10	79	54	9	161	2	340	907	161	26	P2:150-155:
1205	46	15	23	49	50	4	108	1	260	894	186	25	P2:155-163:

NA = NOT ANALYZED

CORE P2, SALT-AND-CARBONATE-FREE DATA, PPM

BA	BR	CO	CR	CU	I	MO	NI	RB	S	SR	ZN	ZR	NAME
9101	41	46	28	318	221	23	403	8	2581	1992	290	73	P2:0-1:
8955	73	44	30	325	229	13	239	9	2494	2203	253	73	P2:1-2:
8524	88	44	27	300	181	2	162	10	2434	2196	245	75	P2:2-3:
8558	91	25	30	243	165	2	124	9	2484	2310	267	72	P2:3-4:
8449	80	26	33	274	130	7	159	9	2789	2430	346	83	P2:4-5:
8687	75	30	38	220	127	10	179	13	2856	2596	343	72	P2:5-6:
8666	66	24	36	342	139	5	196	9	2856	2792	385	94	P2:6-8:
8687	81	27	46	459	102	8	237	10	3499	2943	556	78	P2:8-10:
8828	73	28	48	402	130	8	214	13	3544	3052	577	72	P2:10-12:
8908	53	37	46	302	108	9	229	11	3532	3194	505	85	P2:12-14:
8871	69	48	49	573	128	6	362	11	3985	3402	596	95	P2:14-17:
8687	66	51	47	348	155	9	440	13	3925	3403	566	89	P2:17-20:
8391	207	38	50	345	223	6	303	10	3784	3833	825	92	P2:20-24:
8077	62	47	47	282	141	9	518	14	3685	3526	401	107	P2:24-28:
7426	95	35	46	275	156	12	308	9	3307	3218	387	103	P2:28-32:
7414	79	32	42	269	190	12	257	12	2991	3133	400	91	P2:32-36:
7710	155	41	48	285	245	6	432	13	3378	3164	493	97	P2:36-40:
8018	236	43	53	288	277	6	389	11	3845	3073	537	107	P2:40-44:
7829	214	44	51	254	293	9	416	13	3216	2933	631	129	P2:44-46:
7654	215	46	40	232	307	15	634	12	3105	2510	616	110	P2:46-50:
7214	187	42	36	219	268	11	469	11	2571	2426	471	109	P2:50-55:
7041	264	39	38	202	276	20	450	10	2703	2298	589	98	P2:55-60:
7327	182	32	34	217	243	12	356	12	2033	2292	542	94	P2:60-65:
6901	227	33	36	203	226	14	351	12	2640	2280	524	86	P2:65-70:
6693	110	29	34	189	215	12	316	10	1667	2176	481	94	P2:70-75:
6776	168	23	31	198	209	20	407	11	1997	2015	612	79	P2:75-80:
6674	148	25	31	201	210	21	392	12	1712	2031	574	71	P2:80-85:
6308	106	31	32	203	194	17	346	11	1806	2226	505	77	P2:85-90:
6134	135	30	34	195	170	17	272	7	2656	2378	444	89	P2:90-95:
5990	28	32	30	205	142	16	283	13	1925	2594	413	48	P2:95-100:
5757	76	24	32	187	142	11	186	7	1929	2519	389	87	P2:100-105:
5442	80	22	28	191	135	10	208	11	1625	2250	403	65	P2:105-110:
5615	81	32	30	196	154	12	298	8	2076	2422	375	72	P2:110-115:
5311	35	27	29	191	136	20	297	8	1365	2270	414	90	P2:115-120:
4888	135	21	26	188	132	12	298	8	2168	2101	369	63	P2:120-125:
4622	72	18	26	166	138	11	177	NA	605	1850	331	56	P2:125-130:
4211	209	19	27	163	133	10	142	6	1190	1608	331	42	P2:130-135:
4110	170	16	24	159	137	6	209	4	1077	1651	352	54	P2:135-140:
3974	48	21	23	138	111	15	140	6	379	1714	305	44	P2:140-145:
3615	98	25	22	146	102	8	363	3	1051	1805	311	35	P2:145-150:
3566	114	28	20	157	107	17	318	4	673	1796	319	51	P2:150-155:
2379	90	30	45	97	99	9	213	2	513	1765	366	50	P2:155-163:

NA = NOT ANALYZED

CORE P2, SALT-FREE RATIOS TO ALUMINIUM (x10-4)

BA/AL	CO/AL	CR/AL	CU/AL	MO/AL	NI/AL	RB/AL	S/AL	SR/AL	ZN/AL	ZR/AL	NAME
3334.4	16.8	10.4	116.4	8.4	148.1	2.9	948.5	732.2	106.5	26.8	P2:0-1:
3064.0	15.0	10.2	111.1	4.5	82.1	3.2	855.1	755.3	86.7	24.9	P2:1-2:
3146.5	16.3	9.8	110.7	0.8	59.9	3.6	898.4	810.6	90.2	27.6	P2:2-3:
3260.3	9.5	11.4	92.7	0.9	47.3	3.3	950.0	883.4	102.1	27.7	P2:3-4:
3154.1	9.7	12.4	102.1	2.7	59.4	3.5	1042.7	908.5	129.4	31.0	P2:4-5:
3266.3	11.2	14.1	82.9	3.7	67.2	4.8	1071.4	973.9	128.7	27.0	P2:5-6:
3147.8	8.6	13.2	124.3	1.9	71.1	3.4	1036.4	1013.3	139.9	34.3	P2:6-8:
3023.5	9.3	16.0	159.6	2.8	82.5	3.4	1218.2	1024.6	193.6	27.1	P2:8-10:
2935.4	9.2	15.8	133.6	2.8	71.0	4.2	1177.0	1013.5	191.5	23.8	P2:10-12:
2959.5	12.3	15.2	100.4	2.8	76.1	3.8	1172.7	1060.6	167.8	28.3	P2:12-14:
2978.4	16.0	16.5	192.2	2.0	121.7	3.6	1339.8	1143.6	200.3	32.0	P2:14-17:
3006.5	17.5	16.3	120.5	3.1	152.0	4.6	1356.4	1176.1	195.6	30.9	P2:17-20:
3028.9	13.8	18.0	124.7	2.3	109.4	3.5	1366.7	1384.1	298.0	33.4	P2:20-24:
3066.8	17.9	17.7	107.2	3.6	197.2	5.3	1402.3	1341.6	152.7	40.6	P2:24-28:
3012.2	14.3	18.6	111.4	4.8	125.4	3.7	1344.8	1308.4	157.5	41.8	P2:28-32:
2948.9	12.8	16.8	107.1	4.7	102.0	4.6	1188.9	1245.6	159.2	36.0	P2:32-36:
2840.2	15.2	17.6	105.1	2.2	158.5	4.7	1239.6	1160.9	180.8	35.7	P2:36-40:
2806.5	15.2	18.6	100.8	2.0	136.5	4.0	1349.5	1078.5	188.4	37.5	P2:40-44:
2752.2	15.5	18.1	89.4	3.1	146.4	4.7	1133.3	1033.7	222.2	45.5	P2:44-46:
3088.9	18.6	16.3	93.8	6.2	256.4	4.8	1254.9	1014.4	248.8	44.4	P2:46-50:
3025.6	17.8	14.9	92.0	4.4	197.3	4.4	1080.8	1019.8	198.2	45.7	P2:50-55:
3099.2	17.2	16.7	88.7	8.6	199.0	4.5	1193.9	1015.2	260.1	43.2	P2:55-60:
3050.5	13.4	14.3	90.3	5.2	148.2	5.2	847.6	955.4	226.1	39.2	P2:60-65:
2984.8	14.4	15.6	87.6	6.2	151.4	5.3	1137.3	982.3	225.9	37.0	P2:65-70:
3113.6	13.5	15.8	87.9	5.6	147.1	4.4	775.5	1012.4	223.6	43.8	P2:70-75:
3201.9	10.6	14.9	93.8	9.6	191.5	5.2	940.6	948.8	288.4	37.1	P2:75-80:
3082.6	11.6	14.3	92.7	9.5	180.7	5.5	788.5	935.0	264.5	32.5	P2:80-85:
2993.9	14.8	15.1	96.4	8.0	163.6	5.4	854.2	1053.1	239.0	36.2	P2:85-90:
2961.6	14.3	16.6	94.4	8.3	131.4	3.6	1284.1	1149.8	214.6	42.9	P2:90-95:
2722.5	14.6	13.7	93.2	7.3	128.9	6.0	876.4	1181.1	188.1	22.0	P2:95-100:
2740.8	11.2	15.4	89.1	5.0	88.6	3.3	918.6	1199.3	185.1	41.3	P2:100-105:
2787.0	11.1	14.1	98.0	4.9	106.1	5.6	829.5	1148.6	205.4	33.2	P2:105-110:
2192.8	12.6	11.7	76.6	4.9	116.0	3.2	807.3	942.1	146.0	28.0	P2:110-115:
2793.9	14.1	15.1	100.2	10.3	156.0	4.2	717.6	1193.5	217.8	47.4	P2:115-120:
2889.5	12.3	15.2	111.3	6.8	176.4	4.9	1285.7	1246.0	218.5	37.1	P2:120-125:
2931.2	11.3	16.7	105.6	7.0	112.6	NA	384.6	1176.8	210.5	35.3	P2:125-130:
2736.3	12.5	17.5	106.0	6.2	92.4	4.1	773.8	1045.6	215.1	27.5	P2:130-135:
2798.1	11.0	16.5	108.1	4.1	141.5	3.0	730.8	1119.6	238.9	36.9	P2:135-140:
2794.7	14.7	16.0	97.0	10.3	98.7	4.1	266.7	1205.8	214.8	30.9	P2:140-145:
3149.6	21.8	19.1	127.0	7.3	315.3	2.8	913.8	1568.6	270.3	30.8	P2:145-150:
3084.0	24.1	17.7	135.6	14.8	277.0	3.7	586.2	1564.5	277.9	44.8	P2:150-155:
2348.9	29.8	44.7	95.7	8.5	211.9	2.1	509.8	1752.6	363.8	49.2	P2:155-163:

NA = NOT ANALYZED

CORE P6, UNCORRECTED DATA, PPM

BA	BR	CO	CR	CU	I	MO	NI	RB	S	SR	ZN	ZR	NAME
2726	90	22	18	93	126	28	234	6	2352	1077	170	28	P6:0-1:
2684	89	23	18	86	139	13	158	6	2237	1130	139	27	P6:1-2:
2600	95	21	17	84	123	7	131	6	2305	1137	132	30	P6:2-4:
2512	146	19	17	85	155	8	114	4	2263	1148	197	33	P6:4-6:
2532	89	19	18	89	94	5	112	7	2206	1167	134	22	P6:6-8:
2521	77	18	17	86	86	6	99	4	2026	1175	136	26	P6:8-10:
2442	80	15	16	91	84	6	78	5	2034	1181	130	25	P6:10-12:
2411	76	22	16	91	77	5	71	6	2082	1176	138	29	P6:12-14:
2306	76	12	18	74	73	4	69	8	1967	1132	168	31	P6:14-16:
2175	76	13	15	74	66	2	65	7	1976	1131	135	20	P6:16-18:
2287	82	16	18	82	65	4	66	5	2115	1148	133	25	P6:18-20:
2192	94	10	18	93	65	2	68	5	2317	1144	141	22	P6:20-25:
2206	90	9	19	90	65	4	73	6	2307	1146	110	24	P6:25-30:
2076	117	11	22	103	71	1	98	5	2577	1111	234	27	P6:30-35:
1867	121	14	26	148	92	2	114	6	2521	1093	228	26	P6:35-40:
1732	146	16	31	117	95	1	118	7	2717	1011	227	23	P6:40-45:
1794	131	16	28	102	99	2	116	6	2586	1049	184	21	P6:45-50:
1667	177	15	22	83	113	2	131	4	3284	1081	166	33	P6:50-55:
1645	201	14	23	73	178	3	202	6	2870	1114	169	27	P6:55-60:
1447	291	10	22	68	173	3	160	6	4416	1046	142	28	P6:60-65:
1584	242	9	22	70	181	5	137	6	3817	1099	154	23	P6:65-70:
1459	337	12	18	55	150	7	107	7	7051	1017	116	20	P6:70-75:
1772	219	9	20	61	179	5	120	7	4505	1085	139	19	P6:75-80:
1744	277	12	18	57	148	5	103	7	5086	999	142	24	P6:80-85:
1795	170	9	19	58	120	6	96	7	3571	1042	135	17	P6:85-90:
1546	226	10	16	44	111	9	80	6	4346	997	129	28	P6:90-95:
1849	159	9	20	57	118	7	112	8	3663	1041	148	26	P6:95-100:
1811	177	13	19	53	93	7	91	8	4377	1046	136	29	P6:100-105:
1754	141	10	18	51	78	11	80	7	3255	1067	112	23	P6:105-110:
1745	109	10	19	51	65	9	96	7	2830	1098	107	22	P6:110-115:
1622	157	10	17	50	69	10	86	6	3840	1063	109	27	P6:115-120:
1664	159	12	19	48	65	10	79	6	4119	1045	104	27	P6:120-125:
1763	99	11	19	55	61	8	84	8	2790	1082	110	18	P6:125-130:
1600	181	9	16	55	58	11	88	6	3768	1032	115	24	P6:130-135:
1569	219	10	17	53	72	9	90	5	3664	999	107	27	P6:135-140:
1768	189	12	18	57	76	12	121	5	2860	1050	108	28	P6:140-145:
1639	209	11	17	52	50	12	98	7	3482	1029	97	26	P6:145-150:
1573	175	10	15	51	47	8	92	5	3299	1046	90	22	P6:150-155:
1585	145	9	15	49	47	8	89	4	2348	1061	89	16	P6:155-163:

CORE P6, SALT-FREE DATA, PPM

BA	BR	CO	CR	CU	I	MO	NI	RB	S	SR	ZN	ZR	NAME
2806	37	23	19	95	130	29	241	7	1640	1102	175	29	P6:0-1:
2752	43	24	19	88	143	13	162	6	1680	1153	143	28	P6:1-2:
2682	38	22	18	87	127	7	135	6	1640	1166	136	31	P6:2-4:
2607	80	20	18	88	161	8	118	4	1410	1184	204	34	P6:4-6:
2629	19	20	19	92	98	5	116	7	1340	1203	139	23	P6:6-8:
2575	38	18	18	88	88	6	101	5	1530	1195	139	27	P6:8-10:
2500	37	15	17	93	86	6	80	5	1480	1204	133	26	P6:10-12:
2475	27	23	17	93	79	5	73	6	1450	1201	142	30	P6:12-14:
2364	30	12	18	76	75	4	71	8	1370	1155	172	32	P6:14-16:
2230	30	13	16	76	68	2	67	7	1400	1154	138	21	P6:16-18:
2361	24	17	18	85	67	4	68	6	1400	1178	137	26	P6:18-20:
2284	18	10	19	97	68	2	70	5	1330	1183	147	23	P6:20-25:
2284	25	9	20	93	67	4	76	6	1430	1179	114	25	P6:25-30:
2176	31	12	23	108	74	1	102	5	1560	1154	245	28	P6:30-35:
1945	46	15	28	154	96	2	119	6	1530	1129	238	27	P6:35-40:
1837	40	17	33	124	101	1	125	7	1300	1059	241	24	P6:40-45:
1885	42	17	30	107	104	2	122	6	1370	1090	193	22	P6:45-50:
1782	58	16	24	89	121	2	140	4	1680	1140	177	35	P6:50-55:
1726	118	15	24	76	187	3	212	7	1720	1158	177	28	P6:55-60:
1579	145	11	24	74	189	3	174	6	2330	1120	155	31	P6:60-65:
1669	154	9	23	73	191	5	144	7	2515	1145	162	24	P6:65-70:
1653	129	14	21	63	170	8	121	8	4180	1122	131	23	P6:70-75:
1847	148	9	21	64	187	5	125	7	3480	1121	145	20	P6:75-80:
1861	168	13	19	61	158	5	110	8	3560	1051	152	26	P6:80-85:
1869	99	9	20	60	125	6	99	7	2605	1075	141	18	P6:85-90:
1683	77	11	17	48	121	10	88	6	2300	1066	140	30	P6:90-95:
1925	88	9	20	59	123	7	116	8	2670	1074	154	27	P6:95-100:
1925	69	14	20	56	99	7	97	8	2940	1097	145	31	P6:100-105:
1850	45	11	19	54	82	12	85	8	2020	1113	118	24	P6:105-110:
1805	47	10	20	52	67	9	99	7	2060	1128	111	23	P6:110-115:
1733	38	11	18	53	74	11	92	6	2390	1120	116	29	P6:115-120:
1762	56	13	20	51	69	11	84	7	2860	1093	110	29	P6:120-125:
1815	46	11	19	57	63	8	86	8	2130	1107	113	19	P6:125-130:
1705	69	10	17	59	62	12	94	6	2380	1085	123	26	P6:130-135:
1682	98	11	18	57	77	10	97	6	2130	1055	115	29	P6:135-140:
1834	126	12	18	59	79	12	126	6	2050	1080	112	29	P6:140-145:
1760	84	12	18	56	54	13	105	8	1910	1088	104	28	P6:145-150:
1676	62	11	16	54	50	9	98	5	1890	1100	96	23	P6:150-155:
1639	85	9	15	51	49	8	92	5	1590	1089	92	17	P6:155-163:

CORE P6, SALT-AND-CARBONATE-FREE DATA, PPM

BA	BR	CO	CR	CU	I	MO	NI	RB	S	SR	ZN	ZR	NAME
8614	113	70	58	293	398	88	739	20	5034	3382	537	88	P6:0-1:
8862	138	76	60	283	459	43	522	20	5409	3712	459	89	P6:1-2:
9302	132	75	61	302	440	25	469	21	5687	4043	472	107	P6:2-4:
9166	282	69	62	309	566	29	417	14	4959	4164	719	120	P6:4-6:
9609	70	72	68	337	357	19	424	26	4897	4397	509	84	P6:6-8:
9393	140	67	65	320	320	22	368	17	5581	4360	507	97	P6:8-10:
9619	141	59	64	359	331	24	306	18	5695	4632	512	99	P6:10-12:
9570	105	87	65	360	306	20	281	25	5606	4645	548	115	P6:12-14:
9508	122	49	73	304	301	16	284	31	5510	4644	693	128	P6:14-16:
8916	119	53	62	303	271	8	266	27	5597	4613	553	82	P6:16-18:
10135	101	71	78	364	288	18	294	24	6011	5056	589	111	P6:18-20:
8705	68	40	71	369	258	8	269	18	5069	4507	560	87	P6:20-25:
9611	107	39	84	392	283	17	319	25	6017	4960	479	105	P6:25-30:
8681	125	46	91	432	297	4	409	19	6224	4602	978	113	P6:30-35:
7261	172	54	103	575	358	8	443	24	5712	4216	887	101	P6:35-40:
6091	131	56	110	411	334	4	414	24	4310	3510	798	81	P6:40-45:
6674	149	60	105	378	368	7	432	21	4852	3861	684	78	P6:45-50:
7231	236	65	96	361	490	9	569	17	6818	4626	720	143	P6:50-55:
6968	475	59	96	308	754	13	855	27	6945	4674	716	114	P6:55-60:
6211	570	43	96	292	742	13	686	25	9168	4408	609	120	P6:60-65:
6897	635	39	95	303	788	22	595	27	10396	4735	671	100	P6:65-70:
6372	496	52	80	242	655	31	466	31	16115	4327	507	87	P6:70-75:
7466	596	38	86	258	754	21	506	28	14066	4533	586	80	P6:75-80:
6832	616	47	70	224	580	20	405	29	13070	3858	556	94	P6:80-85:
6768	359	34	73	218	452	23	360	26	9434	3895	509	64	P6:85-90:
5940	271	38	60	171	427	35	309	22	8117	3760	496	108	P6:90-95:
6687	305	33	71	205	427	25	404	28	9275	3732	535	94	P6:95-100:
6878	246	49	71	202	353	27	346	29	10505	3921	516	110	P6:100-105:
6683	161	38	70	194	297	42	306	27	7296	4020	427	88	P6:105-110:
6551	170	38	72	190	244	34	359	25	7474	4093	402	83	P6:110-115:
6681	146	41	70	206	284	41	356	23	9214	4318	449	111	P6:115-120:
6452	205	47	74	188	252	39	306	25	10471	4003	403	105	P6:120-125:
6720	169	42	71	209	233	31	319	29	7885	4099	419	69	P6:125-130:
6265	252	35	61	216	227	43	345	22	8746	3986	450	94	P6:130-135:
5800	336	37	62	195	266	33	333	20	7342	3636	395	100	P6:135-140:
5649	388	38	57	183	243	38	387	17	6316	3328	345	89	P6:140-145:
6162	294	41	63	196	188	45	367	28	6687	3810	365	98	P6:145-150:
6037	223	38	58	196	180	31	352	18	6808	3961	345	84	P6:150-155:
5703	296	32	53	177	169	29	321	16	5533	3791	320	58	P6:155-163:

CORE P6, SALT-FREE RATIOS TO ALUMINIUM (X10-4)

BA/AL	CO/AL	CR/AL	CU/AL	MO/AL	NI/AL	RB/AL	S/AL	SR/AL	ZN/AL	ZR/AL	NAME
1810.6	14.6	12.1	61.5	18.6	155.4	4.3	1058.1	711.0	112.9	18.6	P6:0-1:
1787.3	15.3	12.1	57.0	8.7	105.4	4.1	1090.9	748.6	92.6	18.0	P6:1-2:
1812.3	14.6	11.9	58.8	4.9	91.4	4.2	1108.1	787.6	92.0	20.9	P6:2-4:
1785.3	13.5	12.2	60.1	5.7	81.1	2.8	965.8	810.3	140.0	23.5	P6:4-6:
1838.7	13.8	13.0	64.4	3.6	81.2	4.9	937.1	841.4	97.3	16.0	P6:6-8:
1813.3	12.9	12.5	61.8	4.3	71.0	3.2	1077.5	841.6	97.8	18.7	P6:8-10:
1865.5	11.5	12.3	69.6	4.6	59.3	3.5	1104.5	898.3	99.3	19.1	P6:10-12:
1833.5	16.7	12.4	69.0	3.8	53.8	4.7	1074.1	889.9	105.0	22.1	P6:12-14:
1791.0	9.3	13.8	57.3	3.1	53.4	5.8	1037.9	874.7	130.5	24.1	P6:14-16:
1813.2	10.8	12.7	61.7	1.7	54.1	5.5	1138.2	938.2	112.5	16.7	P6:16-18:
1710.7	12.0	13.2	61.5	3.0	49.6	4.0	1014.5	853.3	99.5	18.7	P6:18-20:
1812.8	8.3	14.8	76.8	1.7	55.9	3.8	1055.6	938.6	116.6	18.2	P6:20-25:
1935.7	7.9	17.0	78.9	3.5	64.2	5.0	1211.9	998.9	96.5	21.1	P6:25-30:
2033.5	10.8	21.3	101.3	1.0	95.8	4.5	1457.9	1078.0	229.2	26.4	P6:30-35:
1984.9	14.9	28.1	157.1	2.1	121.1	6.5	1561.2	1152.5	242.4	27.6	P6:35-40:
1954.3	18.1	35.2	132.0	1.1	132.9	7.8	1383.0	1126.1	256.1	25.9	P6:40-45:
1847.6	16.5	29.1	104.8	2.1	119.6	5.8	1343.1	1069.0	189.5	21.6	P6:45-50:
1665.1	15.0	22.0	83.2	2.0	131.1	3.9	1570.1	1065.3	165.8	33.0	P6:50-55:
1612.7	13.7	22.2	71.4	2.9	198.0	6.2	1607.5	1081.8	165.7	26.5	P6:55-60:
1475.3	10.2	22.8	69.4	3.1	163.0	6.0	2177.6	1047.0	144.7	28.5	P6:60-65:
1516.9	8.6	20.9	66.7	4.8	130.8	6.0	2286.4	1041.3	147.5	22.0	P6:65-70:
1574.2	13.0	19.8	59.8	7.6	115.1	7.6	3981.0	1068.8	125.2	21.6	P6:70-75:
1620.3	8.2	18.7	56.0	4.6	109.8	6.1	3052.6	983.7	127.1	17.4	P6:75-80:
1618.1	11.1	16.6	53.1	4.6	96.0	6.9	3095.7	913.8	131.8	22.3	P6:80-85:
1611.1	8.1	17.4	51.9	5.4	85.8	6.1	2245.7	927.0	121.1	15.3	P6:85-90:
1357.4	8.8	13.6	39.0	7.9	70.6	5.0	1854.8	859.3	113.3	24.6	P6:90-95:
1492.2	7.3	15.7	45.7	5.7	90.3	6.2	2069.8	832.8	119.4	21.0	P6:95-100:
1458.2	10.5	15.1	42.8	5.6	73.4	6.1	2227.3	831.3	109.5	23.3	P6:100-105:
1391.3	7.9	14.5	40.4	8.7	63.7	5.7	1518.8	836.8	88.8	18.2	P6:105-110:
1444.4	8.3	15.8	41.9	7.4	79.1	5.4	1648.0	902.5	88.6	18.2	P6:110-115:
1364.5	8.4	14.3	42.0	8.4	72.7	4.7	1881.9	881.9	91.7	22.7	P6:115-120:
1267.7	9.1	14.6	36.9	7.6	60.1	4.9	2057.6	786.6	79.2	20.6	P6:120-125:
1407.2	8.8	14.9	43.8	6.4	66.8	6.2	1651.2	858.4	87.8	14.4	P6:125-130:
1408.9	7.9	13.7	48.5	9.7	77.7	4.9	1966.9	896.4	101.2	21.1	P6:130-135:
1438.0	9.2	15.3	48.4	8.2	82.7	4.9	1820.5	901.5	98.1	24.7	P6:135-140:
1622.6	11.0	16.3	52.5	11.0	111.3	5.0	1814.2	956.0	99.1	25.7	P6:140-145:
1600.0	10.7	16.3	51.0	11.7	95.4	7.3	1736.4	989.3	94.7	25.4	P6:145-150:
1596.1	10.2	15.4	51.8	8.1	93.0	4.8	1800.0	1047.3	91.3	22.3	P6:150-155:
1655.3	9.4	15.3	51.5	8.4	93.1	4.6	1606.1	1100.4	93.0	16.7	P6:155-163:

CORE P8, UNCORRECTED DATA, PPM

BA	BR	CO	CR	CU	I	MO	NI	RB	S	SR	ZN	ZR	NAME
2499	212	38	123	113	408	11	151	28	1125	180	305	56	P8:0-4:
2546	204	32	124	117	444	1	155	30	955	180	315	75	P8:4-5.5:
2493	188	32	126	123	317	1	169	32	993	178	327	74	P8:5.5-7:
2590	155	29	130	136	270	1	182	32	943	183	342	79	P8:7-8.5:
2622	150	32	133	139	254	1	199	33	914	195	358	81	P8:8.5-10:
2649	154	29	126	129	236	1	193	34	999	205	333	85	P8:10-12:
2690	151	31	127	130	240	1	209	33	995	214	351	75	P8:12-14:
2586	144	40	133	121	217	1	262	34	1093	207	364	71	P8:14-16:
2517	152	37	133	121	211	2	250	35	1055	207	349	81	P8:16-18:
2412	141	38	139	123	211	1	225	35	971	204	341	88	P8:18-21:
2447	152	28	135	118	213	2	186	34	1081	197	331	75	P8:21-24:
2313	187	35	132	119	261	1	183	34	1197	201	312	67	P8:24-28:
2231	174	37	138	118	232	2	199	35	1231	216	320	72	P8:28-32:
2284	202	33	130	114	233	3	185	34	1699	211	308	76	P8:32-36:
2343	173	34	132	116	231	4	176	34	1508	222	300	70	P8:36-40:
2168	207	41	131	111	181	6	171	35	2295	213	283	68	P8:40-45:
2184	269	41	138	118	132	5	195	36	3156	183	274	73	P8:45-50:
2206	287	38	128	114	107	5	160	34	3216	182	272	61	P8:50-55:
2428	178	35	136	122	127	4	148	36	2394	209	299	70	P8:55-60:
2364	242	34	133	118	101	5	172	37	3147	188	298	67	P8:60-65:
2244	229	33	133	116	104	9	162	37	3221	183	289	60	P8:65-70:
2003	263	32	125	105	118	8	143	36	3462	193	264	71	P8:70-75:
2202	236	31	131	111	103	5	146	38	2953	178	289	68	P8:75-80:
2193	215	31	132	113	94	9	161	38	3408	187	286	61	P8:80-85:
2146	261	32	127	111	103	6	161	40	2750	180	278	67	P8:85-90:
2113	233	39	124	118	87	10	177	40	2928	183	287	74	P8:90-95:
2191	185	44	130	123	83	8	161	38	3307	189	292	63	P8:95-100:
2126	236	34	124	121	89	6	158	38	3465	188	287	61	P8:100-105:
1944	253	35	128	111	95	7	233	37	3412	182	261	65	P8:105-110:
1812	241	35	118	105	74	7	174	33	3774	179	256	67	P8:110-115:
2032	156	42	127	116	51	4	157	35	2274	164	281	67	P8:115-120:
1985	200	33	123	112	71	5	155	34	2748	171	273	68	P8:120-125:
1798	236	35	127	102	82	5	156	36	3793	170	236	57	P8:125-130:
1871	239	37	129	108	71	7	160	36	3139	166	233	68	P8:130-135:
2034	242	44	132	121	92	11	185	35	3073	162	252	67	P8:135-140:
1835	266	36	117	111	83	12	148	33	3810	173	228	50	P8:140-145:
1956	207	37	126	109	58	7	137	36	2858	165	236	47	P8:145-150:
1888	215	32	120	110	56	6	159	33	2649	209	249	54	P8:150-155:
2161	194	39	122	119	81	8	166	34	1769	231	275	51	P8:155-160:
2245	231	46	108	116	50	6	263	40	1907	243	272	75	P8:160-165:
2309	174	55	75	95	28	7	310	53	2757	323	228	125	P8:165-170:
2878	161	54	123	114	83	5	272	34	1718	288	277	58	P8:170-175:
2372	145	58	115	215	46	10	277	39	1866	245	341	79	P8:175-183:

CORE P8, SALT-FREE DATA, PPM

BA	BR	CO	CR	CU	I	MO	NI	RB	S	SR	ZN	ZR	NAME
2572	162	39	127	116	420	11	155	29	400	179	314	58	P8:0-4:
2597	170	33	127	119	453	1	158	31	520	179	321	76	P8:4-5.5:
2540	156	33	129	125	323	1	172	32	590	177	333	76	P8:5.5-7:
2633	126	29	132	138	275	1	185	32	580	182	348	80	P8:7-8.5:
2668	120	33	135	142	258	1	203	34	540	194	364	82	P8:8.5-10:
2702	119	30	128	131	241	1	197	34	560	205	340	87	P8:10-12:
2743	116	32	130	133	245	1	213	33	590	214	358	77	P8:12-14:
2638	108	41	135	124	221	1	267	34	670	207	371	72	P8:14-16:
2576	111	38	136	123	216	2	256	36	550	207	357	83	P8:16-18:
2450	113	39	141	125	214	1	229	36	610	204	346	90	P8:18-21:
2498	115	29	138	120	218	2	190	35	600	196	338	76	P8:21-24:
2377	140	36	136	122	268	1	188	35	560	200	321	69	P8:24-28:
2284	133	38	142	121	237	2	204	35	700	216	328	74	P8:28-32:
2380	130	34	136	119	243	3	192	35	800	210	321	79	P8:32-36:
2417	119	35	136	119	238	4	182	35	820	222	309	72	P8:36-40:
2279	120	43	138	117	190	6	180	37	1170	212	298	71	P8:40-45:
2244	224	42	142	121	136	5	200	37	2550	182	281	75	P8:45-50:
2333	194	40	135	120	113	5	170	36	1990	179	288	64	P8:50-55:
2503	125	36	140	126	131	4	152	37	1720	208	308	73	P8:55-60:
2467	170	35	138	123	105	5	180	39	2210	186	311	70	P8:60-65:
2324	169	34	138	120	108	9	168	38	2450	181	299	62	P8:65-70:
2121	166	34	132	111	125	8	152	38	2210	191	280	75	P8:70-75:
2293	168	32	136	115	107	5	152	39	2070	176	301	71	P8:75-80:
2280	148	32	137	117	98	9	167	40	2570	185	297	63	P8:80-85:
2282	157	34	135	118	110	6	172	42	1400	177	296	72	P8:85-90:
2216	152	41	130	124	91	10	185	42	1890	181	301	78	P8:90-95:
2303	97	46	136	129	87	8	170	40	2220	187	307	66	P8:95-100:
2250	138	36	132	128	94	6	168	41	2250	186	304	65	P8:100-105:
2062	153	37	136	118	101	7	247	40	2130	179	277	69	P8:105-110:
1972	95	38	129	114	81	8	189	36	1960	175	279	73	P8:110-115:
2097	101	43	131	120	53	4	162	36	1570	162	290	69	P8:115-120:
2065	132	34	128	116	74	5	161	35	1890	169	284	71	P8:120-125:
1882	159	37	133	107	86	5	163	38	2850	167	247	60	P8:125-130:
1965	155	39	136	113	75	7	169	38	2100	163	245	72	P8:130-135:
2114	177	46	138	126	96	11	192	37	2470	159	262	70	P8:135-140:
2018	103	40	129	122	91	13	162	37	1870	168	251	55	P8:140-145:
2060	117	39	132	115	61	7	145	38	1780	162	249	50	P8:145-150:
1991	123	34	127	116	59	6	168	35	1540	208	263	57	P8:150-155:
2238	133	40	126	123	84	8	172	36	1010	231	285	52	P8:155-160:
2388	125	49	115	123	53	6	279	42	580	244	289	80	P8:160-165:
2495	35	59	81	103	30	8	335	57	1180	331	246	135	P8:165-170:
2970	105	56	127	118	86	5	281	35	1060	290	286	59	P8:170-175:
2465	76	60	119	223	48	10	288	41	1060	246	354	82	P8:175-183:

CORE P8, SALT-FREE RATIOS TO ALUMINIUM (x10-4)

BA/AL	CO/AL	CR/AL	CU/AL	MO/AL	NI/AL	RB/AL	S/AL	SR/AL	ZN/AL	ZR/AL	NAME
328.8	5.0	16.2	14.9	1.4	19.8	3.7	51.2	22.8	40.1	7.4	P8:0-4:
335.8	4.2	16.4	15.5	0.1	20.5	4.0	67.3	23.2	41.6	9.8	P8:4-5.5:
326.2	4.2	16.5	16.1	0.1	22.2	4.1	75.8	22.7	42.8	9.7	P8:5.5-7:
339.0	3.8	17.0	17.8	0.1	23.8	4.2	74.6	23.5	44.8	10.3	P8:7-8.5:
343.3	4.2	17.4	18.2	0.1	26.1	4.3	69.5	25.0	46.9	10.6	P8:8.5-10:
352.7	3.9	16.8	17.1	0.1	25.8	4.5	73.1	26.7	44.3	11.4	P8:10-12:
358.1	4.1	16.9	17.4	0.1	27.8	4.4	77.0	27.9	46.7	10.0	P8:12-14:
347.6	5.4	17.8	16.3	0.1	35.2	4.5	88.3	27.2	48.9	9.5	P8:14-16:
340.1	5.0	18.0	16.3	0.3	33.8	4.7	72.7	27.3	47.2	10.9	P8:16-18:
315.7	5.0	18.2	16.1	0.1	29.5	4.6	78.6	26.2	44.6	11.6	P8:18-21:
321.5	3.7	17.7	15.5	0.3	24.4	4.5	77.2	25.3	43.5	9.8	P8:21-24:
312.6	4.7	17.8	16.0	0.1	24.7	4.6	73.7	26.3	42.2	9.1	P8:24-28:
297.1	4.9	18.4	15.7	0.3	26.5	4.6	91.0	28.1	42.6	9.6	P8:28-32:
309.5	4.5	17.6	15.5	0.4	25.0	4.6	104.0	27.3	41.7	10.3	P8:32-36:
323.2	4.7	18.2	15.9	0.6	24.3	4.7	109.6	29.7	41.4	9.7	P8:36-40:
300.6	5.7	18.2	15.4	0.8	23.7	4.9	154.4	28.0	39.3	9.4	P8:40-45:
279.7	5.2	17.7	15.1	0.6	24.9	4.6	318.0	22.7	35.1	9.3	P8:45-50:
300.6	5.2	17.4	15.5	0.7	21.8	4.7	256.4	23.1	37.1	8.3	P8:50-55:
324.1	4.7	18.2	16.3	0.5	19.7	4.8	222.8	27.0	39.9	9.4	P8:55-60:
326.0	4.7	18.3	16.2	0.7	23.7	5.1	292.0	24.6	41.1	9.3	P8:60-65:
302.0	4.4	17.9	15.6	1.2	21.8	5.0	318.2	23.6	38.9	8.0	P8:65-70:
281.8	4.5	17.6	14.7	1.1	20.2	5.0	293.5	25.4	37.1	10.0	P8:70-75:
298.8	4.2	17.7	15.0	0.7	19.8	5.1	269.9	22.9	39.2	9.2	P8:75-80:
297.9	4.2	17.9	15.3	1.2	21.8	5.2	336.0	24.2	38.9	8.2	P8:80-85:
298.4	4.5	17.7	15.5	0.8	22.5	5.5	183.0	23.2	38.7	9.4	P8:85-90:
284.4	5.2	16.6	15.9	1.3	23.8	5.4	242.6	23.2	38.6	10.0	P8:90-95:
279.5	5.6	16.5	15.7	1.0	20.6	4.8	269.4	22.7	37.2	8.0	P8:95-100:
290.0	4.6	16.9	16.5	0.8	21.6	5.2	289.9	23.9	39.2	8.3	P8:100-105:
272.7	4.9	18.0	15.6	1.0	32.7	5.2	281.7	23.7	36.6	9.1	P8:105-110:
260.0	5.0	16.9	15.1	1.0	24.9	4.7	258.6	23.0	36.7	9.6	P8:110-115:
262.6	5.4	16.4	15.0	0.5	20.3	4.5	196.5	20.3	36.3	8.7	P8:115-120:
261.6	4.3	16.2	14.7	0.7	20.4	4.5	239.5	21.4	36.0	8.9	P8:120-125:
241.1	4.7	17.0	13.7	0.7	20.9	4.8	364.9	21.4	31.6	7.6	P8:125-130:
254.5	5.0	17.6	14.7	1.0	21.8	4.9	272.0	21.1	31.7	9.3	P8:130-135:
274.1	5.9	17.9	16.3	1.5	24.9	4.7	320.4	20.7	34.0	9.1	P8:135-140:
267.5	5.2	17.1	16.1	1.7	21.5	4.9	248.0	22.2	33.2	7.4	P8:140-145:
275.1	5.2	17.7	15.4	1.0	19.3	5.0	237.7	21.6	33.2	6.6	P8:145-150:
276.0	4.7	17.6	16.0	0.9	23.2	4.9	213.6	28.8	36.4	8.0	P8:150-155:
312.7	5.6	17.6	17.2	1.2	24.0	5.0	141.0	32.3	39.8	7.3	P8:155-160:
329.2	6.7	15.8	17.0	0.9	38.5	5.8	80.0	33.6	39.9	11.0	P8:160-165:
342.1	8.1	11.0	14.1	1.0	45.9	7.8	161.8	45.3	33.8	18.5	P8:165-170:
434.7	8.2	18.6	17.3	0.8	41.2	5.2	155.2	42.4	41.8	8.7	P8:170-175:
442.5	10.8	21.4	40.1	1.9	51.7	7.3	190.3	44.1	63.6	14.8	P8:175-183:

PLEIADES BOX CORE, UNCORRECTED DATA, PPM

BA	BR	CO	CR	CU	I	MO	NI	S	SR	ZN	ZR	NAME
2350	76	15	20	103	140	73	307	2460	1087	270	27	PL:2:
2150	88	11	16	92	157	22	213	2220	1107	204	28	PL:4:
2020	115	9	16	89	146	13	167	2510	1130	172	27	PL:6:
1970	101	10	15	86	141	11	171	2360	1131	185	24	PL:8:
2110	89	11	17	96	125	9	194	2430	1159	201	27	PL:10:
2030	103	12	16	94	114	8	155	2420	1166	194	24	PL:12:
2020	89	13	15	95	114	8	152	2310	1169	190	20	PL:14:
1860	83	6	16	79	104	6	81	2230	1149	196	26	PL:16:
1840	91	5	16	79	95	5	83	2240	1144	197	28	PL:18:
1750	101	5	16	83	87	4	96	2370	1138	233	21	PL:20:
1770	91	6	19	94	78	5	111	2380	1159	272	22	PL:24:
1760	101	7	18	81	78	3	116	2390	1160	275	30	PL:28:
1720	87	6	18	89	89	6	113	2160	1155	245	23	PL:32:
1720	87	6	20	112	83	4	131	2320	1154	252	24	PL:36:
1690	92	7	20	101	101	2	121	2390	1161	322	21	PL:40:

PLEIADES BOX CORE, SALT-FREE DATA, PPM

BA	BR	CO	CR	CU	I	MO	NI	S	SR	ZN	ZR	NAME
2434	11	16	21	107	145	76	318	1600	1118	280	28	PL:2:
2223	26	11	17	95	162	23	220	1400	1137	211	29	PL:4:
2119	27	10	17	93	153	14	175	1340	1174	180	28	PL:6:
2040	37	10	16	89	146	11	177	1510	1163	192	25	PL:8:
2186	24	11	18	99	129	9	201	1570	1192	208	28	PL:10:
2115	27	12	17	98	119	8	162	1410	1206	202	25	PL:12:
2088	28	13	16	98	118	8	157	1500	1201	196	21	PL:14:
1911	33	6	16	81	107	6	83	1560	1174	201	27	PL:16:
1907	25	5	17	82	98	5	86	1370	1177	204	29	PL:18:
1817	32	5	17	86	90	4	100	1450	1173	242	22	PL:20:
1839	21	6	20	98	81	5	115	1450	1195	283	23	PL:24:
1825	34	7	19	84	81	3	120	1500	1195	285	31	PL:28:
1783	21	6	19	92	92	6	117	1280	1189	254	24	PL:32:
1777	27	7	21	116	86	4	135	1520	1185	260	25	PL:36:
1748	30	8	21	104	104	2	125	1560	1193	333	22	PL:40:

PLEIADES BOX CORE, SALT-AND-CARBONATE-FREE DATA, PPM

BA	BR	CO	CR	CU	I	MO	NI	S	SR	ZN	ZR	NAME
6491	28	42	55	285	387	202	848	4267	2981	746	75	PL:2:
6443	76	32	48	276	471	66	638	4058	3295	611	84	PL:4:
6631	86	31	53	292	479	43	548	4193	3675	565	89	PL:6:
6578	120	32	50	287	471	37	571	4870	3751	618	80	PL:8:
6915	76	34	56	315	410	29	636	4967	3773	659	88	PL:10:
6822	88	40	54	316	383	27	521	4547	3888	652	81	PL:12:
7088	95	44	53	333	400	28	533	5092	4076	667	70	PL:14:
6965	120	21	60	296	389	22	303	5686	4280	734	97	PL:16:
6729	90	19	59	289	347	18	304	4835	4154	720	102	PL:18:
6486	115	19	59	308	322	15	356	5176	4187	864	78	PL:20:
7561	86	26	81	402	333	21	474	5963	4915	1162	94	PL:24:
6425	120	24	66	296	285	11	423	5280	4205	1004	110	PL:28:
6353	75	22	67	329	329	22	417	4561	4236	905	85	PL:32:
6677	101	25	78	435	322	16	509	5711	4451	978	93	PL:36:
6606	112	29	78	395	395	8	473	5895	4509	1259	82	PL:40:

PLEIADES BOX CORE, SALT-FREE RATIOS TO ALUMINIUM (X10-4)

BA/AL	CO/AL	CR/AL	CU/AL	MO/AL	NI/AL	S/AL	SR/AL	ZN/AL	ZR/AL	NAME
1475.3	9.5	12.6	64.7	45.8	192.7	969.7	677.5	169.5	17.0	PL:2:
1416.1	7.1	10.5	60.6	14.5	140.3	891.7	724.2	134.4	18.4	PL:4:
1349.8	6.2	10.7	59.5	8.7	111.6	853.5	748.0	114.9	18.0	PL:6:
1387.6	6.7	10.6	60.6	7.7	120.4	1027.2	791.2	130.3	16.9	PL:8:
1316.6	6.6	10.6	59.9	5.6	121.1	945.8	718.3	125.4	16.8	PL:10:
1391.8	8.1	11.0	64.4	5.5	106.3	927.6	793.1	133.0	16.5	PL:12:
1382.8	8.6	10.3	65.0	5.5	104.1	993.4	795.2	130.1	13.7	PL:14:
1318.0	4.0	11.3	56.0	4.2	57.4	1075.9	809.9	138.9	18.4	PL:16:
1361.9	3.8	11.8	58.5	3.7	61.4	978.6	840.9	145.8	20.7	PL:18:
1376.4	4.1	12.6	65.3	3.1	75.5	1098.5	888.5	183.2	16.5	PL:20:
1470.9	5.1	15.8	78.1	4.2	92.2	1160.0	956.1	226.0	18.3	PL:24:
1521.2	5.8	15.6	70.0	2.6	100.3	1250.0	995.6	237.7	25.9	PL:28:
1498.0	5.2	15.7	77.5	5.2	98.4	1075.6	999.0	213.4	20.0	PL:32:
1518.7	5.7	17.7	98.9	3.5	115.7	1299.1	1012.5	222.5	21.2	PL:36:
1469.1	6.3	17.4	87.8	1.7	105.2	1310.9	1002.7	279.9	18.3	PL:40:

HALOGEN/ORGANIC CARBON RATIOS($\times 10^{-4}$)

SURFACE SEDIMENTS

I/C_{org}	Br/C_{org}	Sample
128	32	P1:0-2:
156	31	P2:0-1:
479	94	P5:0-1.5:
158	22	PL:2:
167	49	P6:0-1:
360	84	P7:0-2:
167	66	P8:0-4:
388	144	P9:0-2:
325	102	P10:0-2:
337	113	P11:0-3:
313	118	P12:0-1.5:
408	145	P13:0-2:

CORE P1

I/C_{org}	Br/C_{org}	Sample
128	31	P1:0-2:
116	61	P1:2-4:
113	68	P1:4-6:
108	71	P1:6-8:
111	66	P1:8-10:
138	81	P1:10-12:
98	38	P1:12-14:
95	52	P1:14-16:
49	41	P1:16-18:
53	23	P1:18-20:
70	48	P1:20-22:
69	19	P1:22-26:
110	26	P1:26-30:
104	92	P1:30-34:
91	72	P1:34-36:
86	73	P1:36-40:
73	81	P1:40-45:
77	89	P1:45-50:
86	92	P1:50-55:
82	57	P1:55-60:
90	33	P1:60-65:
80	43	P1:65-70:
79	33	P1:70-75:
75	47	P1:75-80:
70	42	P1:80-85:
88	61	P1:85-90:
67	88	P1:90-95:
83	107	P1:95-100:
74	75	P1:100-105:
87	83	P1:105-110:
63	104	P1:110-115:
63	145	P1:115-120:
68	102	P1:120-125:
60	71	P1:125-130:
59	75	P1:130-135:
56	61	P1:135-140:
44	42	P1:140-145:
74	60	P1:145-150:

CORE P2

I/C_{org}	Br/C_{org}	Sample
156	30	P2:0-1:
151	47	P2:1-2:
125	61	P2:2-3:
120	67	P2:3-4:
97	59	P2:4-5:
96	56	P2:5-6:
91	43	P2:6-8:
70	54	P2:8-10:
87	48	P2:10-12:
70	35	P2:12-14:
83	44	P2:14-17:
100	44	P2:17-20:
135	116	P2:20-24:
80	30	P2:24-28:
80	49	P2:28-32:
96	33	P2:32-36:
100	50	P2:36-40:
94	79	P2:40-44:
91	67	P2:44-46:
99	71	P2:46-50:
95	67	P2:50-55:
96	92	P2:55-60:
91	69	P2:60-65:
88	88	P2:65-70:
87	45	P2:70-75:
97	78	P2:75-80:
87	62	P2:80-85:
98	53	P2:85-90:
89	70	P2:90-95:
82	16	P2:95-100:
98	53	P2:100-105:
87	52	P2:105-110:
92	47	P2:110-115:
94	25	P2:115-120:
91	93	P2:120-125:
90	46	P2:125-130:
98	154	P2:130-135:
88	110	P2:135-140:
84	37	P2:140-145:
89	84	P2:145-150:
84	91	P2:150-155:
72	71	P2:155-163:

CORE P6

I/C_{org}	Br/C_{org}	Sample
167	47	P6:0-1:
188	57	P6:1-2:
181	54	P6:2-4:
235	118	P6:4-6:
150	29	P6:6-8:
148	64	P6:8-10:
125	54	P6:10-12:
140	48	P6:12-14:
130	53	P6:14-16:
105	46	P6:16-18:
97	35	P6:18-20:
124	33	P6:20-25:
97	35	P6:25-30:
93	39	P6:30-35:
101	48	P6:35-40:
104	41	P6:40-45:
111	44	P6:45-50:
104	50	P6:50-55:
93	58	P6:55-60:
76	58	P6:60-65:
79	63	P6:65-70:
87	66	P6:70-75:
88	69	P6:75-80:
85	91	P6:80-85:
70	55	P6:85-90:
98	63	P6:90-95:
92	66	P6:95-100:
82	58	P6:100-105:
88	48	P6:105-110:
79	55	P6:110-115:
87	45	P6:115-120:
75	61	P6:120-125:
73	53	P6:125-130:
71	78	P6:130-135:
76	96	P6:135-140:
84	135	P6:140-145:
67	104	P6:145-150:
81	102	P6:150-155:
60	105	P6:155-163:

CORE P8

I/C_{org}	Br/C_{org}	Sample
167	64	P8:0-4:
189	71	P8:4-5.5:
132	64	P8:5.5-7:
114	53	P8:7-8.5:
115	54	P8:8.5-10:
111	55	P8:10-12:
109	52	P8:12-14:
94	46	P8:14-16:
93	48	P8:16-18:
90	47	P8:18-21:
91	48	P8:21-24:
106	55	P8:24-28:
93	52	P8:28-32:
100	53	P8:32-36:
87	50	P8:36-40:
80	51	P8:40-45:
65	108	P8:45-50:
56	96	P8:50-55:
66	63	P8:55-60:
62	100	P8:60-65:
57	88	P8:65-70:
67	89	P8:70-75:
55	86	P8:75-80:
51	78	P8:80-85:
56	80	P8:85-90:
56	93	P8:90-95:
47	52	P8:95-100:
61	92	P8:105-110:
40	76	P8:115-120:
63	117	P8:125-130:
52	96	P8:135-140:
39	74	P8:145-150:
43	67	P8:155-160:
40	45	P8:165-170:
42	67	P8:175-183:

PLEIADES BOX CORE

I/C_{org}	Br/C_{org}	Sample
158	22	PL:2:
160	46	PL:4:
177	40	PL:6:
158	65	PL:8:
162	42	PL:10:
156	39	PL:12:
148	45	PL:14:
119	50	PL:16:
138	37	PL:18:
149	45	PL:20:
142	32	PL:24:
163	53	PL:28:
130	30	PL:32:
114	34	PL:36:
118	37	PL:40:

Table C.3

Interstitial water analyses.

N.D. = not detected.

I.S. = insufficient sample for analysis.

Analyses marked ? are suspect.

INTERSTITIAL WATER ANALYSES

Core P1

Alk. (meq l^{-1})	Fe^{2+} (μM)	Mn (μM)	NH_3 (μM)	PO_4^{3-} (μM)	$Si(OH)_4$ (μM)	SO_4^{2-} (mM)	Sample
2.43	1.1	N.D.	N.D.	3.3	230	25.6	Supernatant
2.64	0.82	N.D.	N.D.	6.1	754	26.4	P1:0-2:
2.55	0.84	6.4	4?	7.6	771	24.7	P1:2-4:
2.50	1.1	11	2?	7.3	804	23.9	P1:4-6:
2.53	0.63	21	1?	8.2	816	24.7	P1:6-8:
2.36	1.9	20	N.D.	I.S.	840	23.5	P1:8-10:
2.53	1.4	20	2?	I.S.	826	24.3	P1:10-12:
2.51	1.0	25	N.D.	9.4	768	23.9	P1:12-14:
2.58	1.3	25	N.D.	11.2	828	24.6	P1:14-16:
2.38	1.8	26	N.D.	I.S.	840	24.0	P1:16-18:
2.56	1.8	25	N.D.	14.3	881	24.5	P1:18-20:
2.32	1.7	29	4?	13.7	864	23.4	P1:20-22:
2.49	1.1	29	N.D.	I.S.	898	25.7	P1:22-26:
2.31	1.3	28	N.D.	I.S.	900	25.1	P1:26-30:
2.51	1.3	29	N.D.	22.6	888	24.4	P1:30-34:
2.69	1.3	29	N.D.	28.1	893	25.0	P1:34-36:
2.68	1.1	32	N.D.	24.9	910	25.4	P1:36-40:
2.76	0.41	29	N.D.	26.1	926	25.7	P1:40-45:
2.62	0.82	31	N.D.	22.1	900	25.6	P1:45-50:
2.73	0.61	33	N.D.	29.4	871	25.3	P1:55-60:
2.76	1.8	34	N.D.	22.5	861	24.4	P1:65-70:
2.69	0.82	40	5	27.0	907	25.3	P1:75-80:
2.64	0.64	36	4?	23.7	847	25.6	P1:85-90:
2.73	0.61	41	4?	28.8	941	25.5	P1:95-100:
2.64	0.50	37	9	30.7	859	25.5	P1:110-115:
2.55	0.61	37	7	26.1	924	24.5	P1:125-130:
2.80	0.82	40	21	23.2	936	24.6	P1:145-150:

INTERSTITIAL WATER ANALYSES

Core P2

Alk (meq l^{-1})	Fe^{2+} (μM)	Mn^{2+} (μM)	NH_3 (μM)	PO_4^{3-} (μM)	$Si(OH)_4$ (μM)	SO_4^{2-} (mM)	Sample
2.53	0.75	N.D.	N.D.	4.2	148	26.5	Supernatant
2.59	1.6	0	3?	10.5	727	25.8	P2:0-1:
	0.57	1.8	N.D.				P2:1-2:
2.44	1.7	18	N.D.	7.9	816	25.1	P2:2-3:
2.59	0.48	35	2?	10.6	814	25.0	P2:3-4:
2.44	0.64	38	4?	10.6	783	23.6	P2:4-5:
	0.57	35	N.D.				P2:5-6:
2.37	1.1	44	N.D.	10.6	797	23.8	P2:6-8:
2.44	1.2	44	N.D.	14.0	879	24.9	P2:8-10:
2.39	1.1	44	N.D.	17.6	864	23.6	P2:10-12:
3.39?	1.5	44	N.D.	I.S.	826	23.5	P2:12-14:
2.35	1.1	44	N.D.	15.8	859	23.3	P2:14-17:
2.22	3.1	47	N.D.	I.S.	862	23.7	P2:17-20:
2.28	0.79	44	N.D.	19.1	852	25.5	P2:20-24:
2.44	0.50	47	N.D.	23.1	867	25.7	P2:24-28:
2.12	0.61	47	N.D.	26.1	910	25.6	P2:28-32:
2.50	0.48	53	2?	27.3	895	25.4	P2:32-36:
2.49	0.66	47	4?	26.1	828	24.9	P2:36-40:
2.62	0.73	56	5	26.1	802	25.7	P2:40-44:
2.69	0.75	62	N.D.	26.1	838	25.8	P2:46-50:
2.75	1.2	55	2?	31.9	895	25.9	P2:55-60:
2.78	0.94	62	4?	30.1	864	25.8	P2:65-70:
2.76	0.36	53	7	29.2	895	25.5	P2:75-80:
2.79	0.36	56	7	31.0	816	25.0	P2:90-95:
2.76	0.39	49	9	27.3	855	25.0	P2:110-115:
2.77	0.36	47	9	29.5	912	24.3	P2:130-135:
2.87	0.84	38	7	30.7	890	24.9	P2:145-150:

INTERSTITIAL WATER ANALYSES

Core P6

Alk (meq l^{-1})	Fe^{2+} (μM)	I (μM)	Mn (μM)	NH_3 (μM)	PO_4^{3-} (μM)	$Si(OH)_4$ (μM)	SO_4^{2-} (mM)	Sample
2.58	0.54	0.76	6.4	5	9.3	182	28.6	Supernatant
2.63	1.5	I.S.	4.6	11	14.4	515	25.5	P6:0-1:
	1.3	1.59	15					P6:1-2:
2.65	1.7	3.09	31	23	17.0	610	24.7	P6:2-4:
2.70	0.82	2.71	38	26	I.S.	652	26.6	P6:4-6:
2.70	0.86	2.71	36	27	16.0	656	26.3	P6:6-8:
2.73	1.7	2.96	56	25	15.8	642	27.1	P6:8-10:
2.69	0.98	3.34	65	15	16.3	649	27.0	P6:10-12:
2.63	1.2	5.74	38	16	19.1	649	26.7	P6:12-14:
2.95?	2.2	4.54	58	19	15.2	650	27.6	P6:14-16:
2.54	1.3	5.04	56	16	14.7	671	26.3	P6:16-18:
2.20	1.7	5.04	51	11	11.4	649	26.1	P6:18-20:
2.41	0.84	4.92	55	19	13.3	601	27.5	P6:20-25:
2.45	3.9	3.78	58	18	13.2	562	28.9	P6:25-30:
2.56	1.4	5.30	59	16	15.2	662	25.2	P6:30-35:
2.60	3.0	5.69	64	15	13.4	654	27.8	P6:35-40:
2.51	5.2	4.29	63	21	15.1	677	29.0	P6:40-45:
2.59	3.9	5.30	61	18	15.8	649	28.7	P6:45-50:
2.54	0.84	7.69	61	21	17.1	618	27.9	P6:55-60:
2.75	0.82	8.95	67	20	17.6	654	29.7	P6:65-70:
2.71	0.84	9.20	68	29	16.5	667	28.8	P6:75-80:
2.77	0.86	6.87	61	31	17.8	643	28.5	P6:85-90:
2.70	1.6	3.78	60	35	18.0	654	29.3	P6:95-100:
2.70	1.1	4.46	60	38	18.3	672	26.4	P6:110-115:
2.67	1.2	2.84	54	37	19.7	680	26.4	P6:125-130:
2.73	0.68	2.71	52	41	19.1	717	26.2	P6:140-145:
2.57	1.1	2.08	55	43	19.6	769	26.2	P6:155-163:

INTERSTITIAL WATER ANALYSES

Core P8

Alk (meq l^{-1})	Fe^{2+} (μM)	I (μM)	Mn^{2+} (μM)	NH_3 (μM)	PO_4^{3-} (μM)	$Si(OH)_4$ (μM)	SO_4^{2-} (mM)	Sample
2.51	1.5?	0.62	N.D.	29?	3.9	224	26.0	Supernatant
2.76	0.68	0.81	N.D.	22	20.9	540	26.2	P8:0-2:
2.52	0.79	0.72	1.8	29	17.4	558	25.1	P8:2-4:
2.68	1.0	0.77	111	36	14.7	606	21.7?	P8:4-5.5:
2.89	1.8	0.85	164	26	19.7	643	24.1	P8:5.5-7:
3.06	2.9	0.91	153	27	23.2	675	24.3	P8:7-8.5:
2.82	1.5	1.03	157	28	18.6	665	24.3	P8:8.5-10:
2.73	3.1	0.98	160	29	16.3	688	24.6	P8:10-12:
2.84	1.6	1.06	173	30	15.5	661	22.9	P8:12-14:
2.82	0.88	1.10	158	34	16.8	663	23.9	P8:14-16:
3.02	1.3	1.11	175	36	20.4	690	24.6	P8:16-18:
4.77?	1.2	1.21	175	32	20.9	721	26.1	P8:18-21:
2.99	0.86	1.23	171	27	19.4	652	26.0	P8:21-24:
3.13	1.3	1.34	177	31	21.2	668	26.2	P8:24-28:
2.98	1.0	1.21	173	30	21.2	692	25.7	P8:28-32:
3.39	1.6	1.27	186	32	29.4	746	24.7	P8:32-36:
3.17	0.81	1.30	178	30	20.9	692	25.3	P8:36-40:
3.25	1.1	1.38	169	36	20.6	649	25.9	P8:40-45:
3.23	0.98	1.34	171	26	22.3	674	26.3	P8:45-50:
3.09	1.9	1.34	182	39	23.0	687	25.8	P8:55-60:
3.70	2.3	1.44	186	37	23.2	711	26.0	P8:65-70:
3.21	1.5	1.36	177	45	24.3	663	25.5	P8:80-85:
3.17	1.1	1.44	171	55	22.1	704	25.8	P8:95-100:
3.21	1.1	1.51	158	50	23.5	676	25.9	P8:115-120:
2.15	1.3	1.50	149	57	24.5	714	24.7	P8:135-140:
1.83	1.1	1.58	137	56	23.7	727	24.5	P8:155-160:
3.01	1.1	1.58	122	65	21.7	676	23.9	P8:170-175:

ACKNOWLEDGMENTS

I would like to thank the officers and crew of R.R.S. Shackleton for their help and co-operation during the May, 1976 Eastern Pacific cruise. Simon Wakefield generously assisted the author with pore water extraction and analysis on board ship.

I am grateful to Professors Sir Frederick Stewart and Gordon Craig for the use of the excellent facilities of the Grant Institute of Geology. Many members of the Grant Institute technical staff were very helpful during the course of this research. Mike Saunders often and freely gave advice on chemical analytical techniques and his genuine interest in many aspects of this study is appreciated. Geoff Angell cheerfully assisted with X-ray fluorescence and diffraction work and Colin Chaplin, Diana Baty, Flo Coxon, and especially Geoff Wilson helped with photography and occasional technical problems in the labs. Eddie Clark carefully manufactured sampling equipment in the workshop; Leo Harrison swiftly and efficiently provided obscure chemicals and assorted hardware from the store-room, often on embarassingly-short notice; and Thea Grieve helpfully procured rare journals and foreign theses, frequently in record time.

I would like to thank Dr. Joris Geiskes of Scripps Institution of Oceanography for kindly making available samples from the Pleiades box core, and Dr. B. L. K. Somayajulu of the Physical Research Laboratory, Ahmedabad, for generously providing some of the radiocarbon dates used in this thesis. I am also obliged to Steve Malcolm for the use of several of his computer programs. I greatly appreciate the efficiency and patience of Lucian Begg who typed the manuscript with great care.

I am particularly indebted to Dr. Brian Price for his excellent supervision and constant interest throughout this research. It has

been a very enjoyable association. I also wish to thank Dr. Ed Sholkovitz for critically commenting on the final draft and for his many suggestions and advice over the past few years.

I gratefully acknowledge the receipt of an Edinburgh University Postgraduate Studentship, without which this research would have been greatly limited.

Finally, I sincerely thank my wife Larraine for her unfailing support and understanding during the course of this work, especially over the interminably-long final stages.

REFERENCES

ABBEY S. (1977) Studies in "standard samples" for use in the general analysis of silicate rocks and minerals. Part 5 : 1977 edition of "usable" values. Can., Geol. Surv., Paper 77-34. Ottawa. 31 pp.

ADELSECK C. G. and ANDERSON T. F. (1978) The late Pleistocene record of productivity fluctuations in the eastern equatorial Pacific Ocean. Geology 6, 388-391.

ARCHER D. (1969) X-ray Analysis of Deep-Sea Sediments. Unpubl. Ph.D. dissert., University of Manchester. 108 pp.

ARRHENIUS G. O. (1952) Sediment cores from the East Pacific. In Repts. Swedish Deep-Sea Exped. (ed. H. Pettersson), Vol. 5, Fasc. 1, 227 pp.

ARRHENIUS G. O. (1963) Pelagic sediments. In The Sea (ed. M. N. Hill), Vol. 3, pp. 655-727. Wiley, London.

ARRHENIUS G. and BONATTI E. (1965) Neptunism and vulcanism in the ocean. In Progress in Oceanography (ed. M. Sears), Vol. 3, pp. 7-22. Pergamon, London.

AUMENTO F., LAWRENCE D. E. and PLANT A. G. (1968) The ferromanganese pavement on San Pablo seamount. Can., Geol. Surv., Paper 68-32, 30 pp.

BENDER M. L., BROECKER W., GORNITZ V., MIDDEL V., KAY R., SUN S. S. and BISCAYE P. (1971) Geochemistry of three cores from the East Pacific Rise. Earth Planet. Sci. Lett. 12, 425-433.

BENDER M. L., FANNING K. A., FROELICH P. N., HEATH G. R. and MAYNARD V. (1977) Interstitial nitrate profiles and oxidation of sedimentary organic matter in the Eastern Equatorial Atlantic. Science 198, 605-609.

BEN-YAAKOV S. and GOLDHABER M. B. (1973) The influence of sea water composition on the apparent constants of the carbonate system. Deep-Sea Res. 20, 87-99.

BERGER W. H. (1970) Planktonic foraminifera : selective solution and the lysocline. Mar. Geol. 8, 111-138.

BERGER W. H. (1973) Deep-sea carbonates : Pleistocene dissolution cycles. J. Foram. Res. 3, 187-195.

BERNER R. A. (1970) Sedimentary pyrite formation. Amer. J. Sci. 268, 1-23.

BERNER R. A. (1971) Principles of Chemical Sedimentology. McGraw-Hill, New York. 240 pp.

BERNER R. A. (1973) Phosphate removal from sea water by adsorption on volcanogenic ferric oxides. Earth Planet. Sci. Lett. 18, 77-86.

BERRANG P. G. and GRILL E. V. (1974) The effect of manganese oxide scavenging on molybdenum in Saanich Inlet, British Columbia. Mar. Chem. 2, 125-148.

BERTINE K. K. (1972) The deposition of molybdenum in anoxic waters. Mar. Chem. 1, 43-53.

BISCAYE P. E. (1965) Mineralogy and sedimentation of recent deep-sea clay in the Atlantic Ocean and adjacent seas and oceans. Geol. Soc. Amer., Bull. 76, 803-832.

BISCHOFF J. L. and KU T. L. (1970) Pore fluids of recent marine sediments : I. Oxidizing sediments of 20°N continental rise to Mid-Atlantic ridge. J. Sediment. Petrology 40, 960-973.

BISCHOFF J. L. and ROSENBAUER R. J. (1977) Recent metalliferous sediment in the North Pacific manganese nodule area. Earth Planet. Sci. Lett. 33, 379-388.

BISCHOFF J. L. and SAYLES F. L. (1972) Pore fluid and mineralogical studies of Recent marine sediments : Bauer depression region of the East Pacific Rise. J. Sediment. Petrology 42, 711-724.

BISCHOFF J. L., GREER R. E. and LUISTRO A. O. (1970) Composition of interstitial waters of marine sediments : temperature of squeezing effect. Science 167, 1245-1246.

BLATT H., MIDDLETON G. and MURRAY R. (1972) Origin of Sedimentary Rocks. Prentice-Hall, New Jersey. 634 pp.

BODINE M. W., HOLLAND H. D. and BORESIK M. (1965) Coprecipitation of manganese and strontium with calcite. In Symposium on Problems of Postmagmatic Ore Deposition, II, pp 401-406. Geol. Surv. Czech., Prague.

BOJANOWSKI R. and PASLAWSKA S. (1970) On the occurrence of iodine in bottom sediments and interstitial waters of the southern Baltic Sea. Acta Geophys. Pol. 18, 277-286.

BONATTI E., FISHER D. E., JOENSUU O. and RYDELL H. S. (1971) Post-depositional mobility of some transition elements, phosphorus, uranium, and thorium in deep-sea sediments. Geochim. Cosmochim. Acta 35, 189-201.

BÖSTROM K. (1973) The origin and fate of ferromanganoan active ridge sediments. Stockholm Contrib. Geol. 27, 149-243.

BÖSTROM K. and PETERSON M. N. A. (1966) Precipitates from hydrothermal exhalations of the East Pacific Rise. Econ. Geol. 61, 1258-1265.

BÖSTROM K. and PETERSON M. N. A. (1969) The origin of aluminium-poor ferromanganoan sediments in areas of high heat flow on the East Pacific Rise. Mar. Geol. 7, 427-447.

BÖSTROM K., PETERSON M. N. A., JOENSUU O. and FISHER D. E. (1969). Aluminium-poor ferromanganoan sediments on active oceanic ridges. J. Geophys. Res. 74, 3261-3270.

BÖSTROM K., JOENSUU O., MOORE C., BÖSTROM B., DALZIEL M. and HOROWITZ A. (1973) Geochemistry of barium in pelagic sediment. Lithos 6, 159-174.

BOWEN H. J. M (1966) Trace Elements in Biochemistry. Academic Press, London. 241 pp.

BOYLE E. A., SCLATER F. R. and EDMOND J. M. (1977) The distribution of dissolved copper in the Pacific. Earth. Planet. Sci. Lett. 37, 38-54.

BRAY J. T., BRICKER O. P. and TROUP B. N. (1973) Phosphate in interstitial waters of anoxic sediments : oxidation effects during sampling procedure. Science 180, 1362-1364.

BRICKER O. P. and TROUP B. N. (1975) Sediment-water exchange in Chesapeake Bay. Estuarine Res. (ed. L. E. Cronin), Vol. 1, pp. 3-27. Academic Press, London.

BROECKER W. S. (1971) Calcite accumulation rates and glacial to interglacial changes in ocean mixing. In The Late Cenezoic Glacial Ages (ed. K. K. Turekian), pp. 239-265. Yale University Press.

BROECKER W. S. (1974) Chemical Oceanography. Harcourt Brace Jovanovich. 214 pp.

BROECKER W. S. and van DONK J. (1970) Insolation changes, ice volumes, and the O^{18} record in deep-sea cores. Rev. Geophys. and Space Phys. 8, 169-198.

BRULAND K. W., KNAUER G. A. and MARTIN J. H. (1978) Zinc in northeast Pacific water. Nature 271, 741-743.

BUNTING W. E. (1944) Determination of soluble silica in very low concentrations. Ind. Eng. Chem., Anal. Ed. 16, 612-615.

BURNS R. G. (1965) Formation of cobalt (III) in the amorphous FeOOH . $2H_2O$ phase of manganese nodules. Nature 205, 999.

BURNS R. G. and BURNS V. M. (1977) Mineralogy. In Marine Manganese Deposits (ed. G. P. Glasby), pp 185-248. Elsevier, Amsterdam.

CALLENDER E. (1976) Transition metal geochemistry of interstitial fluids extracted from manganese-nodule-rich pelagic sediments of the Northeastern Equatorial Pacific Ocean. Abstracts, Joint Oceanogr. Assembly, Edinburgh, p. 85.

CALVERT S. E. (1976) The mineralogy and geochemistry of near-shore sediments. In Chemical Oceanography (eds. J. P. Riley and R. Chester); Vol. 6, pp 187-280. Academic Press, London.

CALVERT S. E. and PRICE N. B. (1970a) Composition of manganese nodules and manganese carbonates from Loch Fyne, Scotland. Contr. Mineral. and Petrol. 29, 215-233.

CALVERT S. E. and PRICE N. B. (1970b) Minor metal contents of recent organic-rich sediments off South West Africa. Nature 227, 593-595.

CALVERT S. E. and PRICE N. B. (1972) Diffusion and reaction profiles of dissolved manganese in the pore waters of marine sediments. Earth Planet. Sci. Lett. 16, 245-249.

CALVERT S. E. and PRICE N. B. (1977) Geochemical variation in ferro-manganese nodules and associated sediments from the Pacific Ocean. Mar. Chem. 5, 43-74.

CANN J. R., WINTER C. K. and PRITCHARD R. G. (1977) A hydrothermal deposit from the Gulf of Aden. Mineral. Mag. 41, 193-199.

CARROLL D. and STARKEY H. C. (1971) Reactivity of clay minerals with acids and alkalies. Clays Clay Minerals 19, 321-333.

CARVAJAL M. C. and LANDERGREN S. (1969) Marine sedimentation processes. The interrelationships of manganese, cobalt and nickel. Stockholm Contrib. Geol. 18, 99-122.

CHAN L. H., DRUMMOND D., EDMOND J. M. and GRANT B. (1977) On the barium data from the Atlantic Geosecs expedition. Deep-Sea Res. 24, 613-649.

CHAPMAN P. and LISS P. S. (1977) The effect of nitrite on the spectrophotometric determination of iodate in sea water. Mar. Chem. 5, 243-249.

CHASE T. E., MENARD H. W. and MAMMERICKX J. (1970) Bathymetry of the North Pacific. IMR Technical Report Series TR-15, Institute of Marine Resources, Scripps Institution of Oceanography.

CHESTER R. (1965) Elemental geochemistry of marine sediments. In Chemical Oceanography. 1st Edition (eds. J. P. Riley and G. Skirrow), Vol. 2. Academic Press, London.

CHURCH T. M. (1970) Marine Barite. Unpubl. Ph.D. dissert., University of California, San Diego. 100 pp.

CLINE J. D. and RICHARDS F. A. (1972) Oxygen deficient conditions and nitrate reduction in the eastern tropical North Pacific Ocean. Limnol. Oceanogr. 17, 885-900.

COOK H. E. and ZEMMELS I. (1971) X-ray mineralogy studies, Leg 8. In Initial Reports of the Deep-Sea Drilling Project (eds. J. I. Tracey, Jr., et al), Vol. VIII, pp. 901-950. U.S. Government Printing Office, Washington, D. C.

COOK H. E. and ZEMMELS I. (1972) X-ray mineralogy studies, Leg 9. Deep-Sea Drilling Project. In Initial Reports of the Deep-Sea Drilling Project (eds. J. D. Hays et al), Vol. IX, pp. 707-777. U.S. Government Printing Office, Washington, D.C.

COPIN-MONTEGUT C. and COPIN-MONTEGUT G. (1972) Chemical analysis of suspended particulate matter collected in the northeast Atlantic. Deep-Sea Res. 19, 445-452.

CORLISS J. B., LYLE M. and DYMOND J. (1978) The chemistry of hydrothermal mounds near the Galapagos Rift. Earth Planet. Sci. Lett. 40, 12-24.

CORLISS J. B., DYMOND J., GORDON L. I., EDMOND J. M., von HERZEN R. P., BALLARD R. D., GREEN K., WILLIAMS D., BAINBRIDGE A., CRANE K. and van ANDEL Tj. H. (1979) Exploration of submarine thermal springs on the Galapagos Rift. Science (submitted).

CORRENS C. W. (1954) Titan in Tiefseesedimenten. Deep-Sea Res. 1, 78-85.

CRONAN D. S. (1974) Authigenic minerals in deep-sea sediments. In The Sea (ed. E. D. Goldberg), Vol. 5, pp. 491-525. Wiley, New York.

CRONAN D. S. (1977) Deep-sea nodules : distribution and geochemistry. In Marine Manganese Deposits (ed. G. P. Glasby), pp. 11-44. Elsevier, Amsterdam.

CULBERSON C. and PYTKOWICZ R. (1968) Effect of pressure on carbonic acid, boric acid and the pH in sea water. Limnol. and Oceanogr. 13, 403-417.

CURRAY J. R. and MOORE D. G. (1964) Pleistocene deltaic progradation of continental terrace, Costa de Nayarit, Mexico. In Marine Geology of the Gulf of California (eds. Tj. H. van Andel and G. J. Shor), Amer. Assoc. Petrol. Geol. Mem. 3, pp. 193-215.

DAMUTH J. E. (1975) Quaternary climate change as revealed by calcium carbonate fluctuations in western Equatorial Atlantic sediments. Deep-Sea Res. 22, 725-743.

DEER W. A., HOWIE R. A. and ZUSSMAN J. (1966) An Introduction to the Rock-Forming Minerals. Longman, London. 528 pp.

DEGENS E. T. (1969) Biogeochemistry of stable carbon isotopes. In Organic Geochemistry (eds. G. Eglington and M. T. J. Murphy), pp. 304-329. Longman, New York.

DEGENS E. T. and MOPPER K. (1976) Factors controlling the distribution and early diagenesis of organic material in marine sediments. In Chemical Oceanography (eds. J. P. Riley and R. Chester), Vol. 6, pp. 59-113. Academic Press, London.

DINKELMAN M. G. (1974) Late Quaternary Radiolarian Paleo-oceanography of the Panama Basin, Eastern Equatorial Pacific. Unpubl. Ph.D. dissert., Oregon State University, Corvallis, Oregon. 123 pp.

DOFF D. H. (1969) The Geochemistry of Recent Oxic and Anoxic Sediments of Oslo Fjord, Norway. Unpubl. Ph.D. dissert., University of Edinburgh. 245 pp.

DOWDING L. G. (1977) Sediment dispersal within the Cocos Gap, Panama Basin. J. Sediment. Petrology 47, 1132-1156.

DYMOND J. and VEEH H. H. (1975) Metal accumulation rates in the Southeast Pacific and the origin of metalliferous sediments. Earth Planet. Sci. Lett. 28, 13-22.

DYMOND J., CORLISS J. B., HEATH G. R., FIELD C. W., DASCH E. J. and VEEH H. H. (1973) Origin of metalliferous sediments from the Pacific Ocean. Geol. Soc. Amer., Bull. 84, 3355-3372.

EDMOND J. M. (1970) High precision determination of titration alkalinity and total carbon dioxide content of sea water by potentiometric titration. Deep-Sea Res. 17, 737-750.

EDMOND J. M. and GIESKES J. M. T. M. (1970) On the calculation of the degree of saturation of sea water with respect to calcium carbonate under in situ conditions. Geochim. Cosmochim. Acta 34, 1261-1291.

EL WAKEEL S. K. and RILEY J. P. (1961) Chemical and mineralogical studies of deep-sea sediments. Geochim. Cosmochim. Acta 25, 110-146.

ELDERFIELD H. (1977) The form of manganese and iron in marine sediments. In Marine Manganese Deposits (ed. G. P. Glasby), pp. 269-289. Elsevier.

EMERY K. O. and RITTENBERG S. C. (1952) Early diagenesis of California Basin sediments in relation to origin of oil. Amer. Assoc. Petrol. Geol., Bull. 36, 735-806.

FANNING K. A. and SCHINK D.R. (1969) Interaction of marine sediment with dissolved silica. Limnol. Oceanogr. 14, 59-68.

FANNING K. A. and PILSON M. E. Q. (1971) Interstitial silica and pH in marine sediments : some effects of sampling procedures. Science 173, 1228-1231.

FANNING K. A. and PILSON M. E. Q. (1974) Diffusion of dissolved silica out of deep-sea sediments. J. Geophys. Res. 79, 1293-1297.

FORSBERGH E. D. (1969) On the climatology, oceanography and fisheries of the Panama Bight. Inter-Am. Tropical Tuna Comm. Bull. 14, 49-385.

FROELICH P. N., BENDER M. L. and HEATH G. R. (1977) Phosphorus accumulation rates in metalliferous sediments on the East Pacific Rise. Earth Planet. Sci. Lett. 34, 351-359.

GARDNER J. V. and HAYS J. D. (1976) Responses of sea-surface temperature and circulation to global climatic change during the past 200,000 years in the Eastern Equatorial Atlantic Ocean. In Investigation of Late Quaternary Paleoceanography and Paleoclimatology (eds. R. M. Cline and J. D. Hays), Geol. Soc. Amer., Mem. 145, pp. 221-246.

GARRELS R. M. and CHRIST G. L. (1965) Solutions, Minerals, and Equilibria. Harper and Row, New York. 450 pp.

GARRELS R. M. and THOMPSON M. E. (1962) A chemical model for sea water at 25°C and one atmosphere total pressure. Amer. J. Sci. 260, 57-66.

GIBBS R. J. (1977) Clay mineral segregation in the marine environment. J. Sediment. Petrology 47, 237-243.

GOLDBERG E. D. and ARRHENIUS G. O. (1958) Chemistry of Pacific pelagic sediments. Geochim. Cosmochim. Acta 13, 153-212.

GOLDHABER M. B., ALLER R. C., COCHRAN J. K., ROSENFELD J. K., MARTENS C. S. and BERNER R. A. (1977) Sulphate reduction, diffusion, and bioturbation in Long Island Sound sediments : report of the FOAM group. Amer. J. Sci. 277, 193-237.

GOLDSCHMIDT V. M. (1954) Geochemistry. Oxford Univ. Press. 730 pp.

GORDON D. C. Jr. (1971) Distribution of particulate organic carbon and nitrogen at an oceanic station in the central Pacific. Deep-Sea Res. 18, 1127-1134.

GORSLINE D. S. and PRENSKY S. E. (1975) Paleoclimatic inferences for late Pleistocene and Holocene from California continental borderland basin sediments. In Quaternary Studies (eds. R. P. Suggate and M. M. Cresswell), Roy. Soc. N.Z., Bull. 13, pp. 147-154.

GREENSLATE J. L., FRAZER J. Z. and ARRHENIUS G. (1973) Origin and deposition of selected transition elements in the seabed. In The Origin and Distribution of Manganese Nodules in the Pacific and Prospects for Exploration (ed. M. Morgenstein), pp. 45-69. Hawaii Inst. of Geophysics, Honolulu.

GRUNDMANIS V. and MURRAY J. W. (1977) Nitrification and denitrification in sediments from Puget Sound. Limnol. Oceanogr. 22, 804-813.

GULBRANDSEN R. A. (1969) Physical and chemical factors in the formation of marine apatite. Econ. Geol. 64, 365-382.

HANOR J. S. (1969) Barite saturation in sea water. Geochim. Cosmochim. Acta 33, 894-898.

HARTMANN M. (1964) Zur Geochemie von Mangan und Eisen in der Ostsee. Meyniana 14, 3-20.

HARTMANN M., MÜLLER P. J., SUESS E., van der WEIJDEN C. H. (1976) Chemistry of Late Quaternary sediments and their interstitial waters from the NW African continental margin. "Meteor" Forsch., Reihe C No. 24, 1-67.

HATHAWAY J. C. and SACHS P. L. (1965) Sepiolite and clinoptilolite from the Mid-Atlantic Ridge. Amer. Mineral. 50, 852-867.

HAY R. L. (1966) Zeolites and zeolitic reactions in sedimentary rocks. Geol. Soc. Amer., Spec. Pap. 85, 130 pp.

HAYS J. D. and PERRUZZA A. (1972) The significance of calcium carbonate oscillations in eastern equatorial Atlantic deep-sea sediments for the end of the Holocene warm interval. Quaternary Res. 2, 355-362.

HAYS J. D., SAITO T., OPDYKE J. D. and BURKLE L. H. (1969) Pliocene-Pleistocene sediments of the equatorial Pacific : their paleomagnetic, biostratigraphic and climatic record. Geol. Soc. Amer., Bull. 80, 1481-1514.

HEATH G. R. (1969) Mineralogy of Cenozoic deep-sea sediments from the equatorial Pacific Ocean. Geol. Soc. Amer., Bull. 80, 1997-2018.

HEATH G. R. and van ANDEL Tj. H. (1973) Tectonics and sedimentation in the Panama Basin : geologic results of Leg 16, Deep-Sea Drilling Project. In Initial Reports of the Deep-Sea Drilling Project (ed. A. G. Kaneps), Vol. XVI, pp. 899-914. U.S. Govt. Printing Office, Washington.

HEATH G. R., MOORE T. C. Jr. and ROBERTS G. L. (1974) Mineralogy of surface sediments from the Panama Basin, Eastern Equatorial Pacific. J. Geol. 82, 145-160.

HEM J. D. (1963) Chemical equilibria and rates of manganese oxidation. U.S. Geol. Surv., Water-Supply Pap. 1667-A. 64 pp.

HEY R. (1977) Tectonic evolution of the Cocos-Nazca spreading centre. Geol. Soc. Amer., Bull. 88, 1404-1420.

HEY R., JOHNSON G. L. and LOWRIE A. (1977) Recent plate motions in the Galapagos area. Geol. Soc. Amer., Bull. 88, 1385-1403.

HIRST D. M. (1962) The geochemistry of modern sediments from the Gulf of Paria - II. The location and distribution of trace elements. Geochim. Cosmochim. Acta 26, 1147-1187.

HOLDEN J. C. and DIETZ R. S. (1972) Galapagos gore, Nazcopac triple junction and Carnegie/Cocos Ridges. Nature 235, 266-269.

HOLDREN G. R., BRICKER D. P. and MATISOFF G. (1975) A model for the control of dissolved manganese in the interstitial waters of Chesapeake Bay. In Marine Chemistry in the Coastal Environment (ed. T. M. Church), pp. 364-381. Amer. Chem. Soc., Washington.

HOLM-HANSEN O. (1969) Determination of microbial biomass in ocean profiles. Limnol. Oceanogr. 14, 740-747.

HORNE R. A. (1969) Marine Chemistry. Wiley, London. 568 pp.

IRVING R. and WILLIAMS R. J. P. (1953) The stability of transition-metal complexes. J. Chem. Soc., Transactions, Part III, Paper 637, 3192-3210.

JONES M. M. and PYTKOWICZ R. (1973) Solubility of silica in sea water at high pressures. Roy. Soc. Sci. Liege, Bull. 42, 118-120.

KAPLAN I. R., EMERY K. O. and RITTENBERG S. C. (1963) The distribution and isotopic abundance of sulphur in recent marine sediments off southern California. Geochim. Cosmochim. Acta 27, 297-331.

KENNETT J. P. (1966) Foraminiferal evidence of a shallow calcium carbonate solution boundary, Ross Sea, Antarctica. Science 153, 191-193.

KLITGORD K. D. and MUDIE J. D. (1974) The Galapagos Spreading Centre : a near-bottom geophysical survey. Geophys. J. Roy. Astr. Soc. 38, 563-586.

KOWSMANN R. O. (1973) Coarse components in surface sediments of the Panama Basin, eastern equatorial Pacific. J. Geol. 81, 473-494.

KOWSMANN R. O. (1973) Coarse components in surface sediments of the Panama Basin, eastern equatorial Pacific. J. Geol. 81, 473-494.

KRAMER J. R. (1964) Sea water - saturation with apatites and carbonates. Science 146, 637-638.

KRAUSKOPF K. B. (1956) Factors controlling the concentrations of thirteen rare metals in sea water. Geochim. Cosmochim. Acta 9, 1-32B.

KRAUSKOPF K. B. (1959) The geochemistry of silica in sedimentary environments. In Silica in Sediments. Soc. Econ. Paleontol. Mineral., Spec. Publ. 7, 4-19.

KYLIN H. (1930) Uber die jodidsaltende Fahigkeit der Phaophycean. Z. Physiol. Chem. 191, 200-210.

LAIRD N. P. (1971) Panama Basin deep water - properties and circulation. J. Mar. Res. 29, 226-234.

LI Y. H. and GREGORY S. (1974) Diffusion of ions in sea water and in deep-sea sediments. Geochim. Cosmochim. Acta 38, 703-714.

LI Y. H., BISCHOFF J. and MATHIEU G. (1969) The migration of manganese in the Arctic Basin sediment. Earth Planet. Sci. Lett. 7, 265-270.

LI Y. H., BROECKER W. S. and TAKAHASHI T. (1969) Degree of saturation of $CaCO_3$ in the oceans. J. Geophys. Res. 74, 5507-5525.

LIDDICOAT M. I., TIBBITTS S. and BUTLER E. I. (1975) The determination of ammonia in sea water. Limnol. Oceanogr. 20, 131-132.

LINGANE J. J. and KARPLUS R. (1946) New method for determination of manganese. Ind. Eng. Chem., Anal. Ed. 19, 191-194.

LONSDALE P. (1977a) Deep-tow observations at the mounds abyssal hydrothermal field, Galapagos Rift. Earth Planet. Sci. Lett. 36, 92-110.

LONSDALE P. (1977b) Inflow of bottom-water to the Panama Basin. Deep-Sea Res. 24, 1065-1101.

LONSDALE P. F. and MALFAIT B. T. (1974) Abyssal dunes of foraminiferal sand on the Carnegie Ridge. Geol. Soc. Amer., Bull. 85, 1697-1712.

LOVE L. G. (1967) Early diagenetic iron sulphide in Recent sediments of the Wash (England). Sedimentology 9, 327-352.

LOWENSTAM H. A. (1974) Impact of life on physical and chemical processes. In The Sea (ed. E. D. Goldberg), Vol. 5, pp. 715-796. Wiley, London.

LUPTON J. E., WEISS R. F. and CRAIG H. (1977) Mantle helium in hydrothermal plumes in the Galapagos Rift. Nature 267, 603-604.

LUZ B. and SHACKLETON N. J. (1975) $CaCO_3$ solution in the tropical East Pacific during the past 130,000 years. Cushman Found. Foraminiferal Res., Spec. Publ. 13, 142-150.

LYLE M. (1978) The Formation and Growth of Ferromanganese Oxides on the Nazca Plate. Unpubl. Ph.D. dissert., Oregon State University, Corvallis. 172 pp.

LYLE M. W. and DYMOND J. (1976) Metal accumulation rates in the Southeast Pacific - errors introduced from assumed bulk densities. Earth Planet. Sci. Lett. 30, 164-168.

LYNN D. C. and BONATTI E. (1965) Mobility of manganese in diagenesis of deep-sea sediments. Mar. Geol. 3, 457-474.

MACDONALD K. C. and MUDIE J. D. (1974) Microearthquakes on the Galapagos Spreading Centre and the seismicity of fast-spreading ridges. Geophys. J. Roy. Astr. Soc. 36, 245-257.

MANGELSDORF P. C., WILSON R. S. and DANIELL E. (1969) Potassium enrichments in interstitial waters of recent marine sediments. Science 165, 171-173.

MANHEIM F. T. (1961) A geochemical profile in the Baltic Sea. Geochim. Cosmochim. Acta 25, 52-71.

MANHEIM F. T. (1970) The diffusion of ions in unconsolidated sediments. Earth Planet. Sci. Lett. 9, 307-309.

MARCH J. (1968) Advanced Organic Chemistry : Reactions, Mechanisms, and Structure. 1st edition. McGraw-Hill, New York. 1098 pp.

MARTIN J. H. and KNAUER G. A. (1973) The elemental composition of plankton. Geochim. Cosmochim. Acta 37, 1639-51.

MASON B. (1966) Principles of Geochemistry. Wiley, London. 329 pp.

McBIRNEY A. R. and WILLIAMS H. (1969) Geology and petrology of the Galapagos Islands. Geol. Soc. Amer., Mem. 118, 197 pp.

MEHRA O. P. and JACKSON M. L. (1959) Iron oxide removal from soils and clays by a dithionite-citrate system buffered with sodium bicarbonate. Proc. Seventh Nat. Conf. Clays Clay Minerals (ed. A. Swineford), pp. 317-327. Pergamon.

MOORE T. C. Jr., HEATH G. R. and KOWSMANN R. O. (1973) Biogenic sediments of the Panama Basin. J. Geol. 81, 458-472.

MORGAN J. J. (1967) Chemical equilibria and kinetic properties of manganese in natural waters. In Principles and Applications of Water Chemistry (ed. S. D. Faust and J. V. Hunter), pp. 561-624, Proc. 4th Rudolfs Res. Conf. Wiley, New York.

MÜLLER P. J. (1977) C/N ratios in Pacific deep-sea sediments : effect of inorganic ammonium and organic nitrogen compounds sorbed by clays. Geochim. Cosmochim. Acta 41, 765-776.

MUMPTON F. A. (1960) Clinoptilolite redefined. Amer. Mineral. 45, 351-369.

MURRAY J. W. (1975) The interaction of metal ions at the manganese dioxide - solution interface. Geochim. Cosmochim. Acta 39, 505-519.

MURRAY J. W. and BREWER P. G. (1977) Mechanisms of removal of iron, manganese and other trace metals from sea water. In Marine Manganese Deposits (ed. G. P. Glasby), pp. 291-325. Elsevier, Amsterdam.

MURRAY J. W., JAHNKE R. and EMERSON S. (1979) The effect of pressure on the alkalinity of deep-sea interstitial water samples. Science (in press).

NAYUDU Y. (1962) Rapid method for studying silt-size sediments and heavy minerals by liquid immersion. J. Sediment. Petrology 32, 326-333.

NIELSEN A. E. (1964) Kinetics of Precipitation. Macmillan, New York.

NORRISH K. and HUTTON J. T. (1969) An accurate X-ray spectrographic method for the analysis of a wide range of geological samples. Geochim. Cosmochim. Acta 33, 431-453.

NRIAGU J. O. (1972) Stability of vivianite and ion-pair formation in the system $Fe_3(PO_4)_2$ - H_3PO_4 - H_2O. Geochim. Cosmochim. Acta 36, 459-470.

PAK H. and ZANEVELD J. R. V. (1973) The Cromwell Current on the east side of the Galapagos Islands. J. Geophys. Res. 78, 7845-7859.

PARKER F. L. and BERGER W. H. (1971) Faunal and solution patterns of planktonic foraminifera in surface sediments of the South Pacific. Deep-Sea Res. 18, 73-107.

PARKIN D. W. and SHACKLETON N. J. (1973) Trade-wind and temperature correlations down a deep-sea core off the Sahara Coast. Nature 245, 455-457.

PATTON J. and REEDER W. (1956) New indicator for titration of Ca with EDTA. Anal. Chem. 28, 1026-1028.

PAVLOVA G. A. and SHISHKINA O. V. (1973) Accumulation of iodine in interstitial water during metamorphism in relation to the iodine distribution in Pacific sediments. Geochem. Int. 10, 804-813.

PETERSON M. N. A. and GOLDBERG E. D. (1962) Feldspar distributions in South Pacific pelagic sediments. J. Geophys. Res. 67, 3477-3492.

PETZING J. and CHESTER R. (1979) Authigenic marine zeolites and their relationship to global volcanism. Mar. Geol. 29, 253-271.

PILIPCHUK M. F. and VOLKOV I. I. (1968) The geochemistry of molybdenum in the Black Sea. Lith. Miner. Res. 4, 389-407.

PISIAS N. G. (1976) Late Quaternary sediment of the Panama Basin : sedimentation rates, periodicities, and controls of carbonate and opal accumulation. In Investigation of Late Quaternary Paleoceanography and Paleoclimatology (eds. R. M. Cline and J. D. Hays), Geol. Soc. Amer., Mem. 145, pp. 375-391.

PRELL W. L., GARDNER J. V., BÉ A. W. H. and HAYS J. D. (1976) Equatorial Atlantic and Caribbean foraminiferal assemblages, temperatures, and circulation : interglacial and glacial comparisons. In Investigation of Late Quaternary Paleoceanography and Paleoclimatology (eds. R. M. Cline and J. D. Hays), Geol. Soc. Amer., Mem. 145, 247-266.

PRESLEY B. J., KOLODNY Y., NISSENBAUM A. and KAPLAN I. R. (1972) Early diagenesis in a reducing fjord, Saanich Inlet, British Columbia - II. Trace element distribution in interstitial water and sediment. Geochim. Cosmochim. Acta 36, 1073-1090.

PRICE N. B. (1967) Some geochemical observations on manganese-iron oxide nodules from different depth environments. Mar. Geol. 5, 511-538.

PRICE N. B. and CALVERT S. E. (1973) The geochemistry of iodine in oxidized and reduced Recent marine sediments. Geochim. Cosmochim. Acta 37, 2149-2158.

PRICE N. B. and CALVERT S. E. (1977) The contrasting geochemical behaviours of iodine and bromine in Recent sediments from the Namibian shelf. Geochim. Cosmochim. Acta 41, 1769-1775.

PRICE N. B., CALVERT S. E. and JONES P. G. W. (1970) The distribution of iodine and bromine in the sediments of the South Western Barents Sea. J. Mar. Res. 28, 22-34.

PROSPERO J. M. and BONATTI E. (1969) Continental dust in the atmosphere of the eastern equatorial Pacific. J. Geophys. Res. 74, 3362-3371.

RAAB W. (1972) Physical and chemical features of Pacific deep-sea manganese nodules and their implications to the genesis of nodules. In Ferromanganese Deposits on the Ocean Floor (ed. D. R. Horn), pp. 31-49. National Science Foundation, Washington.

RANKAMA K. and SAHAMA Th. G. (1950) Geochemistry. University of Chicago Press. 912 pp.

REDFIELD A. C., KETCHUM B. H. and RICHARDS F. A. (1963) The influence of organisms on the composition of sea water. In The Sea (ed. M. N. Hill), Vol. 2, pp. 26-77. Wiley, New York.

REVELLE R., BRAMLETTE M., ARRHENIUS G. O. and GOLDBERG E. D. (1955) Pelagic sediments of the Pacific. Geol. Soc. Amer., Spec. Pap. 62, 221-236.

REYNOLDS R. C. Jr. (1963) Matrix corrections in trace element analysis by X-ray fluorescence : estimation of the mass absorption coefficient by Compton scattering. Amer. Mineral. 48, p.1133.

RILEY J. P. and CHESTER R. (1971) Introduction to Marine Chemistry. Academic Press, London. 465 pp.

ROBBINS J. A. and CALLENDER E. (1975) Diagenesis of manganese in Lake Michigan sediments. Amer. J. Sci. 275, 512-533.

ROBIE R. A. and WALDBAUM D. R. (1968) Thermodynamic properties of minerals and related substances at 298.15°K (25.0°C) and one atmosphere (1.013 bars) pressure and at higher temperatures. U.S. Geol. Surv., Bull. 1259, 256 pp.

ROSENQVIST, I. Th. (1970) Formation of vivianite in Holocene clay sediments. Lithos 3, 327-334.

RYTHER J. H. (1963) Geographic variations in productivity. In The Sea (ed. M. N. Hill), Vol. 2, pp 347-380. Wiley, London.

SAYLES F. L. and BISCHOFF J. L. (1973) Ferromanganoan sediments in the equatorial East Pacific. Earth Planet. Sci. Lett. 19, 330-336.

SAYLES F. L., KU T. L. and BOWKER P. C. (1975) Chemistry of ferromanganoan sediment of the Bauer Deep. Geol. Soc. Amer., Bull. 86, 1423-1431.

SCHINK D. R. and GUINASSO N. L. Jr. (1977) Effects of bioturbation on sediment-sea water interaction. Mar. Geol. 23, 133-154.

SCHINK D. R., FANNING K. A. and PILSON M. E. Q. (1974) Dissolved silica in the upper pore waters of the Atlantic Ocean floor. J. Geophys. Res. 79, 2243-2250.

SCHINK D. R., GUINASSO N. L. Jr. and FANNING K. A. (1975) Processes affecting the concentration of silica at the sediment-water interface of the Atlantic Ocean. J. Geophys. Res. 80, 3013-3031.

SCLATER F. R., BOYLE E. and EDMOND J. M. (1976) On the marine geochemistry of nickel. Earth Planet. Sci. Lett. 31, 119-128.

SHACKLETON N. J. and OPDYKE N. D. (1973) Oxygen isotope and paleomagnetic stratigraphy of equatorial Pacific core V28-238 : oxygen isotope temperatures and ice volumes on a 10^5 and 10^6 year scale. Quaternary Res. 3, 39-55.

SHAW T. I. (1959) The mechanism of iodide accumulation by the brown sea weed Laminaria digitata. I. The uptake of ^{131}I. Roy. Soc. London, Proc. B150, 356-371.

SHAW T. I. (1962) Halogens in algae. In Physiology and Biochemistry of Algae (ed. R. A. Lewin), pp. 247-253. Academic Press, London.

SHISHKINA O. V. and PAVLOVA G. A. (1965) Iodine distribution in marine and oceanic bottom muds and in their pore fluids. Geochem. Int. 2, 559-565.

SHOLKOVITZ E. R. (1973) Interstitial water chemistry of the Santa Barbara Basin sediments. Geochim. Cosmochim. Acta 37, 2043-2073.

SHTERENBERG L. E., GORSHKOVA T. I. and NAKTINAS E. M. (1968) Manganese carbonates in ferromanganese nodules in the Gulf of Riga. Lithol. Miner. Resour. 4, 438-443.

SILLÉN L. G. (1961) The physical chemistry of sea water. In Oceanography (ed. M. Sears), pp. 549-581. Amer. Assoc. Advance. Sci.

SILLÉN L. G. and MARTELL A. E. (1964) Stability constants of metal-ion complexes. Chem. Soc. (London), Spec. Publ. 17.

SOLORZANO L. (1969) Determination of ammonia in natural waters by the phenolhypochlorite method. Limnol. and Oceanog. 14, 799-801.

STEVENSON F. J. and CHENG C. N. (1972) Organic geochemistry of the Argentine Basin sediments : carbon-nitrogen relationships and Quaternary correlations. Geochim. Cosmochim. Acta 36, 653-671.

STEVENSON M. (1970) Circulation in the Panama Bight. J. Geophys. Res. 75, 659-672.

STEVENSON M. R. and TAFT B. A. (1971) New evidence of the Equatorial Undercurrent east of the Galapagos Islands. J. Mar. Res. 29, 103-115.

STRAKHOV N. M. (1969) Principles of Lithogenesis, Vol. 2. Oliver and Boyd, Edinburgh. 609 pp.

STRICKLAND J. P. H. and PARSONS T. R. (1968) A practical handbook of sea water analysis. Fish. Res. Board Can., Bull. 167, 311 pp.

STUMM W. and MORGAN J. J. (1970) Aquatic Chemistry. Wiley, London. 583 pp.

SUGAWARA K. and TERADA K. (1957) Iodine distribution in the western Pacific Ocean. Nagoya Univ., J. Earth Sci. 5, 81-102.

SWANSON V. E., FROST I. C., RADER L. R. and HUFFMAN C. (1966) Metal sorption by northwest Florida humate. U.S. Geol. Surv., Prof. Pap. 550-C, C174-C177.

SWIFT S. A. (1977) Holocene rates of sediment accumulation in the Panama Basin, eastern equatorial Pacific : pelagic sedimentation and lateral transport. J. Geol. 85, 301-319.

SZILAGYI M. (1967) Sorption of molybdenum by humus preparations. Geochem. Int. 4, 1165-1167.

TERRY R. A. (1956) A geological reconnaissance of Panama. Calif. Acad. Sci., Occas. Pap. 23, 91 pp.

THOMPSON G. and BOWEN V. T. (1969) Analyses of coccolith ooze from the deep tropical Atlantic. J. Mar. Res. 27, 32-37.

THOMPSON P. R. and SAITO T. (1974) Pacific Pleistocene sediments : planktonic foraminifera, dissolution cycles, and geochronology. Geology 2, 333-335.

TROUP B. N., BRICKER O. P. and BRAY J. T. (1974) Oxidation effect on the analysis of iron in the interstitial water of recent anoxic sediments. Nature 249, 237.

TRUESDALE V. W. and SPENCER C. P. (1974) Studies on the determination of inorganic iodine in sea water. Mar. Chem. 2, 33-47.

TRUESDALE V. W. and CHAPMAN P. (1976) Optimisation of a catalytic procedure for the determination of total iodine in sea water. Mar. Chem. 4, 29-42.

TSUNOGAI S. (1971) Determination of iodine in sea water by an improved Sugawara method. Anal. Chim. Acta 55, 444-447.

TSUNOGAI S. and SASE T. (1969) Formation of iodide-iodine in the ocean. Deep-Sea Res. 16, 489-496.

TUREKIAN K. K. (1964) The geochemistry of the Atlantic Ocean Basin. Trans. N.Y. Acad. Sci. 26, 312-330.

TUREKIAN K. K. and WEDEPOHL L.H. (1961) Distribution of the elements in some major units of the Earth's crust. Geol. Soc. Amer., Bull. 72, 175-192.

TUREKIAN K. K. and IMBRIE J. (1966) The distribution of trace elements in deep-sea sediments of the Atlantic Ocean. Earth Planet.Sci. Lett. 1, 161-168.

VALENCIA M. (1977) Pacific Pleistocene paleoclimatic stratigraphies : a comparative analysis of results. J. Quaternary Res. 8, 339-354.

VALLENTYNE J. R. (1963) Isolation of pyrite spherules from Recent sediments. Limnol. Oceanogr. 8, 16-30.

van ANDEL Tj. H. (1973) Texture and dispersal of sediments in the Panama Basin. J. Geol. 81, 434-457.

van ANDEL Tj. H., HEATH G. R., MALFAIT B. T., HEINRICKS D. F. and EWING J. I. (1971) Tectonics of the Panama Basin, eastern equatorial Pacific. Geol. Soc. Amer., Bull. 82, 1489-1508.

VANDERBORGHT J. P., WOLLAST R. and BILLEN G. (1977a) Kinetic models of diagenesis in disturbed sediments. Part 1. Mass transfer properties and silica diagenesis. Limnol. Oceanogr. 22, 787-793.

VANDERBORGHT J. P., WOLLAST R. and BILLEN G. (1977b) Kinetic models of diagenesis in disturbed sediments. Part 2. Nitrogen diagenesis. Limnol. Oceanogr. 22, 794-803.

VINOGRADOV A. P. (1939) Iodine in marine muds. To the problem of the origin of iodine-bromine waters in petroliferous regions (In Russian). Tr. Biogeokhim. Lab. Akad. Nauk SSSR 5, 19-32 (English pp. 33-46).

VOLKOV I. I. and FOMINA L. S. (1974) Influence of organic material and processes of sulphide formation on distribution of some trace elements in deep-water sediments of the Black Sea. In The Black Sea - Geology, Chemistry, and Biology (eds. E. T. Degens and D. A. Ross), pp. 456-476. Amer. Assoc. Petrol. Geol., Mem. 20.

WAKEFIELD S. J. (1978) The iodine content of sediments and pore waters from the region of the East Pacific Rise (Abstract). Geol. Soc. London, Quart. J. 135, 478.

WEAVER C. E. and WAMPLER J. M. (1972) The illite-phosphate association. Geochim. Cosmochim. Acta 36, 1-13.

WEISS R. F., LONSDALE P., LUPTON J. E., BAINBRIDGE A. E., CRAIG H. (1977) Hydrothermal plumes in the Galapagos Rift. Nature 267, 600-603.

WILLIAMS H., TURNER F. J. and GILBERT C. M. (1954) Petrography, an introduction to the study of rocks in thin sections. Freeman, San Francisco. 406 pp.

WILSON T. R. S. (1978) Evidence for denitrification in aerobic pelagic sediments. Nature 274, 354-356.

WONG G. T. F. and BREWER P. G. (1974) The determination and distribution of iodate in South Atlantic waters. J. Mar. Res. 32, 25-36.

WONG G. T. F. and BREWER P. G. (1977) The marine chemistry of iodine in anoxic basins. Geochim. Cosmochim. Acta 41, 151-159.

WRIGHT P. L. (1972) The Geochemistry of Recent Sediments of the Barents Sea. Unpubl. Ph.D. dissert., University of Edinburgh. 266 pp.

WYRTKI K. (1965) Surface currents of the eastern tropical Pacific Ocean. Inter-Amer. Tropical Tuna Comm., Bull. 9, 271-304.

WYRTKI K. (1966) Oceanography of the eastern equatorial Pacific Ocean. In Oceanography and Marine Biology Annual Review (ed. H. Barnes), Vol. 4, pp. 33-68. George Allen and Unwin Ltd., London.

WYRTKI K. (1967) Circulation and water masses in the eastern equatorial Pacific Ocean. Int. J. Oceanol. and Limnol. 1, 117-147.

ZEN E. A. (1959) Mineralogy and petrography of marine bottom sediment samples off the coast of Peru and Chile. J. Sediment. Petrology 29, 513-539.